Optimisation of Peptide Linker-based Fluorescent Ligands for the Histamine H_1 Receptor

Zhi Yuan Kok

MPharm. (Hons.)

A Thesis submitted to the University of Nottingham for the degree of Doctor of Philosophy

Dec 2020

Abstract

The histamine H_1 receptor (H_1R) is a class A G protein-coupled receptor (GPCR) and as recent studies suggested, is involved in mediating cell proliferation and thus cancer progression. High affinity H_1R-selective fluorescent ligands with optimum physicochemical properties would serve as a valuable tool to probe in further detail H_1R-related cancer pharmacology and facilitate drug discovery. Fluorescent ligands comprise a receptor binding motif connected to an appropriate fluorophore via a linker moiety, which itself offers an opportunity to modulate the properties of the final compound. Whilst modulating the overall physicochemical properties of the fluorescent ligand, a peptide-based linker could interact with residues which line the ligand entry/exit route through its side chain functional groups, potentially improving the binding affinity of the overall conjugate as well as providing information on structure activity relationships (SARs) along the ligand entry/exit route.

An initial molecular docking study conducted on the H_1R suggested an acidic amino acid (*e.g.* aspartic acid) within the peptide linker could potentially engage in salt bridge interactions with the basic residues of $K179^{ECL2}$ and $K191^{5.39}$; this however failed to generate a useable fluorescent ligand due to non-binding. This led to a more detailed screening approach to try and identify an optimised peptide linker. By incorporating the optimised peptide linker into several series of fluorescent compounds, a library of high affinity H_1R fluorescent ligands was synthesised, where both Copper(I)-catalysed alkyne-azide cycloaddition (CuAAC) and conventional amide coupling approaches were employed for fluorophore attachment. The library afforded compounds with pK_D values ranging from 7.6 to 8.4 determined using NanoBRET saturation binding experiments. Further investigation into the effects of the fluorophore on fluorescent ligand binding affinity suggested that the (*E*)-4-(2-(5,5-difluoro-7-(thiophen-2-yl)-5*H*-5λ^4,6λ^4-dipyrrolo[1,2-*c*:2',1'-*f*][1,3,2]diazaborinin-3-yl)vinyl)phenoxy-based fluorophore (BODIPY 630/650) was a key factor in increasing binding affinity of H_1R fluorescent ligands, overriding the linker SAR. Molecular docking of these ligands into a H_1R model based on the H_1R crystal structure (PDB code: 3RZE) highlighted residues which could interact with the

optimised peptidic linkers and potentially form additional binding site architecture for the fluorescent conjugate.

Acknowledgement

First and foremost, I would like to thank my supervisors Prof. Barrie Kellam, Dr. Shailesh Mistry and Prof. Steve Hill for their constant support, guidance and advice throughout the course of my research as well as my career path.

I would like to extend my utmost appreciation towards Dr. Sarah Mistry and Dr. Leigh Stoddart for their patience in supervising and assisting me in the laboratory and Dr. Nicholas Kindon for his relentless effort in arranging for medicinal chemistry tutorial sessions which I have benefitted from. Many thanks to colleagues within the C-floor corridor and the cell signalling group for the help given as I conduct my experiments as well as companionship throughout my PhD.

I would also like to thank Prof. Rob Leurs for the gastvrijheid during my short stay at the Vrije Universiteit Amsterdam, Dr Henry Vischer and Tamara Mocking for their time and effort in setting up the assays required for the selectivity studies.

My heartfelt gratitude towards my family and friends both in Malaysia and the UK who have been my support pillars throughout my PhD. My special thanks to my parents for constantly believing in what I do; Eric Wei Seong Tee and Yee Seng Tan for never failing to host me when I visit London; Enoch Kan, Sin Yee Wong, Cliff Lim Chee Pui and Elizabeth Ng Yan Xin for the regular indulgence in Ma-La hotpot which I now could not shake off and my comrades at Beeston Braves badminton club for fighting hard together to earn that well-deserved league promotion.

Finally, I am extremely grateful to the University of Nottingham for funding my PhD through the Vice-Chancellor's Scholarship for Research Excellence.

Abbreviation

^{1}H NMR	Hydrogen ^{1}H nuclear magnetic resonance
ACN	acetonitrile
AP-1	Activator protein 1
Ar	aromatic
atm	atmosphere
Boc	tert-butyloxycarbonyl
BODIPY	Boron-dipyrromethene
BODIPY 630/650	(*E*)-4-(2-(5,5-difluoro-7-(thiophen-2-yl)-5*H*-5λ^{4},6λ^{4}-dipyrrolo [1,2-*c*:2',1'-*f*][1,3,2]diazaborinin-3-yl)vinyl)phenoxy-based fluorophore
BRET	Bioluminescence resonance energy transfer
BTTAA	2-(4-((bis((1-(tert-butyl)-1H-1,2,3-triazol-4-yl)methyl)amino) methyl)-1H-1,2,3-triazol-1-yl)acetic acid
BTTES	3-(4-((Bis((1-(*tert*-butyl)-1*H*-1,2,3-triazol-4-yl)methyl)amino) methyl)-1*H*-1,2,3-triazol-1-yl)propane-1-sulfonic acid
BTTPS	3-(4-((bis(1-tert-butyl-1H-1,2,3-triazol-4-yl)methyl)amino) methyl)-1H-1,2,3-triazol-1-yl)-propanol hydrogen sulfate
cAMP	cyclic adenosine monophosphate
$CDCl_3$	Deuterated chloroform
CHO	Chinese hamster ovary
CNS	Central nervous system
CREB	cAMP response element-binding protein
CuAAC	Copper-catalysed alkyne-azide cycloaddition
DAG	Diacylglycerol

DCE	dichloroethane
DCM	Dichloromethane
DDQ	2,3-dichloro-5,6-dicyano-1,4-benzoquinone
DEAD	Diethyl azodicarboxylate
DIAD	Di-isopropyl azodicarboxylate
DIPEA	Diisopropylethylamine
DMAP	4-Dimethylaminopyridine
DMF	Dimethylformamide
DMPK	Drug metabolism and pharmacokinetics
DMSO	Dimethyl sulfoxide
ESI	electrospray ionisation
EtOAc	ethyl acetate
FCS	Fluorescence correlation spectroscopy
Fmoc	Fluorenylmethyloxycarbonyl
GDP	Guanosine diphosphate
GFP	Green fluorescent protein
GPCR	G protein-coupled receptor
gpH_1R/H_2R	Guinea pig H_1R/H_2R
GRK	GPCR kinases
GTP	Guanosine triphosphate
GTPγS	Guanosine 5'-O-[gamma-thio]triphosphate
H_1R	Histamine H_1 receptor
HATU	1-[Bis(dimethylamino)methylene]-1H-1,2,3-triazolo[4,5-b]pyridinium 3-oxide hexafluorophosphate

HBSS	Hank's balanced salt solution
HBTU	2-(1H-benzotriazol-1-yl)-1,1,3,3-tetramethyluronium hexafluorophosphate
HDC	L-histidine decarboxylase
HEK293	Human embryonic kidney 293
HEPES	4-(2-hydroxyethyl)-1-piperazineethanesulfonic acid
HER2	Human epithelial growth factor receptor 2
HOBt	hydroxybenzotriazole
HPLC	High performance liquid chromatography
hr	hour
HRMS	High resolution mass spectrometry
IP_3	Inositol 1,4,5-triphosphate (IP_3)
IκBα	Nuclear factor of kappa light polypeptide gene enhancer in B-cells inhibitor alpha
k_{off}	Dissociation rate
k_{on}	Association rate
LCMS	Liquid chromatography-mass spectrometry
m/z	mass-to-charge ratio
MAPK	Mitogen-activated protein kinase
mdm2	Mouse double minute 2 homolog
MeOH	methanol
min	minute
MW	microwave
NADPH	Nicotinamide adenine dinucleotide phosphate

NAL	Neutral allosteric ligand
NAM	Negative allosteric modulator
NBD	Nitrobenzoxadiazole
NFAT	Nuclear factor of activated T-cells
Nluc	Nano-luciferase
NMR	Nuclear magnetic resonance
PAM	Positive allosteric modulator
PE	petroleum ether
Ph	phenyl
Pip	piperidine
PIP_2	Phosphatidylinositol 4,5-bisphosphate
PKA	Protein kinase A
PKC	Protein kinase C
PLCβ	Phospholipase Cβ
PREP-HPLC	Preparative HPLC
p-TsOH	*para*-toluenesulphonic acid
RBF	round bottom flask
rH_2R	H_2R in rats
RhoEGF	Rho guanine nucleotide exchange factor
Rluc	Renilla luciferase
RP-HPLC	Reverse phase HPLC
RT	room temperature
SAR	Structure-activity relationship

SBD	Sulfobenzoxadiazole
SEM	Standard error of mean
TAMRA	Tetramethylrhodamine
TBTA	Tris[(1-benzyl-1*H*-1,2,3-triazol-4-yl)methyl]amine
TFA	trifluoroacetic acid
THF	tetrahydrofuran
TLC	thin layer chromatography
TOF	time of flight
t_R	retention time
Troc	2,2,2-trichloroethoxycarbonyl
UV	ultraviolet
YFP	Yellow fluorescent protein

Table of Contents

Chapter 1 Fluorescent Ligands as Tools to Study GPCRs 1

1.1 GPCRs 1

1.1.1 GPCR Involvement in Intracellular Signalling 2

1.1.2 GPCR Allostery 5

1.1.3 Conventional Methods of Studying GPCR Pharmacology 6

1.1.3.1 Radioligand Binding Assay 7

1.1.3.2 Functional Assays 7

1.1.3.3 Limitations 9

1.2 Fluorescent Ligands 9

1.2.1 Fluorescent Ligands as Pharmacological Tools 10

1.2.1.1 NanoBRET 11

1.2.1.2 Confocal Microscopy 13

1.2.1.3 Fluorescence Correlation Spectroscopy 13

1.3 Histamine Receptors 14

1.3.1 Histamine Receptors as Therapeutic Targets for Cancer 16

1.3.2 Fluorescent Ligands for Histamine Receptors 16

1.3.2.1 H_1R 17

1.3.2.2 H_2R 19

1.3.2.3 H_3R 21

1.3.2.4 H_4R 26

1.4 Research Aim 27

Chapter 2 Optimisation of the Peptide Linker within the H_1R Fluorescent Ligand 30

2.1 First Generation Fluorescent Ligand 30

2.1.1 Approach and Ligand Design 30

2.1.2 Click Chemistry 34

2.1.2.1 Huisegen 1,3-dipolar Cycloaddition 35

2.1.2.2 Copper-catalysed Alkyne-Azide Cycloaddition 35

2.1.3 Synthesis 37

2.1.3.1 Synthesis of the VUF13816-based Orthosteric Binding Motif 37
2.1.3.2 Synthesis of the Peptide Congener 39
2.1.3.3 Synthesis of the Azido Functionalised BODIPY Fluorophore 41
2.1.3.4 Fluorophore Coupling using CuAAC 42
2.1.4 Fluorescence Spectrscopy and Pharmacology 43
2.1.4.1 Absorption/Emission Spectral Characterisation 43
2.1.4.2 Pharmacology 44
2.2 Sequential Screening of Peptide Linker using Non-fluorescent Peptide Congeners 45
2.2.1 Approach 46
2.2.2 Synthesis 47
2.2.3 Pharmacology 48
2.2.3.1 Series 1 (AA1-A-A) 49
2.2.3.2 Series 2 (V-AA2-A) 51
2.2.3.3 Series 3 (V-S-AA3) 53
2.3 Summary 55

Chapter 3 The Synthesis of New Generation H_1R Fluorescent Ligands 56

3.1 Second Generation Fluorescent Ligands 56
3.1.1 Approach 56
3.1.2 L-Phe-based Congeners 59
3.1.2.1 Synthesis 59
3.1.2.2 Pharmacology 59
3.1.3 Synthesis of Second Generation Fluorescent Ligands 61
3.1.3.1 Synthesis of the Alkyne-Functionalised BODIPY 630/650 Fluorophore 62
3.1.3.2 Synthesis of the Peptide Congener and Fluorophore Coupling 64
3.1.4 Pharmacology 65
3.2 Third Generation Fluorescent Ligands 67

3.2.1 Approach 67
3.2.2 Synthesis 68
3.2.2.1 Synthesis of the Doxepin-based Orthosteric Binding Motif 68
3.2.2.2 Synthesis of the Peptide Congener and Fluorophore Coupling 69
3.2.3 Pharmacology 70
3.2.3.1 Peptide Congener 70
3.2.3.2 Third Generation Fluorescent Ligands 72
3.3 Fourth Generation Fluorescent Ligands 74
3.3.1 Approach 74
3.3.2 Synthesis 75
3.3.3 Pharmacology 76
3.3.4 Confocal Imaging 83
3.4 Summary 84

Chapter 4 The Effects of the Fluorophore on the Binding Affinity of Peptide Linker-based H_1R Fluorescent Ligands and Molecular Docking Studies 85

4.1 Approach and Ligand Design 85
4.2 Synthesis 87
4.2.1 Synthesis of BOIPY A and BODIPY B 87
4.2.2 Synthesis of the Peptide Congener and Fluorophore Coupling 88
4.3 Fluorescence Spectroscopy and Pharmacology 90
4.3.1 Absorption/Emission Spectral Characterisation 90
4.3.2 Pharmacology 90
4.4 Lipophilicity Analysis of H_1R Fluorescent Ligands 96
4.5 Molecular Docking Studies 99
4.6 Summary 103

Chapter 5 **Conclusion and Future Work** 104

5.1 Conclusion 104

5.2 Future Work 105

Chapter 6 **Experimental** 107

6.1 Chemistry 107

6.2 Pharmacology 175

6.3 Computational Modelling 180

Chapter 7 **References** 182

Appendix 196

CHAPTER 1: FLUORESCENT LIGANDS AS TOOLS TO STUDY GPCRs

GPCRs are important drug targets due to their involvement in intracellular signalling and physiological processes, hence it is important for us to have a deeper understanding of GPCR pharmacology. The recent development of fluorescence-based methods for studying GPCR pharmacology have expanded the molecular toolkit we have to achieve this aim which also have the potential to support future drug discovery efforts. Histamine receptors are Class A aminergic GPCRs and have recently been shown to play an important role in cancer progression[1-2], thus fluorescent ligands for the histamine receptors would be useful tools to further the understanding of histamine cancer pharmacology and subsequently contribute towards the fight against cancer. Fluorescent ligands for the H_1R which comprise of peptide linkers have been reported and proven to be useful pharmacological and cell imaging tools[3]. However, the peptide linkers of these fluorescent ligands were not optimised, creating an opportunity to generate fluorescent ligands with higher binding affinities at H_1R with the optimisation of the peptide linker. The H_1R crystal structure revealed several residues along the receptor ligand entry route which could potentially be exploited by the linker moiety[4]. This opens the possibility to further improve the binding affinity of existing H_1R fluorescent ligands and their utility towards studying GPCRs especially in diseased cells in an in vitro and in vivo setting.

1.1 GPCRs

GPCRs are a superfamily of receptor proteins, usually consisting of a 350-400 residue (up to 1100 residues) polypeptide folded into a characteristic seven transmembrane helix structure which spans the plasma membrane. The helices are connected by three intracellular and three extracellular loops, with an extracellular *N*-terminus and an intracellular *C*-terminus (Figure 1.1). GPCRs are inarguably one of the most important class of therapeutic drug targets, with almost 30% of all marketed drugs targeting them, and making up approximately 4% of the protein-encoding human genome[5-7]. The superfamily is divided into five distinct families, with Class A GPCRs (rhodopsin family) being the largest group, containing receptors for most monoamine

neurotransmitters (e.g. histamine, dopamine, serotonin and adrenaline). With many orphan receptors currently present, GPCRs remain an attractive target for drug discovery[6-8]. The first human GPCR crystal structure for the β_2-adrenoceptor (PDB code: 2R4R), solved in 2007 was of great merit as structural determination of non-rhodopsin GPCRs using X-ray crystallography were difficult due to receptor instability after isolation from the plasma membrane[9]. With more than 120 GPCR crystal structures solved, in addition to advances in homology modelling methods and molecular dynamics simulations, *in silico* driven structure-based approaches have become a powerful tool in drug discovery efforts[10].

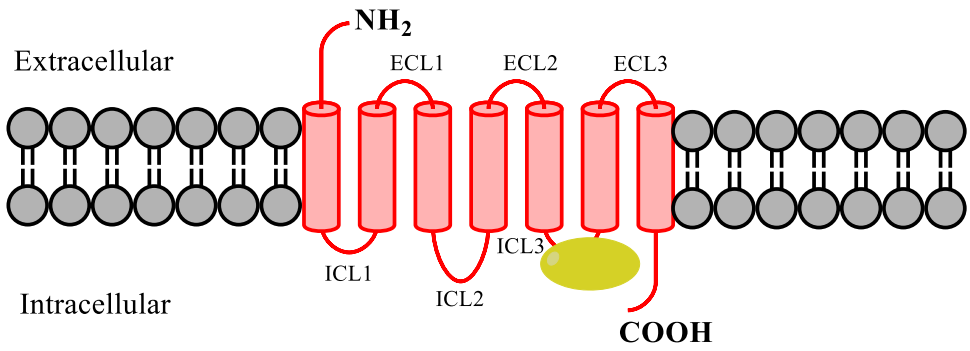

Figure 1.1: Representation of a GPCR (in red) consisting of seven transmembrane domains, three extracellular loops, three intracellular loops, the extracellular *N*-terminus, the intracellular *C*-terminus and the G-protein (in yellow) which binds to intracellular loop 3.

1.1.1 GPCR Involvement in Intracellular Signalling

A heterotrimeric G-protein, the main adaptor protein for the GPCR signalling pathway, is coupled to the 3rd intracellular loop of the receptor (Figure 1.2). The three monomeric units which makes up a G-protein are α, β and γ, with the Gα subunit further divided into four major families, namely G_s, $G_{i/o}$, $G_{q/11}$ and $G_{12/13}$ which vary in terms of downstream signalling activity[11-12]. Receptor activation causes guanosine diphosphate (GDP) bound within the Gα subunit to exchange with guanosine triphosphate (GTP), which then triggers the dissociation of the G-protein, allowing the G-protein subunits to interact with their respective target proteins. The downstream signalling cascade will progress mainly through either the cyclic adenosine monophosphate (cAMP)-dependent, inositol-phospholipid-dependent or

Rho-dependent pathway depending on the Gα subunit involved (Figure 1.2)[12-13]. G-protein independent signalling pathways are mainly mediated by GPCR kinases (GRKs) and β-arrestins. Upon receptor activation, GRKs phosphorylate the intracellular *C*-terminal of the receptor, primarily serine and threonine residues[14]. β-arrestins bind to the phosphorylated sites, leading to G-protein uncoupling, clathrin-mediated receptor endocytosis and subsequently intracellular degradation (or recycling) and desensitisation[12, 15-16]. β-arrestins are also involved in the activation the mitogen-activated protein kinase (MAPK) pathway, the regulation of transcription factors such as mouse double minute 2 homolog (mdm2) and nuclear factor of kappa light polypeptide gene enhancer in B-cells inhibitor alpha (IκBα) as well as its association with transcription cofactors such as p300 and cAMP response element-binding protein (CREB) to promote transcription[14-15, 17-23].

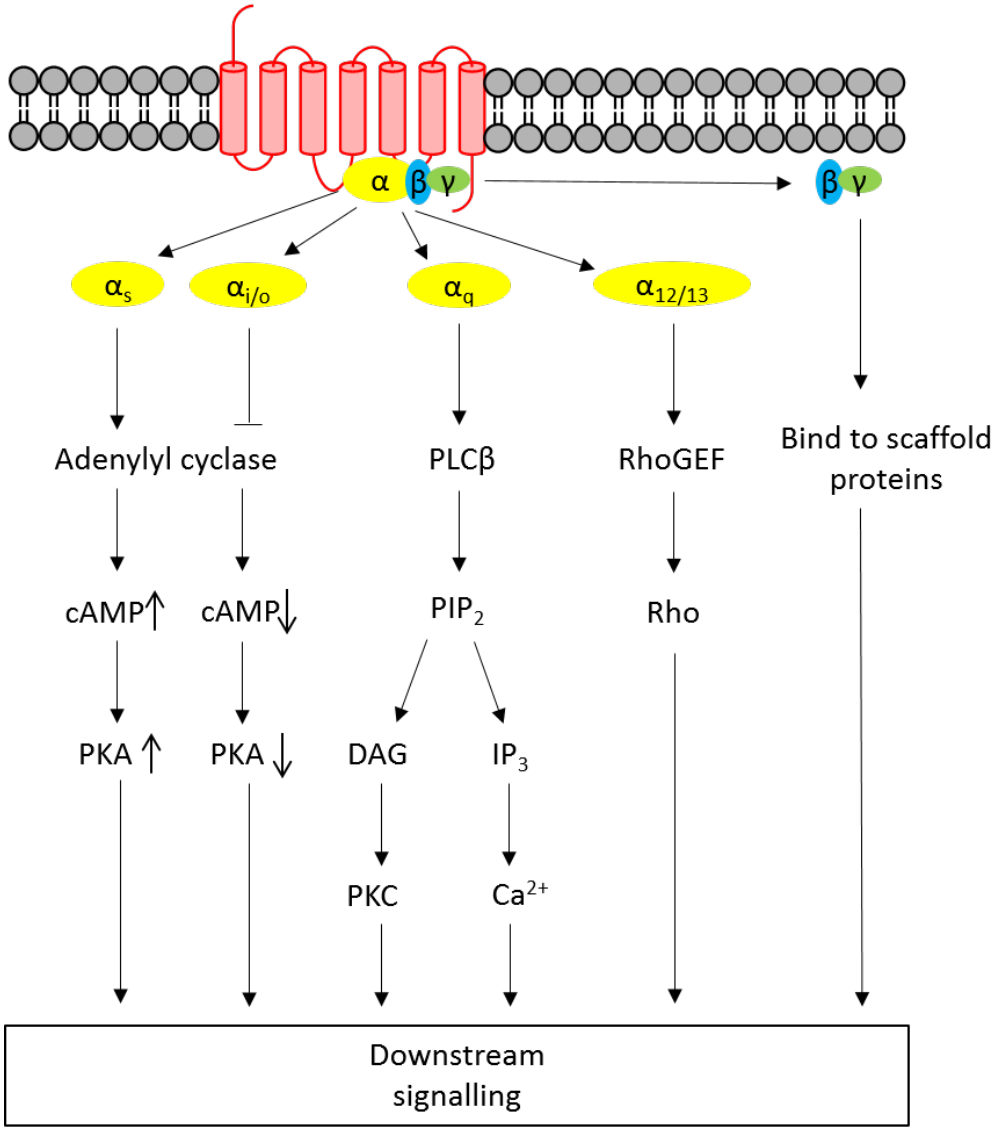

Figure 1.2: G-protein dependent signalling pathway. Upon GPCR activation by an agonist, heterotrimeric G proteins dissociate into separate Gα and Gβγ subunits. Depending on the Gα subunit involved, downstream signalling proceeds via four different pathways. $G\alpha_s$ activates adenylyl cyclase which subsequently increases cAMP production and the phosphorylation of protein kinase A (PKA). $G\alpha_{i/o}$, on the other hand, inhibits adenylyl cyclase which leads to a decrease in intracellular cAMP and decreased PKA activation. $G\alpha_q$ stimulates phospholipase Cβ (PLCβ), promoting the hydrolysis of phosphatidylinositol 4,5-bisphosphate (PIP_2) to diacylglycerol (DAG) and inositol 1,4,5-triphosphate (IP_3) which in turn activates protein kinase C (PKC) and increases intracellular Ca^{2+} respectively. $G\alpha_{12/13}$ activates Rho guanine nucleotide exchange factor (RhoGEF), which subsequently activates Rho GTPases. Gβγ subunit binds to scaffold proteins and could affect downstream signalling[12-13].

1.1.2 GPCR Allostery

Endogenous ligands bind to a specific site in a receptor, namely the orthosteric site to produce a downstream signalling effect. GPCR allostery describes the existence of binding sites on the receptor that are topographically distinct from the orthosteric site, in which a ligand could bind to and subsequently modulate the binding of the natural ligand and/or the coupling of the effectors[24-26]. Allosteric sites can be categorised into five different types, namely ancestral orthosteric site, ligand-entry sites, conformational locks and intracellular signalling protein interface (Figure 1.3)[24]. Ancestral orthosteric site refers to the old orthosteric site for Class A GPCR ligands that has fallen out of use as the receptors evolve to bind at distinct sites. Ligand-entry sites are binding sites in the outer domains of the receptor which allow the transient binding of orthosteric ligands as they make their way into the orthosteric binding site. Conformational locks refer to any other sites located within the hydrophobic core or in extrahelical positions of the receptor that a ligand could bind which subsequently stabilises a receptor conformational state. Allosteric sites could also be found around the intracellular loops of GPCRs where signalling proteins bind to and trigger the signalling cascade.

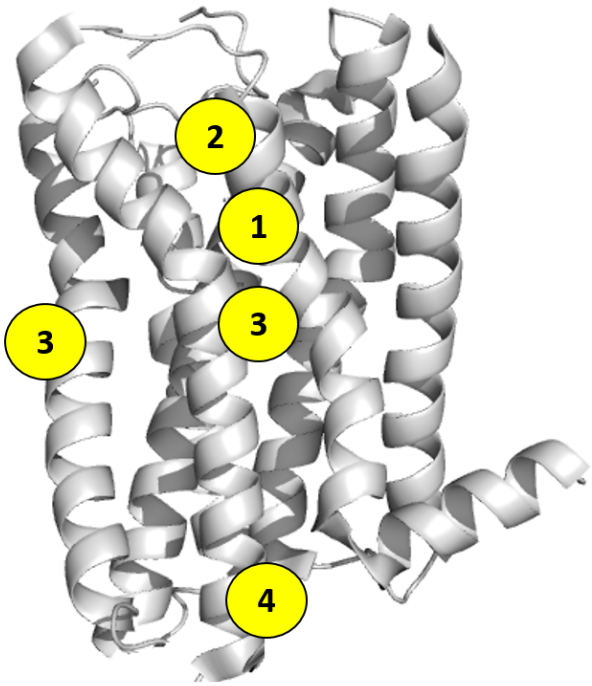

Figure 1.3: Examples of allosteric sites at GPCRs. **1**: ancestral orthosteric site; **2**: ligand-entry sites; **3**: conformational locks; **4**: intracellular signalling protein interface.

Allosteric modulation has emerged as an important approach in drug discovery due the potential it has for regulating receptor binding and activity. Allosteric modulators could be divided into 3 types, namely positive allosteric modulators (PAMs), negative allosteric modulators (NAMs) and neutral allosteric ligands (NALs)[26-27]. One of the key advantages an allosteric modulator offers is its potential ability to bind to its target receptor with greater receptor subtype selectivity. This is attributed to the low sequence homology within the non-conserved allosteric sites as compared to the highly conserved orthosteric site across GPCR subtypes, leading to less off-site binding and effects[27-28]. As such, these modulators could be connected to an orthosteric ligand via a linker to give bitopic ligands with good receptor subtype selectivity and/or affinity profile[29-30]. The availability of co-crystal structures of allosteric modulators bound to GPCRs would offer insight into how allosteric modulators bind to their respective target receptors and subsequently could inform the design of allosteric modulators from a structure-based approach[31-33].

1.1.3 Conventional Methods of Studying GPCR Pharmacology

Given the extensive role played by GPCRs within the physiological functions of the human body, there remains a need to understand these receptors in greater detail to further push forward drug discovery efforts. Drug molecules could exhibit different pharmacological effects at their target and non-target receptors. Full agonists bind to and activate the receptor at full efficacy, partial agonists would only trigger a partial response relative to full agonists, inverse agonists bind to and induce a response which is below the constitutive activity of the receptor whereas antagonists do not induce any response but instead competes with and blocks endogenous ligands from activating the receptor. Radioligand binding assays and functional assays such as cAMP accumulation and Ca^{2+} mobilisation assays are mainstay methods for pharmacological studies of any compound of interest at GPCRs[13]. The binding affinity of the compound of interest are usually reported as K_D, K_i, A_2 or K_B depending on the type of experiments involved. These values could also be reported as the negative logarithm to the base 10, namely pK_D, pK_i, pA_2 or pK_B[34]. K_D and K_i values are reported in saturation and competitive binding experiments respectively. K_D refers to the concentration of a radio- or fluorescently labelled compound needed to occupy 50%

of all targets whereas K_i estimates the binding affinity of an unlabelled compound based on its concentration required to occupy 50% of all targets in the presence of a labelled competitor (see 1.1.3.1). pA_2 and pK_B estimate the dissociation constant of compounds which are antagonists from functional assays. pA_2 refers to the concentration of antagonist required to produce a 2-fold shift in agonist response curve determined from functional assays involving increasing concentrations of the antagonist whereas pK_B estimates the binding affinity of an antagonist in a functional assay setting using the Gaddum equation. The binding affinity of a compound of interest for its target is routinely determined using both binding and functional assays. This orthogonal assay approach allows comparisons to be made between pK_D/pK_i and pA_2/pK_B values, which could potentially highlight assay dependent influences on the obtained data if any as well as provide greater data confidence which is important for determining the direction of the project.

1.1.3.1 Radioligand Binding Assay

Competition radioligand binding assays are useful for determining the binding affinity of the compound of interest at its target receptor but do not provide information on ligand functionality. The K_D and kinetics (association rate (k_{on}), dissociation rate (k_{off})) of a radionuclide-labelled ligand are first determined through saturation and kinetic binding experiments respectively. The radioligand can then be used in competition binding experiments to determine the K_i and kinetics of unlabelled ligands using the Cheng-Prusoff equation[35] and Motulsky-Mahan equation[36] respectively. The biggest disadvantage of this assay is associated with the radioactivity and half-life of radioligands which pose safety, storage and disposal concerns.

1.1.3.2 Functional Assays

Functional assays measure downstream signalling effects after ligand binding and provide useful information about the concentration-response profile of a compound[37]. Measurement of signalling effects could be proximal or distal to receptor activation, each having different advantages, e.g. a lower incidence of false positives and high signal-to-noise ratio respectively[13]. The choice of functional assay is also dependent on the type of G_α subunit the receptor of interest is coupled to.

Guanine nucleotide binding assay measures the binding of a non-hydrolysable radionuclide-tagged GTP analogue such as [^{35}S]GTPγS to the plasma membrane upon GPCR activation by an agonist. As guanine nucleotide exchange is the initial event after GPCR activation, measurements made are not subject to amplification or intracellular regulation and suffer from poor signal-to-noise ratio[38]. As such, this assay is only used to study $G_{i/o}$-coupled receptors due to the abundance of $G_{i/o}$ in most cells and a faster GDP-GTP exchange rate with $G_{i/o}$ as compared to other G proteins[38].

The cAMP assay is useful for screening G_s-coupled receptors in which receptor activation leads to an increase in adenylyl cyclase activity and cAMP production. The increased levels of cAMP would compete against labelled cAMP introduced at the start of the experiment for binding to cAMP antibodies bound to a solid phase and lead to the loss of signal, which could be radioactivity, fluorescence or luminescence based. For G_i-coupled receptors, on the other hand, the assay is considerably more difficult as the stimulation of adenylyl cyclase with forskolin is necessary at the start of the experiment in order to maximise the inhibition signal[13].

Intracellular calcium assay aims to measure changes in intracellular Ca^{2+} concentration after GPCR activation through various means which include IP_3-mediated release of intracellular Ca^{2+} from the endoplasmic reticulum, the influx of Ca^{2+} via ion channels or sequestration and/or efflux of calcium via various mechanisms[13]. This assay utilises cell permeable Ca^{2+} sensitive fluorescent dyes that fluoresce when bound to Ca^{2+} which provide the signal output. Despite not being able to screen for inverse agonists due to non-observable increase in basal intracellular Ca^{2+}, this assay has been proven to be useful for the identification of ligands at orphan GPCRs[13, 39-40].

Reporter gene assay utilises the expression of reporter proteins such as green fluorescent proteins (GFPs) and enzymes to determine the effects of ligand binding on signal transduction at the transcription level. Upon ligand binding, changes in GPCR-mediated secondary messengers such as cAMP or Ca^{2+} will activate or inhibit their respective response elements via CREB and Activator protein 1 (AP1)/Nuclear factor of activated T-cells (NAFT) respectively[13]. This leads to changes in the

expression of the reporter protein and thus readouts which could then be measured to obtain valuable information on ligand pharmacological profile at the receptor of interest[13, 41]. As the signalling event measured is significantly distal in the cascade to receptor activation, it requires long incubation intervals for the effects to take place and is also prone to false-positive results[13].

1.1.3.3 Limitations

Despite their use to quantify receptor-ligand pharmacology, conventional ways of studying GPCR pharmacology using radioligand binding assays and functional assays do not provide information about the detailed events that occur after receptor binding such as receptor localisation, internalisation and protein-protein interaction[42]. This has led to the development of fluorescence-based techniques to study the various aspects of GPCR pharmacology which involve the use of fluorescent donors such as luciferase enzymes and fluorescent acceptors such as fluorescent ligands[43].

1.2 Fluorescent Ligands

Fluorescent ligands for GPCRs are conventionally made by attaching an organic fluorophore such as BODIPYs, Alexa dyes or rhodamine derivatives to an orthosteric or allosteric ligand which can be either a small molecule or peptide, often a known agonist or antagonist for the receptor of interest. A linker between the orthosteric ligand and the fluorophore (Figure 1.4) is usually necessary for small molecule fluorescent ligands as the direct attachment of the fluorophore could impair binding to the orthosteric site. Alternatively, the fluorophore can also be 'designed into' the overall fluorescent ligand structure provided that the final compound retains binding affinity for its target[44-45]. It is also crucial to treat fluorescent ligands as new pharmacological entities which are different from their parent ligand as the fluorophore-linker attachment would usually have an effect on the physical, chemical and biological properties of these new molecules[43, 46-47].

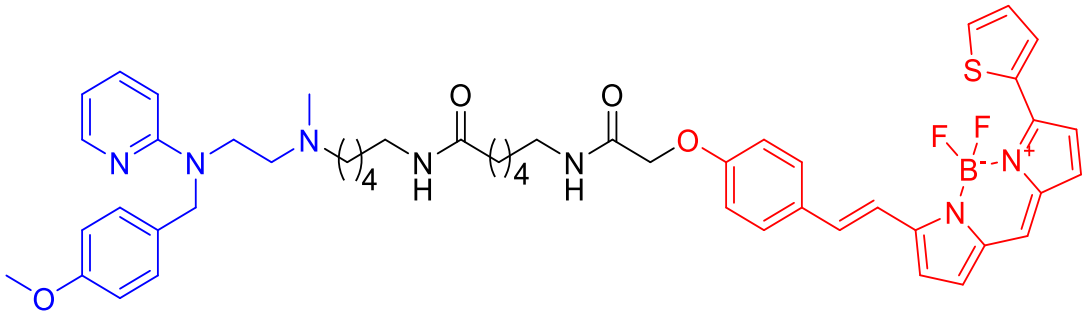

Figure 1.4: An example of a H_1R fluorescent ligand consisting of the H_1R orthosteric ligand mepyramine (**blue**) connected to a fluorophore (**red**) by a linker (**black**)[48].

A fluorescent ligand should possess several pharmacological and fluorescence properties for it to be useful in studying GPCRs. Firstly and most importantly, it should retain the binding affinity and function of its parent ligand and selectively bind to its target with little to no non-specific binding[49]. It should also be significantly quenched in aqueous environments and possess a high quantum yield, which is positively correlated with the brightness of the fluorescence signal when bound to hydrophobic site in proteins[46, 49]. These ensure that the fluorescence signal produced is solely due to the binding of the fluorescent ligand to its target receptor. Auto-fluorescence, an intrinsic cellular property caused by aromatic amino acids, nicotinamide adenine dinucleotide phosphate (NADPH) and flavin coenzymes found in cells should also be taken into consideration when designing GPCR fluorescent ligands[50]. For example, NADPH has maximum absorption/emission wavelengths ($\lambda_{max,ex}/\lambda_{max,em}$) of 340nm/450nm[50]. As such, spectral properties of the fluorescent ligand should be shifted towards longer wavelengths to avoid cell auto-fluorescence as well as spectral crossover with commonly used fluorescent proteins such as GFP and YFP which would affect fluorescence readout[46, 49, 51]. Stokes shift describes the difference between λ_{ex} and λ_{em} of a fluorophore. A fluorescent ligand should have a large stoke shift to prevent self-quenching which would reduce signal output and sensitivity[49].

1.2.1 Fluorescent Ligands as Pharmacological Tools

Fluorescent ligands are of great value in the study of GPCR pharmacology as they provide insight into ligand receptor binding and kinetics, the study and visualisation

of receptor localisation, internalisation, organisation and oligomerisation at a single cell level in living cells using several techniques briefly described below[46, 52].

1.2.1.1 NanoBRET

The term 'NanoBRET' was first coined by Machleidt et al. and involves the use of a luciferase enzyme, Nano-Luciferase (Nluc) as the bioluminescence donor for BRET experiments[53]. Upon oxidation of its substrate furimazine, Nluc transfers energy in the form of light (max λ_{em} of 460nm) to an appropriate fluorescent acceptor *e.g.* GFP, a fluorescent ligand or any protein of interest labelled with a wide range of fluorophores using HaloTag[54], SNAP Tag[55] or CLIP Tag[56] technologies[57-59] which would in turn emit light of a longer wavelength (Figure 1.5). The energy transfer can only take place when the donor and acceptor are in close proximity to one another (<10nm), making it a useful technique for studying protein-ligand and protein-protein interactions between a Nluc-fused protein of interest with a fluorescent ligand and another protein of interest labelled with an appropriate fluorophore respectively[57, 60-61]. Nluc, an optimised derivative of the luciferase found in the deep sea shrimp *Oplophorus gracilirostris* is superior to other widely used luciferases such as renilla luciferase 8 mutant (Rluc8) due to its small size of 19kDa compared to 36kDa (Rluc8), high physical stability and ability to provide sustained luminescence with great intensity within a narrower emission spectrum[53, 58]. This allows experiments to be conducted for a longer duration in time-resolved assays and at greater sensitivity which would allow the detection of protein-protein interactions at low levels[53]. Despite its small size, Nluc-tagged proteins must be validated before conducting NanoBRET experiments as there is a possibility that the Nluc tag may affect ligand binding and the function of the protein of interest. This is especially true for GPCRs with extensive extracellular domains or those whereby the *N*-terminus or the extracellular domains may contribute to ligand binding[62]. The assay should also be validated to rule out the possibility that the furimazine substrate or its associated product furimamide might interfere with ligand binding.

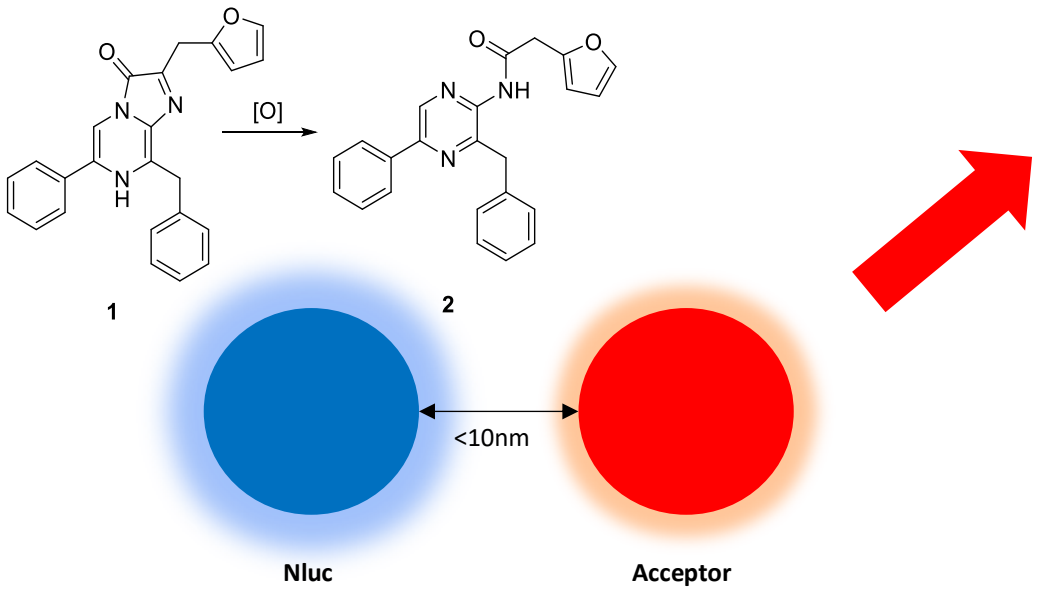

Figure 1.5: Oxidation of furimazine **1** to furimamide **2** by Nluc enables the enzyme to emit light with a peak emission wavelength of 462nm. This energy is then transferred to an acceptor within close proximity (<10nm) which would then emit light with a longer wavelength. The quantification of the fluorescence signal would allow the study of protein-ligand and protein-protein interactions.

Multiple studies have shown that in combination with NanoBRET, fluorescent ligands offer an attractive alternative method to study ligand binding over radioligand-based methods due to advantages over disposal, cost and safety issues associated with the use of radioactive materials[52, 63-73]. NanoBRET binding assays also allow the study of ligand binding in living cells and in real-time with the full intracellular environment intact, taking into account the effects that cellular components such as intracellular proteins have on ligand binding[74]. Perhaps the greatest advantage NanoBRET has over conventional radioligand assays is the ability to study ligand binding kinetics in real-time and requires no wash steps compared to the cumbersome conventional radioligand methods which would require the separation of bound from free ligand at every time point[62, 74]. Binding affinity and kinetics values of various unlabelled ligands obtained from NanoBRET assays are in good agreement with literature values determined from radioligands binding experiments[66-68, 72-73, 75]. A NanoBRET assay was also successful in monitoring in vivo the reversible binding of a propranolol-based fluorescent ligand to Nluc-tagged β_2-adrenoreceptor (β2AR) in breast cancer

tumour mouse models[76]. This will serve as a useful tool to determine the target engagement of drug candidates in vivo to cells within tumours which could hopefully progress cancer drug discovery. An in-depth review of NanoBRET is currently available[77].

1.2.1.2 Confocal Microscopy

In confocal microscopy, a laser is used to illuminate the sample and together with a pinhole eliminates out-of-focus light. This allows the sample to be visualised in a single plane, thus improving image resolution. Whilst there has been some success with the combined use of fluorescent ligands and confocal microscopy for competition and kinetics binding assays, this has now been superseded by the more versatile NanoBRET based assays[47, 78-82]. Nevertheless, fluorescent ligands are still used in confocal microscopy experiments as they allow the visualisation of ligand binding to receptors in whole tissues without the need for tissue fixation, freezing and membrane disruption[3, 42, 70, 76]. This effectively enables receptor localisation (antagonist) and internalisation (agonist) to be studied in native, live cells non-invasively and in real-time, providing valuable information on receptor expression patterns for the interrogation of the physiological importance of the receptors in biological processes and diseases[47, 52, 83-84]. However, issues such as non-specific binding and cell auto-fluorescence must be addressed for these visualisation studies to be meaningful[52].

1.2.1.3 Fluorescence Correlation Spectroscopy

Additionally, fluorescent ligands can be used to study receptor organisation using fluorescence correlation spectroscopy (FCS). FCS provides information on the organisation of the ligand-receptor complexes within a membrane area by measuring the diffusion of molecules labelled with a fluorescent tag through a small defined confocal volume of approximately 0.25fL[85]. Time-dependent fluctuations in fluorescence intensity can be analysed using autocorrelation analysis and diffusion coefficients can be determined, which provide information about the mobility and concentration of subpopulations of the molecules of interest[46, 52, 85]. These subpopulations refer to the unbound fluorescent ligand and at least two states of

ligand-receptor complexes reported in multiple FCS studies involving fluorescent ligands[86]. FCS is proven to be a powerful tool to quantify ligand residence times, allosteric effects and binding kinetics in GPCR microdomains within the cell membrane in providing insights into GPCR biology[48, 87-93].

1.3 Histamine Receptors

Histamine receptors are Class A aminergic GPCRs that share a common endogenous ligand – histamine. There are a total of four histamine receptor subtypes identified to date, namely H_1, H_2, H_3 and H_4[94]. The key characteristics of and differences between these receptors are summarised in Table 1.1 and examples of approved drugs targeting the histamine receptors, all of which are inverse agonists are depicted in Table 1.1 and Figure 1.6.

Receptor	**H_1R**	**H_2R**	**H_3R**	**H_4R**
G-protein	G_q	G_s	$G_{i/o}$	$G_{i/o}$
Tissue localisation	Ubiquitous, mainly lung, blood vessel, CNS	Ubiquitous, mainly stomach, heart, CNS	Neurones	Bone marrow, haematopoietic cells
Main role in physiology	Immuno-modulation	Gastric acid secretion	Neuro-modulation	Immuno-modulation
Pathophysio-logical conditions	Allergy, emesis, sleep-wake disorder	Dyspepsia, gastric ulcers	CNS disorders (schizophrenia, sleep-wake disorder, etc.)	Inflammatory diseases (allergy, asthma, etc.)
Drugs targeting the receptor; Clinical use	Loratidine **3**, fexofenadine **4**; allergy rhinitis	Cimetidine **5**, ranitidine **6**; dyspepsia, gastric ulcer	Pitolisant **7**; narcolepsy	None

Table 1.1: An overview of the four histamine receptor subtypes[94]. CNS: central nervous system.

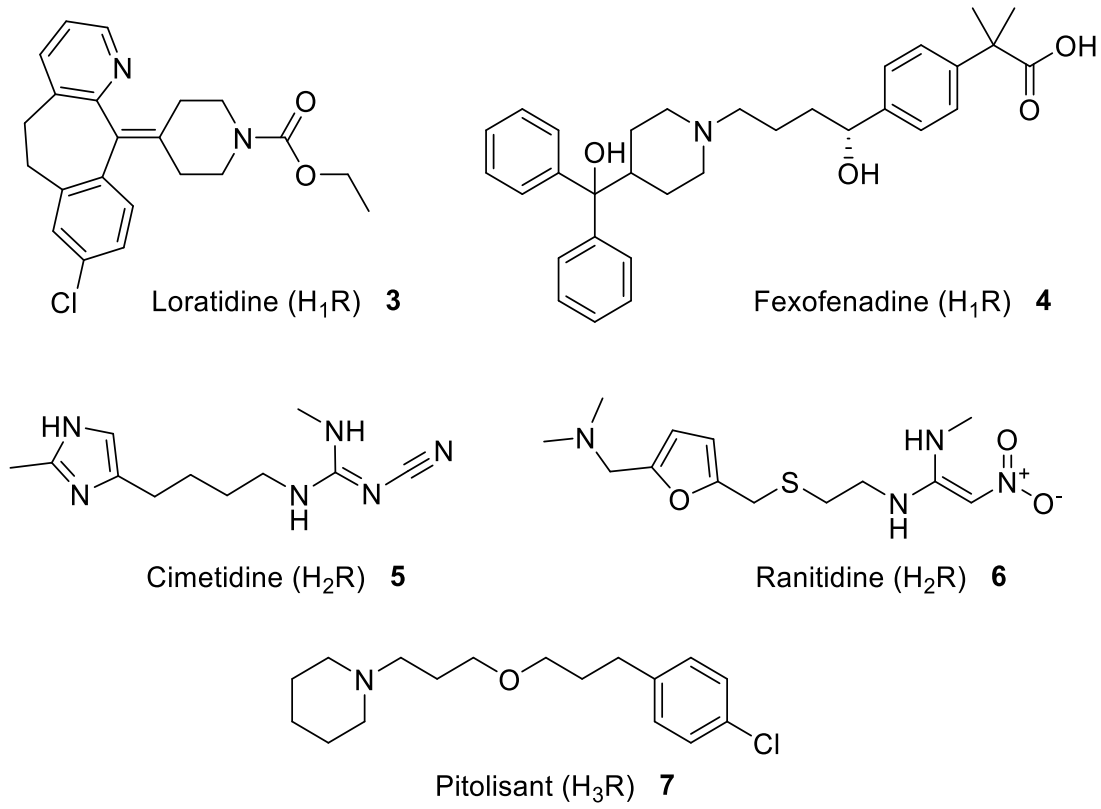

Figure 1.6: Examples of approved small molecule drugs targeting the histamine receptors (subtypes in brackets).

1.3.1 Histamine Receptors as Therapeutic Targets for Cancer

There is a growing body of evidence suggesting that histamine receptors play an important role in cancer progression, due to their involvement in cell proliferation and tumour growth[1-2, 95]. It has also been shown that most malignant cell lines highly express L-histidine decarboxylase (HDC), the histamine-synthesising enzyme and histamine is believed to act as a paracrine or autocrine factor in regulating events associated with cancer, which include angiogenesis, cell invasion, migration, differentiation and immunomodulation[2, 95-97]. This, however, is not the case across all cancer types, as histamine could either promote or suppress tumour growth and is highly dependent on tumour microenvironment, histamine metabolism, the receptor subtypes involved and the local histamine receptor balance[1-2, 95-96]. For example, Massari et al. highlighted the significant reduction of H_4R expression in tumours in comparison with normal tissue in most cancer types, suggesting that an H_4R agonist could potentially exert anti-tumoral effects[1]. The research surrounding histamine receptors and cancers of the colorectal, oesophageal, oral, liver, pancreatic, gastric, skin, breast, lung and blood have been comprehensively summarised[1-2]. Given the complexity of histamine cancer pharmacology, fluorescent ligands which could be agonists or antagonists would serve as valuable tools to understand and probe receptor expression and density, receptor organisation within the plasma membrane and receptor dimerization using techniques described in section 1.2.1 with the hope that a better understanding of cancer pharmacology would realise more successful drug discovery programmes. For example, Fernandez-Nogueira et al. reported that the H_1R is upregulated in human epithelial growth factor receptor 2 (HER2) enriched breast tumour and high H_1R expression is correlated with a worse prognosis and resistance to HER2-targeted therapy[98]. By using fluorescent ligands to image breast cancer tumour cells from patients, those who are more likely to show poor prognosis and/or not respond to HER2-targeted therapy could be identified and their treatment regimens tailored to best suit their needs.

1.3.2 Fluorescent Ligands for Histamine Receptors

Review articles on fluorescent ligands encompassing both peptide and small molecule ligands have been published in recent years, with the first literature review

published in 1996 by McGrath et al.[99]. Since then, work in this field has gained traction, with at least seven review articles published between 2005 and 2019[43, 46, 49, 83-84, 100-101]. For the purpose of this project, the focus of the literature review will be placed on fluorescent ligands targeting histamine receptors.

1.3.2.1 H_1R

There are currently several published articles on H_1R fluorescent ligands. Li et al. synthesised fluorescent ligands of varying linker lengths and fluorophores with mepyramine as the orthosteric ligand[102]. Despite all synthesised compounds displaying lower pA_2 values at guinea pig H_1R (gpH_1R) relative to mepyramine **8** (pA_2 = 9.42), several examples still retained good antagonist affinity. The majority of these contained either the 5- or 6-carboxyfluorescein fluorophores, with pA_2 values in the 8.1-9.0 range. The two compounds with the highest pA_2 at gpH_1R were **9** and **10** (Figure 1.6), containing the 5-carboxyfluorescein and nitrobenzoxadiazole (NBD) fluorophores respectively. In addition, these compounds were found to have pK_B of ~9 in Ca^{2+} mobilisation assays in U373MG human glioblastoma cells. The authors suggested that by using the appropriate linker length, certain fluorophores might be able to interact with extracellular loop regions of the receptor, contributing to an increase in H_1R binding affinity.

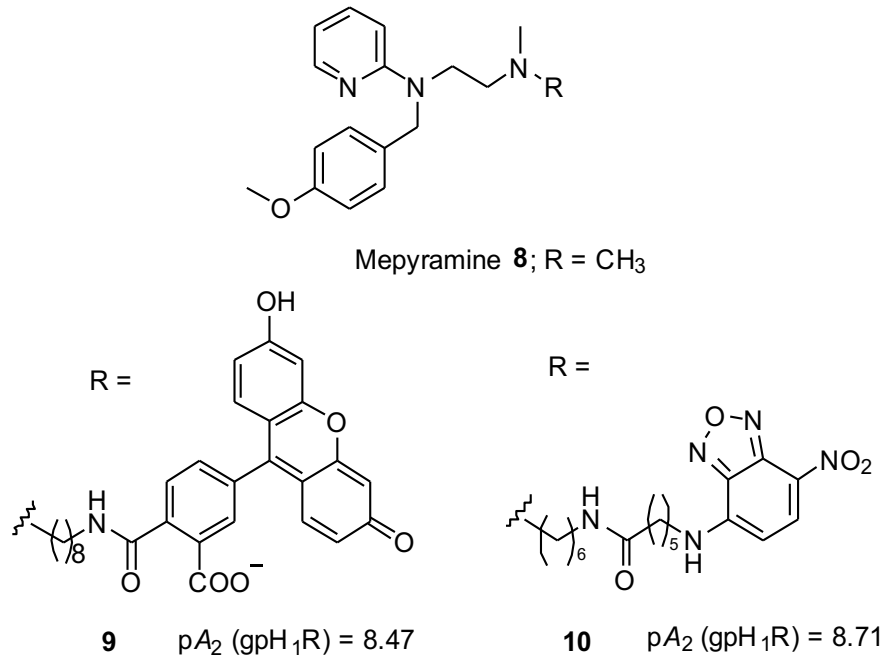

Figure 1.7: The two most potent H_1R fluorescent ligands reported by Li et al. [102]

Rose et al. attached a BODIPY 630/650-X (Invitrogen, Carlsbad, CA) fluorophore to the same mepyramine orthosteric ligand using an alkyl linker to give **11** (Figure 1.8), which exhibited similar apparent dissociation constant (pK_B = 8.9) to mepyramine (pK_B = 8.6) determined using calcium mobilisation assay performed on human H_1R (hH_1R) expressing cells[48]. Compound **11** had a greater effect in suppressing the maximal calcium response to histamine as compared to mepyramine, which the authors suggested was due to the fluorescent ligand having a slower dissociation rate. Significant ligand internalisation was also observed in confocal imaging experiments, possibly due to the lipophilic nature of the fluorophore and linker which caused it to readily cross the cell membrane. Despite this, confocal microscopy revealed specific and displaceable binding to cell surface H_1R, allowing the labelling and visualisation of H_1R in single living cells. FCS was used to determine receptor diffusion rate of the ligand-bound yellow fluorescent protein fused H_1R (H_1R-YFP) compared to the unbound H_1R-FYP, with the former demonstrated to be significantly slower than the latter. Specific binding to intracellular H_1R was also detected using FCS.

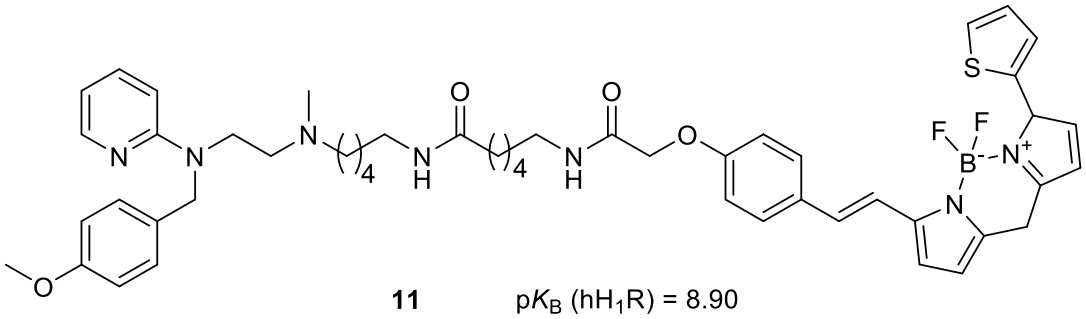

11 pK_B (hH_1R) = 8.90

Figure 1.8: BODIPY630/650-X labelled *N*-desmethylmepyramine.

In 2018, Stoddart et al. reported several BODIPY630/650-X labelled H_1R fluorescent ligands derived from two different orthosteric binding motifs, namely mepyramine and VUF13816, the latter being a highly ligand-efficient fragment for H_1R discovered from in silico screening efforts[3, 103-105]. A wide range of di- or tripeptides were utilised as linkers to give a total of 6 fluorescent ligands with a range of binding affinities (pK_i = 7.6-8.4) at hH_1R. Further pharmacological characterisation of these compounds using calcium mobilisation assay and NanoBRET saturation binding assay in whole cells gave comparable pK_B/pK_D values to pK_i values obtained from radioligand binding assay. When comparing mepyramine-derived fluorescent compound **12** (Figure 1.9;

pK_B = 7.5) to **11** (Figure 1.8; pK_B = 8.9)[48], the introduction of the peptide linker led to a loss in binding affinity but clear visualisation of specific membrane binding on live cells was possible with **12** by confocal microscopy. This was attributed to the reduction in the overall lipophilicity of the conjugate with the use of peptide linkers and hence a decrease in its ability to passively cross the cell membrane. VUF13816-based fluorescent compounds such as **13** were also found to have a slower off-rate and hence longer receptor residence time when compared to their mepyramine counterparts.

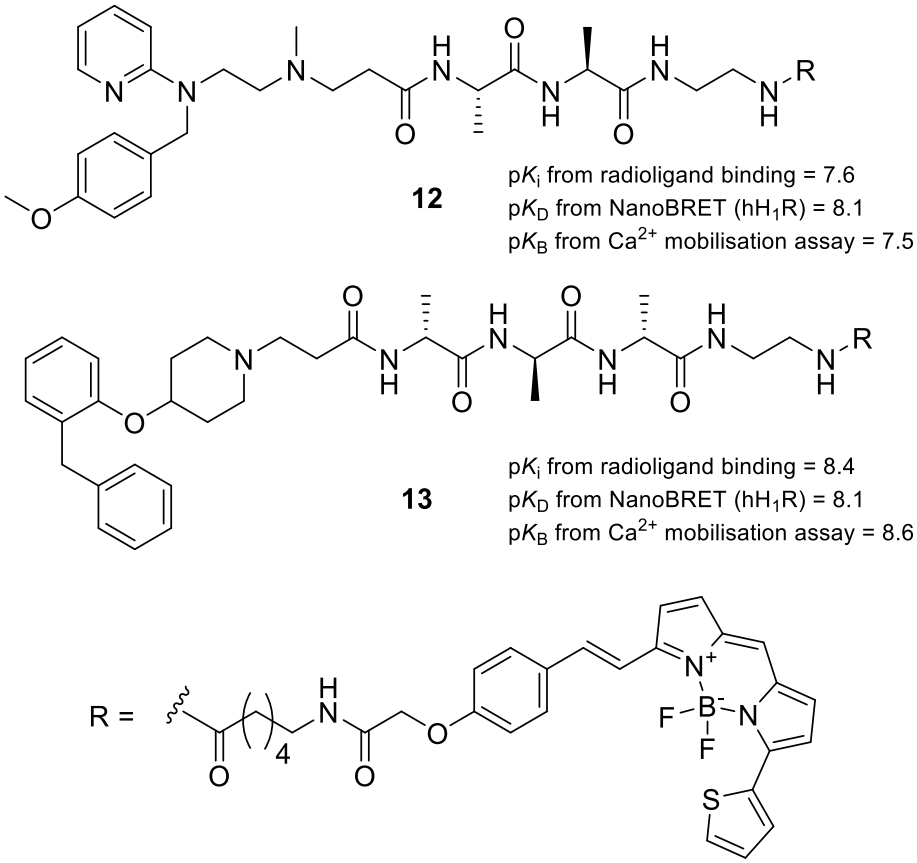

Figure 1.9: High affinity H_1R peptide linker-based fluorescent ligands.

1.3.2.2 H_2R

Limited work has been published on H_2R fluorescent ligands and were mainly by the Buschauer group. Li et al. synthesised 14 H_2R fluorescent ligands by attaching various fluorophores to the aminopotentidine-derived 3-(3-piperidin-1-ylmethylphenoxy)-propylamine orthosteric ligand[106]. It was reported that only those analogues containing the NBD group (such as **14** in Figure 1.10) had significant antagonist

activity, some having pA_2 values ranging from 7.5 to 8.0 at H_2R in isolated guinea pig ileum (gpH_2R), which were comparable to that of famotidine (pA_2 = 7.74), the highest affinity H_2R antagonist to be used clinically. Linkers consisting of 6-8 methylene groups were favourable although the effect of the linker length on binding was unclear as the NBD group may have had an effect on binding by interaction with an extra binding site[106].

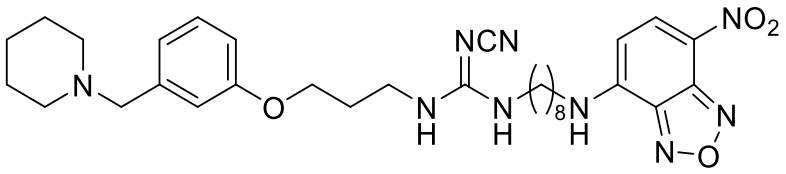

14 pA_2 (gpH_2R) = 7.96

Figure 1.10: The most potent H_2R fluorescent ligand containing the NBD fluorophore reported by Li et al.[106]

Malan et al. also reported 3-aminopotentidine derived H_2R fluorescent ligands and investigated the effects of linker type and length as well as the nature of the fluorophore on ligand binding[107]. They identified four compounds with different fluorophores (methylanthranilate, cyanoisoindole and cyanoindolizine), having pK_i>8 at rat H_2R (rH_2R). The ideal linker was identified as a cyanoguanidine with an ethylene moiety, such as those in **15** and **16** (Figure 1.11). It was also noted that BODIPY based fluorescent ligands despite having the best fluorescent properties among all reported fluorescent compounds, had a much lower binding affinity (pK_i = 6.32-6.90) for the H_2 receptor compared to **15** (pK_i = 8.84) and **16** (pK_i = 8.85).

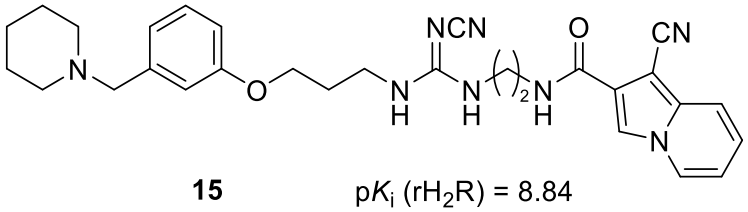

15 pK_i (rH_2R) = 8.84

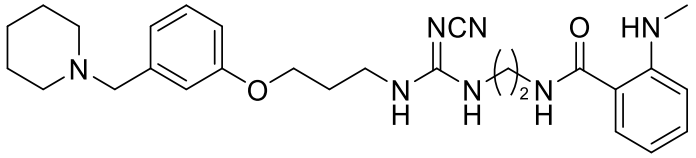

16 pK_i (rH_2R) = 8.85

Figure 1.11: Two fluorescent ligands with nanomolar affinities at H_2R.

Xie et al. attached bulky, commercially available fluorophores such as the cyanine dye S0536 and BODIPY 650/665-X to the same orthosteric ligand-linker congener as in Li et al. and Malan et al[108]. Instead of the expected reduction in binding affinity after the attachment of the S0536 fluorophore, the group observed a 200-fold and 40-fold increase in human (hH_2R) and guinea pig H_2R binding affinity respectively with compound **17** (Figure 1.12) relative to the congener (pK_B = 5.03 and 5.64 for human and guinea pig H_2R respectively). The case was similar for BODIPY containing ligands although the increase in binding affinity was to a lesser extent (pK_B = 6.19-6.59 and 6.72-6.82 for human and guinea pig H_2R respectively). It was suggested the negatively charged sulfate group in the cyanine dye moiety and a resonance stabilised cation had the potential to interact with positively and negatively charged amino acids within the *N*-terminal and/or extracellular loop regions of the H_2R, thus increasing ligand affinity of **17**. Compound **17** was a partial agonist at H_2R in both humans and guinea pigs[108].

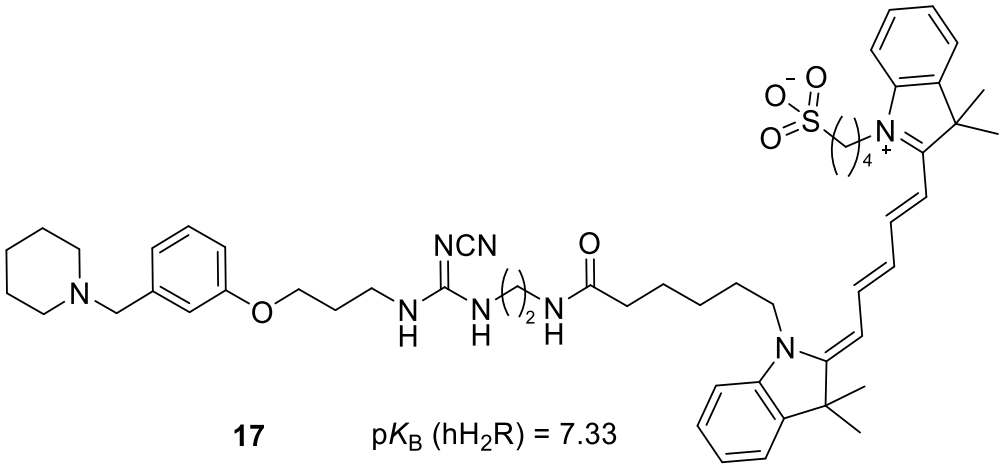

17 pK_B (hH_2R) = 7.33

Figure 1.12: H_2R fluorescent ligand partial agonist **17**.

1.3.2.3 H_3R

The H_3R has received a lot of attention over recent years due to its involvement in modulating neurotransmitter release in the brain. Modulating activity at this receptor could potentially be useful for the treatment of neurological disorders such as schizophrenia and Alzheimer's disease[109-111]. Amon et al. synthesised six H_3R fluorescent ligands based on a piperidine-containing orthosteric binding motif connected to several small fluorophores such as isoindole and NBD by linkers

comprising of 4 to 7 atoms[112]. Compound **18** and **19** (Figure 1.13) had the highest affinity for rat H_3R (rH_3R) across the series and both had a linker length of six atoms which subsequently led to conclusion that the optimum alkyl chain length between the piperidine nitrogen atom and the fluorophore was six atoms. The authors, however, did not investigate how a further increase in chain length would affect H_3R affinity.

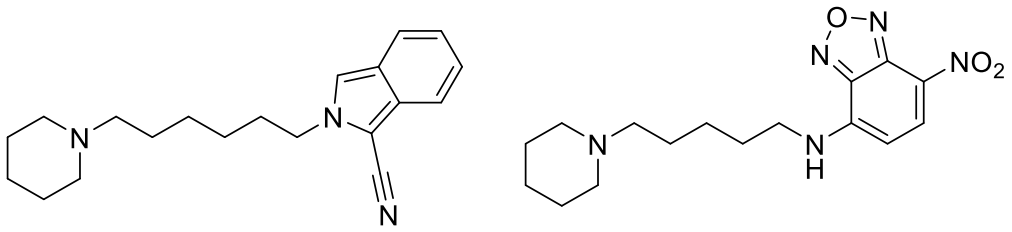

18 pK_i (rH_3R) = 7.51 **19** pK_i (rH_3R) = 7.96

Figure 1.13: H_3R fluorescent ligands containing a basic piperidine orthosteric ligand attached to fluorophores through a six-membered linker.

Cowart et al. synthesised eight H_3R fluorescent ligands by attaching various fluorophores (NBD, sulfobenzoxadiazole (SBD), dansyl, 5- and 6-tetramethyl-rhodamine (TAMRA)) to an orthosteric ligand derived from ABT-239 **20** in the presence and absence of a methylene linker[113]. All but two compounds exhibited pK_i <9 at human H_3R (hH_3R). Fluorescent compounds with the dansyl fluorophore had the lowest affinity (albeit still nanomolar) at hH_3R as compared to the other compounds. Fluorescent compounds containing NBD and SBD had higher binding affinities for hH_3R in the absence of the methylene linker, with compound **21** (Figure 1.14) being the most potent within the series (pK_i = 10). Surprisingly, the 5- and 6-TAMRA fluorescent compounds with a methylene linker (**22** and **23** respectively, Figure 1.14) had sub-nanomolar affinities despite expectations that the large and bulky TAMRA moiety would interfere with binding, especially when a short linker was used. TAMRA-containing analogues were found to have to best fluorescent properties among all the compounds made.

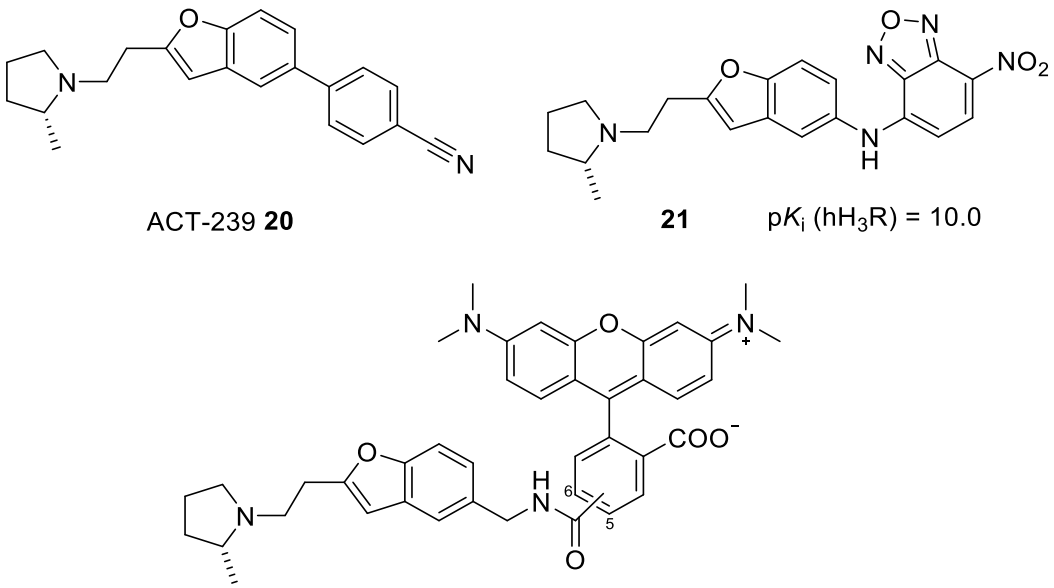

Figure 1.14: NBD and TAMRA based fluorescent ligands which were derived from ACT-239 **20** had sub-nanomolar affinities at hH_3R.

Amon et al. furthered their work and in a second paper reported a series of H_3R fluorescent ligands based on several fluorophores of different physicochemical properties in terms of their size and hydrogen bond donating/accepting capability[114]. The fluorophores were attached to the orthosteric ligand either directly or with a methylene spacer as a linker. All compounds exhibited high affinity for hH_3R (pK_i of 7.82-10.3). The two most potent compounds were **24** and **25** (Figure 1.15) which had the dinitrophenyl and NBD fluorophores respectively (pK_i values >10). Despite lacking a linker moiety, **24** and **25** retained high binding affinity for hH_3R. This suggested that having the fluorophore close to the orthosteric pocket did not interfere with the binding of H_3R fluorescent ligands at their target receptor. The authors subsequently reported that the direct attachment of fluorophores to the orthosteric ligand led to fluorescent ligands of higher potency compared to the incorporation of an additional methylene spacer, although the authors had reservations to this claim as the number of compounds studied were too small.

Kuder et al. investigated the potencies of cyclic isothiourea based fluorescent ligands and concluded that they did not bind to both H_3R and H_4R[115]. In the same paper, they reported compound **26** (Figure 1.15), a methylated analogue of **25** which displayed similar binding affinity for H_3R.

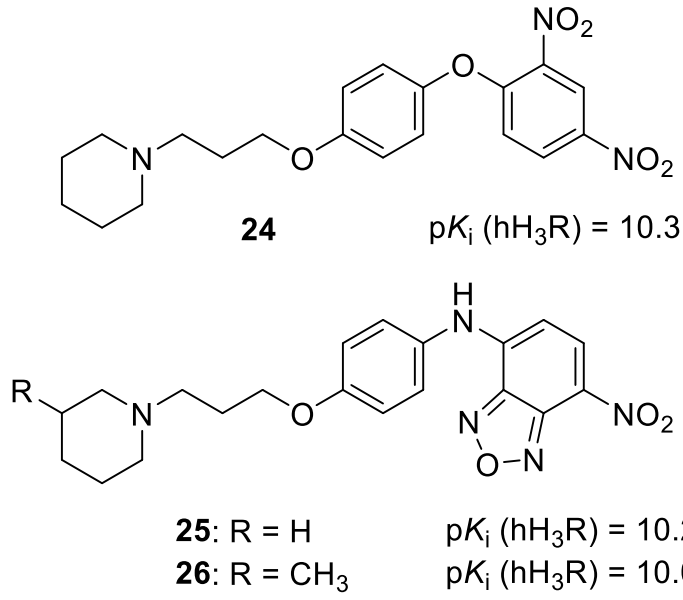

Figure 1.15: Piperidine-based fluorescent ligands with sub-nanomolar affinities at H_3R.

Tomasch et al. reported several chalcone-based fluorescent ligands for H_3R which all exhibited nanomolar affinities at hH_3R and were selective for hH_3R (~10-fold over H_1R and~100-fold over H_4R)[44]. Compound **27** (Figure 1.16) was the most hH_3R-selective fluorescent compound whereas **28** was the least selective. Compounds **28** and **29** were red shifted ($\lambda_{max,ex}/\lambda_{max,em}$ = ~468nm/~670nm) whereas the others including **27** were yellow shifted ($\lambda_{max,ex}/\lambda_{max,em}$ = ~405nm/~567nm). All chalcone compounds were able to bind to and visualise human H_3R in human embryonic kidney (HEK293T) cells using confocal microscopy. The absence of membrane fluorescence when incubated with HEK293T cells that did not transiently express hH_3R confirmed that the binding was specific to hH_3R.

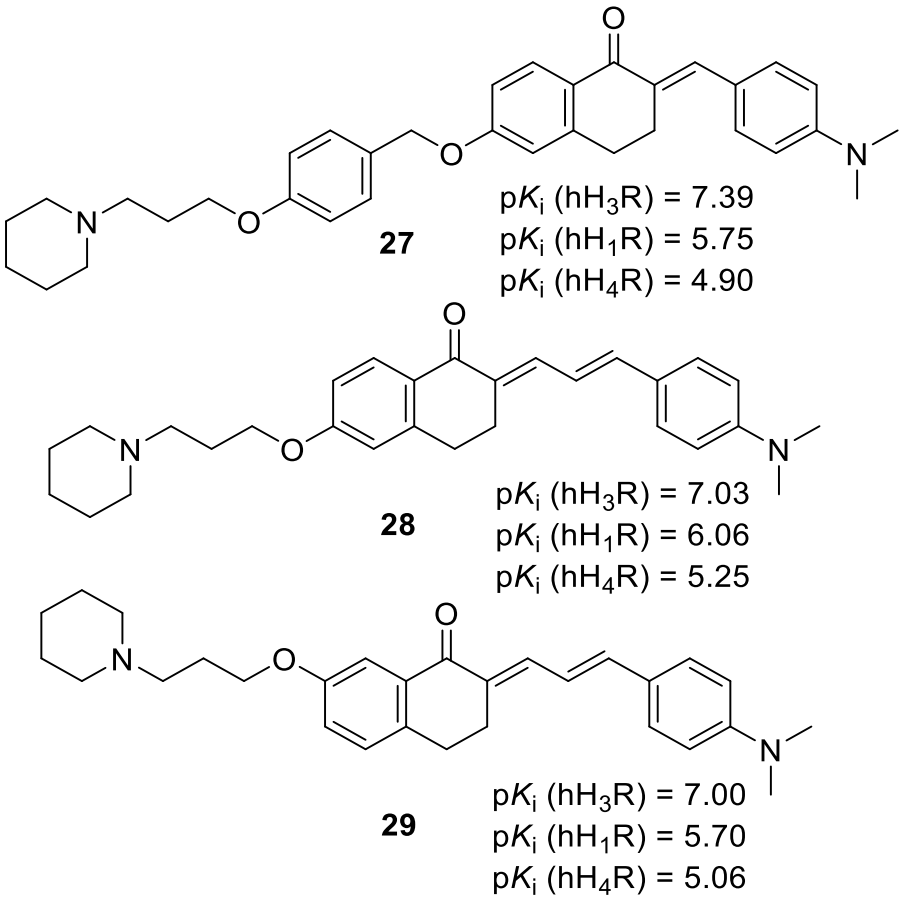

Figure 1.16: Red-shifted **27** ($\lambda_{max,ex}/\lambda_{max,em}$ = 468nm/670nm) and yellow-shifted **28** and **29** ($\lambda_{max,ex}/\lambda_{max,em}$ = ~405nm/~567nm) chalcone based H_3R fluorescent ligands.

Tomasch et al. published a second paper in the same year, this time their approach was to build the BODIPY fluorophore into the structural scaffold[45]. Compound **30** (Figure 1.17), which they named Bodilisant, displayed nanomolar affinity for hH_3R, was ten times more potent than the chalcone fluorescent ligands reported earlier and significantly more selective for hH_3R over hH_1R and hH_4R as well as human dopamine D_1, D_2, D_3 and D_5 receptors. The green-shifted Bodilisant ($\lambda_{max,ex}/\lambda_{max,em}$ = 468nm/494nm and 563nm) had good fluorescent properties in terms of quantum shift and the stability of luminescence. Visualisation of hH_3R in HEK293T cells and in native human brain tissues were successfully achieved using confocal microscopy, suggesting that **30** could potentially be a useful tool for receptor imaging.

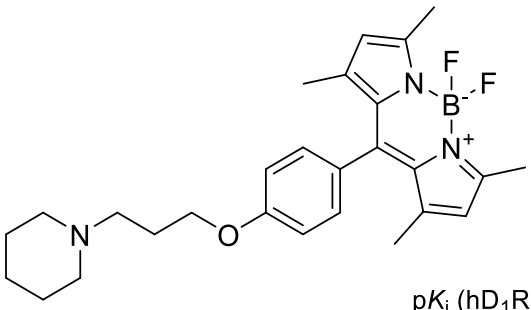

30

pK_i (hH_3R) = 8.19
pK_i (hH_1R) = 5.78
pK_i (hH_4R) = 5.12

pK_i (hD_1R) = 4.90
pK_i (hD_2R) = 5.71
pK_i (hD_3R) = 5.83
pK_i (hD_5R) = 5.28

Figure 1.17: BODIPY bearing H_3R fluorescent ligand with good H_3R affinity and selectivity.

1.3.2.4 H_4R

As the most recent histamine receptor subtype to be discovered there is a need to improve our understanding of H_4R pharmacology and its involvement in immunomodulation. Currently, there are only two reported fluorescent ligands for H_4R, both of which are commercially available and not H_4R selective. BODIPY FL histamine **31** (Figure 1.18) is available from Setareh Biotech (Eugene, OR) but the pharmacological profile of this compound is not provided by the manufacturer. Despite this, Mirhahosseini et al. reported a pK_D of 5.68 measured by flow cytometry for this compound at human H_4R (hH_4R), whereas Mocking et al. reported that **31** did not bind to hH_4R at concentrations of up to 10µM in a NanoBRET saturation binding assay[72, 116]. These results suggest that BODIPY FL Histamine has limited use in studying H_4R pharmacology due to its low binding affinity for the receptor.

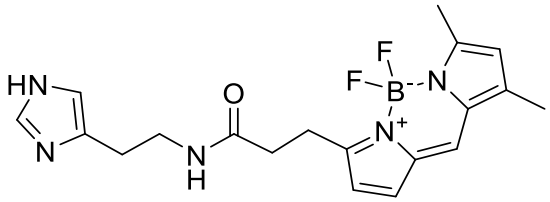

31

pK_D (flow cytometry at hH_4R) = 5.68
pK_D (NanoBRET at hH_3R) = 6.37
pK_D (NanoBRET at hH_4R) < 5

Figure 1.18: BODIPY FL-tagged histamine.

Clobenpropit-based red-shifted fluorescent ligand (Clo-BDY) could be purchased from HelloBio (Bristol, UK) and apparent pK_D values determined from SPAP assay for H_3R, H_1R and H_2R were reported to be 7.09, 6.55 and 5.71 for respectively. Mocking et al. reported pK_D values of 7.89 and 7.15 at H_3R and H_4R respectively for Clo-BDY using NanoBRET saturation binding assay[72]. The structure of this fluorescent ligand was not disclosed by the manufacturer.

1.4 Research Aim

The crystal structure of the human H_1R (PDB code: 3RZE) in complex with doxepin was solved in 2011 (Figure 1.19a), providing useful information about the orthosteric ligand binding site[4]. The main binding pocket was defined by transmembrane regions (TM) 3, -5 and -6 with interactions between doxepin and the binding pocket mediated by an ionic interaction between $D107^{3.32}$ (Ballesteros-Weinstein numbering system) in TM3 and the protonated tertiary amine, as well as aromatic residues $F424^{6.44}$, $W428^{6.48}$ and $F432^{6.52}$ in TMs 5 and 6 with the aromatic moieties of the drug (Figure 1.19b). The X-ray crystal structure also revealed a feature novel to H_1R: a phosphate anion interacting with four residues $Y431^{6.51}$, $K179^{ECL2}$, $K191^{5.39}$ and $H450^{7.35}$ located at the entrance of the binding pocket (Figure 1.19c). It was proposed that this binding site played a role in interacting with the carboxylic acid group present in 2nd generation zwitterionic antihistamines[4].

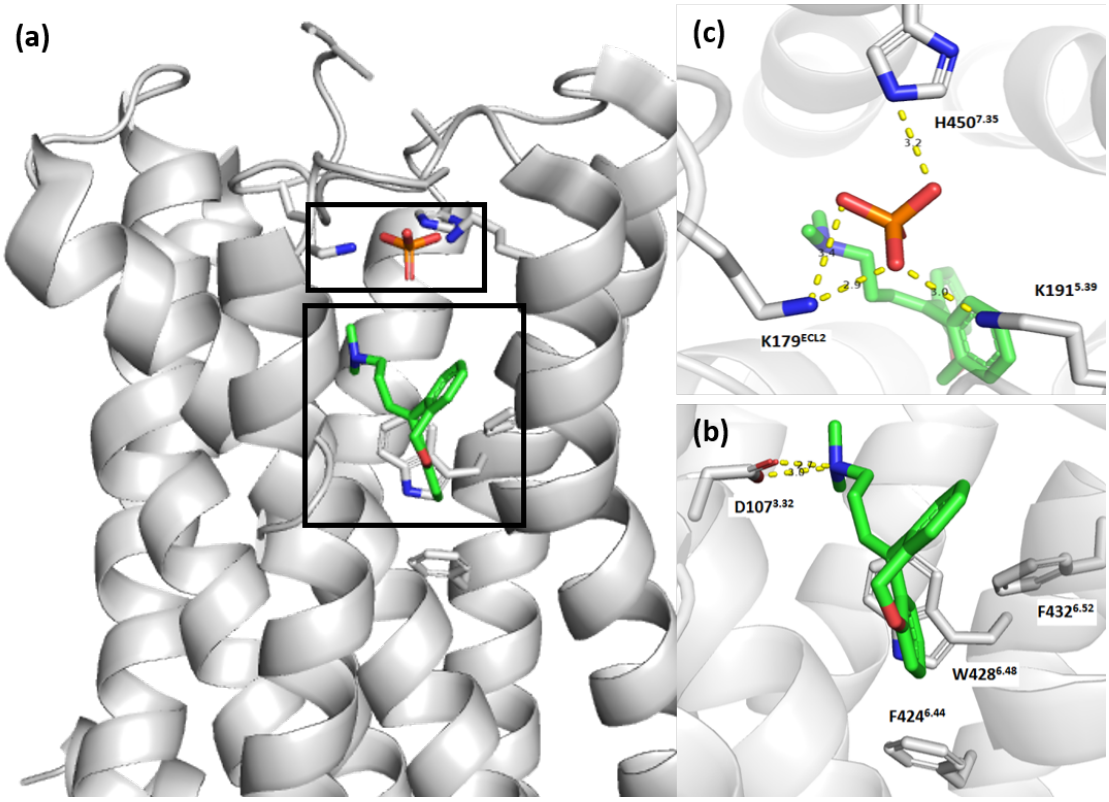

Figure 1.19: (a) Human H_1R crystal structure in complex with doxepin. PDB code: 3RZE. (b) Interaction of doxepin (green) within the H_1R binding pocket formed by D107$^{3.32}$, F424$^{6.44}$, W428$^{6.48}$ and F432$^{6.52}$. (c) Interaction of a phosphate anion (orange) with Y431$^{6.51}$, K179^{ECL2}, K191$^{5.39}$ and H450$^{7.35}$ within the H_1R.

Compound **13**, a peptide linker-based H_1R fluorescent ligand has proven itself to be a useful pharmacological and cell imaging tool[3]. However, the peptide linker of **13** which consists of three alanines is clearly not optimised for H_1R. This creates an opportunity for the synthesis of high affinity H_1R fluorescent ligands with the optimisation of the peptide linker. High affinity fluorescent ligands which selectively bind to their target receptor are highly desirable for in vitro pharmacological studies of wildtype normal and diseased cells. These cells express a wide array of proteins on their surface compared to artificially engineered cell lines which could act as off-site targets for fluorescent ligands if they do not have a high selectivity for their targeted receptor. As quantification of fluorescent ligand selectivity against all potential cell surface proteins is practically impossible, increasing the binding affinity of a fluorescent ligand for its targeted receptor would allow the study of GPCR

pharmacology (i.e. H_1R) in wildtype and diseased cells, as well as in vivo models, to be conducted at the lowest possible ligand concentration, thus reducing off-site binding.

The aim of this research programme was to synthesise high affinity peptide linker-based H_1R fluorescent ligands by optimising fluorescent ligand-receptor interaction along the ligand entry/exit route. This could be achieved by introducing chemical functionalities within the linker moiety which could potentially interact with $Y431^{6.51}$, $K179^{ECL2}$, $K191^{5.39}$ and $H450^{7.35}$ lining the receptor ligand entry/exit route as well as to probe for interactions with other residues along this route. In this project, a similar approach towards the synthesis of compound **13** will be undertaken whereby peptide linkers are incorporated into fluorescent ligands using solid phase peptide synthesis (SPPS). The use of peptides as linkers within fluorescent ligands was utilised by Vernall et al.[47] and was successful in converting a non-selective adenosine receptor antagonist into high affinity adenosine A_3-selective fluorescent ligands through optimisation of the peptide linker which imbued greater affinity and selectivity for the adenosine A_3 subtype. It is hoped that by adopting this strategy, the synthesis of high affinity H_1R selective fluorescent ligands could be achieved.

CHAPTER 2: OPTIMISATION OF THE PEPTIDE LINKER WITHIN THE H_1R FLUORESCENT LIGAND

The overall aim of this programme of research was to further extrapolate our initial investigations[3] by more systematically assessing how the nature of the linker could influence the ultimate pharmacology of a series of histamine receptor fluorescent probes. To this end, molecular modelling initially suggested that simply placing an acidic amino acid (*e.g.* aspartic acid) within the peptide linker could potentially engage in salt bridge interactions with basic side-chain residues as detailed in section 1.4. This hypothesis did not generate a useable fluorescent ligand and this disappointing result led to an alternative and more detailed screening approach to try and identify the ideal peptide linker in a non-fluorescent congener in the first instance. The information obtained from this series of compounds helped identify the most potent congeners which could then be used in the synthesis of the new generation fluorescent ligands.

2.1 First Generation Fluorescent Ligand

The first-generation fluorescent ligand was synthesised to test a hypothesis derived from molecular modelling whereby the basic residues $K179^{ECL2}$, $K191^{5.39}$ and $H450^{7.35}$ within the ligand entry route could be engaged in salt bridge interactions by incorporating an acidic peptide linker within the fluorescent ligand.

2.1.1 Approach and Ligand Design

With prior knowledge regarding the existence of a group of targetable residues along the H_1R ligand entry/exit route (highlighted in section 1.4, depicted in Figure 2.1), we envisaged the generation of high affinity H_1R fluorescent ligands by engaging these mostly basic residues through an acidic functionality within the peptide linker. An initial molecular docking study conducted by Dr. Chris de Graaf using Protein-Ligand ANT System (PLANTS)[3, 117] as described in Stoddart et al. suggested that an Ala-Asp-Gly linker (Figure 2.2) between the VUF13816 ligand (blue in Figure 2.2) and the amino acid handle for fluorophore attachment within the linker would allow for the

exploitation of K179^{ECL2} and K191$^{5.39}$, possibly through salt bridge interaction with acidic aspartate within the linker (Figure 2.1)[3]. The Asp side group within the linker of **32** was modelled to exist as the carboxylic acid form which in physiological pH should exist as the carboxylate form and the rationale behind this was not clear. This in turn could underestimate the predicted free energy of binding during the docking study as the possibility of a salt bridge interaction between the acidic Asp side group and the basic residues would be neglected. However, it was not possible to exclude the existence of microenvironments within the receptor in which the carboxylic acid form could have existed. Nevertheless, the results from the docking study provided the valuable information that it would be possible to incorporate an acidic side group within the linker to be in close proximity to the basic residues.

Despite its usefulness in devising the initial hypothesis of the project, it is important to acknowledge that the molecular docking study performed has fundamentally crucial limitations. A static receptor conformation was assumed and adopted, which in contrast in the actual scenario the receptor does not adopt a fixed conformation. The H_1R crystal structure used in this study was based on the orthosteric binder doxepin which provide high confidence on the receptor conformation limited to the orthosteric binding pocket but not regions further away from it. Lastly, the molecular docking study was also likely performed *in vacuo* without considering the water energies surrounding the ligand-receptor interaction although this was not confirmed with the collaborator.

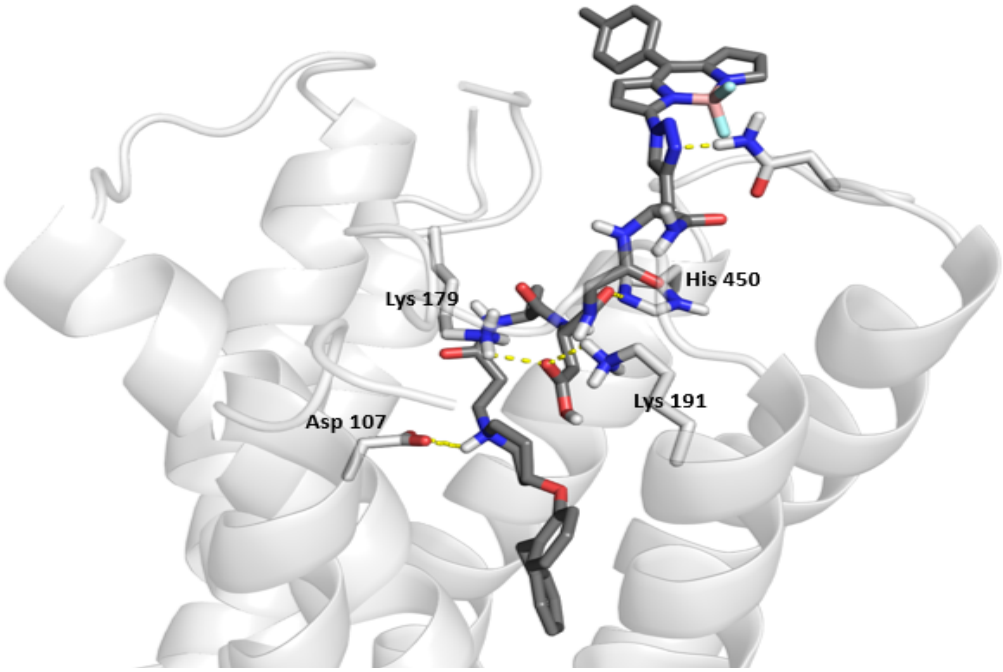

Figure 2.1: H_1R model constructed from the H_1R crystal structure (PDB code: 3RZE) and molecular docking of **32** using PLANTS suggested that an Asp residue within the peptide linker, when placed one amino acid away from the VUF13816 ligand could interact with both $K179^{ECL2}$ and $K191^{5.39}$.

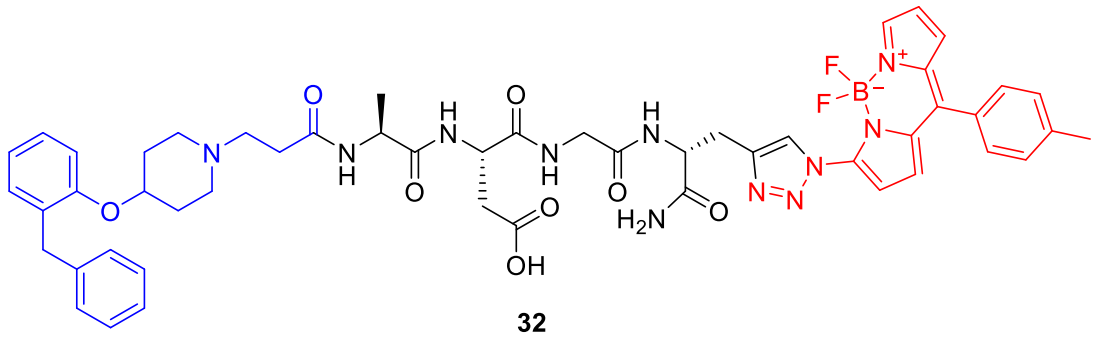

32

Figure 2.2. The chemical structure of the proposed fluorescent ligand with an acidic peptide linker **32**.

Fluorescent probes for GPCRs are conventionally synthesised by attaching an amine-reactive (N-hydroxysuccinimide ester or carboxylic acid) fluorophore to an amine-functionalised congener through amide coupling. This approach, however, limits the chemical functionality that could be incorporated within the congener as introducing nucleophiles within the congener would result in multiple reaction sites which could potentially lead to side reactions. As such, the incorporation of a carboxylic acid

within the amine-containing congener would pose a problem during fluorophore attachment as the congeners could potentially couple to one another under the coupling conditions used to attach the fluorophore. Given that the BODIPY fluorophore is unstable in acidic and basic conditions[118], many protecting group strategies for the carboxylic acid would not be possible as this would require base treatment to liberate the free acid and would potentially degrade the fluorophore of the final product. Therefore, an alternative approach towards fluorophore coupling was employed. In 2014, Chauhan et al. reported an attractive way of making red-shifted BODIPY based fluorescent molecules from cheap starting materials using click chemistry[119]. An azido-functionalised BODIPY fluorophore was reacted with a range of arene-substituted alkynes through copper-catalysed alkyne-azide cycloaddition (CuAAC) to give triazoles, effectively extending the conjugation of the fluorophore and enhancing its fluorescent properties. The exclusivity of the alkyne-azide reaction in CuAAC would allow various electrophilic/nucleophilic groups to be incorporated within the peptide linker without concerns for side reactions and hence was chosen to be the preferred approach for fluorophore coupling in the synthesis of the first-generation fluorescent ligand.

Accordingly, inspired by the work of Chauhan et al., compound **32** was designed with CuAAC as the approach towards fluorophore coupling. The retrosynthesis of **32** is shown in Figure 2.3 and described in four parts: the synthesis of the orthosteric binding motif (**blue**), the peptide congener, the azido functionalised BODIPY (**red**) and the final fluorophore coupling using CuAAC. The alkyne functional group was incorporated into the peptide linker through *D*-propargylglycine, which upon CuAAC led to the transformation into a triazole moiety, could form hydrogen bond interactions with an asparagine residue located at the extracellular vestibule of the receptor as suggested in the molecular docking results (Figure 2.1).

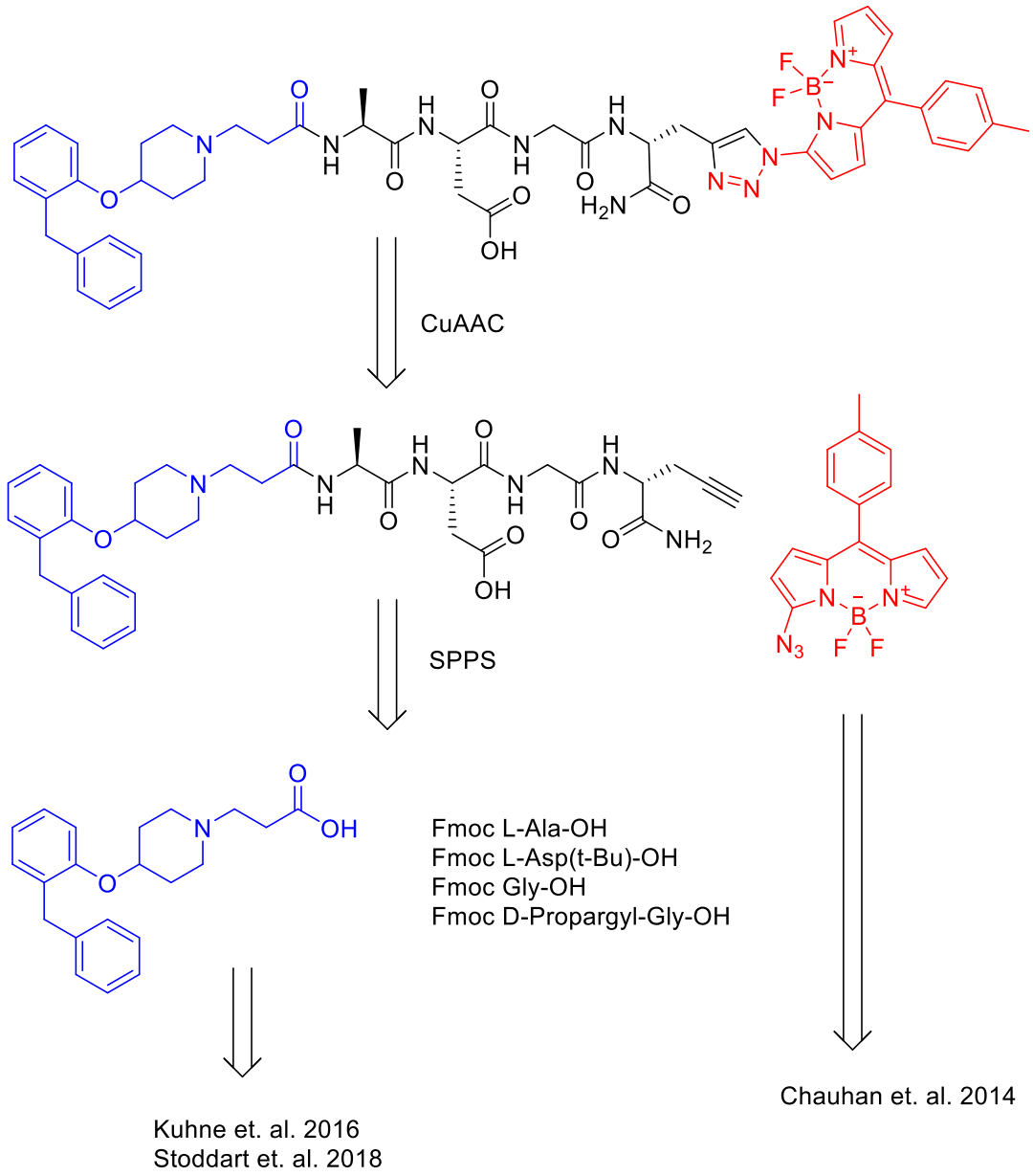

Figure 2.3: The retrosynthesis of **32**.

2.1.2 Click Chemistry

The term 'click chemistry' was first coined in 2001 by Kolb et al.; used to describe reactions that are 'modular, wide in scope, give very high yields, generate only inoffensive by-products that can be removed by nonchromatographic methods, stereospecific, simple reaction conditions, readily available starting materials and simple product isolation'[120-121]. These reactions include cycloadditions and nucleophilic opening of rings such as epoxides and aziridines.

2.1.2.1 Huisgen 1,3-dipolar Cycloaddition

The Huisgen 1,3-dipolar cycloaddition is discovered by Rolf Huisgen and involves the reaction between dipoles (e.g. azides, nitrile imines and nitrile oxides) and dipolarophiles (e.g. alkynes and nitriles) to form five-membered heterocycles which may be aromatic depending on the dipole-dipolarophile pair[122]. One dipole-dipolarophile pair that gained importance in the field of click chemistry is the azide-alkyne combination, which affords an aromatic 1,2,3-triazole.

The original Huisgen reaction was conducted at elevated temperatures in the absence of a catalyst and lacks regioselectivity as it gave rise to a mixture of 1,4- and 1,5-regioisomers. Selectivity for particular regioisomers could be achieved by adding different metal catalysts to the reaction, with a copper catalyst yielding the 1,4-regioisomer and ruthenium catalyst giving the 1,5-regioisomer[123-124] (Figure 2.2).

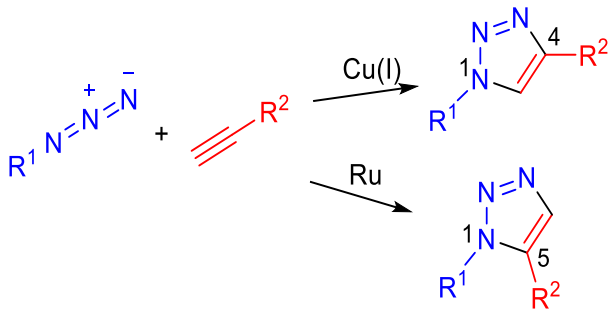

Figure 2.4: Regioselectivity achievable via the use of Copper(I) or Ruthenium catalyst in the dipolar cycloaddition between an azide and an alkyne to give the 1,4-regioisomer and the 1,5-regioisomer respectively.

2.1.2.2 CuAAC

CuAAC is usually carried out at ambient temperature in a polar solvent and the Cu(I) catalyst can be acquired commercially as CuBr, CuI or generated in-situ from Cu(II) salts such as $CuSO_4$ using a mild reducing agent such as sodium ascorbate. Alternative catalyst systems involving the use of various ligands, nitrogen bases, copper complexes and self-assembled polymer-supported solid phase copper catalyst have also reported in recent years[125-128]. Apart from achieving regioselectivity for 1,4-substituted triazoles, the ease of introducing the azide and alkyne functional groups into molecules, their stability against common nucleophiles and electrophiles, the

efficiency of the reaction, high rate acceleration and tolerance to aqueous and oxic conditions of CuAAC are some of the advantages of this reaction[123-124]. The current accepted reaction mechanism for CuAAC involves two copper atoms and is depicted in Figure 2.5[129].

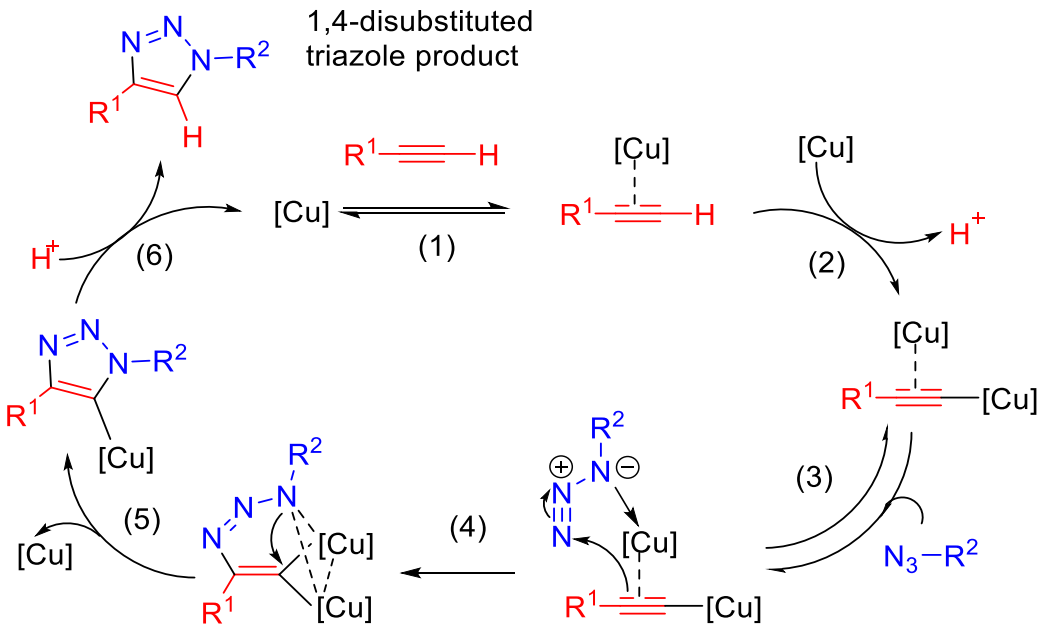

Figure 2.5: Proposed CuAAC mechanism involving two Cu(I) species[129]. The reaction proceeds with the π-complexation of a Cu(I) species to the alkyne functional group **(1)** followed by the coordination of a second Cu(I) species to the alkyne, resulting in the formation of a copper(I) acetylide **(2)**. The π-bound copper atom allows the reversible coordination of an organic azide **(3)** and the subsequent nucleophilic attack at the distal nitrogen atom by the β-carbon of the acetylide **(4)**. Ring closure results in the ejection of one Cu(I) species and the formation of the 5-membered triazolyl-copper derivative **(5)**. Lastly, protonation of the copper derivative gives the 1,4-disubstituted triazole product **(6)** and the restoration of the copper catalyst to complete the catalytic cycle.

The use of CuAAC in biology was initially limited due to copper-associated cytotoxicity but with the discovery of copper-free azide-alkyne cycloaddition and biocompatible copper(I) catalytic systems involving the use of chelating ligands such as 2-(4-((bis((1-(*tert*-butyl)-1*H*-1,2,3-triazol-4-yl)methyl)amino)methyl)-1*H*-1,2,3-triazol-1-yl)acetic acid (BTTAA), 3-(4-((bis((1-(*tert*-butyl)-1*H*-1,2,3-triazol-4-yl)methyl)amino)methyl)-

1*H*-1,2,3-triazol-1-yl)propane-1-sulfonic acid (BTTES) and 3-(4-((bis(1-*tert*-butyl-1*H*-1,2,3-triazol-4-yl)methyl)amino)methyl)-1*H*-1,2,3-triazol-1-yl)-propanol hydrogen sulfate (BTTPS), CuAAC gained prominence in recent years for a wide range of applications in biology, materials and polymer science[123-124, 130-134].

2.1.3 Synthesis

The synthesis of **32** was divided into three parts, namely the synthesis of the orthosteric binding motif and peptide congener, the synthesis of the fluorophore and the final fluorophore coupling through CuAAC.

2.1.3.1 Synthesis of the VUF13816-based orthosteric binding motif

The orthosteric binding motif was synthesised based on the methodology reported by Kuhne et al. and its synthesis route is highlighted in Scheme 2.1[105]. The synthesis began with a Mitsunobu reaction between *N*-Boc-4-hydroxypiperidine and 2-benzylphenol to give the desired product **33** with a comparable yield. Mitsunobu reaction, first reported in 1967 is a dehydration reaction involving a primary or secondary alcohol to a pronucleophile such as a carboxylic acid, phenol or sulphonamide, mediated by dialkyl (e.g. ethyl or isopropyl) azodicarboxylate (DEAD or DIAD) and a trialkyl- or triarylphosphine (e.g. triphenylphosphine)[135-136]. It is conducted at mild, ambient conditions and in various standard reaction solvents[136]. DIAD is usually preferred to DEAD due to toxicity and risk of explosion associated with the latter[137].

The Mitsunobu reaction did not yield the pure product despite silica column purification as the elimination by-product, *tert*-butyl 3,6-dihydropyridine-1(2*H*)-carboxylate had similar retention times, resulting in co-elution. The identity of the side product was confirmed by liquid chromatography-mass spectrometry (LCMS) indicated a $(M+H)^+$ of 184.1 (calculated *M*r value of 184.13) with t_R of 2.88 min and ^{1}H NMR peaks at 5.81ppm and 5.67ppm which corresponded to -C**H**=C**H**-, confirming its presence. The molar ratio of **33** to 1-Boc-2,3,6-trihydropyridine was 1:0.274 as determined by ^{1}H NMR. This however was not a concern for the subsequent reaction step as both **33** and the by-product was subjected to *N*-Boc deprotection in TFA/DCM to give **34** and 1,2,3,6-tetrahydropyridine (b.p. of 108°C) (Scheme 2.1), of which the

latter was removed under rotary evaporation alongside TFA, affording pure **34** confirmed by NMR spectroscopy. Compound **34** was then subjected to a Michael addition reaction with methyl acrylate to afford ester **35**, which following saponification in the presence of NaOH and subsequent acidification afforded carboxylic acid **36**.

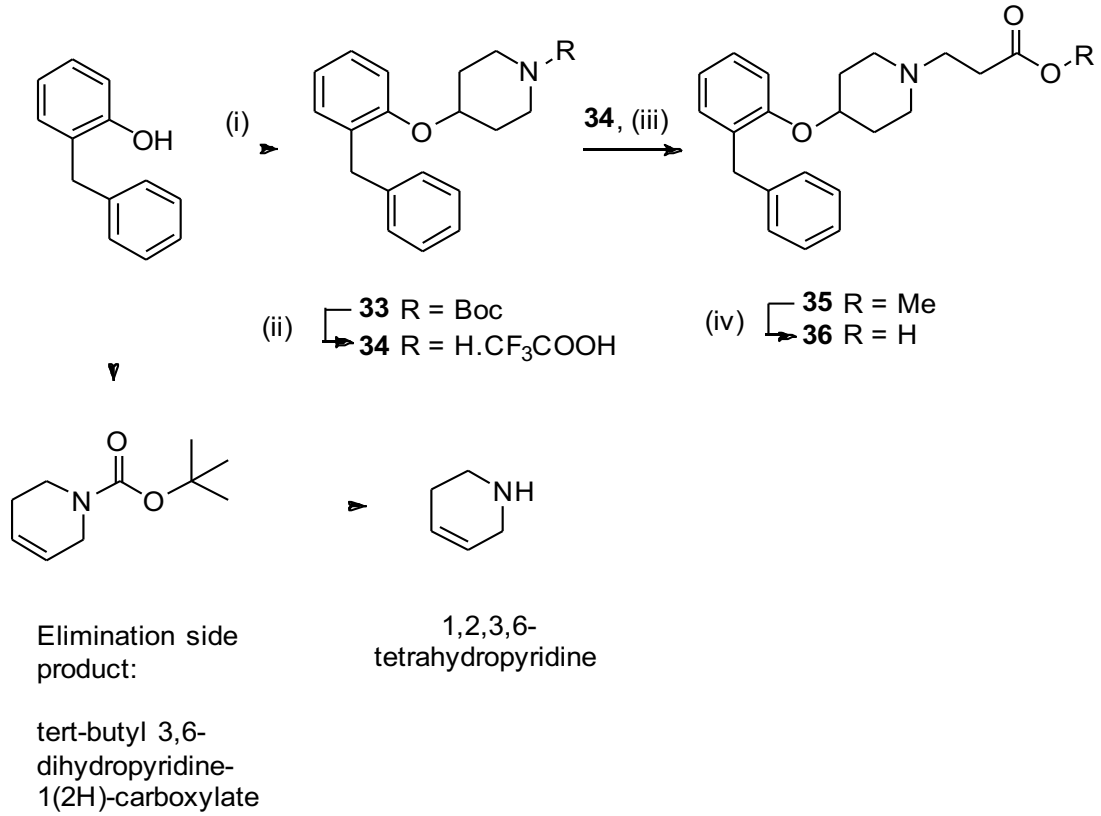

Scheme 2.1: Synthesis of 3-(4-(2-benzylphenoxy)piperidin-1-yl)propanoic acid from 2-benzylphenol. (i) 1-Boc-4-hydroxypiperidine, 2-benzylphenol, PPh_3, DIAD, dry THF, RT, 20hr, 42%. (ii) TFA, DCM, RT, 17hr, 93%. (iii) Methyl acrylate, dichloroethane (DCE), 70^oC, 4 hr, 66%. (iv) NaOH, H_2O/THF, 0^oC, 5 hr, 74%.

2.1.3.2 Synthesis of the peptide congener

The peptide congener was synthesised using standard Fluorenylmethyloxycarbonyl (Fmoc) SPPS protocol on a rink amide resin (Sigma Aldrich 533935)[138]. Fmoc SPPS employs an orthogonal protecting group strategy, utilising the base-labile Fmoc protecting group on the α-amino functionality and acid-labile side chain protecting groups and resin-linkages. This allows the selective removal of the Fmoc amino-protecting group when building the polypeptide chain under basic conditions, usually 20% piperidine in DMF. The acid treatment of 90-95% TFA in water at the end of the polypeptide assembly would remove all side chain protecting groups and liberate the synthesised polypeptide chain from the resin[138]. Fmoc SPPS reaction condition is also considerably milder and safer as compared to the other commonly utilised Boc SPPS which involves the use of hydrogen fluoride for the hydrolytic cleavage of the peptide chain from the resin[138]. Rink amide resin was chosen as upon resin cleavage liberates the *C*-terminus of the peptide congener as the corresponding non-amine reactive carboxamide. 2-(1*H*-benzotriazol-1-yl)-1,1,3,3-tetramethyluroniumhexafluoro-phosphate (HBTU)/hydroxybenzotriazole (HOBt) were chosen as the coupling reagents as they have been reported to activate carboxylates extremely quickly and generally work well for most amino acid coupling reactions as well as reducing racemisation[138]. Large excesses of reagents (up to 4 molar equivalents) in two coupling cycles were used for each of the amino acid additions to push reactions towards completion. Lower equivalencies were employed with Fmoc-*D*-2-propargylglycine and the orthosteric binding motif due to cost considerations. The deprotection step was carried out three times to ensure complete removal of the *N*-Fmoc protecting group. The crude product obtained after work-up was purified by HPLC to give **37** at an overall yield of 17% calculated based on a resin loading of 1.0 mmol/g N loading reported by the manufacturer since the actual resin loading was not experimentally determined. As such, the reported yield would have likely be an underestimate given that the assumed resin loading would not likely be achieved. This applies to all SPPS procedures reported in this thesis. Analytical high-performance liquid chromatography (HPLC) and high-resolution mass spectrometry (HRMS) were used to characterise the purity and confirm the identity of the product.

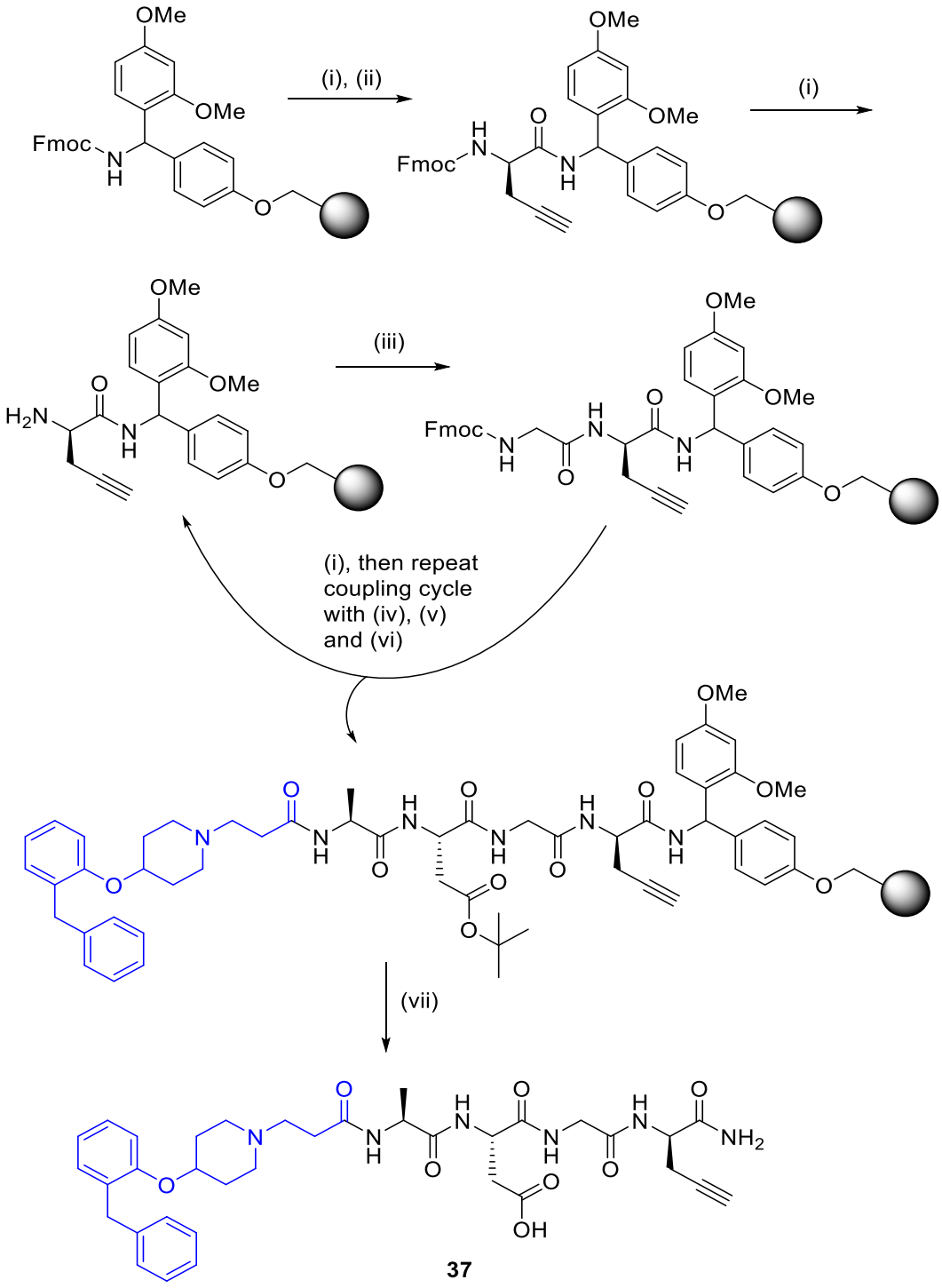

37

Scheme 2.2: Synthesis of Peptide Congener. (i) 20% piperidine/DMF, RT, 5 min. (ii) Fmoc-D-propargylglycine, HBTU, HOBt, DIPEA, DMF, RT, 4 hr. (iii) Fmoc-glycine, HBTU, HOBt, DIPEA, DMF, RT, 4 hr. (iv) Fmoc-L-aspartic acid 4-*tert*-butyl ester, HBTU, HOBt, DIPEA, DMF, RT, 4 hr. (v) Fmoc-L-Alanine, HBTU, HOBt, DIPEA, DMF, RT, 4 hr. (vi) **36**, HBTU, HOBt, DIPEA, DMF, RT, 4 hr. (vii) 95% TFA in water, RT, 6 hr, 17% over seven steps.

2.1.3.3 Synthesis of the azido functionalised BODIPY fluorophore

The fluorophore was synthesised based on experimental procedures reported by Alnoman et al. and Chauhan et al. and is summarised in Scheme 2.3[119, 139]. The first step involved the electrophilic addition of pyrrole to *para*-tolualdehyde, affording meso-(*p*-tolyl)dipyrromethane **38**. The product was dissolved in DMSO-d_6 for NMR spectroscopy as the slightly acidic nature of deuterated chloroform was enough to cause degradation through possibly the polymerisation of **38** involving the pyrrole substituents to give a black solid. Compound **38** was subsequently brominated using *N*-bromosuccinimide (NBS) in dry conditions at -78°C, oxidised by 2,3-dichloro-5,6-dicyano-1,4-benzoquinone (DDQ) and purified using column chromatography to give the monobromo-dipyrromethene **39** with a 29% yield. Double bromination at position 2 in each of the pyrrole rings was observed despite modifications to experimental protocol to reduce the local concentration of NBS (e.g. adding it in a large solvent volume over a long period of time) being made. As the reaction was conducted using 1 molar equivalent of NBS, the consumption of NBS towards the formation of the dibromo-substituted by-product led to the depletion of the bromine source and thus a low-yielding reaction. It was also discovered that the reaction mixture must be purified on the same day as by-products such as succinimide (pK_a = 9.5 determined from Chemdraw 16) and the reduced DDQ 4,5-dichloro-3,6-dihydroxyphthalonitrile (pK_a = 3.7) within the same reaction mixture were acidic, which could have led to the degradation of the product (Figure 2.6).

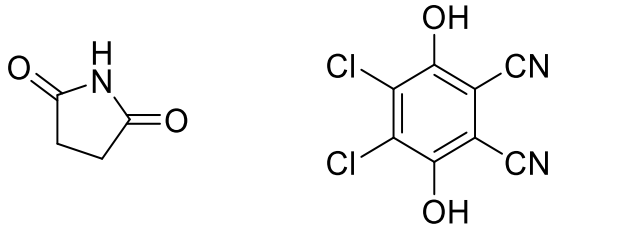

Succinimide

4,5-dichloro-3,6-dihydroxyphthalonitrile

Figure 2.6: The succinimide and 4,5-dichloro-3,6-dihydroxyphthalonitrile by-products were acidic, leading to degradation of **39**.

Compound **39** was then converted into the BODIPY **40** by reacting it with excess $BF_3{\cdot}Et_2O$ in the presence of Et_3N as the base and was purified using column chromatography. Finally, **40** was reacted with sodium azide in 1:1 acetone: water to give pure azido-substituted **41** after work-up, which was used for the subsequent CuAAC reaction without further purification. All intermediates and the final BODIPY **41** were stored at 0°C and protected from light.

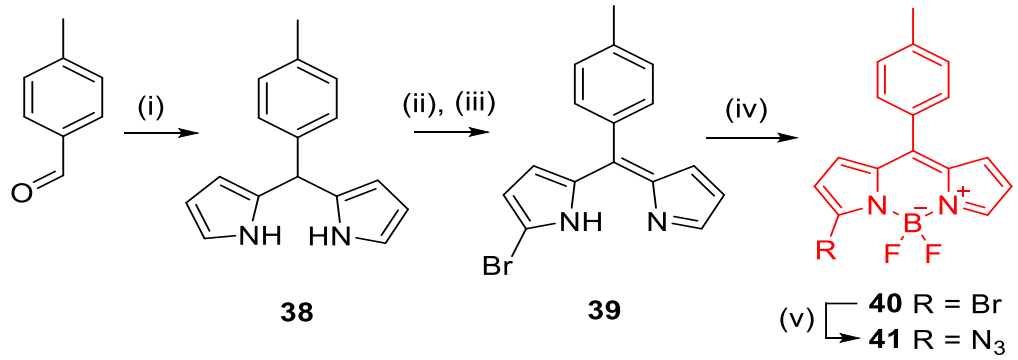

Scheme 2.3: Synthesis of azide substituted BODIPY fluorophore. (i) Pyrrole, $BF_3{\cdot}Et_2O$, RT, 1 hr, 38%. (ii) NBS, dry THF, -78°C, N_2 atm, 3 hr. (iii) DDQ, dry THF, RT, 1 hr, 29%. (iv) $BF_3{\cdot}Et_2O$, Et_3N, DCM, RT, 24 hr, 66%. (v) NaN_3, acetone/water, RT, 24 hr, 90%.

2.1.3.4 Fluorophore coupling using CuAAC

The last step of the synthesis involved the coupling of the fluorophore **41** to the congener **37** by CuAAC to give the final fluorescent compound **32**. The Cu(I) catalyst for CuAAC was generated *in-situ* by dissolving $CuSO_4$ and sodium ascorbate in a 1:3 ratio in water, mixed and stirred with **37** and **41** dissolved in DMF at RT. An excess of the reducing agent was required to prevent Glaser coupling which involves the self-coupling of the acetylene as a side reaction which occurs in oxidative conditions. The reaction did not take place and gradually adding more catalyst was not useful. Black suspending particles were present in the reaction mixture, suggesting that copper(II) oxide was present in significant amounts and that copper(I) ions might not have formed or did not persist long enough before re-oxidisation for reaction catalysis to occur. Addition of tris(benzyltriazolylmethyl)amine (TBTA) which could coordinate and stabilise Cu(I) ions did not solve the problem[140]. Modifications to the reaction conditions were made by changing the water-DMF solvent system to DMSO with

sonication to encourage dissolution of the catalyst system and the addition of 2,6-lutidine, a Lewis base adduct capable of stabilising the Cu(I) ions which was also reported to improve the reaction yield of CuAAC[124, 140,141]. The reaction was successful as the product was observed on the LCMS and HPLC purification yielded the pure desired product **32**. The purity and identity of compound **32** were confirmed with analytical HPLC and HRMS respectively.

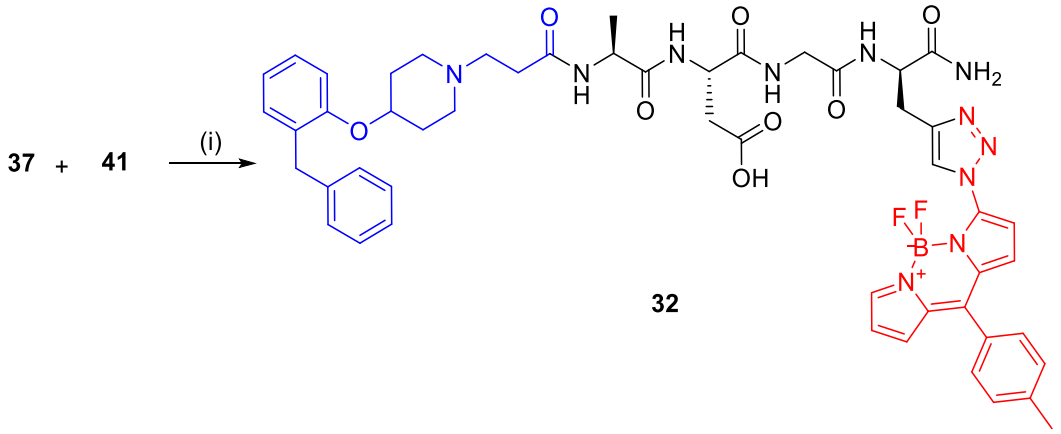

Scheme 2.4: Coupling of peptide congener to the fluorophore. (i) $CuSO_4$, sodium ascorbate, 2,6-lutidine, DMSO, RT, 7 days, 45%.

2.1.4 Fluorescence Spectroscopy and Pharmacology

The absorption/emission spectral profile of **32** in 10% DMSO/Hank's Balanced Salt Solution (HBSS) was determined using FlexStation and its binding affinity along with its corresponding congener **37** were determined through NanoBRET saturation and competition assays respectively.

2.1.4.1 Absorption/Emission Spectral Characterisation

The $\lambda_{max,ex}/\lambda_{max,em}$ of **32** was determined to be 521/536nm (see Appendix for spectra). This suggested that the conjugation of the fluorophore was not extensive enough to shift emission spectrum towards the red region ($\lambda_{max,em}$ > 600nm). Upon revisiting the literature, it was noticed that an arene moiety was unintentionally left out during the design of the final fluorescent compound (Figure 2.7)[119]. Subsequently, **32** was pharmacologically characterised using NanoBRET saturation assay with a suitable light detection filter module on the PheraStar FS plate reader (BMG Labtech, Aylesbury, UK).

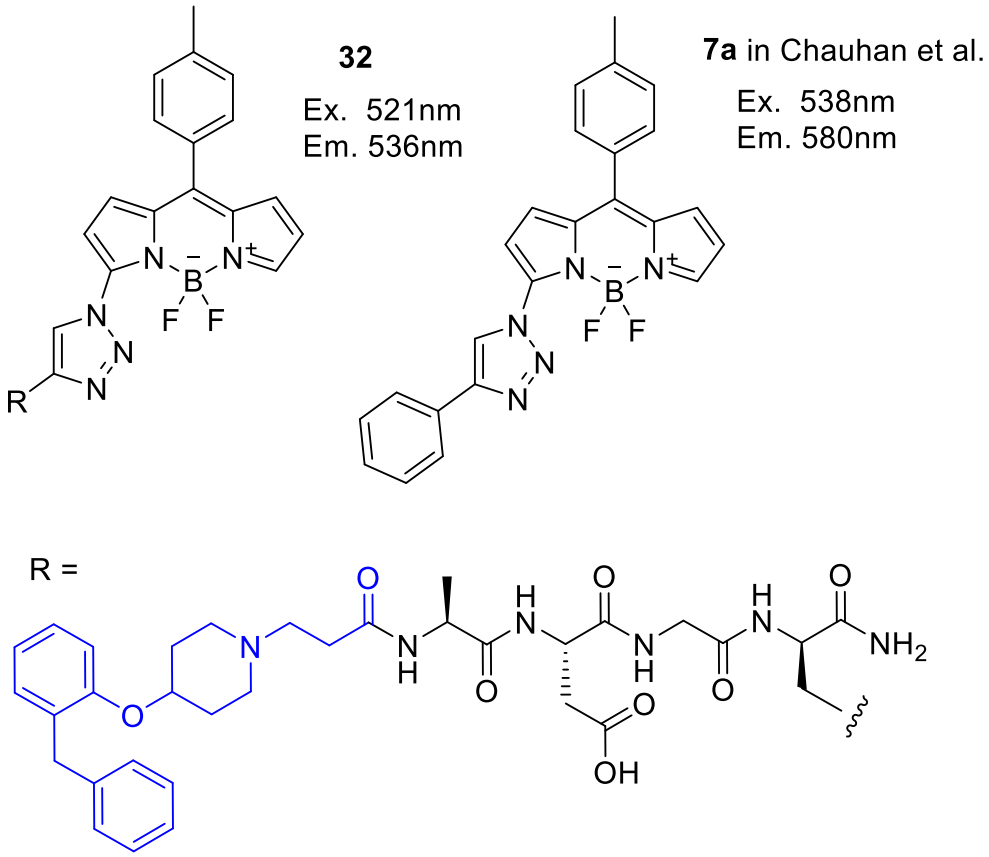

Figure 2.7: Differences in structure between the fluorophore of **32** and the desired fluorophore reported in Chauhan et al. as **7a**.

2.1.4.2 Pharmacology

The binding affinity of **32** at H_1R was determined by a saturation NanoBRET binding assay performed on Nluc-H_1R expressed on HEK293 cells to give its pK_D (Figure 2.10, Left) whereas the binding affinity of the non-fluorescent peptide congener **37** at H_1R was determined by the displacement of the fluorescent ligand **12**[3] (K_D = 8nM) from Nluc-H_1R expressed on HEK293 cells, with final concentrations of **37** ranging from 0.1nM to 0.1mM (Figure 2.8, Right). pK_i was determined using the Cheng-Prusoff equation, with at least three different experiments conducted for each ligand in triplicate. Compounds **32** and **37** displayed low binding affinities at H_1R (pK_D <6 and pK_i <6 respectively), rejecting the initial hypothesis from molecular modelling whereby placing an acidic amino acid (*e.g.* aspartic acid) within the peptide linker could lead to an increase in the binding affinity of the final compounds. This suggested that the proposed linker composition was not optimal and further efforts should be undertaken to identify the ideal peptide linker for the H_1R fluorescent

ligands. The fluorophore, which has been reported to significantly influence fluorescent ligand binding[142], could also have contributed to the lack of binding affinity of **32** and thus its optimisation was also considered.

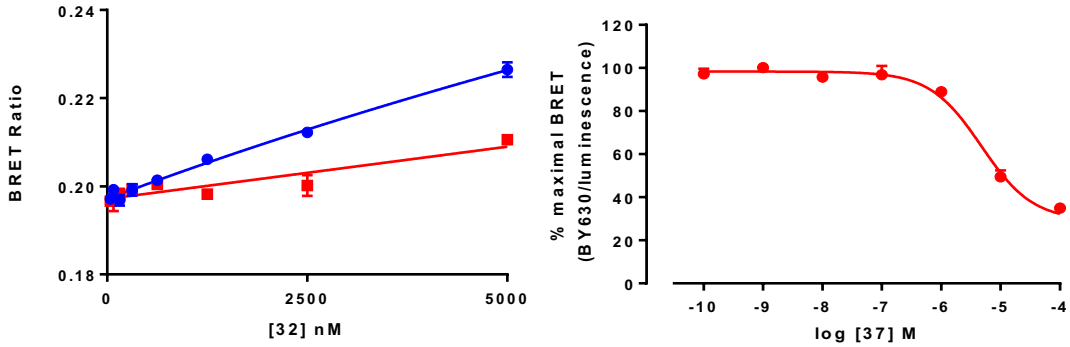

Figure 2.8: (**Left**) Binding curve from NanoBRET experiments in Nluc-H_1R expressing HEK293 cells with increasing concentrations of **32** in the absence (red) or presence (blue) of 10µM mepyramine. The data shown are representative of three independent experiments performed in triplicate and the datapoints are expressed in mean ± SEM. The error bars are within the limits of the symbols. (**Right**) Baseline corrected displacement graph of **37**. Data points represent the baseline corrected mean ± SEM of triplicate determinations from three separate experiments. The error bars are within the limits of the symbols.

2.2 Sequential Screening of Peptide Linker using Non-fluorescent Peptide Congeners

The initial hypothesis derived from molecular modelling led to the design and synthesis of **32**, which was tested to be non-binding at Nluc-H_1R. A systematic approach was undertaken to identify the optimal peptide linker through the synthesis and pharmacological testing of non-fluorescent congeners, which in turn would provide valuable input towards the synthesis of a new generation of peptide linker-based fluorescent ligands.

2.2.1 Approach

In order to optimise the peptide linker for H_1R fluorescent ligands, three series of peptide congeners were synthesised in a sequential manner to identify the amino acid which could provide the greatest improvement in congener binding affinity at amino acid 1 (AA1), amino acid 2 (AA2) and amino acid 3 (AA3), consisting of natural amino acids with distinct functionalities (Figure 2.9). These include the non-functionalised glycine (G); alanine (A) and valine (V) with small, lipophilic side groups; phenyalanine (F) and tyrosine (Y) with large, aromatic side groups; serine (S) and asparagine (N) with polar side groups; histidine (H) and lysine (K) with basic side groups and aspartatic acid (D) with an acidic side group (The structures of these amino acids is available in the Appendix section). *D*-Phe was also incorporated within the congener as the surrogate for the triazole ring – the product of CuAAC as well as to retain the stereochemistry surrounding the triazole moiety in accordance with compound **32**. The peptide linker optimisation was undertaken through unlabelled congeners as it did not require the use of expensive commercially available fluorophores and hence was more cost-effective as compared to carrying out the optimisation effort using fluorescent ligands. In addition, the versatility of SPPS and the commercial availability of a wide range of amino acids also allowed the easy manipulation of the peptide linker functional groups in terms of peptide sequence and type of functionalities.

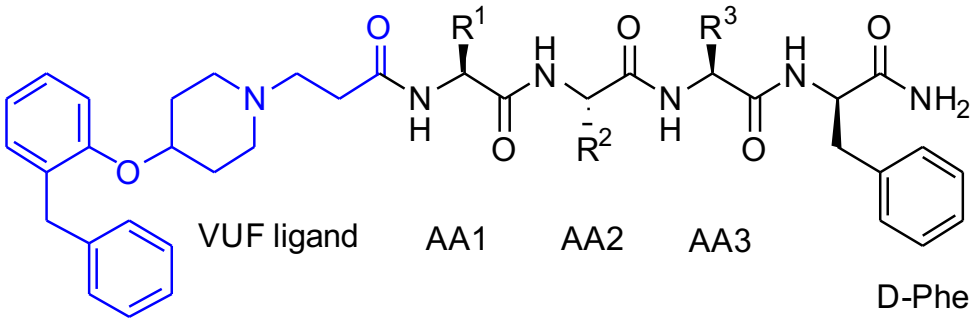

Figure 2.9: General structure of non-fluorescent peptide congeners for the optimisation of the peptide linker.

2.2.2 Synthesis

A total of 28 peptide congeners were synthesised by SPPS in three separate series (Scheme 2.5). Series 1 congeners had Ala fixed as AA2 and AA3, with varying amino acids incorporated at AA1 to optimise the peptide linker at this position and the optimised amino acid at AA1 was identified as Val. This approach was subsequently replicated in the following series of congeners, with AA1 = Val and AA3 = Ala in Series 2 congeners and AA1 = Val and AA2 = Ser in Series 3 congeners. The reaction was conducted in microwave vials at room temperature with mild stirring to avoid the grinding of the resin. Physical removal of DMF rinsing, deprotection and coupling mixtures were achieved by decanting. Despite the main disadvantage of decanting in comparison to flow washing with positive pressure i.e. residual coupling and/or deprotection mixtures which would result in inefficiencies during the synthesis, this approach was adopted as it enabled the three congeners series to be synthesised in a parallel manner. To reduce the synthetic inefficiencies associated with decanting, the coupling/deprotection mixtures were first decanted off and subsequently resins were washed with one-vial full (approximately 5 mL) for three times to remove as much residual mixtures as possible before proceeding to the next step of the synthesis. Meticulous record keeping was conducted to ensure that the peptide congeners synthesised were of the correct sequence. The reactions were straightforward, although overall yields were generally low (<10%) mainly due to reasons as described in 2.1.3.2 and above. Nevertheless, sufficient quantities of pure compounds (>95% except for **53** and **65**) were obtained after RP-HPLC purification for pharmacological characterisation.

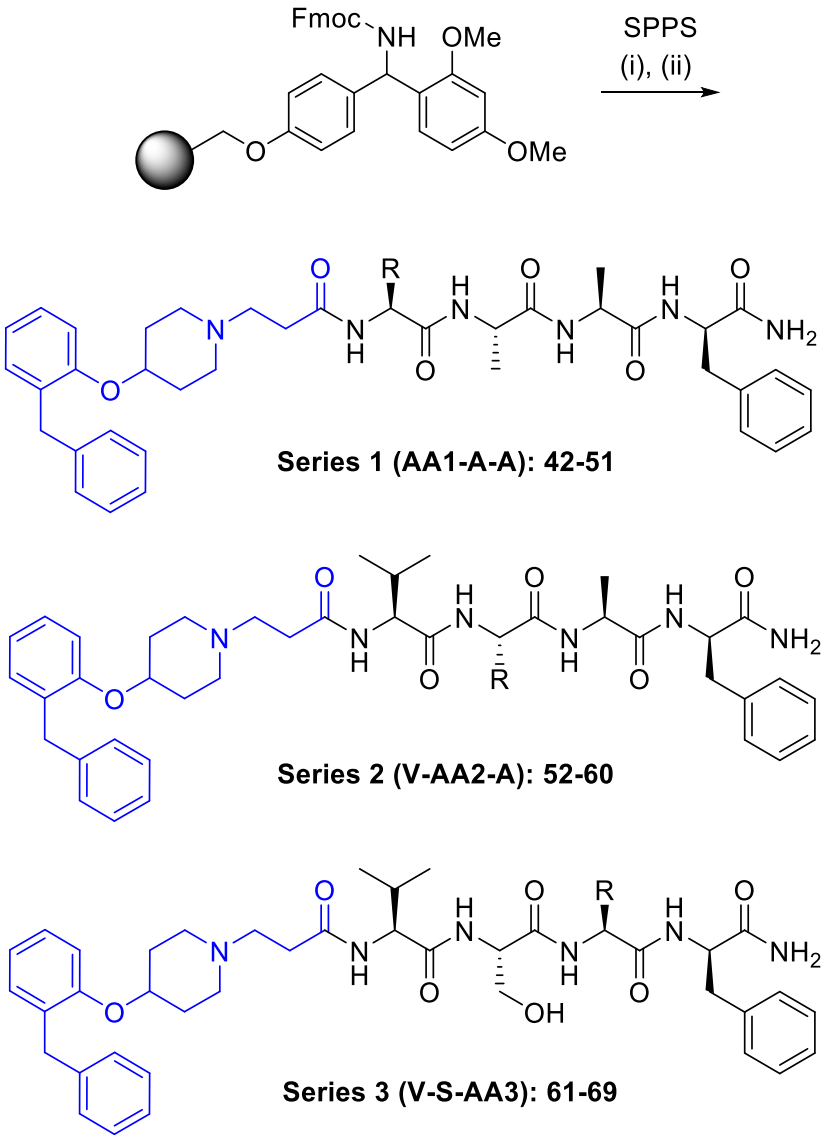

Scheme 2.5: Synthesis of non-fluorescent peptide congeners **42-69** using SPPS. (i) Coupling cycle: Fmoc-amino acid, HBTU, HOBt, DIPEA, DMF, RT, 2-4 hr; deprotection cycle: 20% piperidine in DMF, RT, 5 min. (ii) 95% TFA in water, RT, 6 hr, 1-12% overall yield.

2.2.3 Pharmacology

The binding affinity of the peptide congeners at H_1R were determined by displacement of a previously reported **12**[3] (K_D = 8nM) from Nluc-H_1R expressed on HEK293 cells, with final concentrations of the peptide congener ranging from 0.1mM to 0.1nM. pK_i was determined using the Cheng-Prusoff equation, with at least three separate experiments conducted for each ligand, each in triplicate to give an average value ± SEM with n = 3.

2.2.3.1 Series 1 (AA1-A-A)

Binding affinities in pK_i were between 5.79 to 6.80 across the series, with **44** having the highest binding affinity (pK_i = 6.80 ± 0.12) and showed approximately a 10-fold difference in binding affinity when compared to the compounds with the lowest affinity within the series (**45**, **46**, **50**; pK_i = 5.88 ± 0.21, 5.93 ± 0.17 and 5.79 ± 0.18 respectively) (Table 2.1, Figure 2.10). This suggested that a small and lipophilic side group such as the isopropyl group in the valine side group of **44** is favoured at R^1 compared to the large and bulky aromatic phenylalanine and tyrosine side groups of **45** and **46** respectively. The low binding affinity of **50** at H_1R was possibly attributed to entropic penalty as well as steric clashes within the ligand entry route due to the long and flexible nature of the lysine side group. It was interesting to note that by switching from alanine (**43,** pK_i = 6.04 ± 0.16) to valine (**44**, pK_i = 6.80 ± 0.12) at AA1 congener binding affinity could be increased by approximately 6-fold. Given that **43** shared a similar peptide linker to the fluorescent ligand **12**, it was postulated that optimisation of the peptide linker could lead to fluorescent ligands with binding affinities greater than that of **12** (pK_D = 8.1), provided that the linker SAR could be successfully transferred during the synthesis of these compounds.

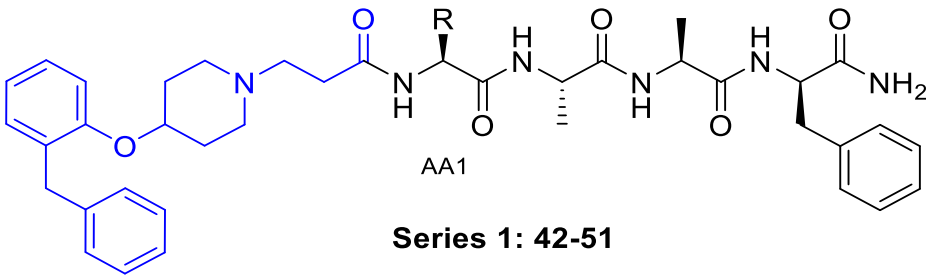

Series 1: 42-51

Cpd	AA1	R	pK_i ± SEM	K_i (nM)	Cpd	AA1	R	pK_i ± SEM	K_i (nM)
42	G	H	6.29 ± 0.21	657 ± 332	**47**	S		6.39 ± 0.15	458 ± 137
43	A	CH_3	6.04 ± 0.16	903 ± 498	**48**	N	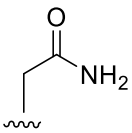	6.25 ± 0.20	709 ± 338
44	V		6.80 ± 0.12	170 ± 45	**49**	H	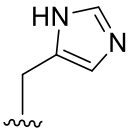	6.03 ± 0.13	932 ± 334
45	F	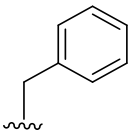	5.88 ± 0.21	1489 ± 492	**50**	K		5.79 ± 0.18	1763 ± 512
46	Y	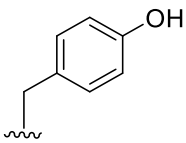	5.93 ± 0.17	1285 ± 427	**51**	D	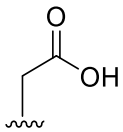	5.99 ± 0.24	1393 ± 734

Table 2.1: Binding affinities (pK_i) of **42-51** at Nluc-H_1R determined by displacement of **12**[3] (K_D = 8nM) from Nluc-H_1R expressed on HEK293 cells and pK_i values obtained using the Cheng-Prusoff equation. The data shown are the means ± SEM from three separate experiments.

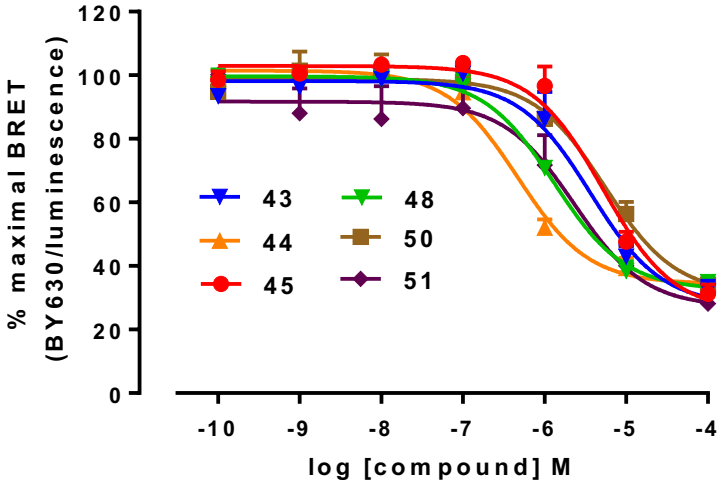

Figure 2.10: Baseline corrected displacement graphs of the congeners **43**, **44**, **45**, **48**, **50** and **51** determined by displacement of **12**[3] (K_D = 8nM) from Nluc-H_1R expressed on HEK293 cells with increasing congener concentration. Data points represent the baseline corrected mean ± SEM of triplicate determinations from three separate experiments.

2.2.3.2 Series 2 (V-AA2-A)

Nine peptide congeners with valine at AA1 were synthesised and tested in Series 2, with pK_i between 5.62 to 6.82 (Table 2.2, Figure 2.11). **56** (pK_i = 6.82 ± 0.06) with a polar serine side group at R^2 was the congener with the highest binding affinity. This was similar to **44** from Series 1 (pK_i = 6.80 ± 0.12) which instead had a small hydrophobic alanine side group at R^2, despite differences in side-chain properties. It was proposed that a small side group such as a methyl or hydroxymethyl group in the alanine and serine side chains of **44** and **56** respectively was preferred at R^2. The binding affinity of **59**, which had lysine at AA2, was 16-fold lower than **56** and had the lowest binding affinity for H_1R across the entire series (pK_i = 5.62 ± 0.06). In addition to the potential issues described previously in Series 1 with regards to the flexible nature of the lysine side group, it was hypothesised that the low binding affinity of **59** could also be attributed to the close proximity between R^2 and the targeted basic residues of $K179^{ECL2}$ and $K191^{5.39}$ which might have resulted in unfavourable electrostatic repulsion. However, having an acidic aspartate side group at R^2 did not increase the binding affinity of its corresponding congener **60** (pK_i = 6.26 ± 0.14)

despite structural evidence indicating the presence of K179^{ECL2} and K191$^{5.39}$ along the ligand entry route. There was a possibility that due to the rigid nature of the peptide linker backbone, the aspartate side group at R^2 (**60**) could not orientate itself towards K179^{ECL2} and K191$^{5.39}$ for the interaction to take place. This hypothesis was subsequently investigated in the synthesis of second-generation fluorescent ligands (section 3.1).

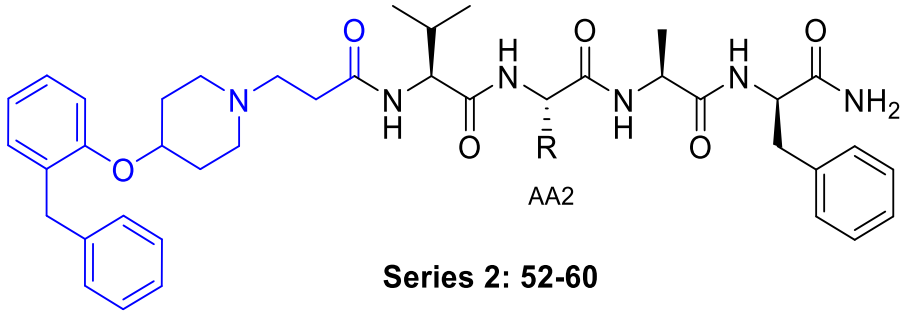

Series 2: 52-60

Cpd	AA2	R	pK_i ± SEM	K_i (nM)	Cpd	AA2	R	pK_i ± SEM	K_i (nM)
52	G	H	6.30 ± 0.07	521 ± 88	**56**	S		6.82 ± 0.06	154 ± 21
44	A	CH_3	6.80 ± 0.12	170 ± 45	**57**	N	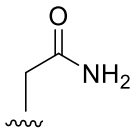	6.08 ± 0.03	832 ± 63
53	V		6.43 ± 0.06	381 ± 51	**58**	H	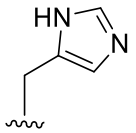	6.16 ± 0.06	711 ± 101
54	F	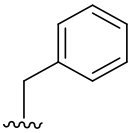	6.10 ± 0.20	993 ± 487	**59**	K		5.62 ± 0.06	2425 ± 469
55	Y	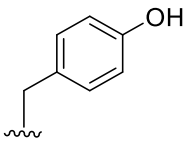	6.36 ± 0.04	445 ± 40	**60**	D	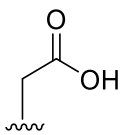	6.26 ± 0.14	606 ± 209

Table 2.2: Binding affinities (pK_i) of **44** and **52-60** at Nluc-H_1R determined by displacement of **12**[3] (K_D = 8nM) from Nluc-H_1R expressed on HEK293 cells and pK_i values obtained using the Cheng-Prusoff equation. The data shown are the means ± SEM from three separate experiments.

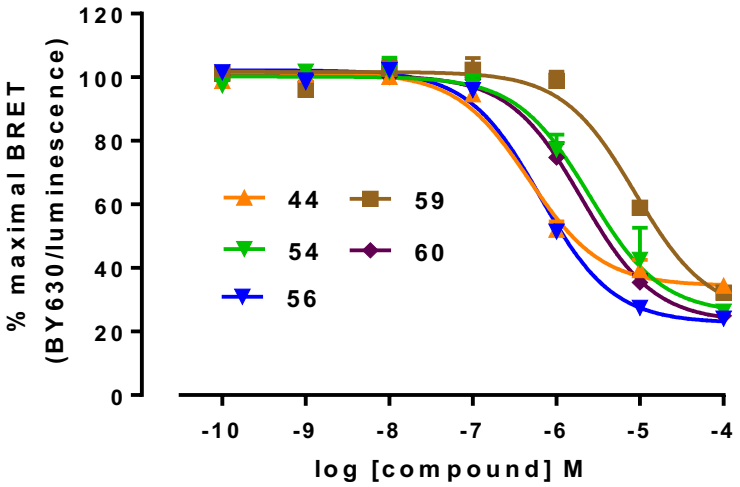

Figure 2.11: Baseline corrected displacement graphs of the congeners **44**, **54**, **56**, **59** and **60** determined by displacement of **12**[3] (K_D = 8nM) from Nluc-H_1R expressed on HEK293 cells with increasing congener concentration. Data points represent the baseline corrected mean ± SEM of triplicate determinations from three separate experiments.

2.2.3.3 Series 3 (V-S-AA3)

Nine peptide congeners with Valine at AA1 and Serine at AA2 were synthesised and tested in Series 3, with pK_i between 6.47 to 7.02 (Table 2.3, Figure 2.12). The congeners with the highest binding affinity in this series were **64** (pK_i = 7.02 ± 0.08) and **66** (pK_i = 7.02 ± 0.08), which was no more than 2-fold better than the rest of congeners in this series, with the exception of **62** and **65**. The greatest difference in binding affinity in this series was approximately 3-fold compared to >10-fold in the previous series, possibly indicating that the amino acid at AA3 had minimal effect on congener binding affinity. It was hypothesised that this was due to R^3 being close to the extracellular vestibule of the receptor and it would be likely that these regions were more solvent exposed. Free energy gained from ligand-receptor interaction was possibly negated due to displacement of solvating water molecules by the hydrophilic amino acid residues which were already present within the region. It was also believed that ligand-receptor interaction at R^3 would involve the long and relatively flexible ECL2, which could adopt multiple conformations to accommodate various substituents at R^3.

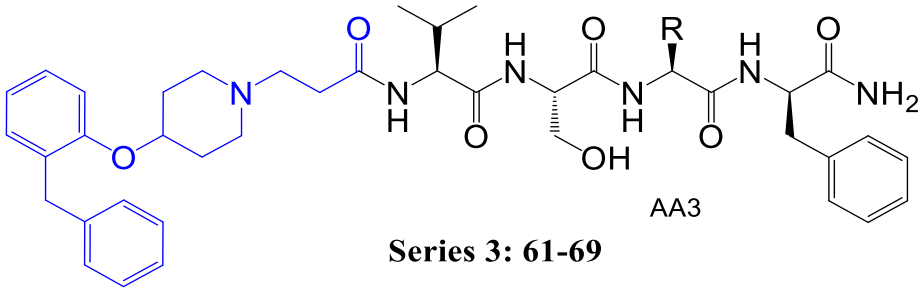

Series 3: 61-69

Cpd	AA 3	R	pK_i ± SEM	K_i (nM)	Cpd	AA3	R	pK_i ± SEM	K_i (nM)
61	G	H	6.80 ± 0.05	159 ± 17	**65**	S		6.47 ± 0.03	338 ± 26
56	A	CH_3	6.82 ± 0.06	154 ± 21	**66**	N	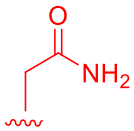	7.02 ± 0.08	99 ± 16
62	V		6.51 ± 0.07	315 ± 49	**67**	H	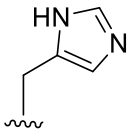	6.90 ± 0.04	130 ± 13
63	F	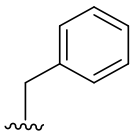	6.96 ± 0.02	111 ± 4	**68**	K		6.73 ± 0.05	187 ± 22
64	Y	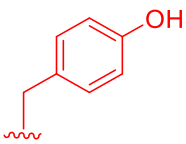	7.02 ± 0.08	98 ± 16	**69**	D	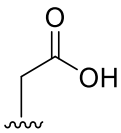	6.76 ± 0.04	174 ± 18

Table 2.3: Binding affinities (pK_i) of **56** and **61-69** at Nluc-H_1R determined by displacement of **12**[3] (K_D = 8nM) from Nluc-H_1R expressed on HEK293 cells and pK_i values obtained using the Cheng-Prusoff equation. The data shown are the means ± SEM from three separate experiments.

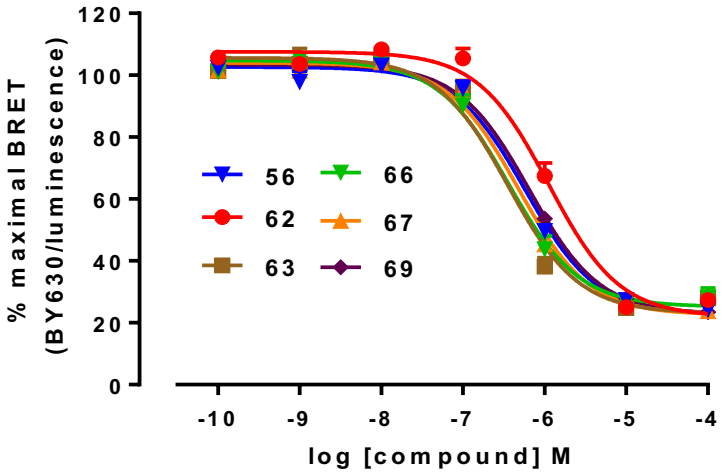

Figure 2.12: Baseline corrected displacement graphs of the congeners **56**, **62**, **63**, **66** **67** and **69** determined by displacement of **12**[3] (K_D = 8nM) from Nluc-H_1R expressed on HEK293 cells with increasing congener concentration. Data points represent the baseline corrected mean ± SEM of triplicate determinations from three separate experiments.

2.3 Summary

The first-generation fluorescent ligand **32** was designed based on molecular modelling findings and attempted to engage K179^{ECL2} and K191$^{5.39}$ by possessing an acidic aspartate side chain at R^2. This compound, however, exhibited low binding affinity at the H_1R. The low binding affinity of its associated congener **37** suggested that the peptide linker composition was not ideal and could instead be further optimised. A detailed screening approach was subsequently undertaken to identify the ideal peptide linker in a non-fluorescent congener. Through the synthesis and testing of three series of peptide congeners, **64** (V-S-Y linker) and **66** (V-S-N linker) were identified to have the highest binding affinity for H_1R (pK_i >7) and thus their associated linker was postulated to be ideal for H_1R. It was also interesting to note that the binding affinities of **64** and **66** were approximately 10-fold higher compared to **43** which shared a similar A-A-A linker to the fluorescent ligand **13**, indicating the possibility of further improving fluorescent ligand binding affinity with the optimisation of its peptide linker. This information was subsequently used in the synthesis of new fluorescent ligands and is described in Chapter 3.

Chapter 3: The Synthesis of New Generation H_1R Fluorescent Ligands

A detailed screening approach towards peptide linker optimisation involving the use of non-fluorescent congeners led to the discovery of V-S-N or V-S-Y as the best candidate peptide linkers for H_1R fluorescent ligands. These were subsequently taken into consideration in the synthesis of second-generation fluorescent ligands, with the fluorophore ultimately attached using CuAAC. The lack of difference in binding affinities of second-generation fluorescent ligands despite having different peptide linker composition led to the design and synthesis of third-generation fluorescent ligands, which aimed to study the effect of the orthosteric binding motif and linker length on overall ligand affinity. Finally, fourth-generation fluorescent ligands were synthesised to further probe the role of the peptide linker in influencing final binding affinity of H_1R fluorescent ligands.

3.1 Second Generation Fluorescent Ligands

Second generation H_1R fluorescent ligands were synthesised based on the ideal peptide linker composition determined from the congener screen, using CuAAC for the coupling of the BODIPY 630/650 fluorophore to the congener.

3.1.1 Approach

As previously discussed in Chapter 2, it was proposed that the low binding affinity of the first-generation H_1R fluorescent ligand **32** was attributed to its peptide linker composition and/or the fluorophore. With the ideal linker identified through efforts described in section 2.2, choosing the appropriate fluorophore for this generation of fluorescent ligand was also important as it would affect the binding affinity of the final fluorescent compound. In this instance BODIPY 630/650 was preferred, due to previous success with this fluorophore in the synthesis of Class A GPCR fluorescent ligands[47, 62, 142-144]. The second generation H_1R fluorescent ligands were subsequently designed and retrosynthesis performed, with CuAAC as the method towards fluorophore-congener coupling (Figure 3.1).

An azido functionalised BODIPY 630/650 fluorophore, a novel organic azide would present potential explosion risk associated with its long-term storage as well as its total synthesis, especially when conducted on a large scale. As such, it was decided that the BODIPY 630/650 should be instead alkyne functionalised for CuAAC. Having studied the structure of commercially available BODIPY 630/650 fluorophores, the attachment point (circled in red in Figure 3.1) was determined to be a suitable point of modification for the introduction of the alkyne group. Retrosynthesis of the proposed fluorophore **70** (Figure 3.1) led to a general BODIPY synthesis method involving the condensation of two functionalised pyrrole moieties, namely 5-(thiophen-2-yl)-1*H*-pyrrole-2-carbaldehyde **71** and (*E*)-2-(4-(prop-2-yn-1-yloxy)styryl)-1*H*-pyrrole **72** in the presence of phosphorus oxychloride and subsequent boron coordination under basic conditions (Figure 3.1)[145].

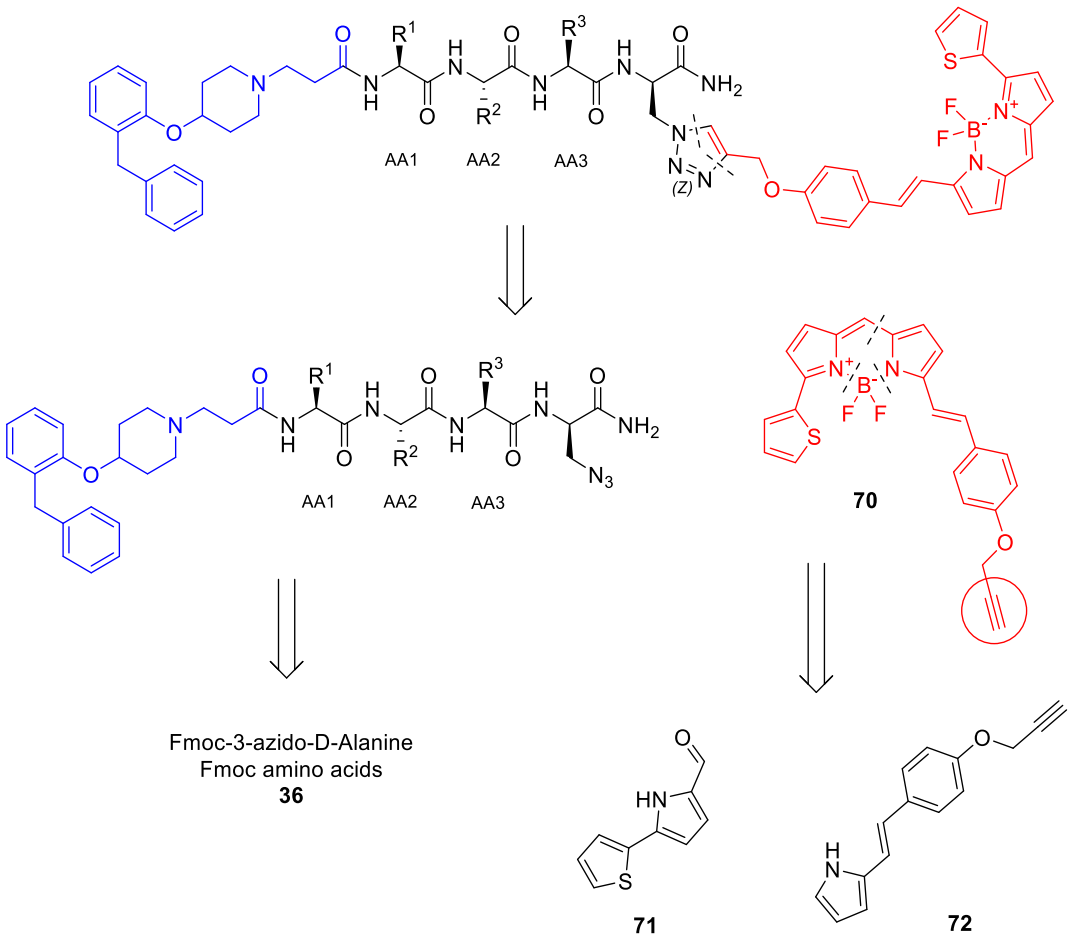

Figure 3.1: Retrosynthesis of the second-generation fluorescent ligands and alkyne-functionalised BODIPY 630/650-based fluorophore.

The azido-functionalised peptide congener on the other hand could be easily synthesised using SPPS in a similar way described in section 2.2.2 with the appropriate amino acids. Azido-functionalised amino acid such as Fmoc-3-azido-*D*-alanine would be incorporated as the first amino acid, with the *D*-isomer preferred to retain the stereochemistry surrounding the triazole moiety in accordance with compound **32**, followed by the desired peptide linker sequence and finally the VUF13816-based ligand **36**. At a later stage of the project, however, it was found out that only Fmoc-3-azido-*L*-alanine was commercially available and not the desired *D*-isomer. The incorporation of the *L*-amino acid instead of its *D*-enantiomer would have led to a change in the stereochemistry and hence possibly biological properties of the final product. This posed an issue with regards to the validity of the SAR information obtained from the previous congener screen which was conducted using *D*-Phe based peptide congeners (Figure 3.2). A preliminary experiment involving *L*-Phe-based peptide congeners with the ideal V-S-N or V-S-Y linker was therefore undertaken to investigate the effects of the opposite stereochemistry of the phenylalanine (* in Figure 3.2) on congener binding affinity, prior to utilising the commercially available Fmoc-3-azido-L-alanine towards congener synthesis.

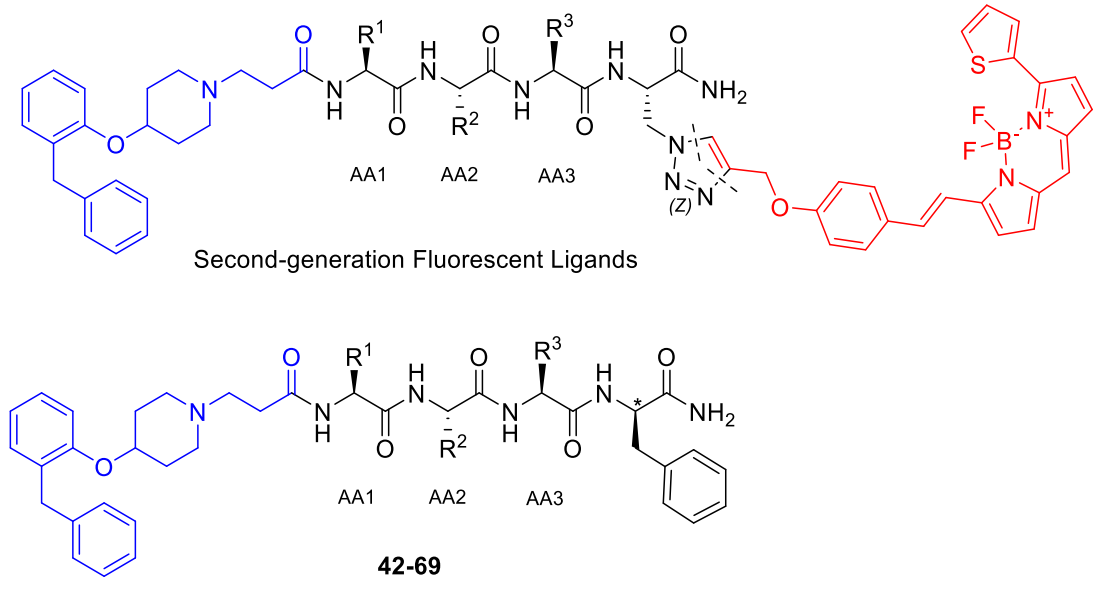

Figure 3.2: Difference in stereochemistry between second-generation fluorescent ligands synthesised from Fmoc-3-azido-(*L*)-alanine and the peptide congeners **42-69.**

3.1.2 L-Phe-based Congeners

3.1.2.1 Synthesis

Two *L*-Phe-based peptide congeners with the V-S-N and V-S-Y linkers were synthesised through SPPS as previously described in section 2.2.2.

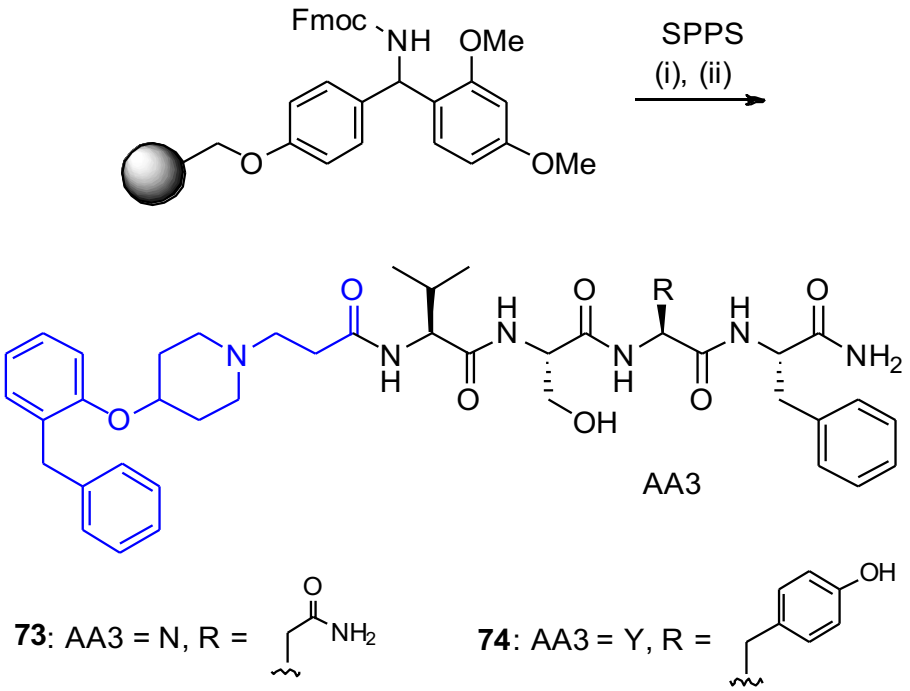

Scheme 3.1: Synthesis of VUF13816-based peptide congeners **73-74** using SPPS. (i) Coupling cycle: Fmoc-amino acid or **36**, HBTU, HOBt, DIPEA, DMF, RT, 2-4 hr; deprotection cycle: 20% piperidine in DMF, RT, 5 min. (ii) 95% TFA in water, RT, 6 hr, 2-6% overall yield.

3.1.2.2 Pharmacology

The binding affinity of **73-74** at H_1R was determined by the displacement of **12**[3] with a K_D of 8nM from Nluc-H_1R expressed on HEK293 cells, with final concentrations of the peptide congener ranging from 0.1mM to 0.1nM. pK_i was determined using the Cheng-Prusoff equation, with at least three different experiments were conducted for each ligand in triplicate to give an average value ± SEM with n = 3 (Table 3.1, Figure 3.3). Compound **73** (pK_i = 7.05 ± 0.20) was no different from its *D*-Phe based counterpart **66** (pK_i = 7.02 ± 0.08) in terms of binding affinity at H_1R. For compound **74** (pK_i = 6.36 ± 0.22) however, there was an approximately 5-fold decrease in binding

affinity compared to its *D*-Phe based counterpart **64** (pK_i = 7.02 ± 0.08). Since the stereochemistry at phenylalanine did not affect the V-S-N congener H_1R binding affinity, it was decided that Fmoc-3-azido-*L*-Alanine should be utilised in the synthesis of second-generation fluorescent ligands with the exclusion of V-S-Y as an optimal peptide linker.

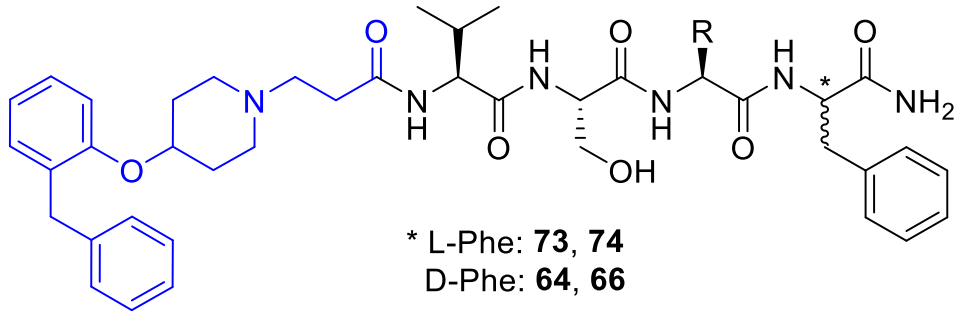

R	Cpd (L-Phe)	pK_i ± SEM	K_i (nM)	Cpd (D-Phe)	pK_i ± SEM	K_i (nM)
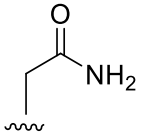	**73**	7.05 ± 0.20	89 ± 40	**66**	7.02 ± 0.08	99 ± 16
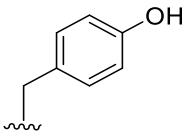	**74**	6.36 ± 0.22	437 ± 211	**64**	7.02 ± 0.08	98 ± 16

Table 3.1: Binding affinities (pK_i) of **73-74** compared to their *D*-Phe-based counterpart **64** and **66** at Nluc-H_1R determined by displacement of **12**[3] (K_D = 8nM) from Nluc-H_1R expressed on HEK293 cells and pK_i values obtained using the Cheng-Prusoff equation. The data shown are the means ± SEM from three separate experiments.

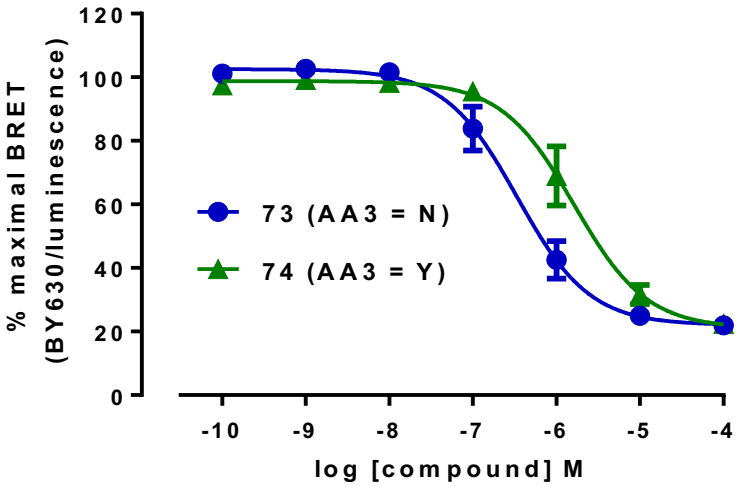

Figure 3.3: Baseline corrected displacement graphs of *L*-Phe-based congeners **73-74** determined by displacement of **12**[3] (K_D = 8nM) from Nluc-H_1R expressed on HEK293 cells with increasing congener concentration. Data points represent the baseline corrected mean ± SEM of triplicate determinations from three separate experiments.

3.1.3 Synthesis of Second-Generation Fluorescent Ligands

Congeners with the V-S-N linker (**73** and **66**) had similar pK_i values regardless of differences in stereochemistry of the phenylalanine surrogate as described in section 3.1.1, which suggested that the V-S-N linker might be suitable for fluorescent ligands synthesised from Fmoc-3-azido-*L*-alanine. In addition to V-S-N (**75**), two other linker compositions were considered in the synthesis of second-generation fluorescent ligands (Figure 3.4). Fluorescent ligand with a V-E-N linker **76** was synthesised to further test the initial hypothesis whereby an acidic side group at R^2 could form salt bridge interactions with $K179^{ECL3}$ and $K191^{5.39}$. This would hopefully be possible given the greater flexibility of the glutamate side group arising from an additional methylene group compared to the aspartate side group in the first-generation fluorescent ligand. Compound **77** containing an unoptimised A-A-A linker, similar to that in **12** would act as a control for investigating the effects of the optimised linker on fluorescent ligand binding affinity.

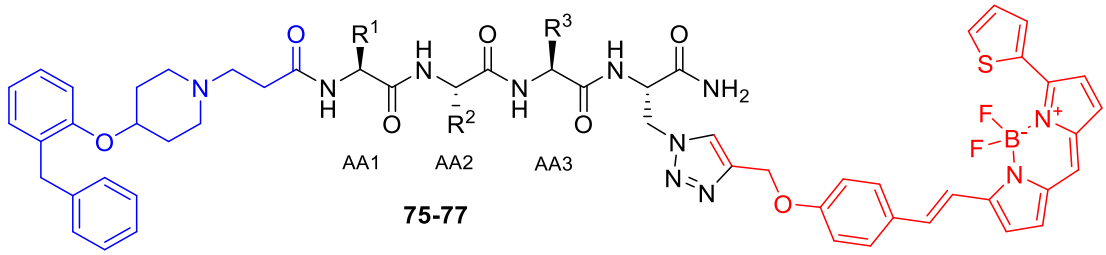

75-77

AA1-AA2-AA3 for **75-77**:

75: V-S-N
76: V-E-N
77: A-A-A

R^1, R^2, R^3 =
side chains of amino acids
at AA1, AA2 and AA3
respectively

Figure 3.4: Second-generation H_1R fluorescent ligands synthesised using CuAAC as final fluorophore coupling step.

The synthesis of the second generation of fluorescent ligands is described in two parts, namely, (i) the synthesis of the alkyne functionalised BODIPY630/650 fluorophore and (ii) the synthesis of the peptide congener and the coupling of the fluorophore to the congener through CuAAC.

3.1.3.1 Synthesis of the Alkyne-Functionalised BODIPY630/650 Fluorophore

5-(Thiophen-2-yl)-1*H*-pyrrole-2-carbaldehyde (**71**) was synthesised from 2-formyl pyrrole in five steps (summarised in Scheme 3.2), starting with Boc protection of the pyrrole-NH and acetal protection of the aldehyde group to give **78**, which proceeded efficiently in high yields and did not require chromatographic purification. The subsequent step involved boronation at C5 using triisopropyl borate in the presence of lithium diisopropylamide as a strong base followed by acidic deprotection of the Boc protecting group, the acetal group and the boronic ester in the presence of water to afford **79**. Diluted strong acids such as 0.1M HCl should not be used in the acid deprotection step as it was observed to have led to protodeboronation and subsequently acid-catalysed polymerisation of the 2-formylpyrrole to give a thin black film which was insoluble in various solvents. Instead, weak acids such as 10% sodium bisulphate heated to 70°C would be suitable to yield the desired product. Compound **79** was subjected to a Suzuki coupling with 2-bromothiophene to afford **71**.

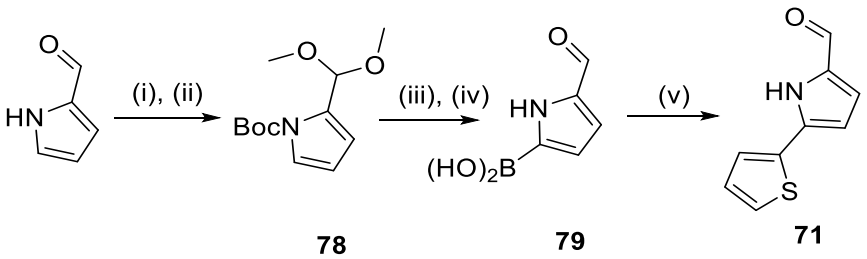

78 79 71

Scheme 3.2: Synthesis of 5-(thiophen-2-yl)-1*H*-pyrrole-2-carbaldehyde **71**. (i) Boc anhydride, triethylamine, DMAP, DCM, RT, 30 min, 99% (ii) trimethyl orthoformate, p-TsOH, MeOH, RT, 3 hr, 87%. (iii) triisopropylborate, lithium diisopropylamide, THF, 0°C, N_2, 1 hr. (iv) NH_4Cl quenching, 10% $NaHSO_4$, 70^{c}C, 2 hr, 34°C, 34% over two steps. (v) 2-bromo-thiophene, Na_2CO_3, $Pd(PPh_3)_2Cl_2$, 10% H_2O/1,4-dioxane, 100°C, N_2, 3 hr, 32%.

The synthesis of **72** (summarised in Scheme 3.3) began with the generation of a Wittig reagent **80** from para-methoxybenzyl chloride and tributylphosphine which was subsequently treated with NaOH under sonication for 5 minutes and then subjected to a Wittig reaction with 2-formylpyrrole at 100°C under microwave conditions. The coupling constant of R-C**H**=C**H**-R' was 16.5Hz, confirming that the product obtained was the (*E)*-isomer **81.** The aryl methoxy group was then demethylated using sodium ethanethiolate to yield the corresponding phenol and was isolated through an aqueous workup before subjecting it to K_2CO_3 treatment and subsequent alkylation with propargyl bromide to afford **72** with an overall yield of 57% across 5 steps.

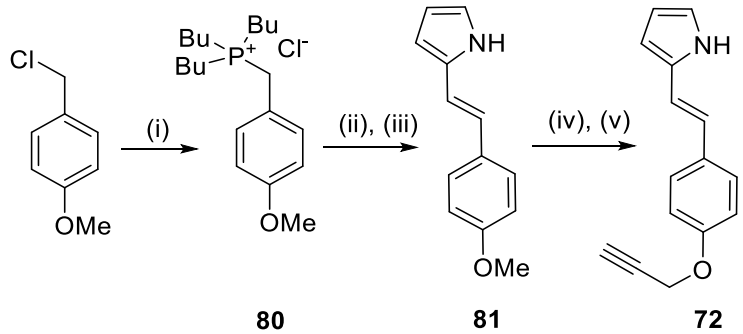

80 81 72

Scheme 3.3: Synthesis of (*E*)-2-(4-(prop-2-yn-1-yloxy)styryl)-1*H*-pyrrole **72.** (i) Tributylphosphine, anhydrous toluene, heated under reflux, N_2 atm, 15 hr, 85%. (ii) NaOH (aq), H_2O, RT, sonicate 5 mins. (iii) 2-formylpyrrole, 100°C MW, 30 mins, 76%. (iv) Sodium ethanethiolate, anhydrous DMF, heated under reflux, N_2 atm, 15 hr. (v) Propargyl bromide, K_2CO_3, ACN, heated to reflux, 15 hr, 88% over two steps.

Compound **71** was then condensed with **72** in the presence of $POCl_3$ overnight and subsequently treated with excess DIPEA and $BF_3{\cdot}Et_2O$ which after purification by silica column chromatography gave a red iridescent solid **70** in 69% yield (Scheme 3.4). Characterisation by LCMS, HRMS and NMR (^1H and ^{13}C) confirmed product identity.

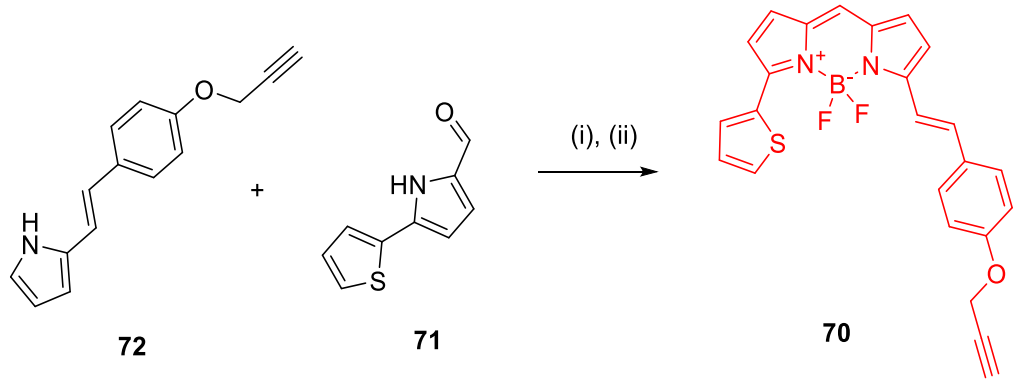

Scheme 3.4: Synthesis of alkyne-functionalised BODIPY 630/650 fluorophore **70**. (i) $POCl_3$, anhydrous DCM, RT, N_2 atm, 15 hr. (ii) $BF_3{\cdot}Et_2O$, DIPEA, DCM, RT, 2 hr, 69%.

3.1.3.2 Synthesis of the Peptide Congener and Fluorophore Coupling

Peptide congeners with the desired R^1, R^2 and R^3 side chains were synthesised through SPPS as previously described in section 2.2.2. The fluorophore was then coupled to congeners **82-84** through CuAAC to give the final fluorescent compounds **75-77**.

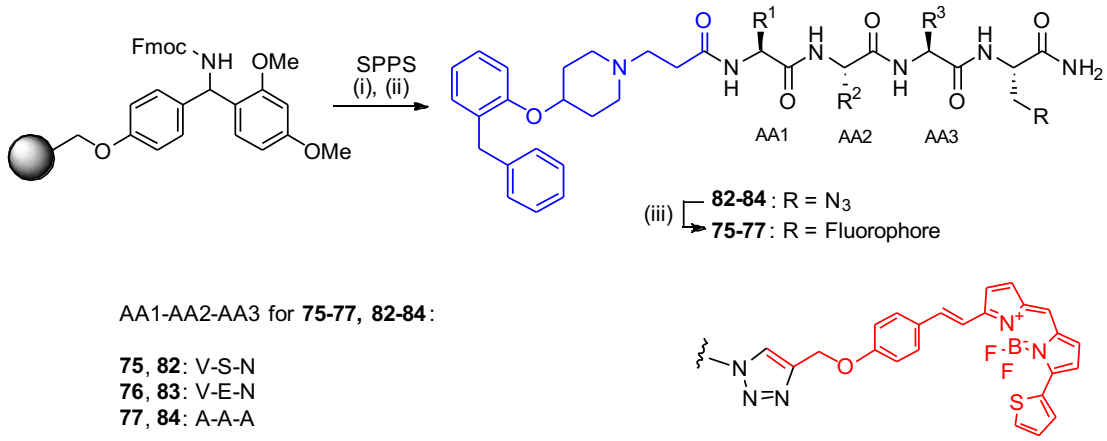

Scheme 3.5: Synthesis of azido-functionalised peptide congeners and second-generation fluorescent ligands. (i) Coupling cycle: Fmoc-amino acid or **36**, HBTU, HOBt, DIPEA, DMF, RT, 2-4 hr; deprotection cycle: 20% piperidine in DMF, RT, 5 min. (ii) 95% TFA in water, RT, 6 hr, 2% overall yield. (iii) **70**, $CuSO_4$, sodium ascorbate, 2,6-lutidine, DMSO, RT, 18 hours, 60-79%.

3.1.4 Pharmacology

The binding affinity of the fluorescent ligands **75-77** at H_1R was determined using a NanoBRET saturation binding assay performed on Nluc-H_1R expressed on HEK293 cells. The given pK_D values are mean values ± SEM of five independent repeats (Table 2.6). Concentration-dependent and saturable binding was observed for all three fluorescent compounds (Figure 3.5). Compound **75** (V-S-N linker; pK_D = 7.55 ± 0.07) and **77** (A-A-A linker; pK_D = 7.70 ± 0.05) had similar pK_D values, suggesting that the optimised peptide linker could not improve fluorescent ligand affinity, in stark contrast to what was observed during the congener screen whereby the V-S-N congener **66** displayed a 10-fold improvement in binding affinity over the A-A-A congener **43**. This could possibly be attributed to the significant changes in the overall size and physicochemical properties of the final compound which occur after fluorophore conjugation, resulting in fluorescent compounds which are significantly different from their corresponding non-fluorescent peptide congeners. This suggested that information regarding the linker SAR from the congener screen could not be directly transferred towards the synthesis of fluorescent compounds. There remained evidence that the linker still played a role, albeit a minor one in influencing overall fluorescent ligand binding affinity in which a switch from V-S-N (**75**, pK_D = 7.55 ± 0.07) to V-E-N (**76,** pK_D = 6.79 ± 0.04) resulted in a 5-fold loss of binding affinity. The acidic V-E-N peptide linker failed to increase the binding affinity of H_1R fluorescent ligands for H_1R despite additional side chain flexibility at R^2. Taking into consideration the observations from the first-generation fluorescent ligand and congener screen (Chapter 2), it appears that incorporating an acidic amino acid at AA2 within the peptide linker could not increase the binding affinity of H_1R fluorescent ligands.

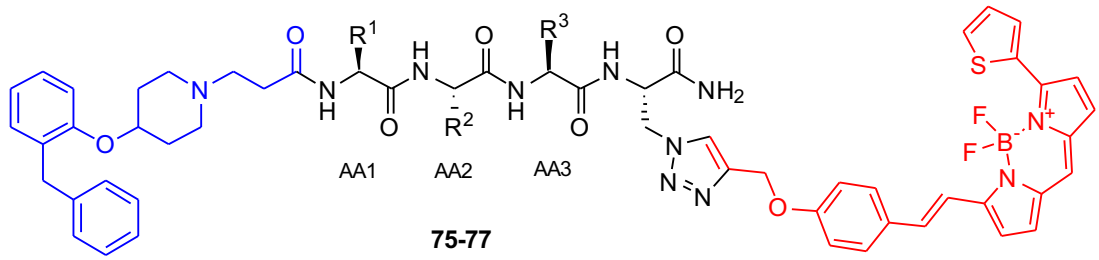

75-77

Cpd	AA1-AA2-AA3	pK_D ± SEM	K_D (nM)
75	V-S-N	7.55 ± 0.07	31 ± 5
76	A-A-A	7.70 ± 0.05	21 ± 1
77	V-E-N	6.79 ± 0.04	164 ± 16

Table 3.2: Binding affinities (pK_D) of fluorescent ligands **75-77** at Nluc-H_1R determined using a NanoBRET saturation binding assay performed on Nluc-H_1R expressed on HEK293 cells. The data shown are the means ± SEM from five experiments.

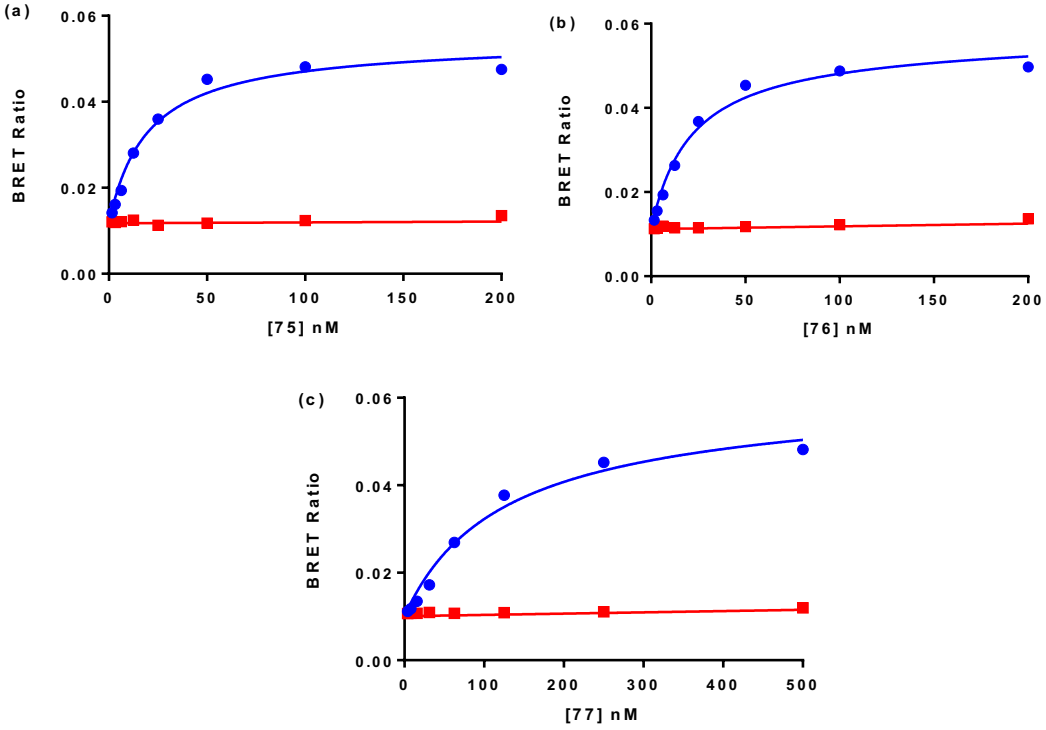

Figure 3.5: Saturation binding curves from NanoBRET experiments in Nluc-H_1R expressing HEK293 cells with increasing concentrations of fluorescent ligands **75 (a)**, **76 (b)** and **77 (c)** in the absence (red) or presence (blue) of 10µM mepyramine. The data shown are representative of five independent experiments performed in triplicate and the data points are expressed in mean ± SEM and error bars are within the limits of the symbols.

3.2 Third Generation Fluorescent Ligands

In the second generation H_1R fluorescent ligands, the optimised V-S-N peptide linker was unable to improve the binding affinity of peptide linker-based fluorescent ligands for H_1R. The synthesis of third generation H_1R fluorescent ligands was undertaken to investigate other factors which might affect final fluorescent ligand binding affinity e.g. linker length and the orthosteric binding motif.

3.2.1 Approach

Doxepin is one of only a few ligands which has a sub-nanomolar binding affinity for the H_1R (pK_i = 9.70 as an *E*:*Z* mixture of 85:15) at the orthosteric pocket and is at least 30-fold higher than VUF13816 (pK_i = 8.20)[103]. In this instance, two sets of fluorescent ligands based on either VUF13816 or doxepin were synthesised to investigate the effects of the orthosteric binding motif on fluorescent ligand binding affinity at H_1R (Figure 3.6). Third generation fluorescent ligands would also contain either the V-S-N or A-A-A linkers, with a similar overall linker length to compound **13.** This was achieved by incorporating Fmoc-5-azido-L-norvaline and an additional β-Alanine before the desired AA1-AA2-AA3 (Figure 3.6). Third generation VUF13816-based fluorescent ligands were then compared to their second-generation counterpart to study the effect of the change in linker length on binding affinity.

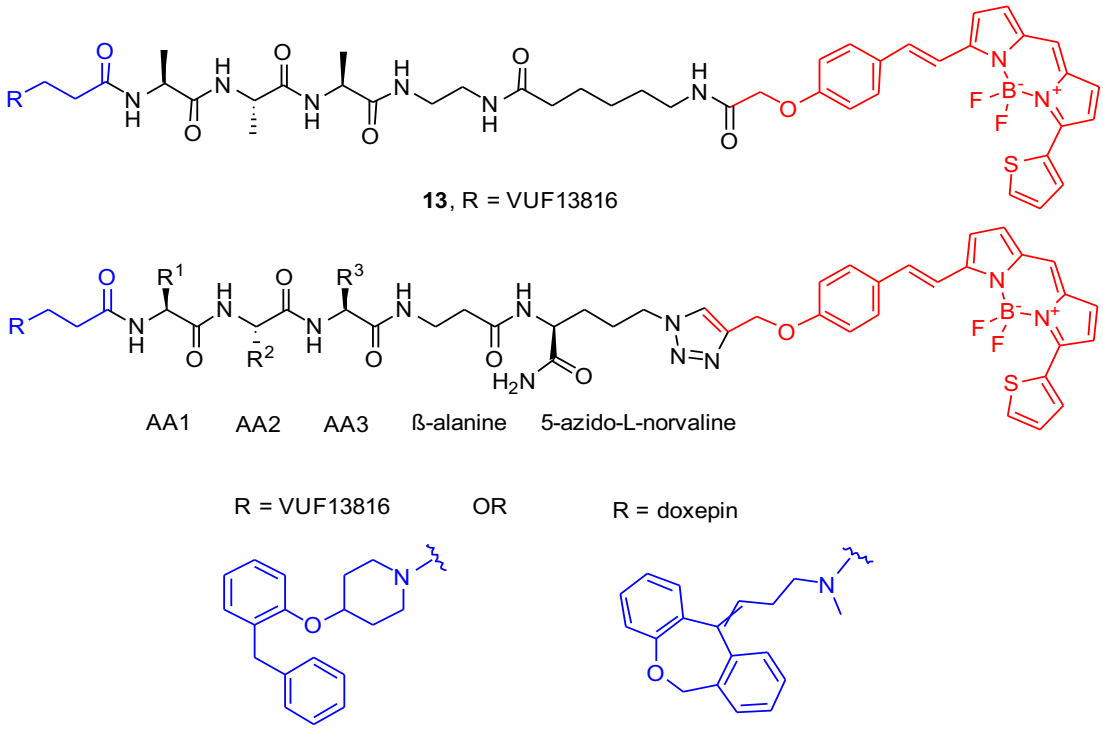

Figure 3.6: VUF13816 and doxepin-based third generation fluorescent ligands which shared a greater similarity to **13** in terms of overall ligand length as compared to the second-generation fluorescent ligands.

3.2.2 Synthesis

The synthesis of third generation of fluorescent ligands is described in two parts, namely, (i) the synthesis of the doxepin-based orthosteric binding motif and (ii) the synthesis of the peptide congener and fluorophore coupling through CuAAC.

3.2.2.1 Synthesis of the Doxepin-based Orthosteric Binding Motif

Doxepin hydrochloride was purchased from Tocris Bioscience (Bristol, UK) with a reported *E*:*Z* ratio of 85:15. The doxepin starting material was subjected to *N*-demethylation by reacting it with trichloroethyl chloroformate to form the trichloroethoxycarbonyl (Troc) group and its subsequent reductive cleavage using zinc powder in the presence of a weak acid (1M NaH_2PO_4) to afford desmethyldoxepin **85** with an *E*:*Z* ratio of 79:21. Silica gel column chromatography purification involved in step (i) and (ii) could have led to the enrichment of the *Z*-isomer. However, the *E*:*Z* ratio of the commercially acquired doxepin hydrochloride starting material was not experimentally determined and hence cannot be ruled out as one of the potential

reasons for the changes in the *E*:*Z* ratios. Compound **85** was converted to **86** by Michael addition with methyl acrylate in the presence of a base, heated under reflux in DCE. Ester hydrolysis in excess NaOH and subsequent acidification yielded free acid **87** with an *E*:*Z* ratio of 78:22. 1H and 13C NMR data were reported for the *E*-isomer only as the *Z*-isomer signal significantly overlapped with the *E*-isomer signal in 1H NMR (apart from the signal which corresponded to the alkene-H) whereas a combination low abundance of the *Z*-isomer and carbon-13 in the sample led to poor *Z*-isomer 13C NMR signal.

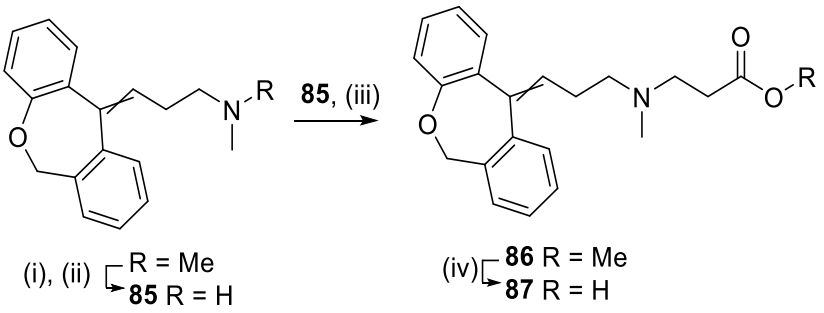

Scheme 3.6: Synthesis of the doxepin-based orthosteric binding motif. (i) trichloroethyl chloroformate, DCM, triethylamine, RT, N_2, 6 hr. (ii) Zn powder, 1M NaH_2PO_4, THF, RT, N_2, 15 hr, 45%. (iii) Methyl acrylate, DIPEA, DCE, 75°C, 15 hr, 69%. (iv) NaOH, H_2O/THF, RT, 1 hr, 96%.

3.2.2.2 Synthesis of the Peptide Congener and Fluorophore Coupling

The desired peptide congeners **88-91** were synthesised through SPPS as previously described in section 2.2.2. The fluorophore **70** was then coupled to the congeners using CuAAC to give the final fluorescent compounds **92-95** (Scheme 3.7). The *E*:*Z* ratio surrounding the doxepin orthosteric binding motif of the final fluorescent compounds **92-95** were not determined and the final fluorescent compounds were likely tested as a mixture. The effects of having a doxepin *E*:*Z* ratio different from 85:15 were unclear as a search on the ChEMBL database revealed that the activity of the *E*- and *Z*-isomer of doxepin were never separately determined.

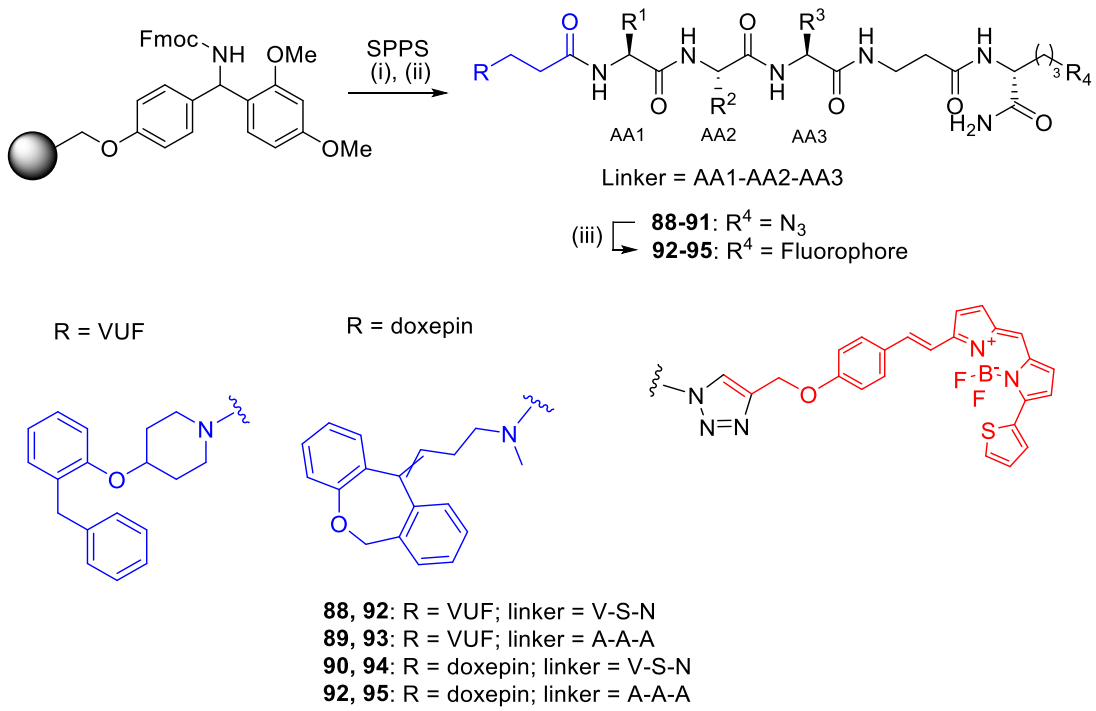

Scheme 3.7: Synthesis of VUF13816, doxepin-based peptide congeners and third generation fluorescent ligands. (i) Coupling cycle: Fmoc-amino acid, HBTU, HOBt, DIPEA, DMF, RT, 2-4 hr; deprotection cycle: 20% piperidine in DMF, RT, 5 min. (ii) 95% TFA in water, RT, 6 hr, 5-11% overall yield. (iii) **70**, $CuSO_4$, sodium ascorbate, 2,6-lutidine, DMSO, RT, 18 hr, 33-54%.

3.2.3 Pharmacology

The binding affinity of the congeners **88-91** and fluorescent ligands **92-95** were subsequently determined using NanoBRET competition and saturation binding assays respectively.

3.2.3.1 Peptide Congener

The binding affinity of the non-fluorescent congeners **88-91** at H_1R was determined by the displacement of **12**[3] from Nluc-H_1R expressed on HEK293 cells, with final concentrations of **88-91** ranging from 0.1mM to 0.1nM. pK_i was determined using the Cheng-Prusoff equation, with at least three different experiments were conducted for each ligand in triplicate to give an average value ± SEM with n = 3 (Table 3.3, Figure 3.7). There was little difference observed (less than 2-fold) in the binding affinity across the four peptide congeners of varying orthosteric binding motifs and peptide linkers, indicating that neither the orthosteric binding motif nor the peptide linker

affected the binding affinities of the azido-functionalised peptide congeners. Despite the differences in orthosteric binding motif and peptide linker whereby the of the parent ligand doxepin (K_i = 0.2 nM) has a significantly higher binding affinity (>30-fold) compared to VUF13816 (K_i = 6.3 nM), the binding affinity of congeners derived from these ligands at H_1R did not reflect this difference. This observation was in close agreement with the current consensus regarding fluorescent ligands as highlighted in section 1.2, whereby fluorescent ligands or their congeners are significantly different than their parent ligands and *must* be treated as new pharmacological entities in their own rights rather than simple extensions of the original orthostere. This also suggested that the linker SAR might only be restricted to the initial congener screen and would not usefully translate to synthesising other congeners and fluorescent ligands.

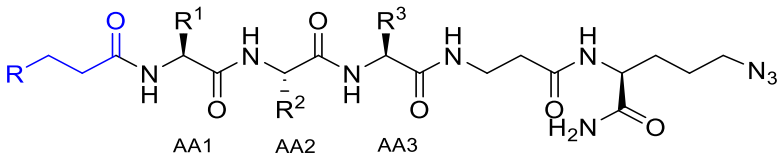

88, **89**: R = VUF13816 **90**, **91**: R = doxepin

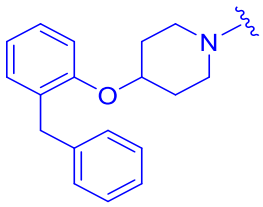

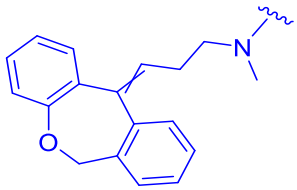

	VUF13816-based			**Doxepin-based**		
AA1-AA2-AA3	Cpd	pK_i ± SEM	K_i (nM)	Cpd	pK_i ± SEM	K_i (nM)
V-S-N	**88**	6.70 ± 0.05	200 ± 21	**90**	6.77 ± 0.12	182 ± 46
A-A-A	**89**	6.65 ± 0.14	252 ± 88	**91**	6.91 ± 0.12	134 ± 38

Table 3.3: Binding affinities (pK_i) of **88-91** at Nluc-H_1R determined by displacement of **12**[3] (K_D = 8nM) from Nluc-H_1R expressed on HEK293 cells and pK_i values obtained using the Cheng-Prusoff equation. The data shown are the means ± SEM from three separate experiments..

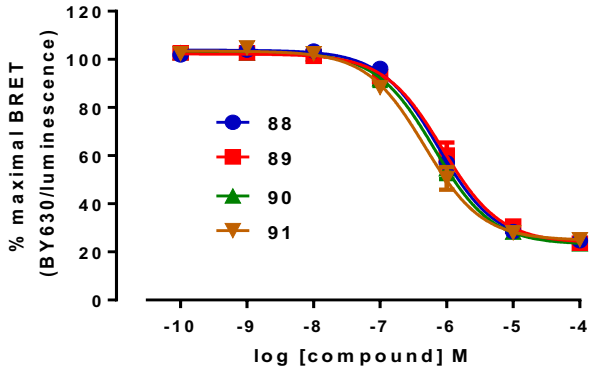

Figure 3.7: Baseline corrected displacement graphs of **88**-**91** determined by displacement of **12**[3] (K_D = 8nM) from Nluc-H_1R expressed on HEK293 cells with increasing congener concentration. Data points represent the baseline corrected mean ± SEM of triplicate determinations from three separate experiments.

3.2.3.2 Third Generation Fluorescent Ligands

The binding affinity of **92-95** at H_1R were determined by NanoBRET saturation binding assays performed on Nluc-H_1R expressed on HEK293 cells. The listed pK_D values are mean values ± SEM of four independent repeats (Table 3.4). Concentration-dependent and saturable binding was observed for all four fluorescent compounds (Figure 3.8). pK_D values were similar across **92-95**, with only the doxepin-based **95** having a pK_D >8 (sub 10-nM K_D) and H_1R binding affinity was at most 3-fold higher than **92-94**. Compound **92** (pK_D = 7.71 ± 0.05) and **93** (pK_D = 7.86 ± 0.06) and their second-generation fluorescent ligand counterpart **82** (pK_D = 7.55 ± 0.07) and **83** (pK_D = 7.70 ± 0.05) had similar binding affinities at H_1R. Neither the orthosteric binding motif nor the length of the linker significantly influenced fluorescent ligand binding affinity. This builds upon observations from previous work carried out on H_1R fluorescent compounds whereby a total of 6 VUF13816- and mepyramine-based fluorescent compounds with differences in linker length and composition had comparable pK_D values across various assays[3]. Fluorophore attachment increased fluorescent ligand binding affinity by approximately 10-fold as seen in **92-95** (pK_D = 7.71-8.27) compared to their corresponding peptide congeners **88-91** (pK_i = 6.65-6.91). This could be attributed to the lipophilic fluorophore orientating itself away from the extracellular aqueous environment and potentially embedding in the lipophilic lipid bilayer, subsequently acting as a tether[3].

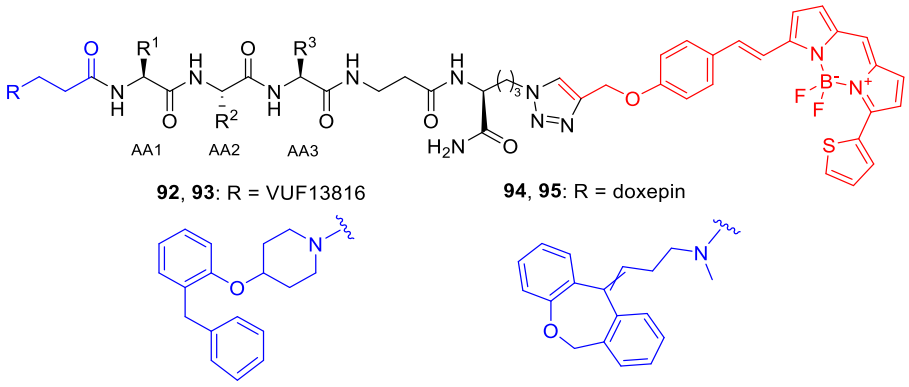

	VUF13816-based			Doxepin-based		
AA1-AA2-AA3	Cpd	pK_D ± SEM	K_D (nM)	Cpd	pK_D ± SEM	K_D (nM)
V-S-N	**92**	7.71 ± 0.05	20 ± 2	**94**	7.72 ± 0.11	20 ± 6
A-A-A	**93**	7.86 ± 0.06	14 ± 2	**95**	8.27 ± 0.05	6 ± 1

Table 3.4: Binding affinities of **92-95** at Nluc-H_1R determined using a NanoBRET saturation binding assay performed on Nluc-H_1R expressed on HEK293 cells. The data shown are the means ± SEM from four experiments.

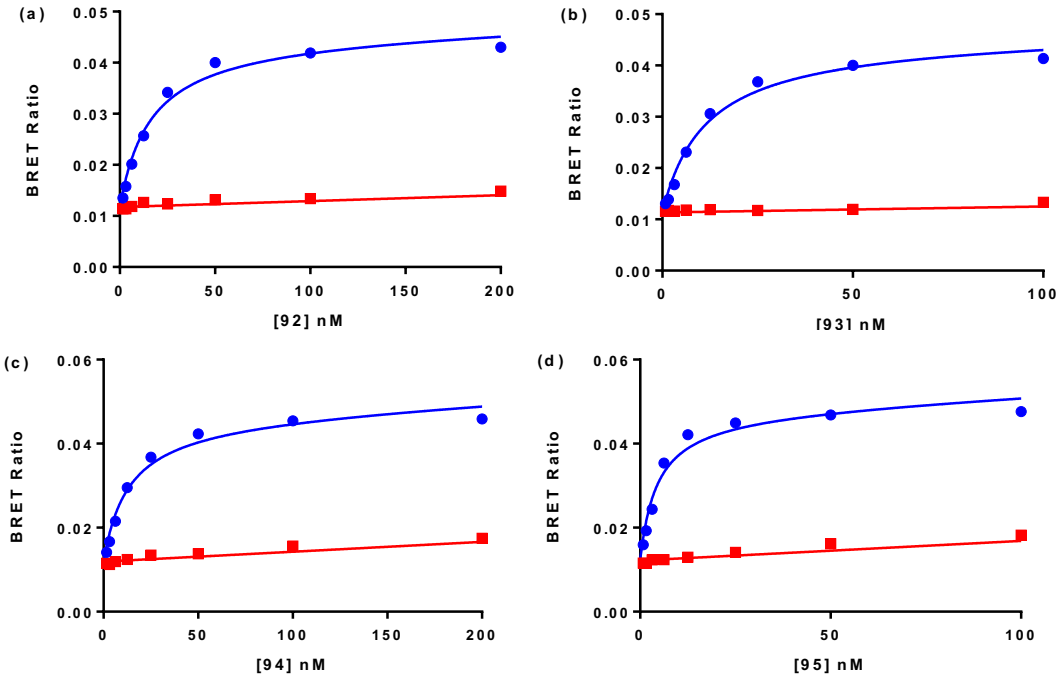

Figure 3.8: Saturation binding curves from NanoBRET experiments in Nluc-H_1R expressing HEK293 cells with increasing concentrations of fluorescent ligands **92 (a)**, **93 (b)**, **94 (c)** and **95 (d)** in the absence (red) or presence (blue) of 10µM mepyramine. The data shown are representative of four independent experiments performed in triplicate and the data points are expressed in mean ± SEM and error bars are within the limits of the symbols.

3.3 Fourth-Generation Fluorescent Ligands

The second- and third-generation fluorescent ligands exhibited comparable binding affinities despite differences in peptide linker composition, overall linker length and orthosteric binding motif. The synthesis of fourth-generation fluorescent ligands was aimed to study the effects of peptide linker on fluorescent ligand binding affinities in greater detail. This was achieved by the synthesis and pharmacological characterisation of fluorescent ligands with a wide range of peptide linkers designed based on the findings of the congener screen (section 2.2). The fluorescent ligand with the highest binding affinity was subsequently used in confocal imaging to determine the lowest concentration required for cell imaging experiments and to determine the extent of intracellular accumulation.

3.3.1 Approach

Fourth generation fluorescent ligands were synthesised to explore the potential existence of synergistic effects within the peptide linkers whereby amino acids in certain combination within the peptide linker could significantly increase fluorescent ligand binding affinity. A total of eleven fluorescent ligands with a wide range of peptide linkers were synthesised based on information obtained from the congener screen. A 2x2x2 matrix approach towards the linker (AA1-AA2-AA3) design was adopted, with AA1 = V or T, AA2 = S or A and AA3 = N or Y to give eight fluorescent ligands with V-S-N, V-A-N, T-S-N, T-A-N, V-S-Y, V-A-Y, T-S-Y and T-A-Y linkers (**107-114** in Scheme 3.8). Fluorescent ligands with I-S-N and L-S-N linkers were also synthesised to further explore the SAR around R^1 given that having a Val at AA1 was observed to be favourable in the congener screen, alongside a fluorescent ligand with an unoptimised F-A-A linker as a control for investigating the effects of the optimised linker on fluorescent ligand binding affinity. Amide coupling of the fluorophore was preferred as fourth-generation fluorescent ligands did not possess any competing nucleophilic side groups at R^1, R^2 or R^3 (except for Tyr). This was achieved by incorporating L-Lysine within the fluorescent ligands which served as the attachment point for the amide coupling of an in-house synthesised carboxylic acid-functionalised BODIPY 630/650 fluorophore (BODIPY 630/650-COOH). Subsequently,

fourth generation fluorescent ligands would share great similarity to **13** in terms of orthosteric binding motif, linker length, fluorophore and the congener-fluorophore coupling approach, with differences in linker composition (Figure 3.9).

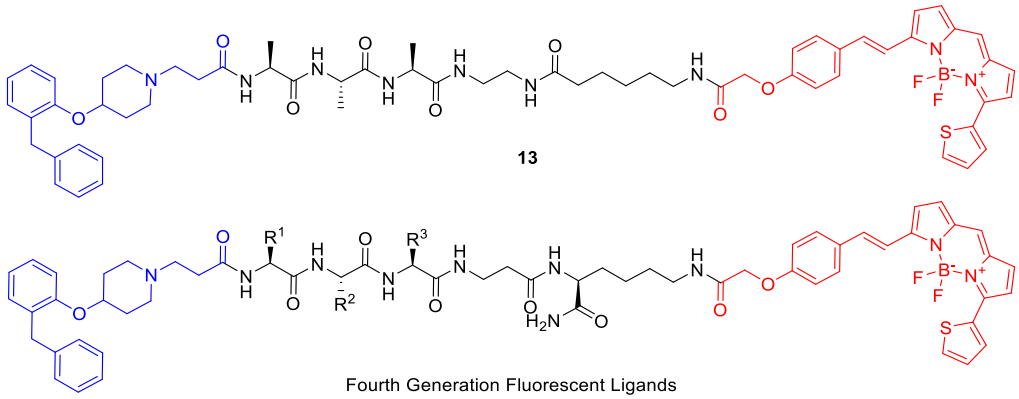

Figure 3.9: Conventional amide coupling of the fluorophore was proposed for the synthesis of fourth generation fluorescent ligands which were highly similar to **13**.

3.3.2 Synthesis

Peptide congeners with the desired linker composition were synthesised using SPPS. BODIPY 630/650-COOH fluorophore was then coupled to each of the congeners **96-106** in DMF at room temperature with 1-[Bis(dimethylamino)methylene]-1*H*-1,2,3-triazolo[4,5-b]pyridinium 3-oxide hexafluorophosphate (HATU) as the coupling reagent and purified using preparative HPLC to give **107-117** (Scheme 3.8). Purity and identity of the compounds were confirmed using HPLC and HRMS respectively.

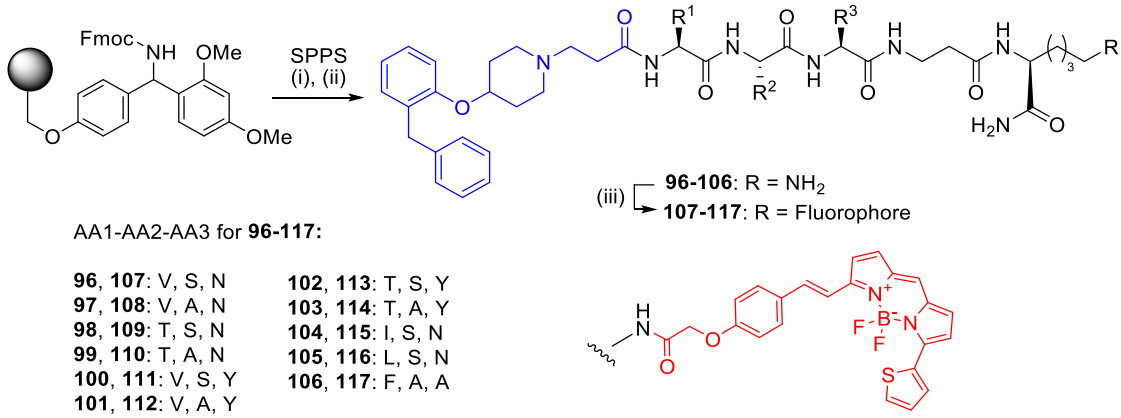

Scheme 3.8: Synthesis of VUF13816-based amide coupled fluorescent ligands. (i) Coupling cycle: Fmoc-amino acid, HBTU, HOBt, DIPEA, DMF, RT, 2-4 hr; deprotection cycle: 20% piperidine in DMF, RT, 5 min. (ii) 95% TFA in water, RT, 6 hr, 4-8% overall yield. (iii) BODIPY 630/650-COOH, HATU, DIPEA, DMF, RT, 2 hours, 27-45%.

3.3.3 Pharmacology

The binding affinities of the final fluorescent compounds **107**-**117** at H_1R were determined by a saturation binding assay performed on Nluc-H_1R expressed on HEK293 cells. The given pK_D values are mean values ± SEM of four independent repeats (Table 3.5). Concentration-dependent and saturable binding was observed for all eleven fluorescent compounds (Figure 3.10 and Figure 3.11). All 11 fluorescent ligands exhibited comparable pK_D values (pK_D = 7.80-8.40), with 8 out of 11 compounds having pK_D values of higher than 8 regardless of differences in peptide linker. Compound **107** (V-S-N linker) had the highest average binding affinity for the H_1R (pK_D = 8.40 ± 0.08), which was only 3-fold greater compared to **117** (F-A-A linker, pK_D = 7.92 ± 0.08) despite a 13-fold difference in pK_D between their corresponding congener counterparts **66** (pK_D = 7.02 ± 0.08, Table 2.3) and **45** (pK_D = 5.88 ± 0.21, Table 2.1) respectively. These results further confirmed the findings obtained from the synthesis of second and third generation fluorescent ligands whereby the peptide linker composition had little effect on fluorescent ligand binding affinity.

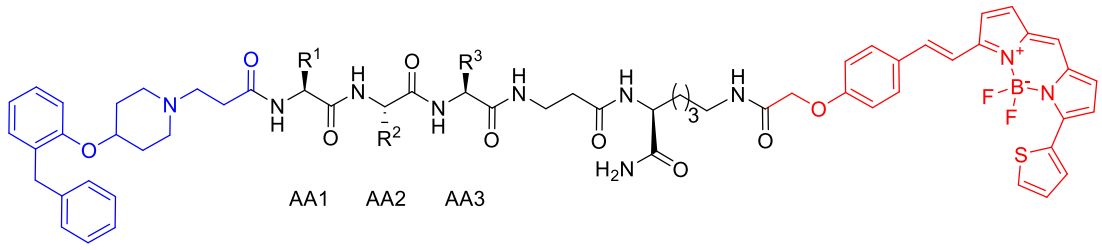

107-117

Cpd	AA1-AA2-AA3	pK_D ± SEM	K_D (nM)	Cpd	AA1-AA2-AA3	pK_D ± SEM	K_D (nM)
107	V-S-N	8.40 ± 0.08	4 ± 1	**113**	T-S-Y	8.16 ± 0.12	8 ± 2
108	V-A-N	8.34 ± 0.09	5 ± 1	**114**	T-A-Y	8.23 ± 0.17	8 ± 3
109	T-S-N	8.20 ± 0.07	7 ± 1	**115**	L-S-N	8.33 ± 0.09	5 ± 1
110	T-A-N	8.29 ± 0.07	5 ± 1	**116**	I-S-N	8.23 ± 0.06	6 ± 1
111	V-S-Y	7.80 ± 0.11	17 ± 4	**117**	F-A-A	7.92 ± 0.08	13 ± 3
112	V-A-Y	7.96 ± 0.11	12 ± 4				

Table 3.5: Binding affinities of **107-117** at Nluc-H_1R determined using a NanoBRET saturation binding assay performed on Nluc-H_1R expressed on HEK293 cells. The data shown are the means ± SEM from four experiments.

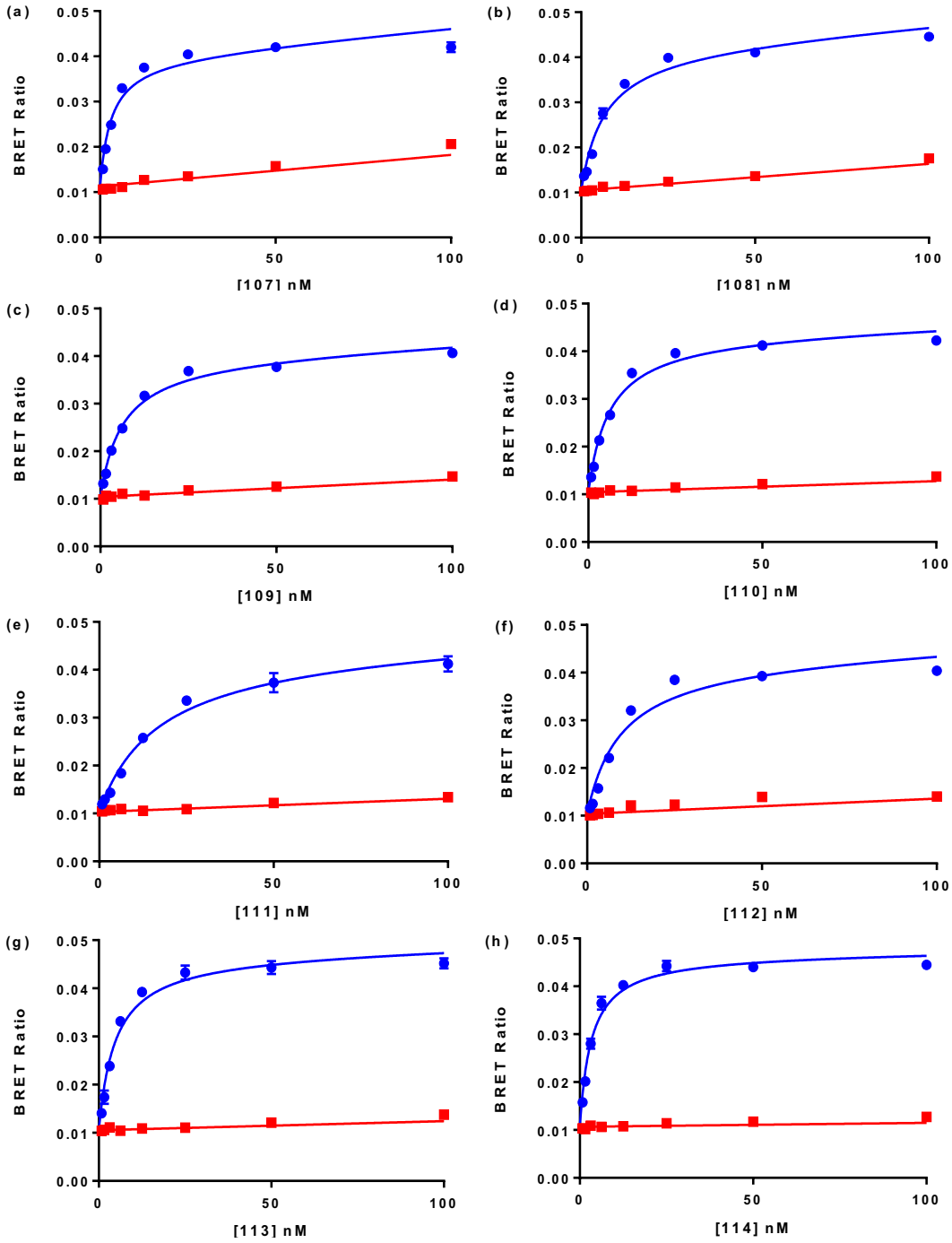

Figure 3.10: Saturation binding curves from NanoBRET experiments in Nluc-H_1R expressing HEK cells with increasing concentrations of fluorescent ligands **107 (a)**, **108 (b)**, **109 (c)**, **110 (d)**, **111 (e)**, **112 (f)**, **113 (g)** and **114 (h)** in the absence (red) or presence (blue) of 10µM mepyramine. The data shown are representative of four independent experiments performed in triplicate and the data points are expressed in mean ±SEM and error bars are within the limits of the symbols.

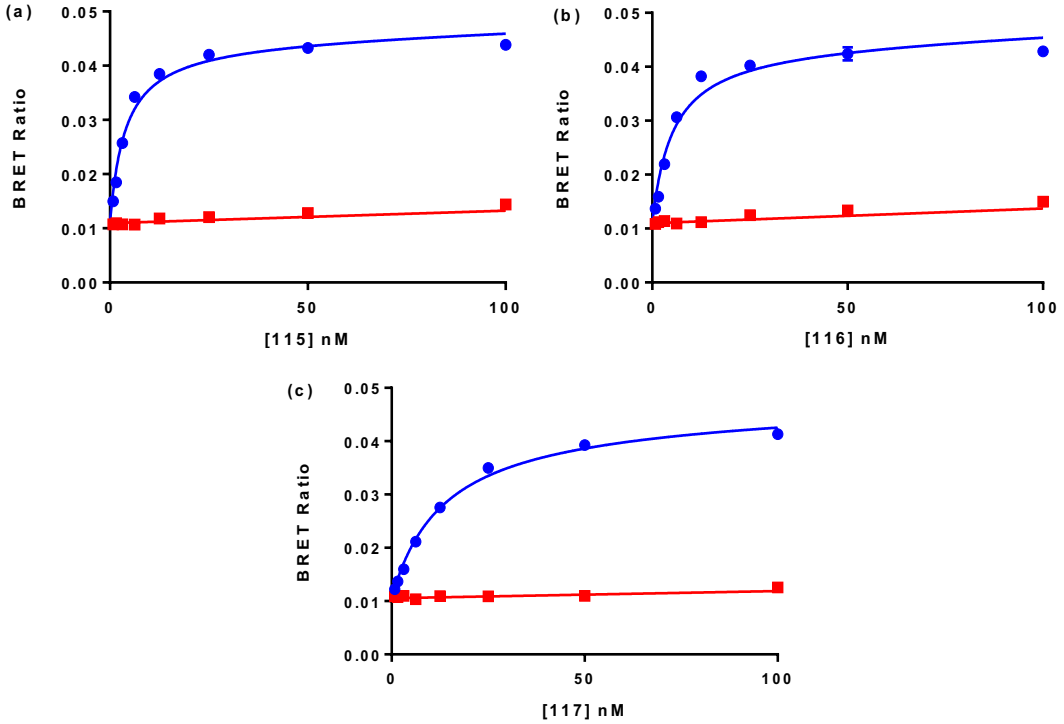

Figure 3.11: Saturation binding curves from NanoBRET experiments in Nluc-H_1R expressing HEK cells with increasing concentrations of fluorescent ligands **115 (a)**, **116 (b)** and **117 (c)** in the absence (red) or presence (blue) of 10µM mepyramine. The data shown are representative of four independent experiments performed in triplicate and the data points are expressed in mean ±SEM and error bars are within the limits of the symbols.

Compound **107** (V-S-N linker) and **117** (F-A-A linker) were subjected to further pharmacological characterisation in order to investigate the effects of the optimised peptide linker on other pharmacological properties such as H_1R selectivity and binding kinetics. To this end, a BRET saturation binding assay was also carried out using **107** and **117** on cell membrane preparations from Nluc-H_3R and Nluc-H_4R HEK293T cells to determine their binding affinities at H_3R and H_4R and subsequently their selectivity for H_1R. The assay was performed in the presence of a commercially available (HelloBio, Bristol) clobenpropit-based BODIPY 630/650 H_3R fluorescent ligand (**Clo-BDY**) as a positive control in the same assay plate. Clobenpropit was used to determine non-specific binding at both receptors. Concentration-dependent and saturable binding was observed for **Clo-BDY** at H_3R and H_4R (Figure 3.12), with pK_D values of 7.36 ± 0.05 and 7.51 ± 0.04 respectively (Table 2.10) and agreed well with existing literature values (7.89 and 7.15 respectively; see section 1.3.2.4)[72]. Compound **107** and **117** on the other hand exhibited little to no binding at H_3R and H_4R at concentrations of up to 1µM (Figure 2.24), indicating that they bind selectively to H_1R with at least 250- and 83-fold selectivity respectively.

Cpd	**Nluc-H_3R**		**Nluc-H_3R**	
	pK_D ± SEM	K_D (nM)	pK_D ± SEM	K_D (nM)
107	<6	<1000	<6	<1000
117	<6	<1000	<6	<1000
Clo-BDY	7.36 ± 0.05	44 ± 3	7.51 ± 0.04	31 ± 2

Table 3.6: Binding affinities of **107, 117** and **Clo-BDY** at NLuc-H_3R and NLuc-H_4R determined using a NanoBRET saturation binding assay performed on cell membrane preparations from Nluc-H_3R and Nluc-H_3R expressing HEK293T cells. The data shown are the means ± SEM from three experiments.

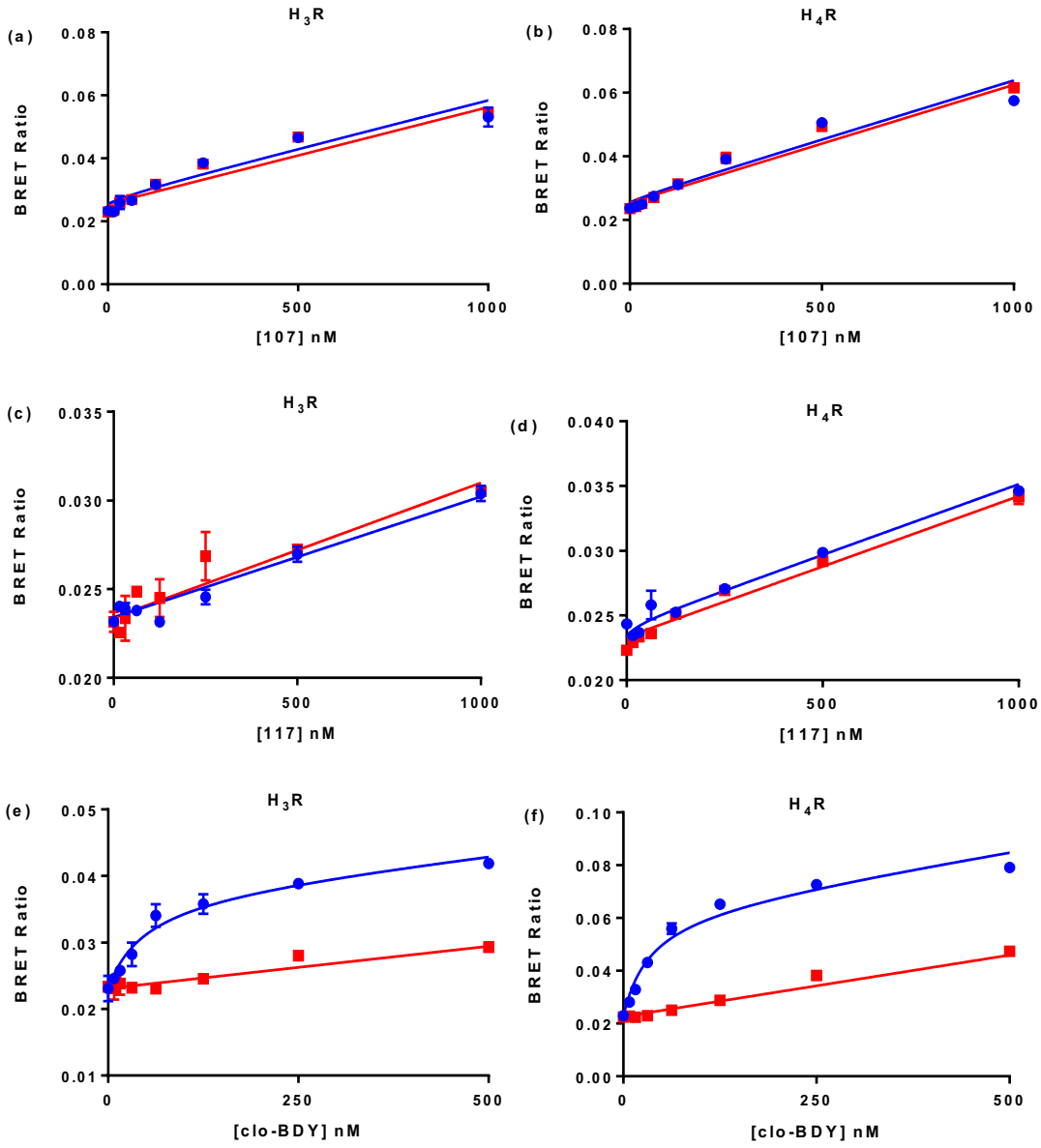

Figure 3.12: Saturation binding curves from NanoBRET experiments in cell membrane preparations from Nluc-H_3R (**a**, **c**, **e**) and Nluc-H_4R HEK293T cells (**b**, **d**, **f**) with increasing concentrations of fluorescent ligands **107** (**a, b**), **117** (**c, d**) and **Clo-BDY** (**e, f**) in the absence (red) or presence (blue) of 10µM clobenpropit. The data shown are representative of three independent experiments performed in duplicate and the data points are expressed in mean ± SEM and error bars are within the limits of the symbols if not shown.

The lack of efficacy of drug candidates in drug discovery programmes have led to a growing appreciation for evaluating binding kinetics of biologically active compounds for GPCRs over the recent years[146-149]. Biological activity of drug candidates is usually reported as K_D, K_B, K_i or IC_{50} determined from *in vitro* assays, which are performed under conditions whereby the ligand and receptor are present at a fixed concentration irrespective of time throughout the course of the experiment and ligand binding equilibrium is achieved[148]. These assessments of biological activity however, do not mimic *in vivo* conditions whereby the concentration of the ligand to which the target receptor is exposed is not fixed but varies with time after dosing due to partitioning to other parts of the body and clearance, as well as a non-equilibrium state in ligand binding[148]. As such, it is proposed that ligand binding kinetics parameters such as k_{on}, k_{off} and especially ligand-receptor residence time (T_r) should be determined to provide a more holistic picture on the *in vivo* biological activity of a ligand to guide candidate progression during drug discovery as well as to provide information on duration of action of the ligand at the receptor of interest. For instance, levocetirizine which has a reported T_r of 142 mins (slightly more than > 2 hours) was found to have a long duration of action (at least 24 hours) in the inhibition of histamine-induced wheal and flare response[150-151].

In the context of fluorescent ligands, having a long T_r at the receptor of interest would allow fluorescent ligands remain bound on the receptor and the receptor reversibly fluorescent-tagged for a longer period of time. This would enable *in vivo* studies for assessing drug-target engagement be performed using fluorescent ligands such as that demonstrated by Alcobia et. al[76]. Compound **13** had a T_r of approximately 1 hour and it would be interested to know whether linker optimisation had an effect on overall fluorescent ligand binding kinetics[3]. To study the effects of the peptide linker on the binding kinetics of the final fluorescent compound, a NanoBRET association kinetics study was performed using **107** and **117** on Nluc-H_1R expressing HEK293 cells, with BRET monitored at room temperature every minute for 90 minutes (Figure 3.13). The k_{on}, k_{off}, residence time (T_r) and pK_D values were determined and expressed in mean values ± SEM of four independent repeats (Table 3.7). Binding kinetics of the two compounds were similar and comparable to that of **13** which also had a T_r of almost an hour[3]. The pK_D values determined from binding kinetics experiments were

slightly lower than that obtained from saturation binding experiments (4-fold and 2-fold for **107** and **117** respectively). It was concluded that the peptide linker composition had a limited effect on the binding affinity and kinetics of the final fluorescent compound.

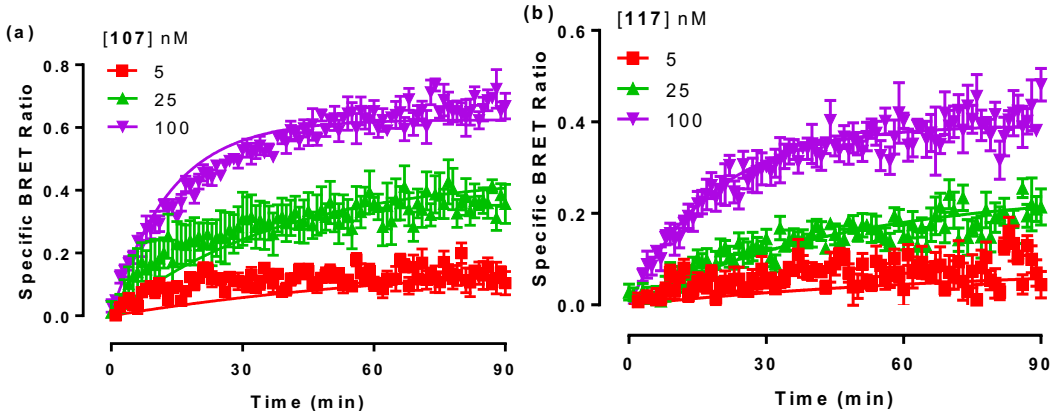

Figure 3.13: NanoBRET association kinetic studies performed on Nluc-H_1R HEK293T cells treated with the indicated concentrations of **107 (a)** and **117 (b**), with BRET monitored at room temperature every min for 90 mins. The data points shown are mean ± SEM and representative examples from five (**107**) or four (**117**) independent experiments performed in triplicates.

Cpd	AA1-AA2-AA3	k_{on} (x $10^6 M^{-1}$ min^{-1})	k_{off} (min^{-1})	T_r (min)	pK_D	n
107	V-S-N	0.839 ± 0.103	0.0144 ± 0.002	75.6 ± 10.2	7.75 ± 0.04	5
117	F-A-A	0.686 ± 0.244	0.0142 ± 0.003	78.8 ± 14.4	7.64 ± 0.12	4

Table 3.7: Association rate, dissociation rate, residence time and pK_D values of **107** and **117** determined from real-time NanoBRET binding kinetics experiment performed on Nluc-H_1R HEK293T cells.

3.3.4 Confocal Imaging

The fluorescent ligand with the highest binding affinity at H_1R **107** was subsequently used for visualising the receptor at the single cell level using confocal microscopy to further investigate its utility in conducting cell imaging experiments. Varying concentrations of **107** (1nM, 5nM, 10nM and 25nM) were incubated with Chinese Hamster Ovary (CHO) cells expressing H_1R-YFP at 37°C in the presence and absence of 10µM mepyramine pre-treatment, to determine non-specific binding. The cells were visualised using two different channels, both separately and combined. The green channel (BP505-30 filter) allowed only the visualisation of the receptor whereas the red channel (650nM long pass filter) for the red-shifted fluorescent ligand.

Confocal imaging revealed that **107** was localised to the plasma membrane of the cells with no intracellular accumulation across all ligand concentrations, which suggested its inability to cross the plasma membrane. This could be attributed to the hydrophilicity of the peptide linker which led to a decrease in overall ligand lipophilicity and its ability to cross the plasma membrane[3]. Receptor binding was specific and displaceable as shown in the overlay of the green and red channels (top right panel, Figure 3.14) as well as the lack of signal in the red channel in the wells containing a high concentration of mepyramine (bottom middle panel, Figure 3.14). No signal was observed in the red channel at 1nM and 5nM of **107**, suggesting that at these concentrations **107** would not be useful for confocal imaging purposes. In one independent experiment, however, where the incubation time was approximately 1 hour instead of 30 minutes, ligand binding was observed with 5nM of **107**, indicating that 5nM concentration of **107** could also be useful for cell imaging if incubated for a longer period. This could be attributed to the low k_{on} of **107** and hence a longer incubation time would be required to reach the equilibrium state. Residual signal was observed on the red channel at 25nM of **107** in the presence of mepyramine and was believed to be due to ligand aggregation on cellular debris. A concentration of 10nM of **107** would be ideal for H_1R confocal imaging studies as receptor binding could be observed with little to no non-specific binding, resulting in confocal images with good signal-to-noise ratio.

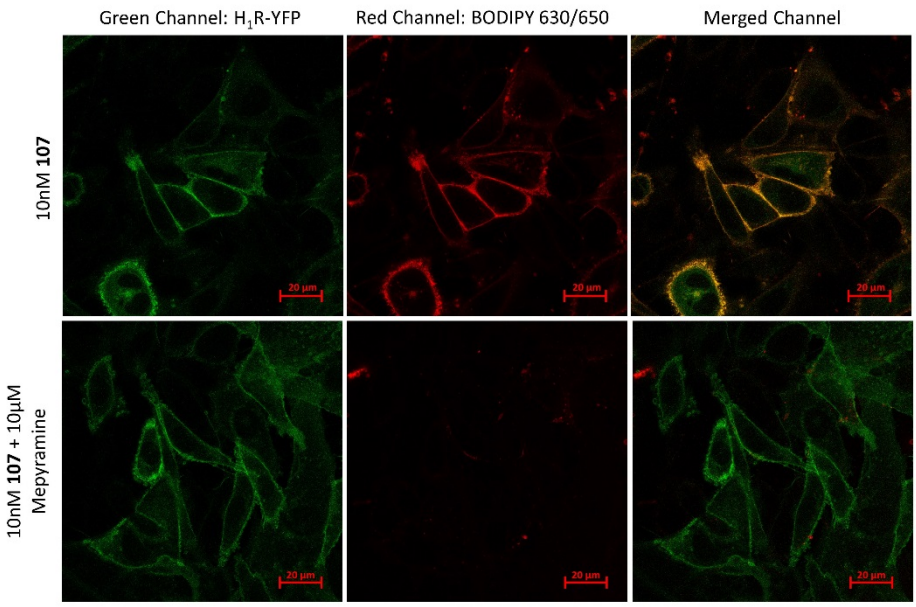

Figure 3.14: Confocal images of H_1R-YFP expressing CHO cells at 10nM of **107** in the absence and presence of 10μM mepyramine observed under the red and green channels separately and together. The data shown represented one of three independent experiments performed.

3.4 Summary

Efforts towards the synthesis of new generation H_1R fluorescent ligands based on the ideal peptide linker reported in section 2.2 yielded a high affinity H_1R selective fluorescent ligand **107** (pK_D = 8.40 ± 0.08) which could be used for cellular imaging at 10nM concentration. The binding affinity and binding kinetics of **107** at H_1R, however, were similar to that of **13** and **117** despite having the optimised V-S-N linker. In addition, fluorescent ligands with the optimised V-S-N linker have similar binding affinities compared to their counterpart across all three new generations of fluorescent ligand. It appears that the peptide linker does not play a major role in influencing the binding affinity of the final fluorescent ligand and the fluorophore maybe playing an important role in influencing the binding affinity of the final fluorescent ligand. This was subsequently investigated and is described in Chapter 4.

CHAPTER 4: THE EFFECTS OF THE FLUOROPHORE ON THE BINDING AFFINITY OF PEPTIDE LINKER-BASED H_1R FLUORESCENT LIGANDS AND MOLECULAR DOCKING STUDIES

Efforts to improve the binding affinity of H_1R fluorescent ligands by optimisation of the peptide linker as described in Chapter 3 highlighted the possibility that the fluorophore might be heavily influencing the overall binding affinity of H_1R fluorescent ligands and overriding the linker SAR. NanoBRET saturation binding experiment and calcium mobilisation assay involving fluorescent ligands with either the V-S-N or A-A-A peptide linkers coupled to varying fluorophores in combination with lipophilicity analysis provided convincing evidence that the fluorophore did indeed played a significant role in influencing the binding affinity of H_1R fluorescent ligands. Finally, molecular docking prediction highlighted several amino acid residues lining the receptor entry route which could interact with the peptide linker as well as a possible ligand-receptor interaction surrounding the fluorophore.

4.1 Approach and Ligand Design

Efforts undertaken for the optimisation of the peptide linker did not have a significant effect on the binding affinity of the new generation of H_1R fluorescent ligands and led to the hypothesis that the fluorophore was in fact significantly influencing the binding affinity of these fluorescent ligands. To study this, peptide congeners **96** and **106** were synthesised and attached to commercially available fluorophores such as BODIPY 630/650-X, BODIPY FL, BODIPY FL-X (Molecular Probes, Eugene, OR) and Sulfo-Cy5 (Lumiprobe, Hunt Valley, MD) via amide coupling. The hydrophilic sulfonic acid containing Sulfo-Cy5 fluorophore was included to explore whether overall ligand affinity following fluorophore conjugation was mainly lipophilicity-driven. Two hybrid fluorophores (BODIPY A and BODIPY B) were designed based on the BODIPY 630/650 and BODIPY FL fluorophores and had clogP values and fluorophore sizes between that of BODIPY 630/650 and BODIPY FL fluorophores (clogP values of the fluorophore-COOH) were calculated using ChemBioDraw Ultra 14). This allowed the effects of the gradual decrease in lipophilicity and size of the fluorophore on overall conjugate

affinity be studied (Figure 4.1). BODIPY A and B were carboxy-functionalised to allow for facile conjugation via amide coupling. A total of 12 fluorescent ligands, with either the V-S-N or the F-A-A linker, were synthesised and their binding affinities at the H_1R determined through NanoBRET binding and calcium mobilisation assays.

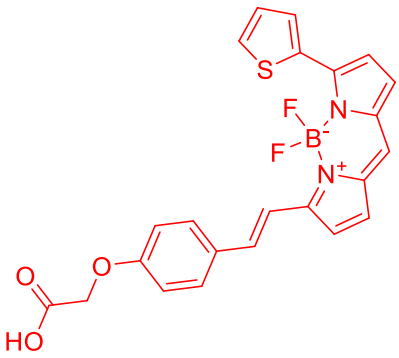

BODIPY 630/650-COOH
cLogP = 6.55

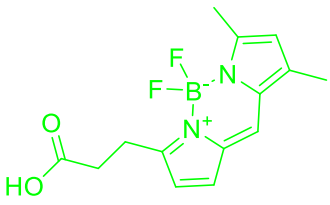

BODIPY FL-COOH
cLogP = 3.50

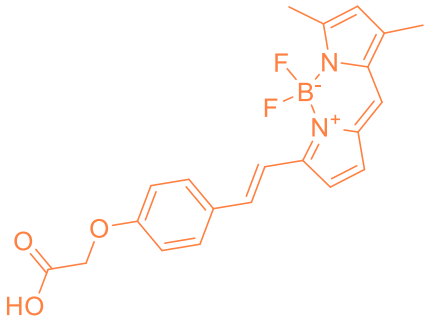

BODIPY A-COOH
cLogP = 5.59

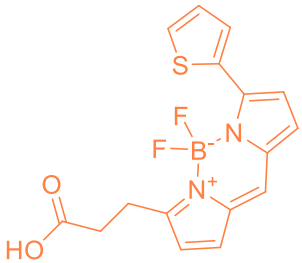

BODIPY B-COOH
cLogP = 4.46

Figure 4.1: Structure of BODIPY 630/650-COOH, BODIPY FL-COOH and the two hybrid fluorophores BODIPY A-COOH and BODIPY B-COOH. cLogP values were calculated from ChemBioDraw Ultra 14.

4.2 Synthesis

Syntheses of fluorescent ligands are described in two parts, namely, (i) the synthesis of BODIPY A and BODIPY B and (ii) the synthesis of the peptide congener and the coupling of the fluorophore through an amide bond.

4.2.1 Synthesis of BODIPY A and BODIPY B

The synthesis of BODIPY A is summarised in Scheme 4.1. Compound **76** (section 3.1.3.1) was subjected to demethylation using sodium ethanthiolate and subsequent alkylation with methyl bromoacetate yielded methyl (*E*)-2-(4-(2-(1*H*-pyrrol-2-yl)vinyl)phenoxy)-acetate **118**. Compound **118** was then condensed with 3,5-dimethyl-1*H*-pyrrole-2-carbaldehyde in the presence of $POCl_3$ and $BF_3{\cdot}Et_2O$ afforded the BODIPY ester **119**. The free acid **120** was liberated by stirring **119** in a weak acid such as H_3PO_4 for approximately 4 days.

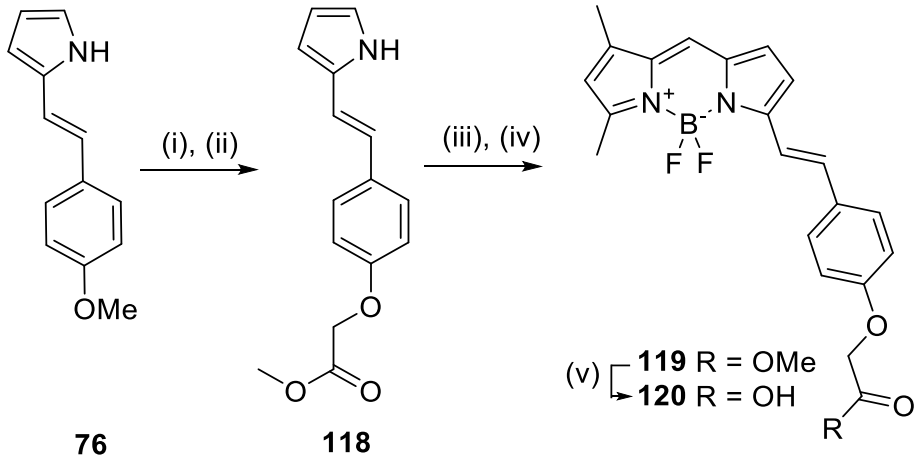

Scheme 4.1: Synthesis of BODIPY A **120**. (i) Sodium ethanethiolate, anhydrous DMF, heated under reflux, N_2, 15 hr. (ii) methyl bromoacetate, K_2CO_3, ACN, heated to reflux, 15 hr, 69%. (iii) $POCl_3$, anhydrous DCM, RT, 15 hr. (iv) 3,5-dimethyl-1*H*-pyrrole-2-carbaldehyde, $BF_3{\cdot}Et_2O$, DIPEA, DCM, RT, 2 hr, 19%. (v) 85% H_3PO_4, THF/H_2O:2:1, 65°C, N_2 atm, 90 hr, 92%.

The synthesis of BODIPY B is summarised in Scheme 4.2. BODIPY B was synthesised from **71** and methyl 3-(1*H*-pyrrol-2-yl)propanoate in the presence of $POCl_3$ and $BF_3{\cdot}Et_2O$, with subsequent acid cleavage of the ester to give the free acid product **121**.

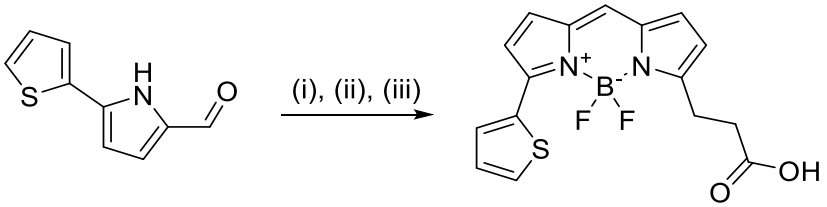

71 **121**

Scheme 4.2: Synthesis of BODIPY B. (i) Methyl 3-(1*H*-pyrrol-2-yl)propanoate, $POCl_3$, anhydrous DCM, RT, 15 hr. (ii) $BF_3{\cdot}Et_2O$, DIPEA, DCM, RT, 2 hr, 17%. (iii) 85% H_3PO_4, THF/H_2O:2:1, 65^oC, N_2 atm, 90 hr, 63%.

4.2.2 Synthesis of the Peptide Congener and Fluorophore Coupling

Peptide congeners with the V-S-N **96** and F-A-A linker **106** were synthesised through SPPS and coupled to six different fluorophores through amide bond formation in the presence of HATU for BODIPY A and BODIPY B (**123-124** and **129-130**) and absence of HATU for BODIPY630/650-X-NHS ester, BODIPY-FL-NHS ester, BODIPY FL-X-NHS ester and Sulfo-Cy5-NHS ester fluorophores (**122**, **125-128** and **131-133**) to give twelve H_1R fluorescent ligands, which upon HPLC purification afforded **122-133** (Scheme 4.3). Purity and identity of the compounds were confirmed using analytical HPLC and HRMS respectively.

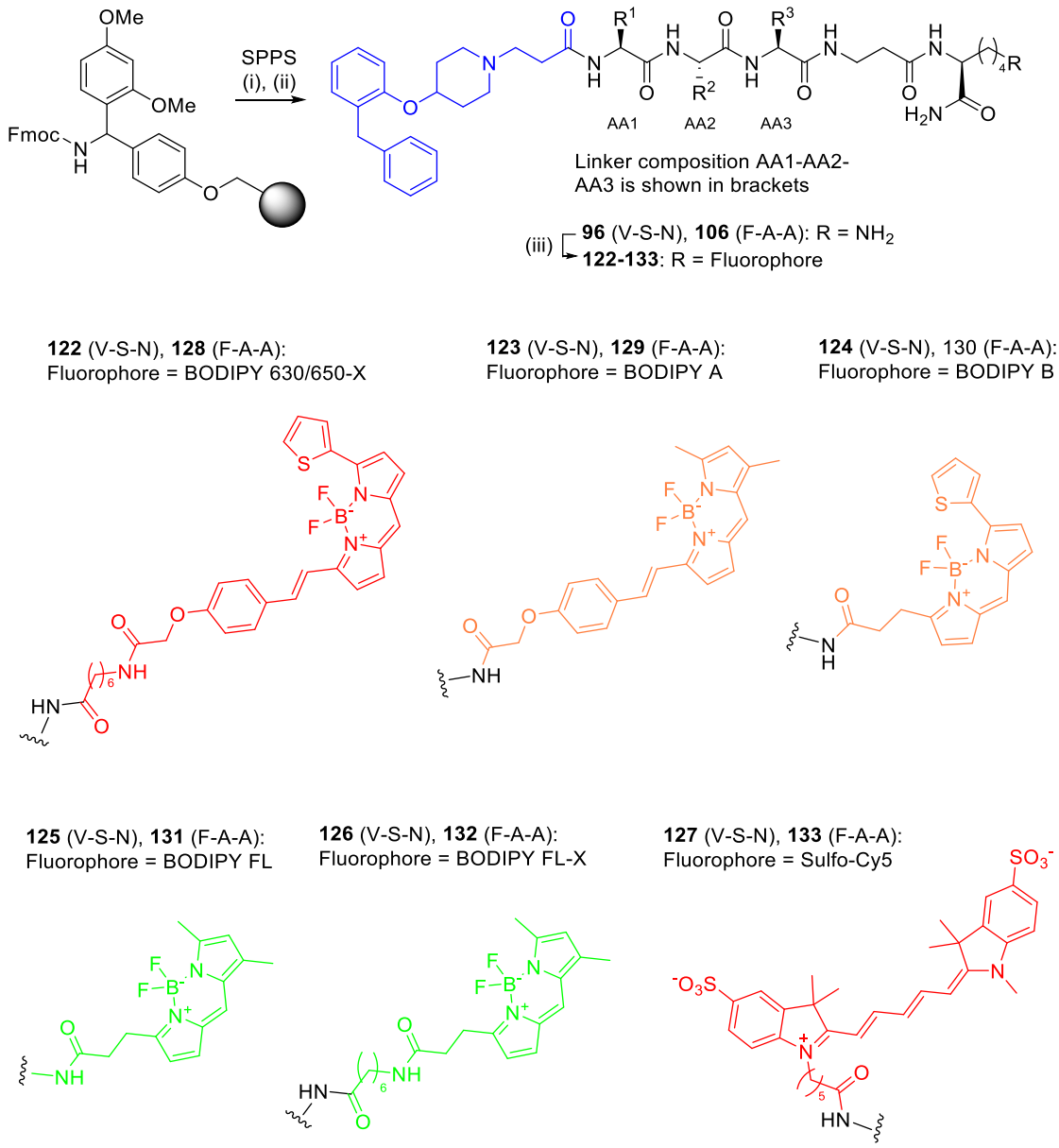

Scheme 4.3: Synthesis of twelve VUF13816-based fluorescent ligands with varying peptide linkers and fluorophores. (i) Coupling cycle: Fmoc-amino acid, HBTU, HOBt, DIPEA, DMF, RT, 2-4 hr; deprotection cycle: 20% piperidine in DMF, RT, 5 min. (ii) 95% TFA in water, RT, 6 hr, 4-8% overall yield. (iii) **122**, **125-128, 131-133**: Fluorophore-NHS ester, DMF, RT, 2 hr; **123**, **129**: BODIPY A, HATU, DIPEA, DMF, RT, 2 hr, 41-82%; **124**, **130**: BODIPY B, HATU, DIPEA, DMF, RT, 2 hr; 58-79%.

4.3 Fluorescence Spectroscopy and Pharmacology

123, **124**, **129** and **130** were spectrally characterised on a multi-well fluorometric imaging plate reader FlexStation3 (Molecular Devices, Sunnyvale, CA) in order to determine their absorption/emission spectral profiles and filters suitable to carry out the NanoBRET experiments on the Pherastar FS plate reader. Subsequently, **122-133** were pharmacologically characterised through NanoBRET experiments and calcium mobilisation assays.

4.3.1 Absorption/Emission Spectral Characterisation

The $\lambda_{max,ex}/\lambda_{max,em}$ of **123**, **124**, **129** and **130** were determined in both 10% DMSO/HBSS and 100% DMSO at a concentration of 100µM (Table 4.1; spectra available in Appendix). The $\lambda_{max,ex}/\lambda_{max,em}$ of **123**, **124**, **129** and **130** were in the orange region (560-572nm/570-594nm) and not the red region due to the reduction in conjugation in the hybrid fluorophore structures compared to the red-shifted BODIPY 630/650. Subsequently, NanoBRET saturation experiments performed on **123**, **124**, **129** and **130** would utilise a light detection filter module of a shorter wavelength (550nm-long pass) on the PheraStar FS plate reader.

	Fluorophores	10% DMSO/HBSS		100% DMSO	
		$\lambda_{max,ex}$ (nm)	$\lambda_{max,em}$ (nm)	$\lambda_{max,ex}$ (nm)	$\lambda_{max,em}$ (nm)
123	BODIPY A	570	586	574	594
124	BODIPY B	562	570	566	576
129	BODIPY A	572	584	576	594
130	BODIPY B	560	570	566	576

Table 4.1: Excitation/emission profile of **123**, **124**, **129** and **130** in 10% DMSO/HBSS and 100% DMSO determined using a multi-well fluorometric imaging plate reader FlexStation3 (Molecular Devices, Sunnyvale, CA).

4.3.2 Pharmacology

The binding affinities of the fluorescent ligands at H_1R were determined by NanoBRET saturation binding assay performed on NLuc-H_1R expressed on HEK293 cells. The given pK_D values are mean values ± SEM of four independent repeats (Table 4.2). Concentration-dependent and saturable binding was observed for all twelve fluorescent compounds (Figure 4.2 and Figure 4.3). Saturation binding curves of

BODIPY FL-based fluorescent ligands (**125**, **126**, **131** and **132**) indicated a small difference between total binding (absence of mepyramine) and non-specific binding signals (presence of mepyramine) (Figure 4.3(c), (d), (e), (f)). This was possibly attributed to the significant emission spectral overlap of Nluc ($\lambda_{max,em}$ = 460nm) and BODIPY FL ($\lambda_{max,em}$ = 512nm) which led to the bleed-through of the BRET luminescence signal from Nluc into the fluorescence channel (detection at 530-535nm)[53]. Nevertheless, specific binding curves generated from subtracting the non-specific binding signal from the total binding signal indicated that the binding of BODIPY FL-based fluorescent ligands **125-126** and **131-132** were indeed concentration-dependent and saturable (Figure 4.4).

Fluorophore	**AA1-AA2-AA3 = V-S-N**			**AA1-AA2-AA3 = F-A-A**		
	Cpd	pK_D ± SEM	K_D (nM)	Cpd	pK_D ± SEM	K_D (nM)
BODIPY 630/650	**107**	8.40 ± 0.08	4 ± 1	**117**	7.92 ± 0.08	13 ± 3
BODIPY 630/650-X	**122**	7.74 ± 0.06	19 ± 2	**128**	7.98 ± 0.01	11 ± 1
BODIPY A	**123**	7.18 ± 0.11	74 ± 16	**129**	7.36 ± 0.03	44 ± 3
BODIPY B	**124**	6.68 ± 0.10	224 ± 46	**130**	6.14 ± 0.06	749 ± 96
BODIPY FL	**125**	5.89 ± 0.10	1411 ± 382	**131**	5.84 ± 0.13	1624 ± 435
BODIPY FL-X	**126**	5.28 ± 0.06	5400 ± 818	**132**	5.57 ± 0.05	2757 ± 322
Sulfo-Cy5	**127**	5.66 ± 0.02	2206 ± 94	**133**	5.66 ± 0.06	2264 ± 323

Table 4.2: Binding affinities of **107**, **117** and **122-133** using a NanoBRET saturation binding assay performed on Nluc-H_1R expressed on HEK293 cells. The data shown are the means ± SEM from three experiments.

The BODIPY 630/650-based fluorescent ligands **107 117**, **122** and **128** had the highest binding affinity at H_1R, with pK_D of greater than or approximately 8. Interestingly, as the lipophilicity of the fluorophore decreases from BODIPY 630/650 to the water soluble Sulfo-Cy5 for fluorescent ligands with either linkers, binding affinity of the fluorescent ligands decreases gradually. This suggested that the fluorophore did indeed played a significant role in influencing the binding affinities of the fluorescent ligands. There was little or no difference (less than 4-fold) in binding affinity at H_1R for fluorescent ligands with the optimised V-S-N linker (**107**, **122-127**) compared to their counterpart with the unoptimized F-A-A linker (**117**, **128-133**). These findings provided further evidence that the peptide linker exerted little effect on overall fluorescent ligand binding affinity and that the lipophilicity of the fluorophore was

playing an overarching role in influencing the binding affinities of the fluorescent ligands[142]. BODIPY FL-based fluorescent ligands (**125-126, 131-132**) had similar pK_D values (5.28~5.89) compared to their Sulfo-Cy5-based counterparts (**127**, **133**) despite significant differences in the properties of their fluorophores in terms of lipophilicity and size. This would suggest that solely having a lipophilic fluorophore such as that of BODIPY FL could not improve overall fluorescent ligand binding affinity and there might be a certain minimal threshold in terms of lipophilicity or size of the fluorophore for the fluorophore to contribute positively to the binding affinity of fluorescent ligands. The fluorescent ligands with the additional hexanyl spacer (**122**, **128**, **125**, **131**) had similar binding affinities compared to their counterparts without the spacer (**107**, **117**, **124**, **130**), indicating that the hexanyl spacer too had limited influence in H_1R fluorescent ligand binding affinity.

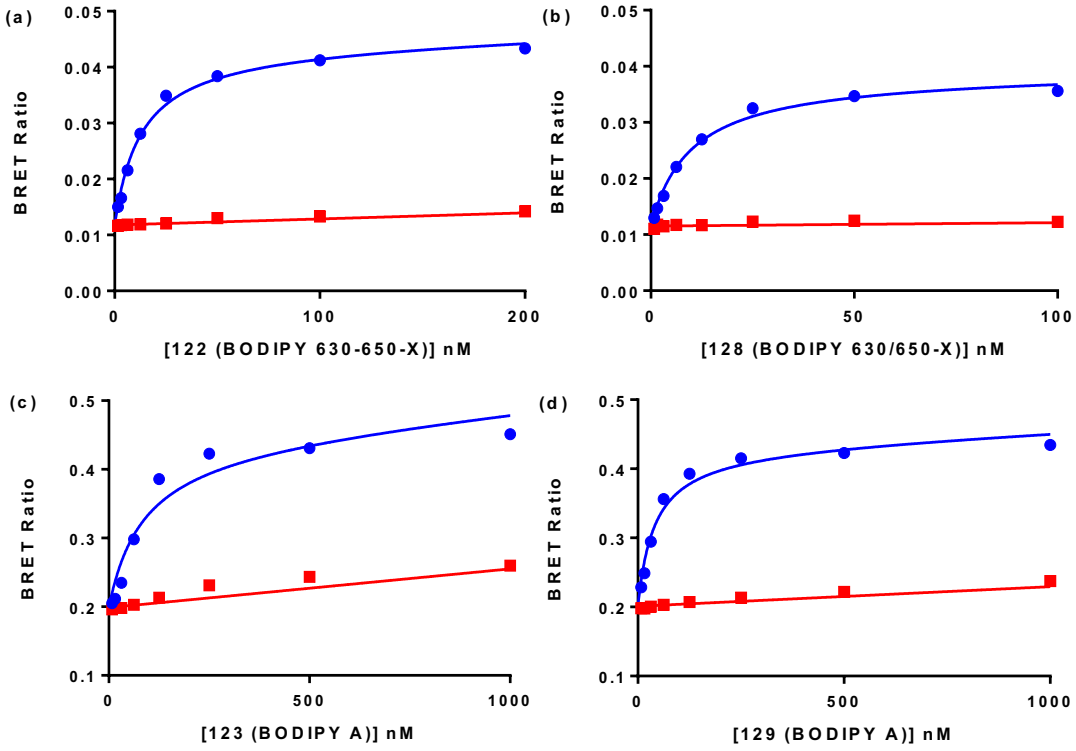

Figure 4.2: Saturation binding curves from NanoBRET experiments in NLuc-H_1R expressing HEK cells with increasing concentrations of fluorescent ligands **122 (a)**, **128 (b)**, **123 (c)** and **129 (d)** in the absence (red) or presence (blue) of 10µM mepyramine. The data shown are representative of four independent experiments performed in triplicate and the data points are expressed in mean ± SEM and error bars are within the limits of the symbols.

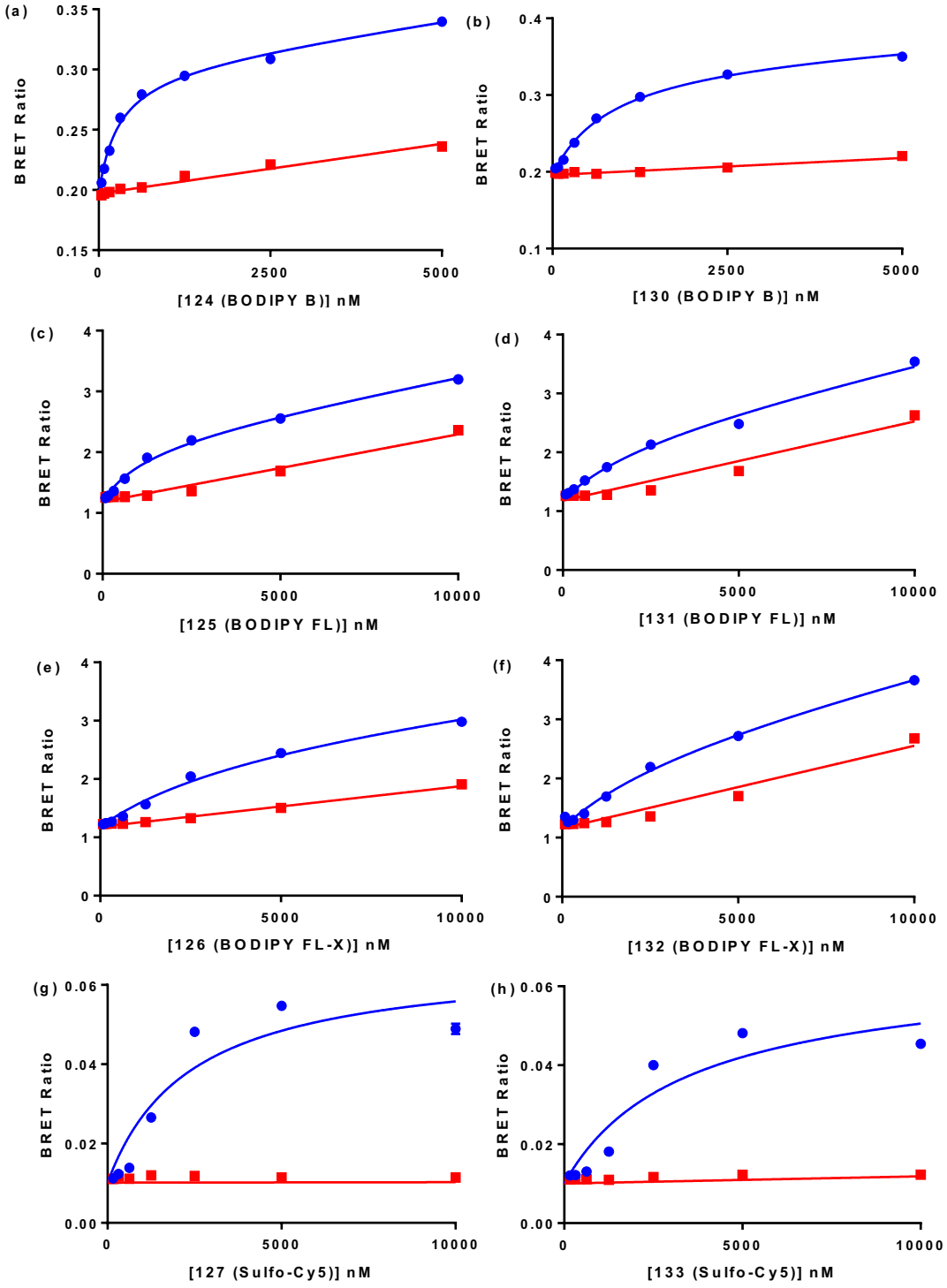

Figure 4.3: Saturation binding curves from NanoBRET experiments in NLuc-H_1R expressing HEK cells with increasing concentrations of fluorescent ligands **124 (a)**, **130 (b)**, **125 (c)**, **131 (d)**, **126 (e)**, **132 (f)**, **127 (g)** and **133 (h)** in the absence (red) or presence (blue) of 10µM mepyramine. The data shown are representative of four independent experiments performed in triplicate and the data points are expressed in mean ± SEM and error bars are within the limits of the symbols.

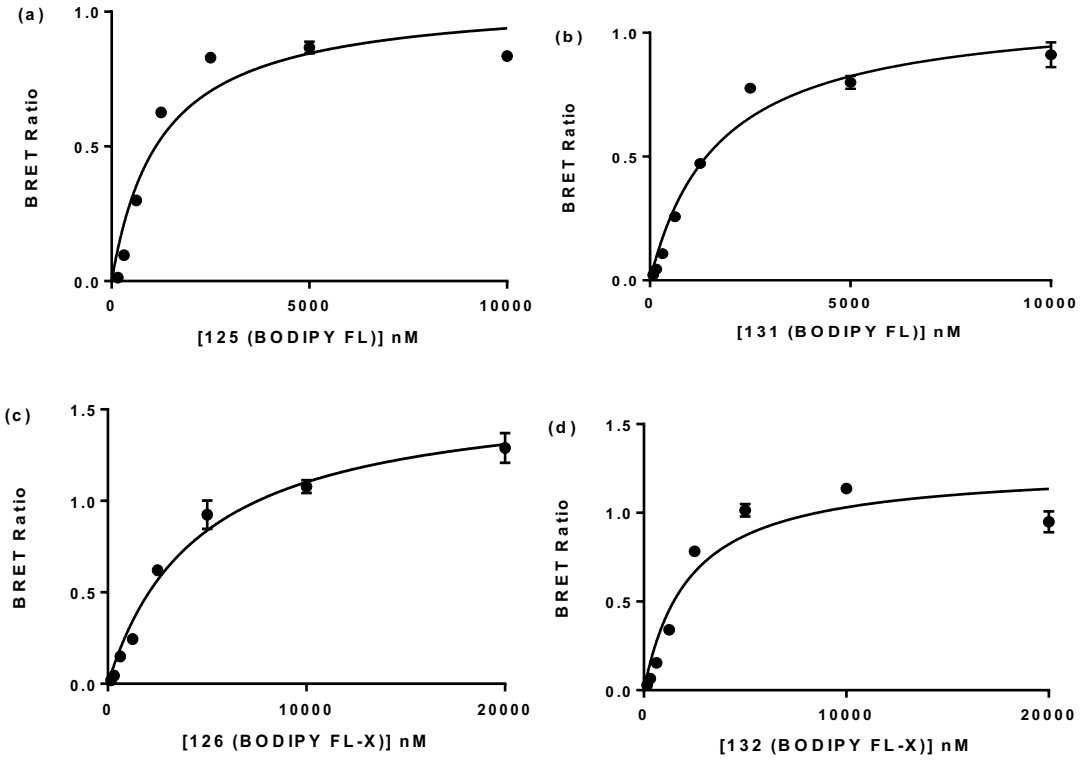

Figure 4.4: Specific binding curves of **125 (a)**, **131 (b)**, **126 (c)** and **132 (d)** indicating that binding was saturable. The data shown are representative of four independent experiments performed in triplicate and the data points are expressed in mean ± SEM and error bars are within the limits of the symbols.

The binding affinity at H_1R of ten selected fluorescent ligands **107**, **117**, **123-125, 127, 129-131** and **133** were also determined using calcium mobilisation assay in CHO cells expressing H_1R. All ten compounds exerted a rightward-shift in histamine mediated concentration response curves, indicating receptor antagonism (Figure 4.4). Maximum calcium response was not achieved in the presence of all fluorescent ligands due to the measurement of transient response and the non-equilibrium kinetics of calcium mobilisation assay (Figure 4.5)[152]. Estimation of antagonist affinity using the dose ratio in an agonist-stimulated calcium response assumes that a state of equilibrium is achieved between the agonist and the antagonist. However, due to the slow fluorescent antagonist dissociation kinetics of the compounds this equilibrium state was believed to be unachievable, coupled with the transient response measurement by the assay, leading to the phenomenon of an apparent insurmountable antagonism[152]. Hence, to minimise the influence of hemi-equilibrium on the estimation of the affinity of the fluorescent antagonists, dose ratios at low

agonist responses such as EC_{25} instead of EC_{50} were used as described by Kenakin et al. whereby in insurmountable antagonism pA_2 will tend towards pK_B at low agonist occupancy[153-154]. pK_B values obtained were similar to pK_D values determined from NanoBRET assay with differences of less than three-fold across all fluorescent ligands, with the exception of BODIPY FL-based fluorescent ligands **125** and **131**, providing further evidence that a gradual decrease in fluorophore lipophilicity and size led to a gradual decrease in binding affinity of the fluorescent ligands (Table 4.3).

Fluorophore	AA^1-AA^2-AA^3 = V-S-N			AA^1-AA^2-AA^3 = F-A-A		
	Cpd	pK_D ± SEM[a]	pK_B ± SEM[b]	Cpd	pK_D ± SEM[a]	pK_B ± SEM[b]
BODIPY 630/650	**107**	8.40 ± 0.08	8.69 ± 0.13	**117**	7.92 ± 0.08	8.39 ± 0.08
BODIPY A	**123**	7.18 ± 0.11	7.00 ± 0.09	**129**	7.36 ± 0.03	6.92 ± 0.05
BODIPY B	**124**	6.68 ± 0.10	6.55 ± 0.17	**130**	6.14 ± 0.06	6.29 ± 0.04
BODIPY FL	**125**	5.89 ± 0.10	6.98 ± 0.10	**131**	5.84 ± 0.13	7.34 ± 0.10
Sulfo-Cy5	**127**	5.66 ± 0.02	5.28 ± 0.16	**133**	5.66 ± 0.06	5.88 ± 0.16

Table 4.3: Binding affinities of **107, 117, 123-125, 127, 129-131** and **133** determined from NanoBRET assay[a] performed on Nluc-H_1R expressed on HEK293 cells and calcium mobilisation assay[b] performed on H_1R expressed on CHO cells. The data shown are the means ± SEM from four experiments.

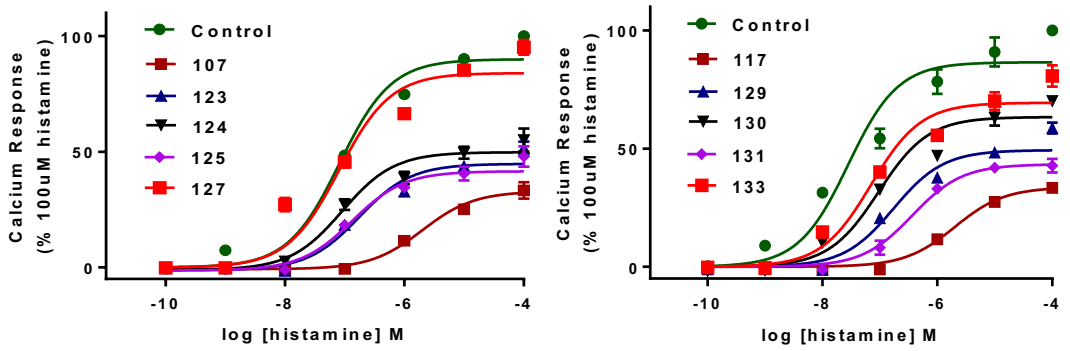

Figure 4.5: Rightward shift of histamine mediated calcium release response curves in the presence of the fluorescent ligands at a concentration of 1 µM. Data were normalized to basal (in the absence of histamine or antagonist) and 100 µM histamine for each experiment. The data shown represent the mean ± SEM of four experiments performed in duplicate.

4.4 Lipophilicity Analysis of H_1R Fluorescent Ligands

In order to investigate the relationship between the lipophilicity of the fluorescent ligands and their binding affinity at H_1R, the pK_D of ten fluorescent ligands (**107**, **117**, **123-125, 127, 129-131, 133**) were plotted against their cLogP values calculated using ChemBioDraw 14 on GraphPad Prism 7 and linear regression analysis was performed (Table 4.4, Figure 4.6). There was a weak positive correlation between the cLogP and pK_D of the fluorescent ligands (r^2 = 0.472, P = 0.028; Figure 4.6). This was consistent with pharmacological data indicating that although fluorescent ligands with the F-A-A linker (**117, 129-131** and **133**) were more lipophilic than their V-S-N linker counterpart (**107**, **123-125** and **127**) with differences in cLogP value of at least 2 units, they had similar if not slightly lower pK_D values. Therefore, lipophilicity of the overall fluorescent ligand does not appear to have a major role in influencing fluorescent ligand binding affinity.

Compound (V-S-N)	cLogP	pK_D (NanoBRET)	Compound (F-A-A)	cLogP	pK_D (NanoBRET)
107	6.650	8.40 ± 0.08	**117**	9.111	7.92 ± 0.08
123	6.088	7.18 ± 0.11	**129**	8.549	7.36 ± 0.03
124	4.005	6.68 ± 0.10	**130**	6.466	6.14 ± 0.06
125	4.073	5.89 ± 0.10	**131**	6.534	5.84 ± 0.13
127	-1.377	5.66 ± 0.02	**133**	1.084	5.66 ± 0.06

Table 4.4: cLogP values of fluorescent compounds calculated using ChemBioDraw 14 and their associated pK_D values determined from NanoBRET saturation binding assay performed on Nluc-H_1R expressed on HEK293 cells.

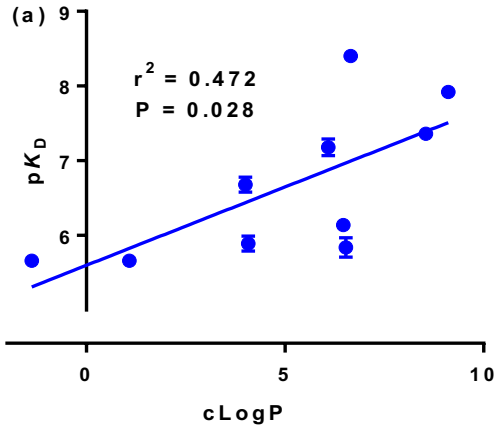

Figure 4.6: Linear regression analysis between pK_D against cLogP values of fluorescent compounds indicated weak positive correlation r^2 = 0.472, P = 0.028. The data points are expressed in mean ± SEM and error bars are within the limits of the symbols.

Throughout the study it was clear that the fluorophore played an indispensable role in influencing the binding affinity of the final fluorescent ligand at H_1R. The relationship between the binding affinity of fluorescent ligands (pK_D) and the lipophilicity (cLogP) of their respective fluorophores up to the amide bond was subsequently investigated by plotting the two parameters using GraphPad Prism 7 separately for fluorescent ligands with the V-S-N and F-A-A linkers and linear regression analysis was performed (Table 4.5, Figure 4.7). The analysis suggested a positive correlation between binding affinity (pK_D) and the lipophilicity of the fluorophore (r^2 = 0.668, P = 0.091 and r^2 = 0.617, P = 0.115) for florescent ligands with V-S-N linker (blue) and F-A-A linker (green) respectively; Figure 4.7a). Exclusion of **127** and **133** (sulfo Cy5-based fluorescent ligands) in the analysis indicated a very strong positive correlation between the lipophilicity of the BODIPY fluorophore and fluorescent ligand binding affinity (r^2 = 0.967, P = 0.017 and r^2 = 0.957, P = 0.022 for florescent compounds with V-S-N linker and F-A-A linker respectively; Figure 4.7b). This analysis, however, could not rule out the effects of fluorophore size on the binding affinity of fluorescent ligands as the lipophilicity and size of the BODIPY fluorophore are closely related to each other. Nevertheless, it is clear that the properties of the fluorophore do have a profound effect in the binding affinity of the final fluorescent ligand which could possibly be attributed to an improved ligand-receptor interaction surrounding the fluorophore space through hydrophobic effect.

Fluorophore	cLogP	Cpd (V-S-N linker)	pK_D (NanoBRET)	Cpd (F-A-A linker)	pK_D (NanoBRET)
BODIPY 630/650	6.411	**107**	8.40 ± 0.08	**117**	7.92 ± 0.08
BODIPY A	5.455	**123**	7.18 ± 0.11	**129**	7.36 ± 0.03
BODIPY B	4.428	**124**	6.68 ± 0.10	**130**	6.14 ± 0.06
BODIPY FL	3.472	**125**	5.89 ± 0.10	**131**	5.84 ± 0.13
Sulfo-Cy5	-1.377	**127**	5.66 ± 0.02	**133**	5.66 ± 0.06

Table 4.5: cLogP values of fluorophores calculated using ChemBioDraw 14 and pK_D values of their associated fluorescent ligands determined using NanoBRET saturation binding assay with either the optimised V-S-N or the unoptimised F-A-A peptide linker.

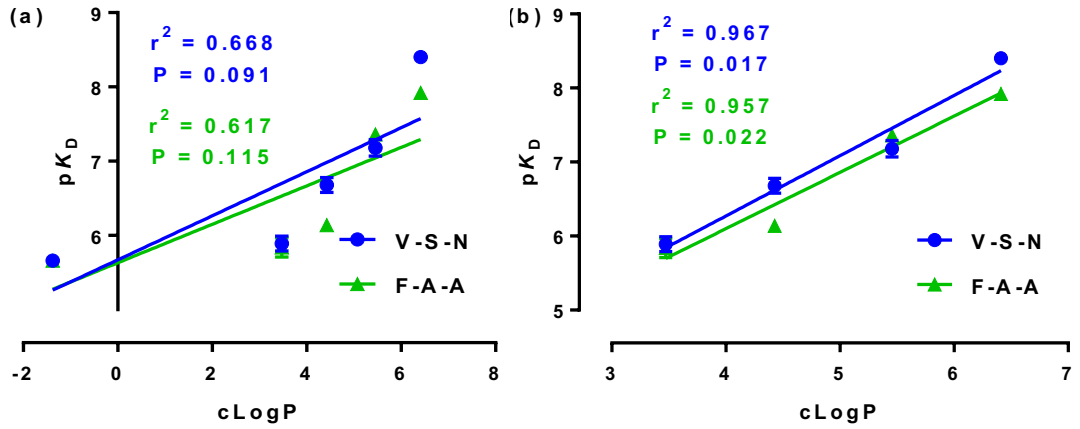

Figure 4.7: (a) Linear regression analysis was performed on the fluorophore lipophilicity of compound **107**, **117**, **123-125**, **127**, **130-133** and **133** and their respective pK_D values at Nluc-H_1R indicated strong positive correlation regardless of peptide linker composition, with r^2 = 0.668, P = 0.091 and r^2 = 0.617, P = 0.115 for the fluorescent compounds with the V-S-N and F-A-A linker respectively. (b) The exclusion of sulfo-Cy5-bearing fluorescent compounds **127** and **133** (analysis conducted using **107**, **117**, **123-125** and **129-131**) from the analysis resulted in a stronger positive correlation between lipophilicity and pK_D, with r^2 = 0.967, P = 0.017 and r^2 = 0.957, P = 0.022 for the fluorescent compounds with the V-S-N and F-A-A linker respectively. The data points are expressed in mean ± SEM and error bars are within the limits of the symbols.

4.5 Molecular Docking Studies

Compound **107** was subsequently docked in vacuo into a H_1R model derived from the H_1R crystal structure (PDB code: 3RZE) using Glide within the Schrödinger Molecular Modelling suite (see Experimental Section) to give a single docking pose (Green) which was subsequently overlaid with the binding pose of doxepin (Purple) retrieved from the H_1R crystal structure (Figure 4.8).

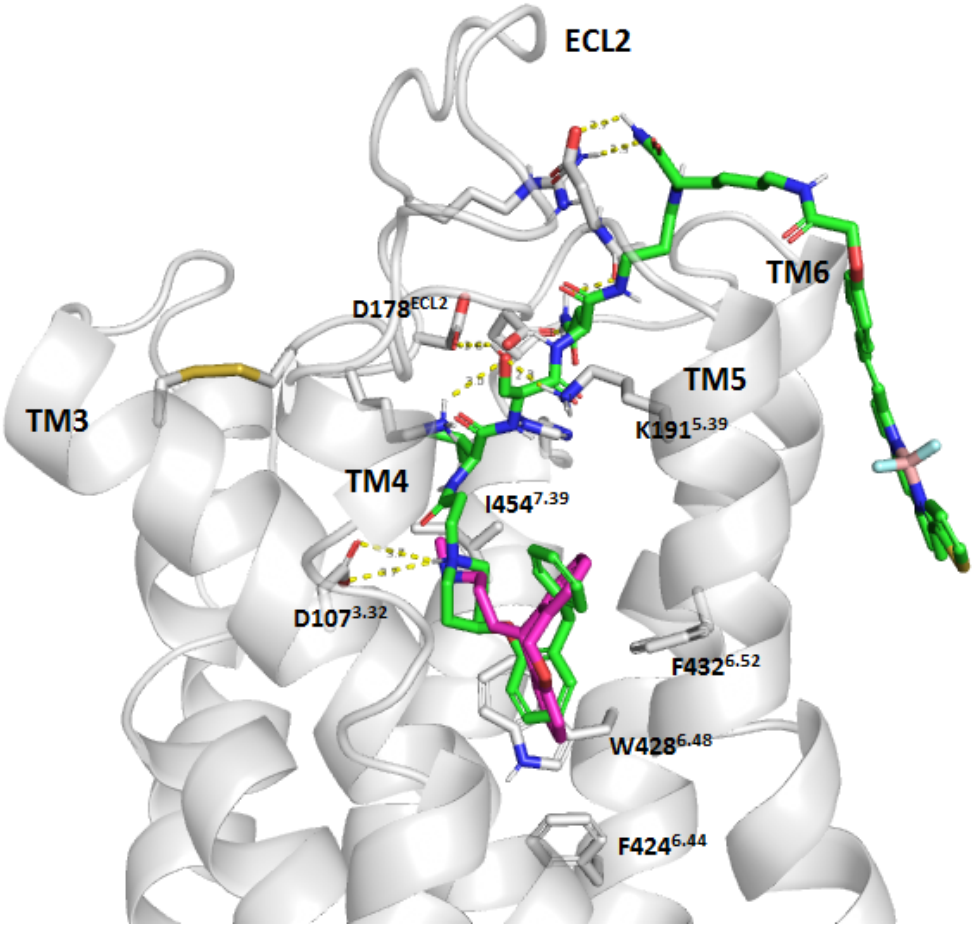

Figure 4.8: Binding pose prediction of **107** in a H_1R model using Glide docking (Green) overlaid with the binding pose of doxepin (Purple) retrieved from the H_1R crystal structure (PDB code: 3RZE) The transmembrane helices (TM) and amino acid residues interacting with the **107** binding pose are labelled.

The docking results suggested that the VUF13816 orthosteric binding motif of **107** could fit nicely within the orthosteric binding pocket surrounded by F424$^{6.44}$, W428$^{6.48}$ and F432$^{6.52}$ as well as forming the crucial salt bridge interaction between D107$^{3.32}$ and the protonated piperidine nitrogen (Figure 4.9a).

Residues lining the receptor ligand entry route which could interact with the peptide linker of **107** were also highlighted. The small and hydrophobic isopropyl group of Val (AA1) at R^1 was thought to be able to position itself in a hydrophobic space between I454$^{7.39}$ and H450$^{7.35}$ (Figure 4.9b). This would lead to the displacement of water molecules occupying this space, thus increasing the free energy of ligand binding and ligand binding affinity due to hydrophobic effect. This receptor space was also reported to be linked to the combined affinity/kinetics profile of rupatadine and its analogues[155]. Steric constraints surrounding this space as well as a lack of flexibility surrounding the peptide bonds within the linker to allow for side group orientation could have limited the variety of side groups which could be accommodated at this space. This might explain why the binding affinity of the V-A-A unlabelled congener (**44**, pK_i = 6.80 ± 0.12) was at least half a log unit better than the other congeners across the series 1 congeners.

The hydroxymethyl group of Ser (AA2) at R^2 was in close proximity with D178^{ECL2} (2.6Å), K179^{ECL2} (3.0Å) and K191$^{5.39}$ (2.3Å) and could potentially form hydrogen bond interactions (Figure 4.9c). The proximity of the acidic D178^{ECL2} to the basic residues of K179^{ECL2} and K191$^{5.39}$ could explain why fluorescent ligands (**32**, **76**) and congeners (**37**, **60**) with R^2-acidic peptide linkers did not have a high binding affinity at H_1R, which was due to unfavourable electrostatic repulsion between D178^{ECL2} and the R^2-acidic side groups. The Asn (AA3) side group at R^3 could form hydrogen bond interactions with N443^{ECL3} (2.3Å) and E447$^{7.32}$ (1.7Å) (Figure 4.9d). Despite providing information on the potential ligand-receptor interaction at R^2 and R^3, it was important to acknowledge that the proposed residues interacting with the linker at R^2 and R^3 were hydrophilic and mainly located within the extracellular loop of the receptor (except for K191$^{5.39}$ and E447$^{7.32}$). As such, ligand-receptor interactions at R^2 and R^3 would be formed at the expense of existing water hydrogen bond network, with the free energy gained from hydrogen bonding between the interaction

offsetting the energy required to disrupt this water network. The flexible nature of the extracellular loop region would likely suggest that a fixed conformation for this region is not adopted, making the extracellular vestibule of the receptor hard to target for improving ligand-receptor interaction. This is likely to explain why optimisation of the peptide linker at R^2 and R^3 did not improve the binding affinity of Series 2 and 3 unlabelled congeners and the improvements in unlabelled congener binding affinity through linker optimisation was mainly attributed to the Val side group at R^1.

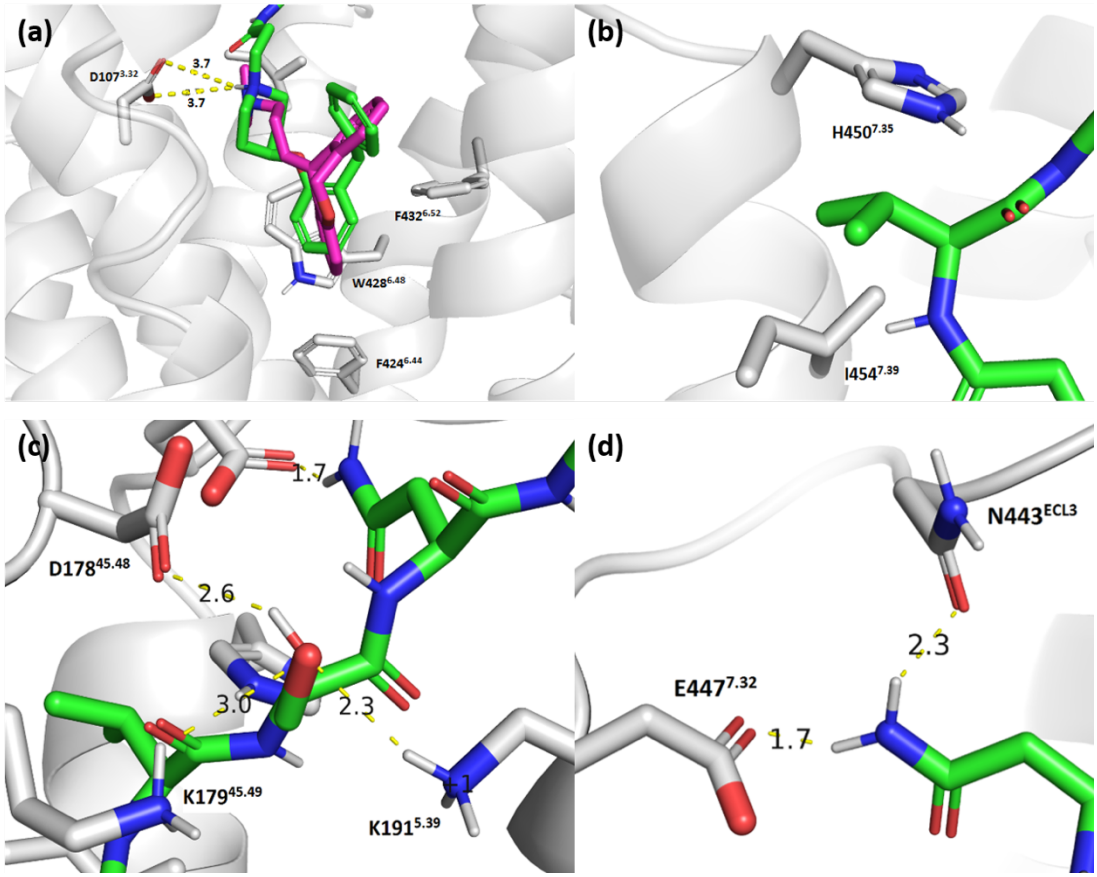

Figure 4.9: (a) VUF13816 based motif binding to the orthosteric pocket and overlays well with the doxepin binding pose from the H_1R crystal structure. (b) Val side group at R^1 engaging the hydrophobic space between $H450^{7.35}$ and $I454^{7.39}$. (c) The hydroxyl group of Ser at R^2 could engage in hydrogen bonding with the surrounding $D178^{45.48}$, $K179^{45.49}$ and $K191^{5.39}$. (d) Potential hydrogen bonding interactions between the carboxamide group of Asn at R^3 and the amino acid residues of $N443^{ECL3}$ and $E447^{7.32}$.

The phospholipid bilayer was modelled around the T4 lysozyme-truncated H_1R crystal structure using ProBLM web server[156] and aligned with the binding pose of compound **107** using PyMOL (Figure 4.10). The lipophilic BODIPY fluorophore was predicted to be positioned away from the aqueous extracellular environment and possibly be embedded in the lipid bilayer in cells driven by hydrophobic effect. This agreed well with the molecular dynamic simulation findings reported by Stoddart et al[3]. It was postulated that the gain in free energy from the hydrophobic effect attributed to the fluorophore increased the free energy of binding of the fluorescent ligand as well as allowed the receptor to adopt non-energy minimum conformations to accommodate the various linker side groups. This could potentially explain why fluorophore attachment had a significant effect on fluorescent ligand binding affinity as well as limiting the linker SAR role in influencing the binding affinity of the final fluorescent ligands.

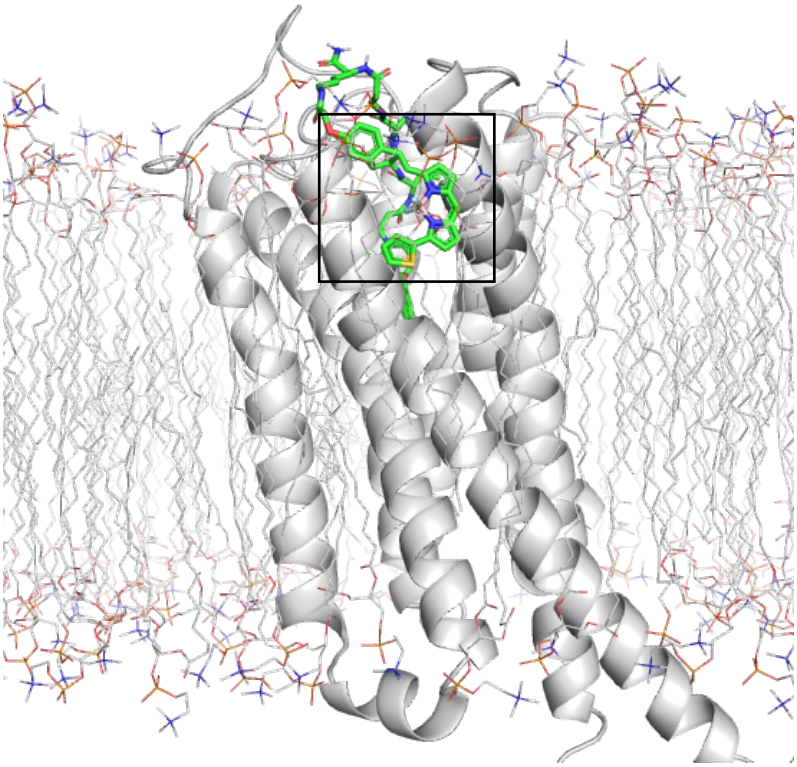

Figure 4.10: Molecular modelling of **107** (green) bound to the human H_1R embedded in the membrane bilayer. The BODIPY 630/650 fluorophore (black box) is positioned within the membrane bilayer, away from the aqueous extracellular environment.

4.6 Summary

The synthesis and pharmacological characterisation of fluorescent ligands with a wide range of fluorophores provided convincing evidence that the fluorophore did exert a profound effect on overall binding affinity of the final fluorescent ligands. Linear regression analysis indicated that the lipophilicity of the fluorophore and not the overall ligand lipophilicity which was positively correlated to the binding affinity of the fluorescent ligands, suggesting that the fluorophore might be involved in ligand-receptor interaction. Molecular docking studies involving **107** docked into a H_1R model highlighted the residues lining the ligand entry route which could potentially interact with the peptide linker of **107**. The fluorophore was predicted to be embedded in what would be the plasma membrane in cells. This was believed to have led to an increase in the binding affinity of the fluorescent ligand at H_1R through hydrophobic effect, which could explain its influence in the binding affinity of the final H_1R fluorescent ligands as well as the insignificance of the linker SAR in the final fluorescent ligands.

CHAPTER 5: CONCLUSION AND FUTURE WORK

5.1 Conclusion

A range of H_1R fluorescent ligands with varying receptor binding motifs, linker length and composition as well as fluorophores were successfully synthesised and pharmacologically characterised. This led to compound **107**, a high affinity (pK_D = 8.40 ± 0.08) H_1R selective fluorescent ligand capable of producing high quality confocal images at concentrations as low as 10nM.

Linker optimisation using unlabelled congeners should be reconsidered for future fluorescent ligand linker approaches as the linker SAR obtained from congener screening might not be completely transferrable towards the synthesis of fluorescent ligands. This is due to the significant structural and physicochemical differences between the two since the fluorophore makes up approximately one-third of the overall mass of the fluorescent ligand. In contrary to the objective of this thesis which aims to synthesise high affinity H_1R fluorescent ligands through the optimisation of the peptide linker, it is clear that it is the fluorophore instead which plays a major role in influencing the binding affinity of fluorescent ligands, with BODIPY630/650-based fluorescent ligands having the highest binding affinity at H_1R compared to fluorescent ligands bearing other fluorophores and linker SAR had limited effect on the binding affinity of H_1R fluorescent ligands. The peptide linker, however, does have a big influence on the overall physicochemical properties of the overall fluorescent ligand which allow these ligands to bind to the cell surface receptors with very limited uptake into the cell and should be considered when designing fluorescent ligands for GPCR receptors.

Molecular modelling served as a valuable tool for the initial ligand design and the rationalisation of pharmacology results. However, docking results should be studied in greater detail to provide an insight into the residues lining the ligand entry route and should not be focussing solely on a specific site. Water energies should also be taken into consideration when conducting molecular modelling due to their major role in the free energy of the system. Focus should be placed on identifying lipophilic hotspots, hydrogen bonding sites and salt bridge interactions within the inner

vestibule of the receptor. Solvent exposed hydrogen bonding sites located at the receptor extracellular vestibule are of minimal importance as energy input to disrupt existing water networks present offset free energy gain from ligand-receptor interactions as seen in R^2 and R^3 of the peptide linker as well as the flexible nature of the receptor extracellular loops meant that these regions of the receptor would be hard to target for improving ligand-receptor interaction.

Lastly, a novel, BODIPY 630/650-based alkyne-functionalised 'clickable' fluorophore was successfully synthesised and could be attached to any azido-functionalised congener through CuAAC. This would expand the utility of peptide linkers for the modulation of physicochemical and pharmacological properties of fluorescent ligands as it would allow the incorporation of a larger variety of side groups within the linker, which was not always favourable with the conventional amide coupling approach for fluorophore conjugation over concerns regarding side reactions.

5.2 Future Work

Compound **107** which has a high binding affinity and selectivity at H_1R and its inability to cross the plasma membrane could serve to be a useful tool for studying H_1R expression on cancer tissues in vitro using confocal microscopy. If a sufficiently large and representative patient biopsy is sampled, H_1R expression data could be used to identify correlations between receptor expression and treatment outcome or prognosis[98]. This could be then used to inform treatment plans based on information on H_1R expression determined from patient cancer biopsies. Alternatively, **107**, if possess good drug metabolism and pharmacokinetics (DMPK) properties, could be used in an in vivo setting to determine and study the drug-target engagement in the investigation of cancer therapeutics targeting H_1R in a similar manner employed by Alcobia et al[76].

The effects of the fluorophore on binding affinity of fluorescent ligands should also be investigated in other GPCR receptors which could hopefully provide valuable input for the synthesis of better GPCR fluorescent ligands. Molecular docking and molecular dynamic studies conducted by in this project and Stoddart et al. predicted

that the fluorophore could embed itself in the plasma membrane, surrounded by the extrahelical surface of the receptor and the lipid bilayer[3]. A crystal structure of **107** bound to the H_1R would be crucial to understand the nature of the linker interaction with the ligand entry route as well as the fluorophore effect on overall ligand affinity.

CHAPTER 6: EXPERIMENTAL

6.1 Chemistry

Materials

All chemicals and solvents were obtained from Fischer Scientific UK, Acros Organics, Sigma-Aldrich, Merck Millipore, Fluorochem or Tocris Bioscience and used without further purification. TLC was performed using Merck TLC Silica gel 60Å F_{254} plates. TLC plate visualisations were conducted under UV light (256 & 366 nm). Column chromatography was carried out using Sigma Aldrich silica gel (pore size 60Å, 230-440 mesh, 0.040-0.063 mm). BODIPY630/650-X-NHS (D10000), BODIPY-FL-NHS (D2184) and BODIPY FL-X-NHS (D6102) were purchased from Molecular Probes (Eugene, OR) whereas Sulfo-Cy5-NHS (23320) was purchased from Lumiprobe (Hunt Valley, MD).

LC-MS

LC-MS was recorded on a Shimadzu UFLCXR HPLC system combined with an Applied Biosystems MDS SCIEX API2000 electrospray ionisation mass spectrometer. The column used was a gemini 3µm C18 110Å, LC Column 50 x 2mm and the solvent system was an increasing gradient (from 5 to 95% over 5 mins) of acetonitrile in water containing 0.1% formic acid, flowing at 0.5mL/min.

NMR

NMR spectroscopy were recorded on a Bruker-AV 400 equipped with a 5mm dual $^{1}H/^{13}C$ helium-cooled cryoprobe which recorded the ^{1}H and ^{13}C NMR at 400.13 MHz and 101.62 MHz respectively. The data was processed using iNMR (version 5.5.7), which referenced the spectra to those of the residual solvents. Chemical shifts (δ) were quoted in parts per million (ppm) and coupling constants (J) were reported to the nearest 0.1Hz along with peak multiplicities using the following abbreviations: s, singlet; d, doublet; t, triplet; q, quartet; m, multiplet and br, broad.

HRMS

HRMS was done with a Brucker microTOF II mass spectrometer using electrospray ionisation (ESI-TOF). Adducts within errors of ±6 ppm were reported.

HPLC

Analytical, semi-preparative and preparative RP-HPLC were performed on a Waters 2767 sample manager coupled to Waters 2525 binary-gradient module and a Waters 2457 dual-wavelength absorbance detector or manually on a Rheodyne 7725i injector coupled to Waters 515 HPLC Pump and a Waters 996 photometric diode array detector.

Analytical HPLC was performed to identify compound purity.

System 1: YMC reverse phase C8 column (150 x 4.6mm), a flow rate of 1.00 mL/min and UV detection at 220, 254 and 330 nm. Linear gradient 5% to 95% solvent B over 25 min. Solvent A:0.1% formic acid in water; solvent B: 0.1% formic acid in acetonitrile.

System 2: Phenomenex Gemini® 5µm reverse phase C18 column (250 x 4.6mm), a flow rate of 1.00 mL/min and UV detection at 220, 254 and 330 nm. Linear gradient 5% to 95% solvent B over 25 min. Solvent A:0.05% TFA in water; solvent B: 0.1% formic acid in acetonitrile.

Semi-/Preparative HPLC was conducted to purify the congeners and final fluorescent compound.

YMC reverse phase C8 column (150 x 10mm), a flow rate of 5.00 mL/min and UV detection at 220, 254 and 330 nm and at various gradients. Solvent A:0.1% formic acid in water; solvent B: 0.1% formic acid in acetonitrile.

System 3: 5% to 45% solvent B over 5 min, then 45% to 47% solvent B over 20 min.

Phenomenex Gemini® 5µm reverse phase C18 column (250 x 21.2mm), a flow rate of 20.00 mL/min, UV detection at 254 nm and at various gradients. Solvent A:0.05% TFA in water; solvent B: 0.05% TFA in acetonitrile.

System 4: 5% to 65% solvent B over 15 min.

System 5: 20% to 50% solvent B over 10 min.

System 6: 40% to 70% solvent B over 10 min.

Phenomenex Gemini® 5µm reverse phase C18 column (250 x 10mm), a flow rate of 5.00 mL/min, UV detection at 254 nm and at various gradients. Solvent A: 0.1% formic acid in water; solvent B: 0.1% formic acid in acetonitrile.

System 7: 5% to 50% solvent B over 15 min.

System 8: 30% to 60% solvent B over 15 min.

System 9: 20% to 50% solvent B over 15 min.

General Procedure 1: SPPS performed in a small glass column

All coupling, deprotection and washing steps involved mild stirring by gentle N_2 bubbling. Rink amide resin (Aldrich 533935) (200mg for **36** or 50mg for **88**-**91**) with a reported resin loading of 1mmol/g (0.05mmol) was weighed and swelled in DCM overnight. The swelled resin was transferred to a small glass column, draining off DCM and the resin were washed by DMF (3 x 5 mL). The deprotection step was done using 20% piperidine in DMF (3 x 2 mL) followed by DMF washings (3 x 5 mL). Peptide coupling was done using a coupling mixture of 4 equiv. of amino acid, 4 equiv. of HBTU, 2 equiv. of HOBt hydrate and 8 equiv. of DIPEA dissolved in DMF (2 mL for **36**, 0.5 mL for **88**-**91**) for two hrs. Two coupling cycles were carried out for each required amino acid. 5-minute Fmoc deprotection cycle was done using 20% piperidine in DMF (3 x 2 mL). The resins were washed with DMF (3 x 5 mL) between each coupling and deprotection cycle. Final coupling of the orthosteric ligand was done using coupling mixture of 2 equiv. of **36**, 2 equiv. of HBTU, 1 equiv. of HOBt hydrate and 4 equiv. of DIPEA dissolved in DMF (2 mL for **36**, 0.5 mL for **xx**) for four hr as a single coupling cycle. The resin was then washed with DMF (3 x 5 mL), DCM (3 x 5 mL) and hexane (3 x 5 mL) successively and left to dry overnight. The dried resins were transferred to a scintillation vial and treated with cleavage mixture 90% TFA:10% water (5 mL for **36**, 3 mL for **88**-**91**) and left for 3 hr under mild stirring. The mixture was then pipetted into a round bottom flask, concentrated *in vacuo*, dissolved in DMSO, filtered, purified by Prep HPLC and subsequent lyophilisation to afford the oligopeptide product.

General Procedure 2: SPPS performed in a microwave vial

The removal of solvents, coupling/deprotection mixtures and washings for this procedure were achieved through decanting. All coupling, deprotection and washing steps involved mild stirring by a stirrer bar. 50mg of Rink amide resin (Aldrich 533935) with a reported resin loading of 1mmol/g (0.05mmol) was weighed into a 5 mL microwave vial and swelled in DCM overnight. DCM was decanted off the vial and the

resins were washed with DMF (3 x 5 mL). Three 5-min deprotection cycles were done using 20% piperidine in DMF to deprotect the resin followed by DMF washings (3 x 5 mL). Peptide coupling was done using a coupling mixture of 4 equiv. of amino acid (0.2mmol), 4 equiv. of HBTU (76mg, 0.2mmol), 2 equiv. of HOBt hydrate (16mg, 0.1mmol) and 8 equiv. of DIPEA (70µL, 0.4mmol) dissolved in 0.5mL of DMF for two hr. Two coupling cycles were carried out for each required amino acid. Fmoc deprotection step was done using 20% piperidine in DMF with 3 x 5-min cycles. The resins were washed with DMF (3 x 5 mL) between each coupling and deprotection cycle. Final coupling of the orthosteric ligand was done using coupling mixture of 2 equiv. of **36** (34mg, 0.1mmol), 2 equiv. of HBTU (38mg, 0.1mmol), 1 equiv. of HOBt hydrate (8mg, 0.05mmol) and 4 equiv. of DIPEA (35µL, 0.2mmol) dissolved in 0.5mL of DMF for four hr as a single coupling cycle. The resins were washed with DMF (3 x 5 mL), DCM (1 x 5 mL) and hexane (1 x 5 mL) successively and left to dry overnight. 3mL of cleavage mixture 90% TFA:10% water is added and left for 3 hr under mild stirring. The mixture was then pipetted into a round bottom flask, concentrated *in vacuo*, dissolved in DMSO, filtered, purified by Prep HPLC and subsequent lyophilisation afforded the oligopeptide product.

General Procedure 3: BODIPY Coupling through CuAAC

1 Equiv of the azide congener was dissolved in 0.25mL/ µmol of DMSO and transferred to a small microwave vial. 1.1 equiv of the alkyne-functionalised BODIPY, 3 equiv of $CuSO_4 \cdot 5H_2O$ and 9 equiv of sodium ascorbate were dissolved in 0.25mL/µmol of DMSO in a scintillation vial and sonicated for 5 mins. The sonicated mixture was added to the microwave vial followed by three drops of 2,6-lutidine and left to stir overnight. The reaction mixture was purified using PREP HPLC followed by lyophilisation to give the product.

General Procedure 4: BODIPY Coupling through amide bond formation with HATU

1 Equiv of the amine congener was dissolved in 1mL/µmol of DMF, treated with 0.9 equiv of carboxylic acid functionalised fluorophore, 1.2 equiv of HATU and 6 equiv of DIPEA and left to stir for 1 hr in the dark. The reaction mixtures were diluted with DMF, purified using Prep HPLC followed by lyophilisation to give the product. The

fluorophores are BODIPY630/650-COOH for **107-117**, BODIPY A for **123**, **129** and BODIPY B for **124**, **129**.

General Procedure 5: Fluorophore Coupling through NHS Ester

1mg (1.2μmol) of the amine congener and the 1.2μmol of the desired fluorophore (0.8mg of BODIPY630/650-X-NHS (D10000), 0.5mg of BODIPY-FL-NHS (D2184), 0.6mg of BODIPY FL-X-NHS (D6102), 0.9mg of Sulfo-Cy5-NHS (23320)) were dissolved in 1mL of DMF, treated with a few drops of DIPEA and left to stir for 2 hrs in the dark. The reaction mixtures were purified using Prep HPLC followed by lyophilisation to give the product.

***tert*-Butyl 4-(2-benzylphenoxy)piperidine carboxylate 33[105].**

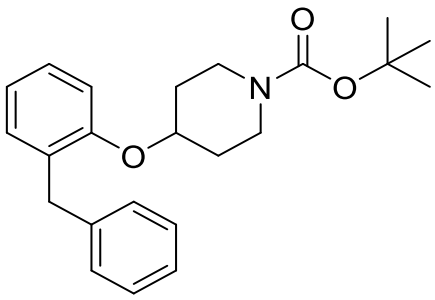

1000mg (5.43mmol) of 2-benzylphenol and 1092mg (5.43mmol) of 1-Boc-4-hydroxypiperidine were dissolved in 5mL of dry THF in a scintillation vial before being transferred to a dry 25mL 2-necked RBF. 1566mg (5.97mmol) of triphenylphosphine and 1175µL (5.97mmol) of DIAD was added to the solution and left to react overnight. Reaction mixture was filtered, filtrate collected and triturated with hexane. The mixture was filtered again, the filtrate collected and dried using rotary evaporator, subsequently dissolved in 100mL of EtOAc, washed once with 1M NaOH, followed by brine wash, drying with magnesium sulphate, filtered, concentrated using rotary evaporator and purified using silica gel column chromatography (PE:EtOAc:Et_3N=99:1:1). Pale yellow oil was obtained (957mg) which consisted of a mixture of the desired product and the elimination product *tert*-butyl 3,6-dihydropyridine-1(2*H*)-carboxylate in a molar ratio of 1:0.274 as determined by ^{1}H NMR. The desired product was calculated to be 842mg (88 wt. %, 2.29mmol, 42%) and product mixture was used in the next step without further re-purification.

^{1}H NMR (400 MHz, $CDCl_3$) δ 7.40 – 7.02 (m, 7H, Ar-C**H**), 7.02 – 6.72 (m, 2H, Ar-C**H**), 4.52 – 4.46 (m 1H, -C**H**), 3.99 (s, 2H, Benzyl C**H_2**), 3.53 – 3.42 (m, 2H, Piperidine C**H_2**), 3.42 – 3.28 (m, 2H, Pip C**H_2**), 1.90 – 1.77 (m, 2H, Pip C**H_2**), 1.77 – 1.61 (m, 2H, Pip C**H_2**), 1.48 (s, 9H, -C**(**C**H_3)$_3$**).

^{13}C NMR (101 MHz, $CDCl_3$) δ 171.17, 154.92, 141.20, 131.11, 130.58, 128.86, 128.27, 127.46, 125.88, 120.60, 112.53, 79.56, 71.41, 40.46, 36.56, 30.45, 28.54.

LCMS: *m/z* of $(M+H)^+$ = 368.1; t_R = 3.35 min.

4-(2-Benzylphenoxy)piperidine 34[105].

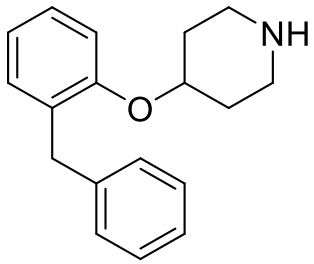

884mg of **33** (778mg as 88 % by weight, 2.12mmol) was dissolved in 10mL of DCM in a 25mL RBF and 1mL of TFA was added and left to react overnight. Reaction mixture was dried using rotary evaporator, dissolved in EtOAc, washed with $NaHCO_3$ thrice, followed by brine wash, drying with $MgSO_4$, filtering through filter paper, dried using rotary evaporator under high vacuum pump. A yellow oil was obtained (525mg, 1.97mmol, 93%).

^{1}H NMR (400 MHz, $CDCl_3$) δ 7.30 – 7.23 (m, 2H, Ar-C**H**), 7.23 – 7.10 (m, 5H, Ar-C**H**), 6.93 – 6.79 (m, 2H, Ar-C**H**), 4.48 – 4.38 (m, 1H, -C**H**), 3.99 (s, 2H, Benzyl C**H_2**), 3.06 – 2.97 (m, 2H, Pip C**H_2**), 2.91 (br s, 1H, N**H**), 2.79 – 2.69 (m, 2H, Pip C**H_2**), 2.03 – 1.91 (m, 2H, Pip C**H_2**), 1.74 – 1.61 (m, 2H Pip C**H_2**).

^{13}C NMR (101 MHz, $CDCl_3$) δ 155.02, 141.36, 131.08, 130.68, 128.95, 128.32, 127.45, 125.91, 120.56, 112.68, 72.01, 43.22, 36.58, 31.58.

LCMS: *m/z* of $(M+H)^+$ = 267.9; t_R = 2.22 min.

Methyl 3-(4-(2-benzylphenoxy)piperidin-1-yl)propanoate 35.

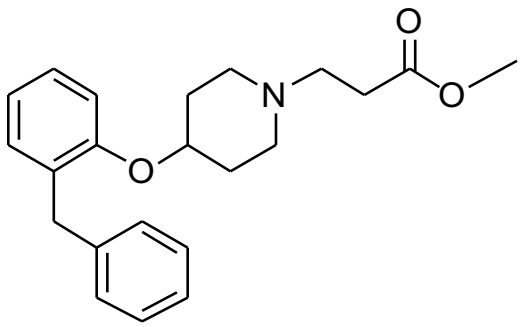

525mg (1.97mmol) of **34** was dissolved in 2mL of 1,2-dichloroethane (DCE) in a 25mL RBF and heated to 70°C. 890µL (10mmol) of methyl acrylate was added into the RBF and left to react for 4 hrs. DCE and excess methyl acrylate were removed using rotary evaporator and the crude was purified using column chromatography (PE:EtOAc:Et_3N= 60:40:2). Pale yellow oil was obtained as the product (454mg, 1.29mmol, 66%).

^{1}H NMR (400 MHz, $CDCl_3$) δ 7.39 – 7.03 (m, 7H, Ar-C**H**), 6.97 – 6.74 (m, 2H, Ar-C**H**), 4.42 – 4.28 (m, 1H, -C**H**), 3.98 (s, 2H, Benzyl C**H_2**), 3.69 (s, 3H, -COOC**H_3**), 2.72 – 2.63 (m, 2H, Pip C**H_2**), 2.67 (t, *J* = 7.4 Hz, 2H, -C**H_2**-), 2.50 (t, *J* = 7.4 Hz, 2H, -C**H_2**-), 2.38 – 2.28 (m, 2H, Pip C**H_2**), 1.98 – 1.87 (m, 2H, Pip C**H_2**), 1.85 – 1.73 (m, 2H, Pip C**H_2**).

^{13}C NMR (101 MHz, CDCl3) δ 173.13, 155.15, 141.37, 131.00, 130.61, 128.99, 128.31, 127.41, 125.84, 120.42, 112.60, 71.66, 53.68, 51.77, 50.14, 36.50, 32.40, 30.80.

LCMS: *m/z* of $(M+H)^+$ = 353.8; t_R = 2.32 min.

3-(4-(2-Benzylphenoxy)piperidin-1-yl)propanoic acid 36.

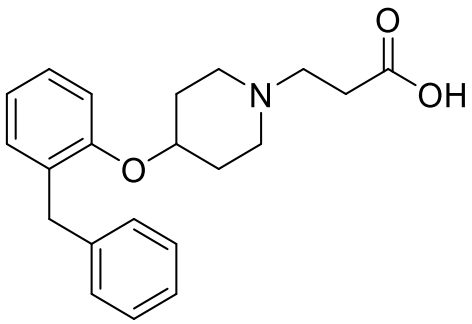

342mg (0.97mmol) of **35** was dissolved in 5mL of THF in a 25mL RBF placed in an ice bath and 120mg (3mmol) of NaOH dissolved in 4mL of de-ionised water was added to it and left to stir for 5 hrs. THF was removed by rotary evaporation and the pH of the reaction mixture was adjusted to pH 6 using 2M aqueous HCl. De-ionised water was added to dilute the mixture and the mixture was extracted with chloroform for three times, followed by brine wash of the organic layer, drying with $MgSO_4$, filtration and dried using rotary evaporator to yield a pale yellow gum (244mg, 0.72mmol, 74%).

^{1}H NMR (400 MHz, CD_3OD) δ 7.32 – 7.19 (m, 4H, Ar-C**H**), 7.22 – 7.10 (m, 3H, Ar-C**H**), 7.00 – 6.90 (m, 2H, Ar-C**H**), 4.70 (p, *J* = 3.8 Hz, 1H, -C**H**), 4.01 (s, 2H, Benzyl C**H$_2$**), 3.21-3.10 (m, 2H, pip C**H$_2$**), 3.03 (t, *J* = 6.7 Hz, 2H, -C**H$_2$-**), 2.84 – 2.59 (m, 2H, pip C**H$_2$**), 2.52 (t, *J* = 6.7 Hz, 2H, -C**H$_2$**-), 2.12 – 1.90 (m, 4H, 2 x pip C**H$_2$**).

^{13}C NMR (101 MHz, CD_3OD) δ 176.73, 155.56, 143.37, 132.90, 130.80, 129.58, 129.40, 129.06, 127.07, 122.01, 113.19, 67.58, 54.86, 49.85, 37.91, 30.68, 28.58.

LCMS: *m/z* of $(M+H)^+$ = 339.8; t_R = 2.32 min

(*S*)-4-((2-(((*R*)-1-Amino-1-oxopent-4-yn-2-yl)amino)-2-oxoethyl)amino)-3-((*S*)-2-(3-(4-(2-benzylphe-noxy)piperidin-1-yl)propanamido)propanamido)-4-oxobutanoic acid 37

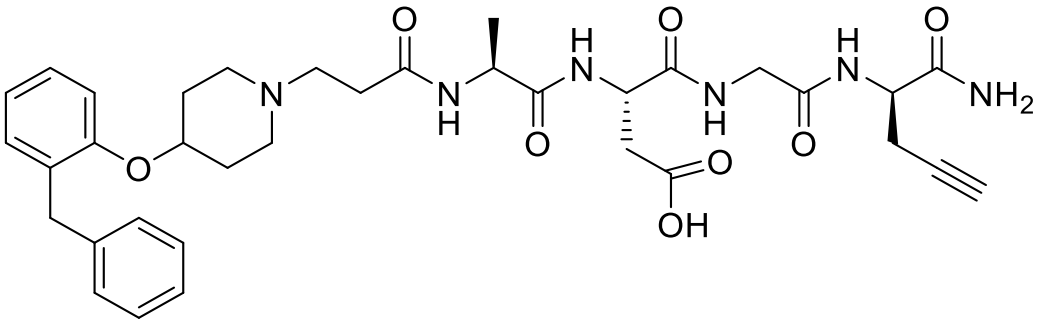

Compound synthesised using General Procedure 1 and purified using System 3 to give a white solid (18mg, 0.027mmol, 17%).

HRMS (Bruker MicroTOF)(*m/z*): Calculated $(M+H)^+$ for $C_{35}H_{44}N_6O_8$ = 677.3293; Measured = 677.3315; Error = 3ppm. **Analytical HPLC** (System 1): 93% purity; t_R = 20.16 min.

2,2'-(*p*-tolylmethylene)bis(1*H*-pyrrole) 38[139]

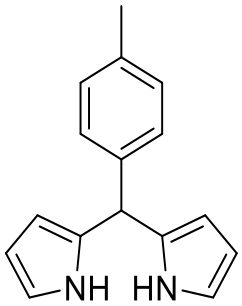

1.2mL (0.01mmol) of para-tolualdehyde was added to 20mL of pyrrole in a 50mL RBF and stirred at room temperature for 25 mins. 124µL (1µmol) of $BF_3{\cdot}Et_2O$ was added and stirred at room temperature for another 30 mins. TLC (PE:EtOAc:Et_3N=9:1:0.1) indicated presence of product (R_f=0.25). The reaction mixture was concentrated using rotary evaporator to remove excess pyrrole and subsequently dissolved in 50mL of DCM, followed by two washings with 150mL of 0.1M NaOH, brine wash, drying with $MgSO_4$, concentrated using rotary evaporator and purified using column chromatography (PE:EtOAc:Et_3N=9:1:0.1). Tan solid product was obtained (901mg, 3.82mmol, 38%).

^{1}H NMR (400 MHz, DMSO-d_6) δ 10.50 (s, 2H, Pyrrole N-**H**), 7.07 (d, *J* = 8.1 Hz, 2H, PhC2**H**), 7.03 (d, *J* = 8.3 Hz, 2H, PhC3**H**), 6.59 (td, *J* = 2.7, 1.6 Hz, 2H, Pyrrole-C1**H**), 5.88 (q, *J* = 2.7 Hz, 2H, Pyrrole-C2**H**), 5.66-5.60 (m, 2H, Pyrrole-C3**H**), 5.29 (s, 1H, -C**H**(Pyrrole)$_2$), 2.25 (s, 3H -C**H$_3$**).

^{13}C NMR (101 MHz, DMSO-d_6) δ 140.83, 134.93, 133.28, 128.52, 127.96, 116.70, 106.78, 105.91, 43.08, 20.59.

LCMS: *m/z* of $(M+H)^+$ = 236.8; t_R = 2.92 min

(*Z*)-2-((2*H*-Pyrrol-2-ylidene)(*p*-tolyl)methyl)-5-bromo-1*H*-pyrrole 39[119]

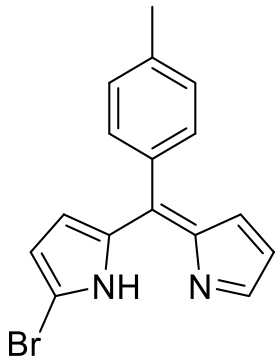

300mg (1.27mmol) of **38** was dissolved in 15mL dry THF placed under nitrogen environment, which was then cooled to -78°C in a dry ice acetone bath. 227mg (1.27mmol) of NBS was dissolved in 15mL of dry THF and added in 1mL batches, dropwise over 90 mins. Reaction mixture was left to stir for another 90 mins. The reaction mixture was left to warm to room temperature and 289mg of 2,3-dichloro-5,6-dicyano-1,4-benzoquinone (1.27mmol) was added and allowed to react for 1 hr. The reaction mixture was concentrated using rotary evaporator and purified using column chromatography (PE:DCM:Et_3N=98:1:1) to give dark orange oil as the product (114mg, 0.37mmol, 29%).

^{1}H NMR (400 MHz, $CDCl_3$) δ 12.36 (s, 1H, Pyrrole N-**H**), 7.37 (d, *J* = 8.1 Hz, 2H, PhC2**H**), 7.31 (dd, *J* = 2.5, 1.4 Hz, 1H, Right Pyrrole C5**H**), 7.25 (d, *J* = 8.0 Hz, 2H, PhC3**H**), 6.73 (d, *J* = 4.3 Hz, 1H, Left Pyrrole C4**H**), 6.46 – 6.40 (m, 2H, Pyrrole C**H** x 2), 6.28 (dd, *J* = 3.9, 2.4 Hz, 1H, Right Pyrrole C4**H**), 2.45 (s, 3H, -C**H$_3$**).

^{13}C NMR (101 MHz, $CDCl_3$) δ 146.80, 146.04, 141.84, 139.46, 136.63, 133.60, 132.85, 130.97, 129.22, 128.54, 125.76, 123.54, 111.87, 21.51.

LCMS: *m/z* of (M (^{79}Br/^{81}Br)+H)$^+$ = 313.1 and 314.9; t_R = 3.28 min

3-Bromo-5,5-difluoro-10-(*p*-tolyl)-5*H*-5λ^4,6λ^4-dipyrrolo[1,2-*c*:2',1'-*f*][1,3,2]diaza-borinine 40[119]

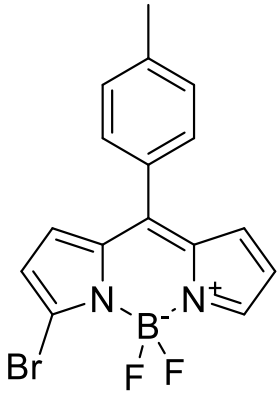

114mg (0.37mmol) of **39** was dissolved in 10mL of DCM, subsequently treated with 404µL (2.96mmol) of Et_3N and 540µL (4.44mmol) of $BF_3{\cdot}Et_2O$ and left to stir overnight. The reaction mixture was washed with 0.1M NaOH and deionised water, followed by brine wash, dried with $MgSO_4$, filtered, concentrated using rotary evaporator and purified using silica gel column chromatography (PE:EtOAc:Et_3N=90:10:0.1 to yield a red-orange solid as the product (86mg, 0.24mmol, 65%).

^{1}H NMR (400 MHz, $CDCl_3$) δ 7.95 (s, 1H, Pyrrole-C5**H**), 7.43 (d, *J* = 8.0 Hz, 2H, PhC2**H**), 7.33 (d, *J* = 7.8 Hz, 2H, PhC3**H**), 6.94 (d, *J* = 4.3 Hz, 1H, Ar-C**H**), 6.85 (d, *J* = 4.3 Hz, 1H, Ar-C**H**), 6.62 – 6.53 (m, 1H, Ar-C**H**), 6.52 (d, *J* = 4.3 Hz, 1H, Ar-C**H**), 2.47 (s, 3H, -C**H$_3$**).

^{13}C NMR (101 MHz, $CDCl_3$) δ 145.85, 144.56, 141.63, 135.78, 134.94, 131.85, 131.72, 131.55, 130.68, 130.45, 129.39, 122.05, 119.08, 21.63.

LCMS: *m/z* of $(M(^{79}Br)+H)^+$ = 361.2; tR = 3.14 min

3-Azido-5,5-difluoro-10-(*p*-tolyl)-5*H*-5λ^4,6λ^4-dipyrrolo[1,2-*c*:2',1'-*f*][1,3,2]diaza-borinine 41[119]

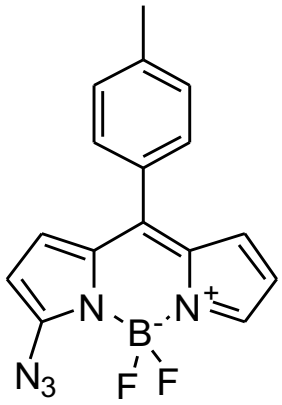

20mg (0.056mmol) of **40** was dissolved in 2mL of acetone, treated dropwise with 4.32mg of NaN_3 (2.4eq) dissolved in 2mL of deionised water and left to stir for 24 hrs. The reaction mixture was diluted with 20mL of ethyl acetate and washed thrice with deionised water, followed by brine wash, drying with $MgSO_4$, filtered and concentrated using rotary evaporator. Flask was placed under constantly flowing nitrogen gas to dry. Dark reddish solid was obtained (16mg, 0.049mmol, 88%).

^{1}H NMR (400 MHz, $CDCl_3$) δ 7.80 (s, 1H, Pyrrole-C5**H**), 7.42 (d, *J* = 8.1 Hz, 2H, PhC2**H**), 7.32 (d, *J* = 7.8 Hz, 2H, PhC3**H**), 6.98 (d, *J* = 4.6 Hz, 1H, Ar-C**H**), 6.82 (d, *J* = 4.1 Hz, 1H, Ar-C**H**), 6.54 – 6.46 (m, 1H, Ar-C**H**), 6.35 (d, *J* = 4.6 Hz, 1H, Ar-C**H**), 2.47 (s, 3H, -C**H$_3$**).
^{13}C NMR (101 MHz, $CDCl_3$) δ 152.81, 144.41, 141.16, 134.15, 133.54, 133.07, 130.77, 130.69, 130.60, 129.32, 129.07, 117.55, 110.16, 21.60.
LCMS: *m/z* of $(M+H)^+$ not observed; t_R = 3.09 min

(*S*)-4-((2-(((*R*)-1-Amino-3-(1-(5,5-difluoro-10-(*p*-tolyl)-5*H*-5λ^4,6λ^4-dipyrrolo[1,2-*c*:2',1'-*f*][1,3,2]diaza-bor-inin-3-yl)-1*H*-1,2,3-triazol-4-yl)-1-oxopropan-2-yl)amino)-2-oxoethyl)amino)-3-((S)-2-(3-(4-(2-benzyl-phenoxy)piperidin-1-yl)propanamido) propanamido)-4-oxobutanoic acid 32

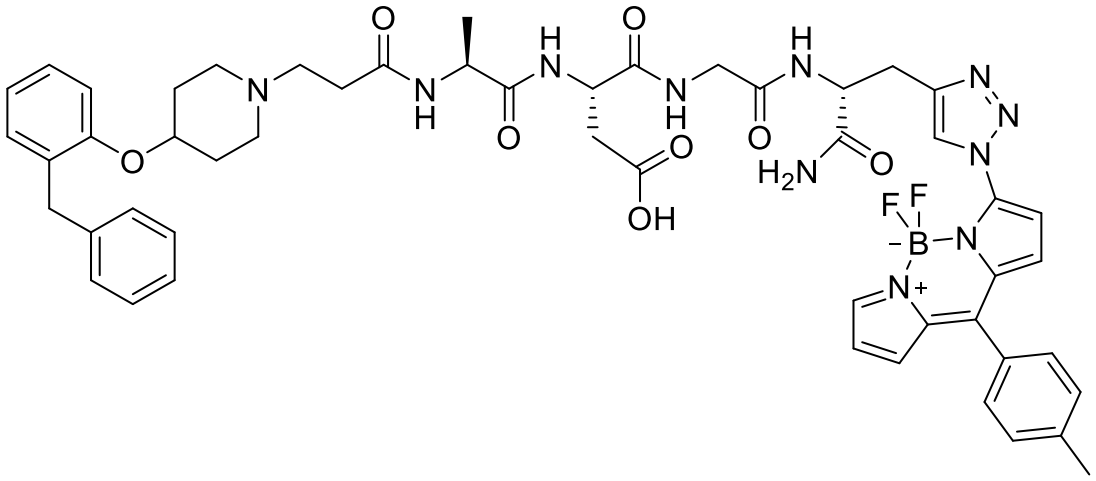

3mg (4.44μmol) of **37** and 1.5mg (4.6μmol) of **41** were dissolved in 5mL of DMSO and treated with 5.7mg (35.5μmol) of $CuSO_4 \cdot 5H_2O$ and 21mg (107μmol) of sodium ascorbate were weighed and dissolved in 1mL of DMSO in a scintillation vial. A few drops of 2,6-lutidine were added to the catalyst mixture and the mixture was added dropwise into the reaction flask and left to react over a few days. The reaction mixture was purified using prep HPLC (System 3) and subsequent lyophilisation gave a red solid (2mg, 2μmol, 45%).

HRMS (Bruker MicroTOF)(*m/z*): Calculated $(M+H)^+$ for $C_{51}H_{56}B_1F_2N_{11}O_8$ = 1000.4443; Measured = 1000.4447; Error = 1.3ppm. **Analytical HPLC** (System 1): 98% purity; t_R = 20.43 min.

(*S*)-*N*-((*R*)-1-Amino-1-oxo-3-phenylpropan-2-yl)-2-((*S*)-2-(2-(3-(4-(2-benzylphen-oxy) piperidin-1-yl)propanamido)acetamido)propanamido)propanamide 42.

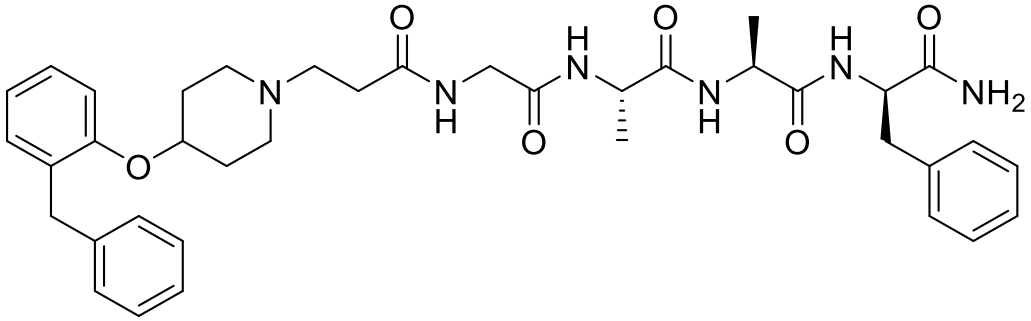

Compound synthesised using General Procedure 2 and purified using *System 4* to give a white solid (0.33mg, 0.5µmol, 1%). **HRMS** (Bruker MicroTOF)(*m/z*): Calculated $(M+H)^+$ for $C_{38}H_{48}N_6O_6$ = 685.3708; Measured = 685.3716; Error = 1.2ppm. **Analytical HPLC** (System 2): 98% purity; t_R = 13.73 min.

(*S*)-*N*-((*R*)-1-Amino-1-oxo-3-phenylpropan-2-yl)-2-((*S*)-2-((*S*)-2-(3-(4-(2-benzylphen-oxy)piperidin-1-yl)-propana-mido)propanamido)propanamido)propanamide 43.

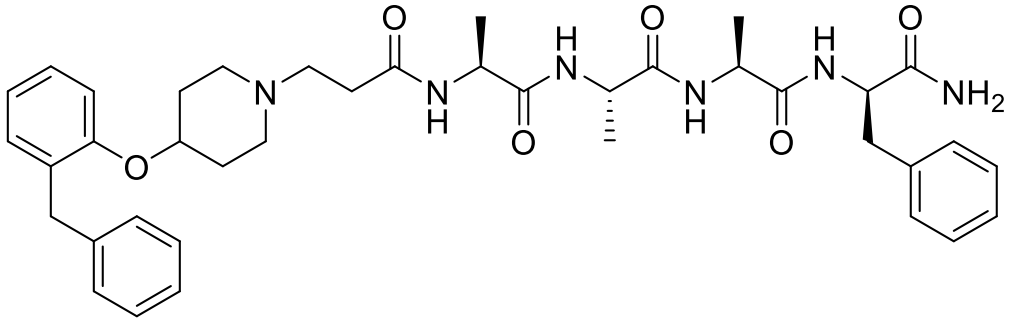

Compound synthesised using General Procedure 2 and purified using *System 4* to give a white solid (0.21mg, 0.3µmol, 1%). **HRMS** (Bruker MicroTOF)(*m/z*): Calculated $(M+H)^+$ for $C_{39}H_{50}N_6O_6$ = 699.3865; Measured = 699.3871; Error = 0.9ppm. **Analytical HPLC** (System 2): 99% purity; t_R = 13.66 min.

(*S*)-*N*-((*S*)-1-(((*S*)-1-(((*R*)-1-Amino-1-oxo-3-phenylpropa-n-2-yl)amino)-1-oxopropan-2-yl)amino)-1-oxo-propan-2-yl)-2-(3-(4-(2-benzylphenoxy)piperidin-1-yl)propana-mido)-3-methylbutanamide 44.

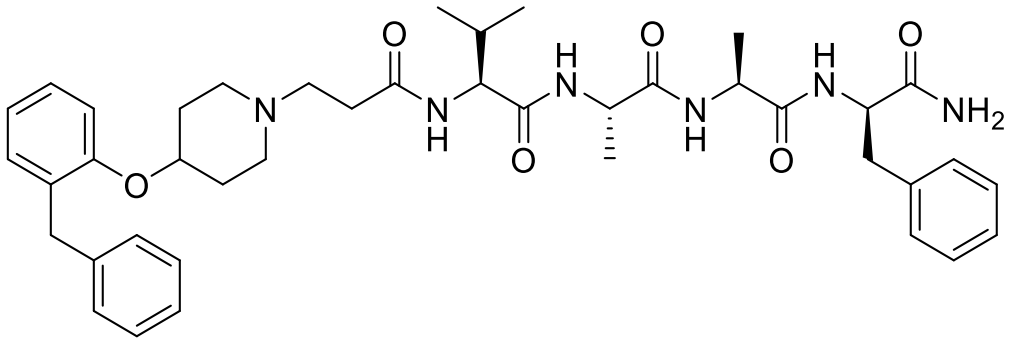

Compound synthesised using General Procedure 2 and purified using *System 4* to give a white solid (0.52mg, 0.7µmol, 2%). **HRMS** (Bruker MicroTOF)(*m/z*): Calculated $(M+H)^+$ for $C_{41}H_{54}N_6O_6$ = 727.4178; Measured = 727.4188; Error = 1.4ppm**. Analytical HPLC** (System 2): 99% purity; t_R = 14.21 min.

(*S*)-*N*-((*S*)-1-(((*S*)-1-(((*R*)-1-Amino-1-oxo-3-phenylpropa-n-2-yl)amino)-1-oxopropan-2-yl)amino)-1-oxo-propan-2-yl)-2-(3-(4-(2-benzylphenoxy)piperidin-1-yl)propana-mido)-3-phenylpropanamide 45.

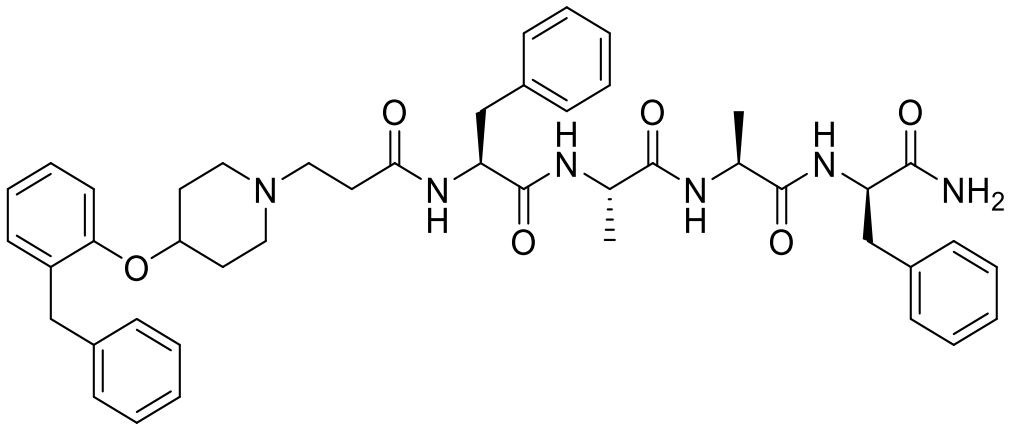

Compound synthesised using General Procedure 2 and purified using *System 4* to give a white solid (0.28mg, 0.4µmol, 1%). **HRMS** (Bruker MicroTOF)(*m/z*): Calculated $(M+H)^+$ for $C_{45}H_{54}N_6O_6$ = 775.4178; Measured = 775.4154; Error = 3ppm. **Analytical HPLC** (System 2): 99% purity; t_R = 14.08 min.

(*S*)-*N*-((*S*)-1-(((*S*)-1-(((*R*)-1-Amino-1-oxo-3-phenylpropa-n-2-yl)amino)-1-oxopropan-2-yl)amino)-1-oxopropan-2-yl)-2-(3-(4-(2-benzylphenoxy)piperidin-1-yl)propanami-do)-3-(4-hydroxyphenyl)-propanamide 46.

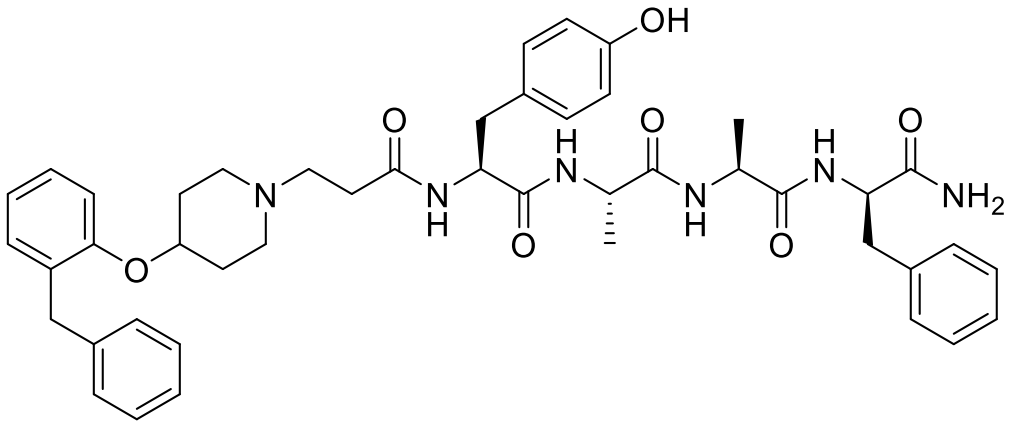

Compound synthesised using General Procedure 2 and purified using *System 4* to give a white solid (0.26mg, 0.3µmol, 1%). **HRMS** (Bruker MicroTOF)(*m/z*): Calculated $(M+H)^+$ for $C_{45}H_{54}N_6O_7$ = 791.4127; Measured = 791.4130; Error = 0.4ppm. **Analytical HPLC** (System 2): 98% purity; t_R = 14.08 min.

(*S*)-*N*-((*S*)-1-(((*S*)-1-(((*R*)-1-Amino-1-oxo-3-phenylpropa-n-2-yl)amino)-1-oxopropan-2-yl)amino)-1-oxopropan-2-yl)-2-(3-(4-(2-benzylphenoxy)piperidin-1-yl)propanami-do)-3-hydroxypropanamide 47.

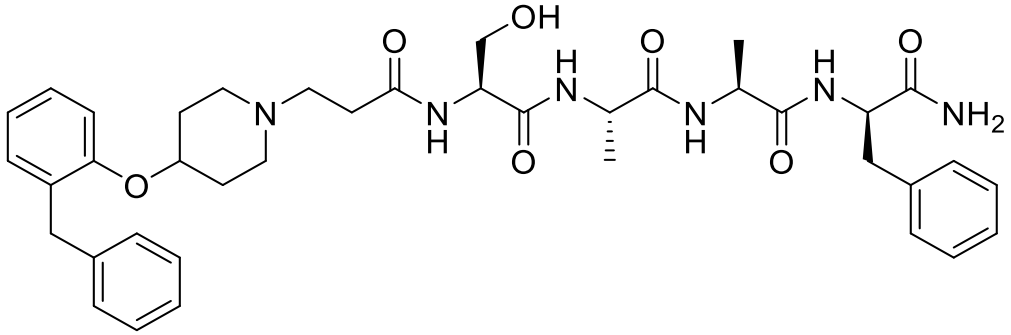

Compound synthesised using General Procedure 2 and purified using *System 4* to give a white solid (0.46mg, 0.6µmol, 2%). **HRMS** (Bruker MicroTOF)(*m/z*): Calculated $(M+H)^+$ for $C_{39}H_{50}N_6O_7$ = 715.3814; Measured = 715.3835; Error = 2.9ppm. **Analytical HPLC** (System 2): 98% purity; t_R = 13.42 min.

(*S*)-*N*-((S)-1-(((*S*)-1-(((*R*)-1-Amino-1-oxo-3-phenyl-propa-n-2-yl)amino)-1-oxopropa n-2-yl)amino)-1-oxopro-pan-2-yl)-2-(3-(4-(2-benzylphenoxy)piperidin-1-yl)-propan -amido)succinamide 48.

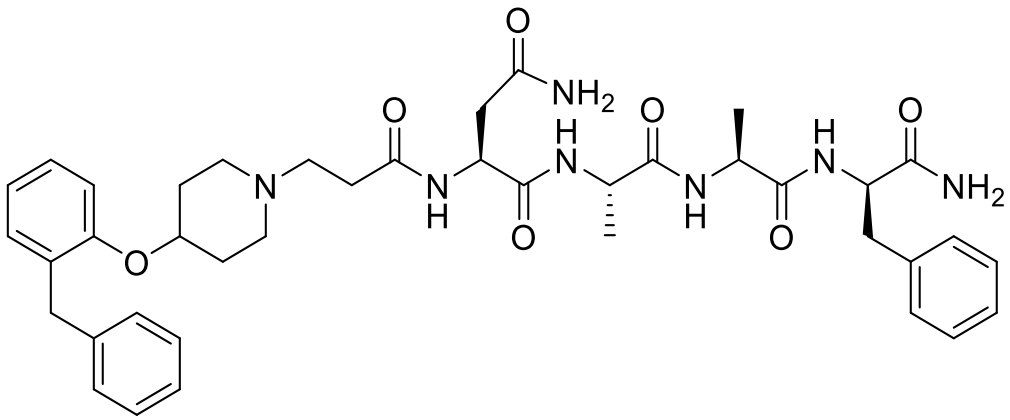

Compound synthesised using General Procedure 2 and purified using *System 4* to give a white solid (0.50mg, 0.7µmol, 2%). **HRMS** (Bruker MicroTOF)(*m/z*): Calculated $(M+H)^+$ for $C_{40}H_{51}N_7O_7$ = 742.3923; Measured = 742.3923; Error = 0.1ppm. **Analytical HPLC** (System 2): 97% purity; t_R = 13.35 min.

(*S*)-*N*-((S)-1-(((*S*)-1-(((*R*)-1-Amino-1-oxo-3-phenylpropa-n-2-yl)amino)-1-oxopro-pan-2-yl)amino)-1-oxopropan-2-yl)-2-(3-(4-(2-benzylphenoxy)piperidin-1-yl)pro-panemi-do)-3-(1*H*-imidazol-5-yl)propanamide 49.

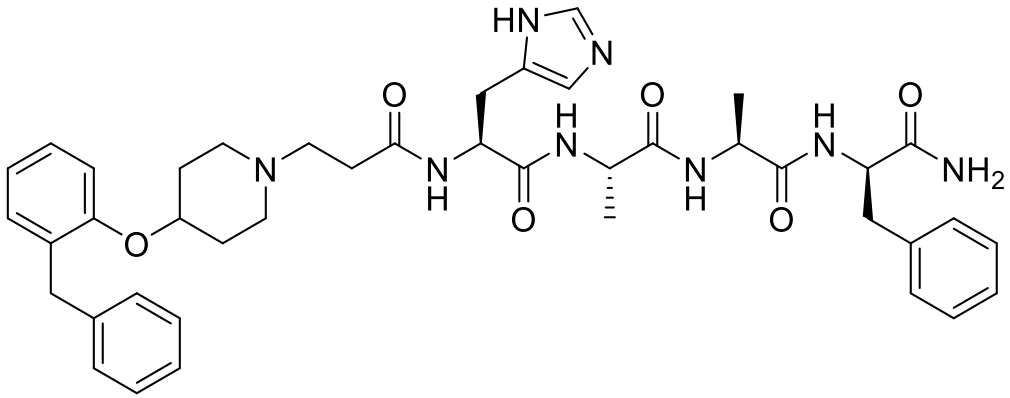

Compound synthesised using General Procedure 2 and purified using *System 4* to give a white solid (0.27mg, 0.3µmol, 1%). **HRMS** (Bruker MicroTOF)(*m/z*): Calculated $(M+Na)^+$ for $C_{42}H_{52}N_8O_6$ = 787.3882; Measured $(M+Na)^+$ = 787.3882; Error = 2.5ppm. **Analytical HPLC** (System 2): 95% purity; t_R = 11.82 min.

(*S*)-6-Amino-*N*-((*S*)-1-(((*S*)-1-(((*R*)-1-amino-1-oxo-3-phe-nylpropan-2-yl)amino)-1-oxopropan-2-yl)-amino)-1-oxo-propan-2-yl)-2-(3-(4-(2-benzylphenoxy)piperidin-1-yl)-propanamido)hexanamide 50.

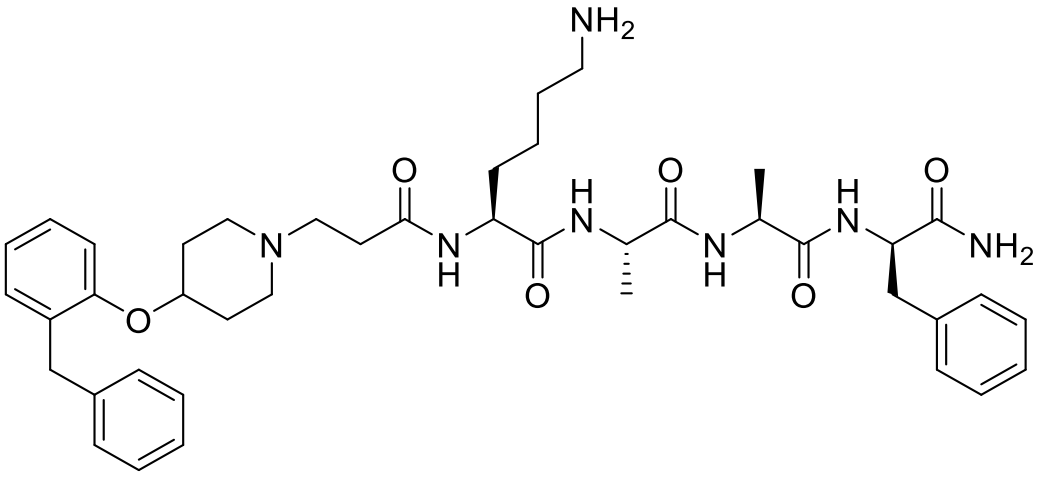

Compound synthesised using General Procedure 2 and purified using *System 4* to give a white solid (0.53mg, 0.7µmol, 2%). **HRMS** (Bruker MicroTOF)(*m/z*): Calculated $(M+H)^+$ for $C_{42}H_{57}N_7O_6$ = 756.4443; Measured = 756.4428; Error = 2ppm. **Analytical HPLC** (System 2): 99% purity; t_R = 11.77 min.

(*S*)-4-(((*S*)-1-(((*S*)-1-(((*R*)-1-Amino-1-oxo-3-phenylpropa-n-2-yl)amino)-1-oxopro-pan-2-yl)amino)-1-oxopro-pan-2-yl)amino)-3-(3-(4-(2-benzylphenoxy)piperidin-1-yl)prop-anamido)-4-oxobutanoic acid 51.

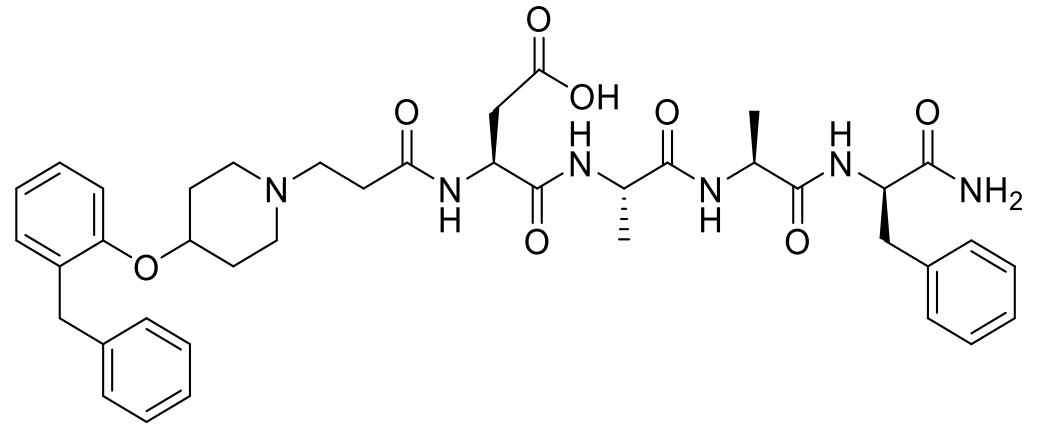

Compound synthesised using General Procedure 2 and purified using *System 4* to give a white solid (0.67mg, 0.9µmol, 1%). **HRMS** (Bruker MicroTOF)(*m/z*): Calculated $(M+H)^+$ for $C_{40}H_{50}N_6O_8$ = 743.3763; Measured = 743.3765; Error = 0.3ppm. **Analytical HPLC** (System 2): 99% purity; t_R = 13.60 min.

(*S*)-*N*-(2-(((*S*)-1-(((*R*)-1-Amino-1-oxo-3-phenylpropan-2-yl)amino)-1-oxopropan-2-yl)amino)-2-oxoethyl)-2-(3-(4-(2-benzylphenoxy)piperidin-1-yl)propanamido)-3-me-thylbutanamide 52.

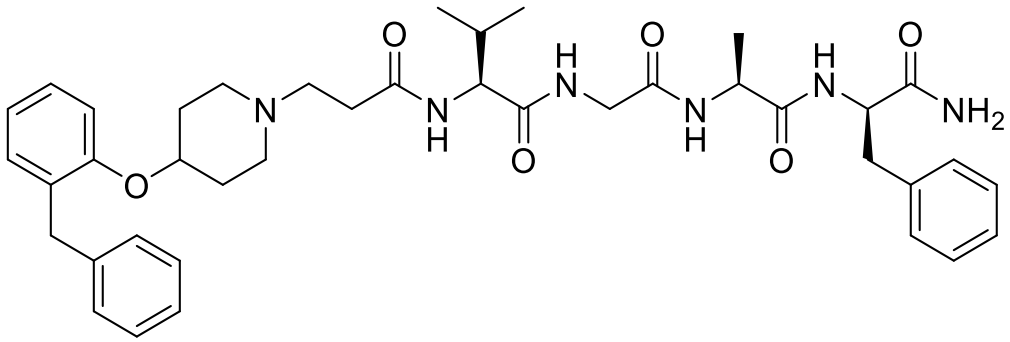

Compound synthesised using General Procedure 2 and purified using *System 4* to give a white solid (1.27mg, 1.8µmol, 4%). **HRMS** (Bruker MicroTOF)(*m/z*): Calculated $(M+H)^+$ for $C_{40}H_{52}N_6O_6$ = 713.4021; Measured = 713.4048; Error = 3.7ppm. **Analytical HPLC** (System 2): 97% purity; t_R = 14.69 min.

(*S*)-*N*-((*S*)-1-(((*R*)-1-Amino-1-oxo-3-phenylpropan-2-yl)amino)-1-oxopropan-2-yl)-2-((*S*)-2-(3-(4-(2-benzyl-ph-enoxy)piperidin-1-yl)propanamido)-3-methylbutanami-do)-3-methylbutanamide 53.

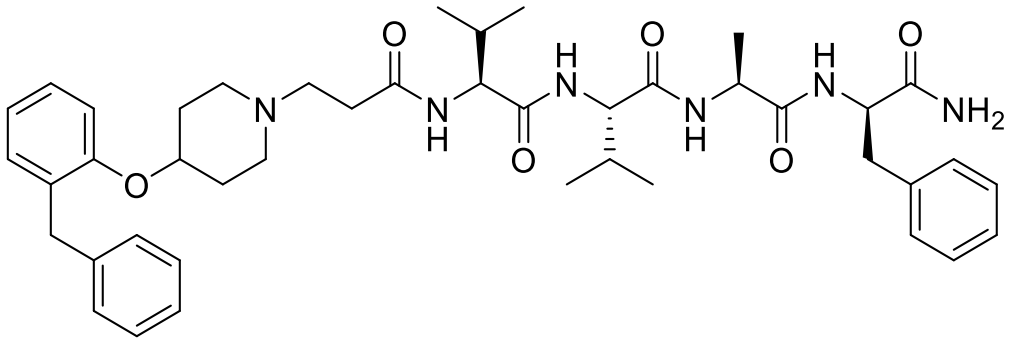

Compound synthesised using General Procedure 2 and purified using *System 4* to give a white solid (1.62mg, 2.1µmol, 5%). **HRMS** (Bruker MicroTOF)(*m/z*): Calculated $(M+H)^+$ for $C_{43}H_{58}N_6O_6$ = 755.4491; Measured = 755.4515; Error = 3.2ppm. **Analytical HPLC** (System 2): 90% purity; t_R = 15.34 min.

(*S*)-*N*-((*S*)-1-(((*S*)-1-(((*R*)-1-Amino-1-oxo-3-phenylpropa-n-2-yl)amino)-1-oxopropan-2-yl)amino)-1-oxo-3-phen-ylpropan-2-yl)-2-(3-(4-(2-benzylphenoxy)piperidin-1-yl)-propanamido)-3-methylbutanamide 54.

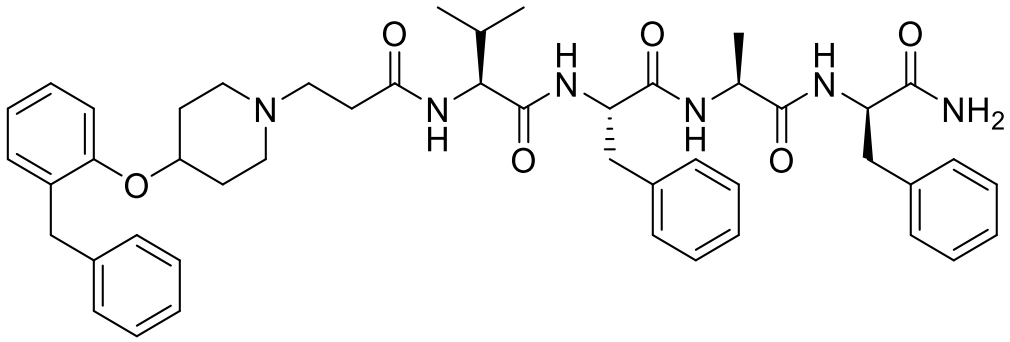

Compound synthesised using General Procedure 2 and purified using *System 4* to give a white solid (1.94mg, 2.4µmol, 6%). **HRMS** (Bruker MicroTOF)(*m/z*): Calculated $(M+H)^+$ for $C_{47}H_{58}N_6O_6$ = 803.4491; Measured = 803.4510; Error = 2.4ppm. **Analytical HPLC** (System 2): 99% purity; t_R = 16.28 min.

(*S*)-*N*-((*S*)-1-(((*S*)-1-(((*R*)-1-Amino-1-oxo-3-phenylpropa-n-2-yl)amino)-1-oxopropan-2-yl)amino)-3-(4-hydroxy-phenyl)-1-oxopropan-2-yl)-2-(3-(4-(2-benzylphenoxy)-piperidin-1-yl)propanamido)-3-methylbutanamide 55.

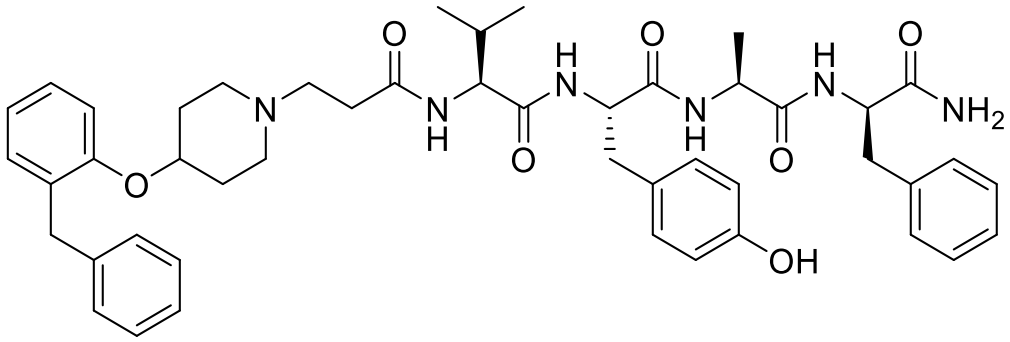

Compound synthesised using General Procedure 2 and purified using *System 4* to give a white solid (2.36mg, 2.9µmol, 7%). **HRMS** (Bruker MicroTOF)(*m/z*): Calculated $(M+H)^+$ for $C_{47}H_{58}N_6O_7$ = 819.4440; Measured = 819.4457; Error = 2.1ppm. **Analytical HPLC** (System 2): 96% purity; t_R = 15.32 min.

(*S*)-*N*-((*S*)-1-(((*S*)-1-(((*R*)-1-Amino-1-oxo-3-phenylpropa-n-2-yl)amino)-1-oxopropan-2-yl)amino)-3-hydroxy-1-oxo-propan-2-yl)-2-(3-(4-(2-benzylphenoxy)piperidin-1-yl)-propanamido)-3-methylbutanamide 56.

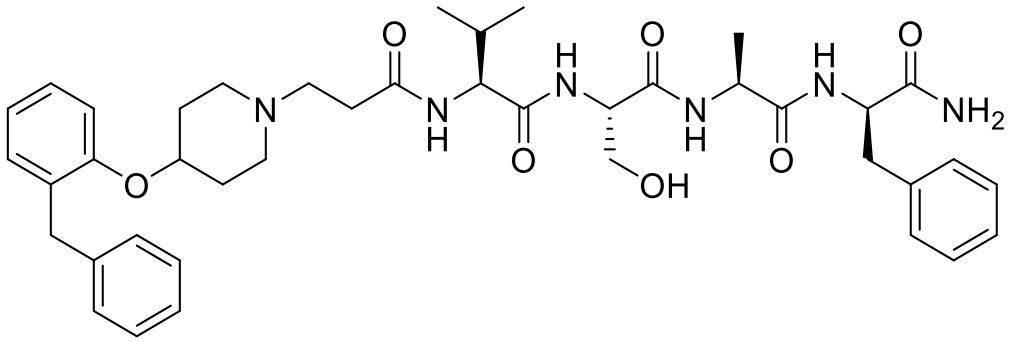

Compound synthesised using General Procedure 2 and purified using *System 4* to give a white solid (2.87mg, 3.9µmol, 10%). HRMS (Bruker MicroTOF)(*m/z*): Calculated $(M+H)^+$ for $C_{41}H_{54}N_6O_7$ = 743.4127; Measured = 743.4153; Error = 3.5ppm. Analytical HPLC (System 2): 99% purity; t_R = 14.47 min.

(*S*)-*N*1-((*S*)-1-(((*R*)-1-Amino-1-oxo-3-phenylpropan-2-yl)amino)-1-oxopropan-2-yl)-2-((*S*)-2-(3-(4-(2-benzyl-phenoxy)piperidin-1-yl)propanamido)-3-methylbutanamido)succinamide 57.

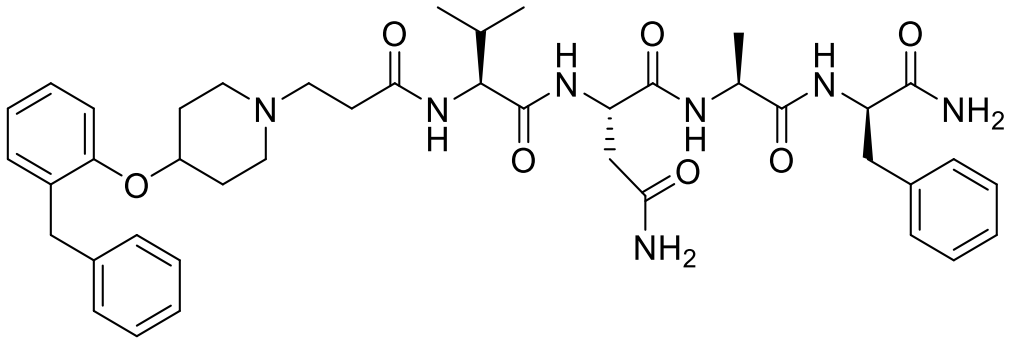

Compound synthesised using General Procedure 2 and purified using *System 4* to give a white solid (2.86mg, 3.7µmol, 9%). **HRMS** (Bruker MicroTOF)(*m/z*): Calculated $(M+H)^+$ for $C_{42}H_{55}N_7O_7$ = 770.4236; Measured = 770.4266; Error = 3.9ppm. **Analytical HPLC** (System 2): 99% purity; t_R = 14.28 min.

(*S*)-*N*-((*S*)-1-(((*S*)-1-(((*R*)-1-Amino-1-oxo-3-phenylpropa-n-2-yl)amino)-1-oxopropan-2-yl)amino)-3-(1*H*-imidazol-5-yl)-1-oxopropan-2-yl)-2-(3-(4-(2-benzylphenoxy)pipe-ridin-1-yl)propanamido)-3-methylbutanamide 58.

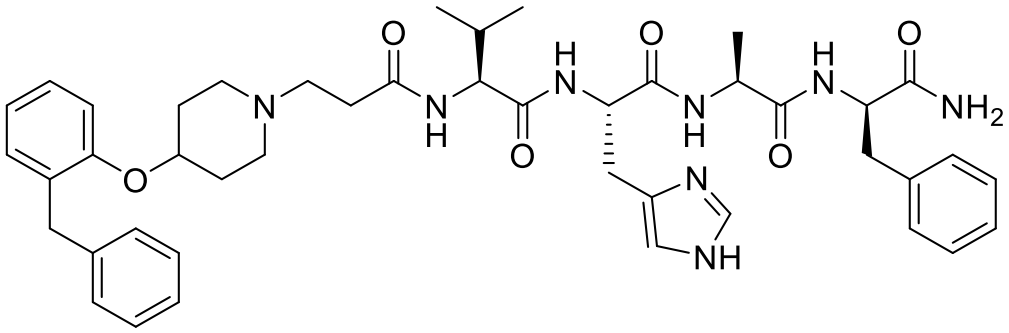

Compound synthesised using General Procedure 2 and purified using *System 4* to give a white solid (3.12mg, 3.9µmol, 10%). **HRMS** (Bruker MicroTOF)(*m/z*): Calculated $(M+H)^+$ for $C_{44}H_{56}N_8O_6$ = 793.4396; Measured = 793.4412; Error = 2.0ppm. **Analytical HPLC** (System 2): 99% purity; t_R = 13.14 min.

(*S*)-6-Amino-*N*-((*S*)-1-(((*R*)-1-Amino-1-oxo-3-phenylpropan-2-yl)amino)-1-oxopropan-2-yl)-2-((*S*)-2-(3-(4-(2-benzylphenoxy)piperidin-1-yl)propanamido)-3-methyl butanamido)hexanamide 59.

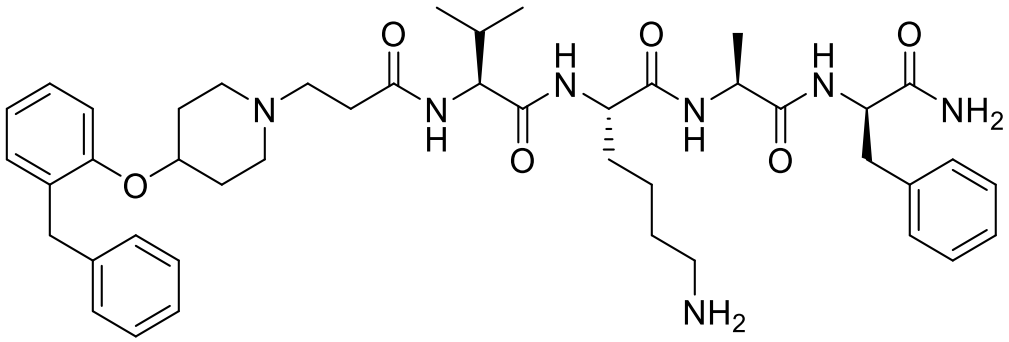

Compound synthesised using General Procedure 2 and purified using *System 4* to give a white solid (2.92mg, 3.7µmol, 9%). **HRMS** (Bruker MicroTOF)(*m/z*): Calculated $(M+H)^+$ for $C_{44}H_{61}N_7O_6$ = 784.4756; Measured = 787.4772; Error = 2ppm. **Analytical HPLC** (System 2): 99% purity; t_R = 12.97 min.

(*S*)-4-(((*S*)-1-(((*R*)-1-Amino-1-oxo-3-phenylpropan-2-yl) amino)-1-oxopropan-2-yl)amino)-3-((*S*)-2-(3-(4-(2-ben-zylphenoxy)piperidin-1-yl)propanamido)-3-methylbuta namido)-4-oxobutanoic acid 60.

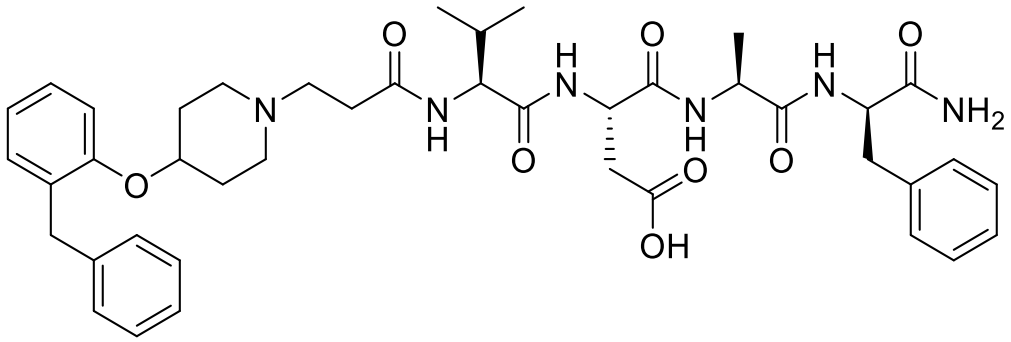

Compound synthesised using General Procedure 2 and purified using *System 4* to give a white solid (3.71mg, 4.8µmol, 12%). **HRMS** (Bruker MicroTOF)(*m/z*): Calculated $(M+H)^+$ for $C_{42}H_{54}N_6O_8$ = 771.4076; Measured = 771.4082; Error = 0.8ppm. **Analytical HPLC** (System 2): 99% purity; t_R = 14.60 min.

(*S*)-*N*-((*S*)-1-((2-(((*R*)-1-Amino-1-oxo-3-phenylpropan-2-yl)amino)-2-oxoethyl)-amino)-3-hydroxy-1-oxopropan-2-yl)-2-(3-(4-(2-benzylphenoxy)piperidin-1-yl)propanamido)-3-methylbutanamide 61.

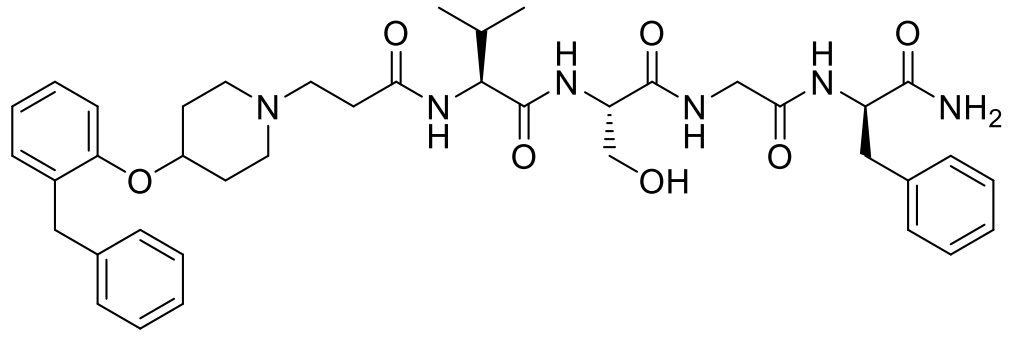

Compound synthesised using General Procedure 2 and purified using *System 4* to give a white solid (2.67mg, 3.7µmol, 9%). **HRMS** (Bruker MicroTOF)(*m/z*): Calculated $(M+H)^+$ for $C_{40}H_{52}N_6O_7$ = 729.3970; Measured = 729.3984; Error = 1.8ppm. **Analytical HPLC** (System 2): 97% purity; t_R = 14.23 min.

(*S*)-*N*-((*R*)-1-Amino-1-oxo-3-phenylpropan-2-yl)-2-((*S*)-2-((*S*)-2-(3-(4-(2-benzylphenoxy)piperidin-1-yl)propanamido)-3-methylbutanamido)-3-hydroxypropanamido)-3-methylbutanamide 62.

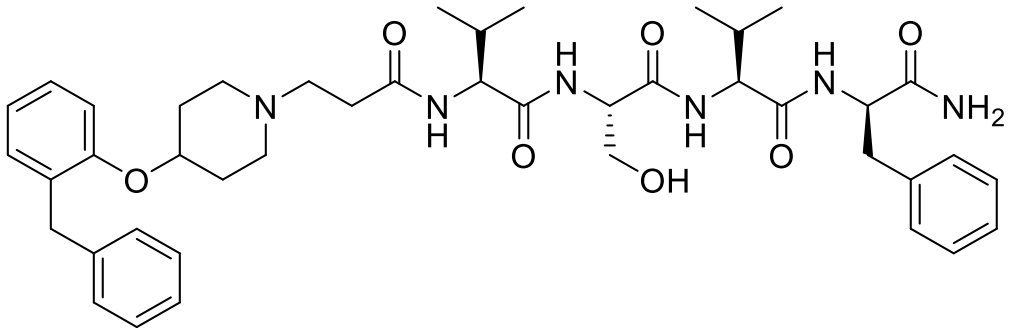

Compound synthesised using General Procedure 2 and purified using *System 4* to give a white solid (1.58mg, 2.1µmol, 5%). **HRMS** (Bruker MicroTOF)(*m/z*): Calculated $(M+H)^+$ for $C_{43}H_{58}N_6O_7$ = 771.4440; Measured = 771.4452; Error = 1.6ppm. **Analytical HPLC** (System 2): 99% purity; t_R = 15.14 min.

(*S*)-*N*-((*S*)-1-(((*S*)-1-(((*R*)-1-Amino-1-oxo-3-phenylpropan-2-yl)amino)-1-oxo-3-phenylpropan-2-yl)amino)-3-hydroxy-1-oxopropan-2-yl)-2-(3-(4-(2-benzylphenoxy)piperidin-1-yl)propanamido)-3-methylbutanamide 63.

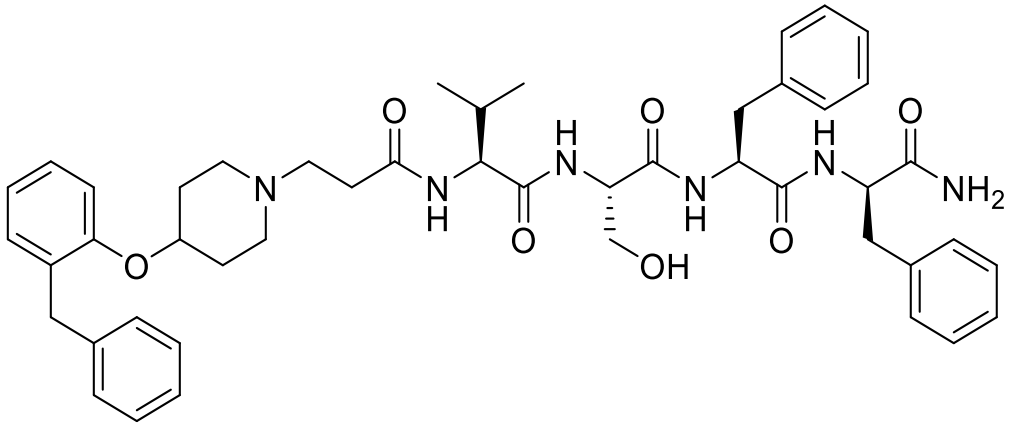

Compound synthesised using General Procedure 2 and purified using *System 4* to give a white solid (2.35mg, 2.9µmol, 7%). **HRMS** (Bruker MicroTOF)(*m/z*): Calculated $(M+H)^+$ for $C_{47}H_{58}N_6O_7$ = 819.4440; Measured = 819.4474; Error = 4.2ppm. **Analytical HPLC** (System 2): 99% purity; t_R = 15.85 min.

(*S*)-*N*-((*S*)-1-(((*S*)-1-(((*R*)-1-Amino-1-oxo-3-phenylpropa-n-2-yl)amino)-3-(4-hydroxyphenyl)-1-oxopropan-2-yl)amino)-3-hydroxy-1-oxopropan-2-yl)-2-(3-(4-(2-benzylphenoxy)piperidin-1-yl)propanamido)-3-methylbutanamide 64.

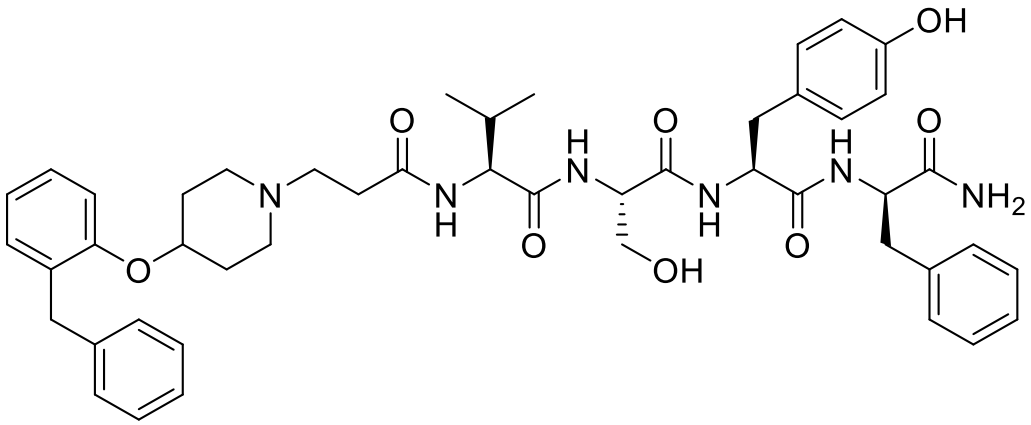

Compound synthesised using General Procedure 2 and purified using *System 4* to give a white solid (2.31mg, 2.8µmol, 7%). **HRMS** (Bruker MicroTOF)(*m/z*): Calculated $(M+H)^+$ for $C_{47}H_{58}N_6O_8$ = 835.4389; Measured = 835.4398; Error = 1.1ppm. **Analytical HPLC** (System 2): 99% purity; t_R = 14.78 min.

(*S*)-*N*-((*S*)-1-(((*S*)-1-(((*R*)-1-Amino-1-oxo-3-phenylpropa-n-2-yl)amino)-3-hydroxy-1-oxopropan-2-yl)amino)-3-hydroxy-1-oxopropan-2-yl)-2-(3-(4-(2-benzylphenoxy) piperidin-1-yl)propanamido)-3-methylbutanamide 65.

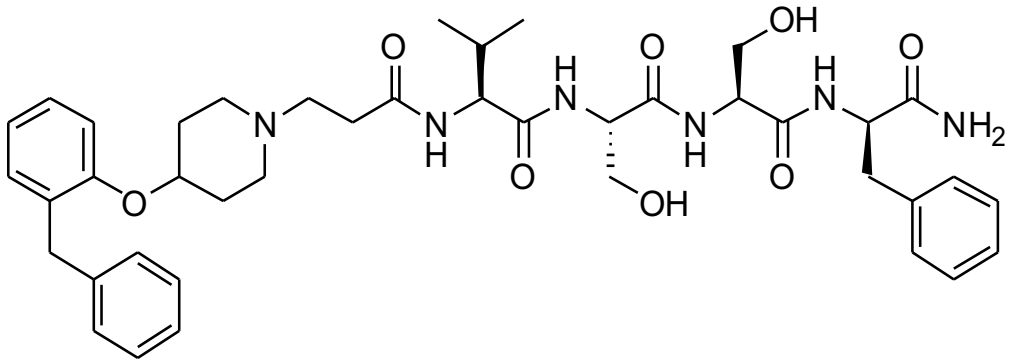

Compound synthesised using General Procedure 2 and purified using *System 4* to give a white solid (0.39mg, 0.5µmol, 1%). **HRMS** (Bruker MicroTOF)(*m/z*): Calculated $(M+H)^+$ for $C_{41}H_{54}N_6O_8$ = 759.4076; Measured = 759.4088; Error = 1.6ppm. **Analytical HPLC** (System 2): 89% purity; t_R = 14.07 min.

(*S*)-*N*1-((*R*)-1-Amino-1-oxo-3-phenylpropan-2-yl)-2-((*S*)-2-((*S*)-2-(3-(4-(2-benzyl-phenoxy)piperidin-1-yl)propanamido)-3-methylbutanamido)-3-hydroxypropan-amido)-succinamide 66.

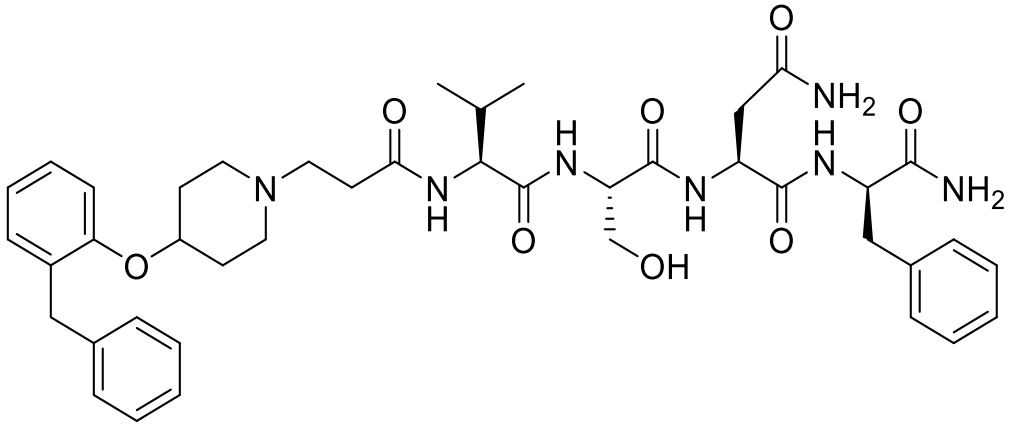

Compound synthesised using General Procedure 2 and purified using *System 4* to give a white solid (1.90mg, 2.4µmol, 6%). **HRMS** (Bruker MicroTOF)(*m/z*): Calculated $(M+H)^+$ for $C_{42}H_{55}N_7O_8$ = 786.4185; Measured = 786.4192; Error = 1.0ppm. **Analytical HPLC** (System 2): 99% purity; t_R = 13.90 min.

(*S*)-*N*-((*S*)-1-(((*S*)-1-(((*R*)-1-Amino-1-oxo-3-phenylpropa-n-2-yl)amino)-3-(1*H*-imidazol-4-yl)-1-oxopropan-2-yl)amino)-3-hydroxy-1-oxopropan-2-yl)-2-(3-(4-(2-benzylphenoxy)piperidin-1-yl)propanamido)-3-methylbutanamide 67.

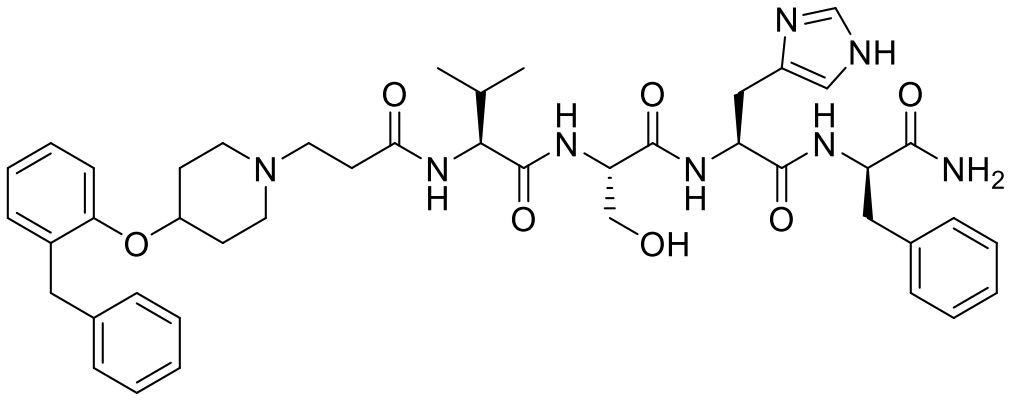

Compound synthesised using General Procedure 2 and purified using *System 4* to give a white solid (3.03mg, 3.7µmol, 9%). **HRMS** (Bruker MicroTOF)(*m/z*): Calculated $(M+H)^+$ for $C_{44}H_{56}N_8O_7$ = 809.4345; Measured = 809.4345; Error = 0ppm. **Analytical HPLC** (System 2): 99% purity; t_R = 12.67 min.

((*S*)-6-Amino-*N*-((*R*)-1-amino-1-oxo-3-phenylpropan-2-yl)-2-((*S*)-2-((*S*)-2-(3-(4-(2-benzylphenoxy)-piperidin-1-yl)propanamido)-3-methylbutanamido)-3-hydroxypropanamido)hexanamide 68.

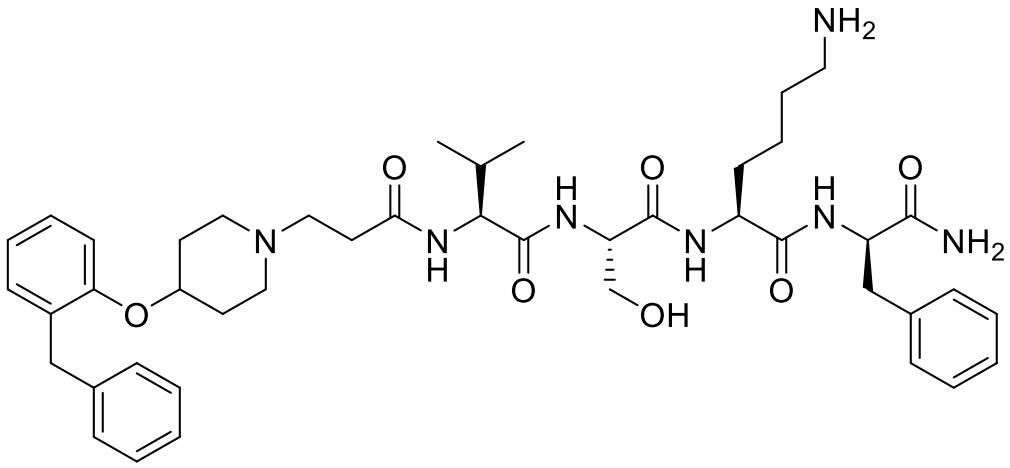

Compound synthesised using General Procedure 2 and purified using *System 4* to give a white solid (2.79mg, 3.5µmol, 9%). **HRMS** (Bruker MicroTOF)(*m/z*): Calculated $(M+H)^+$ for $C_{44}H_{61}N_7O_7$ = 800.4705; Measured = 800.4681; Error = 3.10ppm. **Analytical HPLC** (System 2): 99% purity; t_R = 12.52 min.

(*S*)-4-(((*R*)-1-Amino-1-oxo-3-phenylpropan-2-yl)amino)-3-((*S*)-2-((*S*)-2-(3-(4-(2-benzylphenoxy)-piperidin-1-yl)propanamido)-3-methylbutanamido)-3-hydroxypropana-mido)-4-oxobutanoic acid 69.

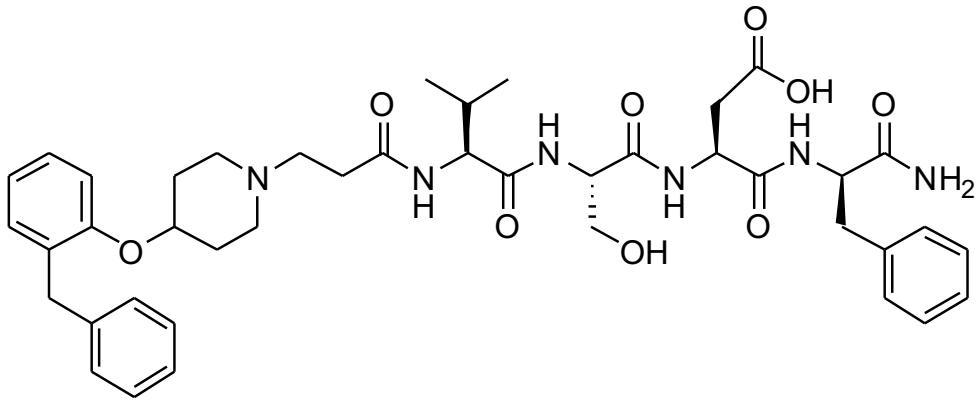

Compound synthesised using General Procedure 2 and purified using *System 4* to give a white solid (1.98mg, 2.5µmol, 6%). **HRMS** (Bruker MicroTOF)(*m/z*): Calculated $(M+H)^+$ for $C_{42}H_{54}N_6O_9$ = 787.4025; Measured = 787.4044; Error = 2.4ppm. **Analytical HPLC** (System 2): 99% purity; t_R = 14.23 min.

(*S*)-*N1*-((*S*)-1-Amino-1-oxo-3-phenylpropan-2-yl)-2-((*S*)-2-((*S*)-2-(3-(4-(2-benzylphenoxy)piperidin-1-yl)propanamido)-3-methylbutanamido)-3-hydroxypropanamido) succinamide 73

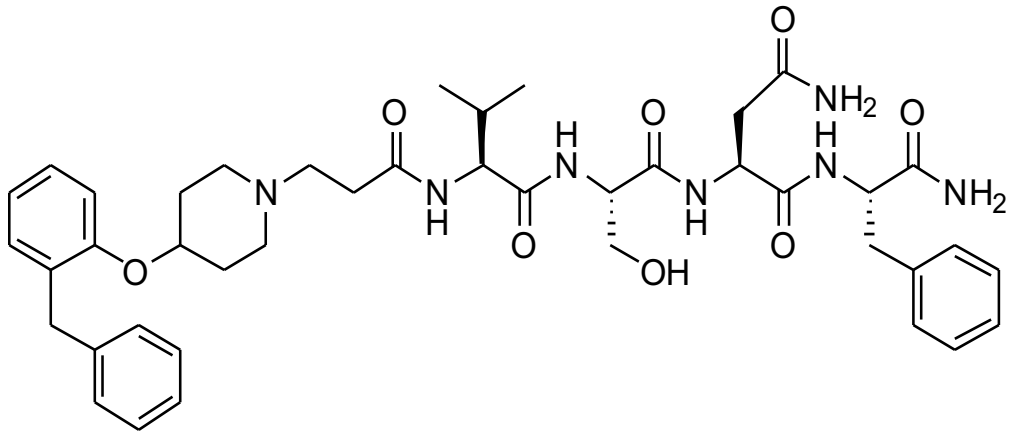

Compound synthesised using General Procedure 2 and purified using *System 4* to give a white solid (1.07mg, 1.4µmol, 3%). **HRMS** (Bruker MicroTOF)(*m/z*): Calculated $(M+H)^+$ for $C_{42}H_{55}N_7O_8$ = 786.4185; Measured = 785.4197; Error = 1.6ppm. **Analytical HPLC** (System 2): 99% purity; t_R = 14.17 min.

(*S*)-*N*-((*S*)-1-(((*S*)-1-(((*S*)-1-Amino-1-oxo-3-phenylpropan-2-yl)amino)-3-(4-hydroxyphenyl)-1-oxopropan-2-yl)amino)-3-hydroxy-1-oxopropan-2-yl)-2-(3-(4-(2-benzylphenoxy)piperidin-1-yl)propanamido)-3-methylbutanamide 74

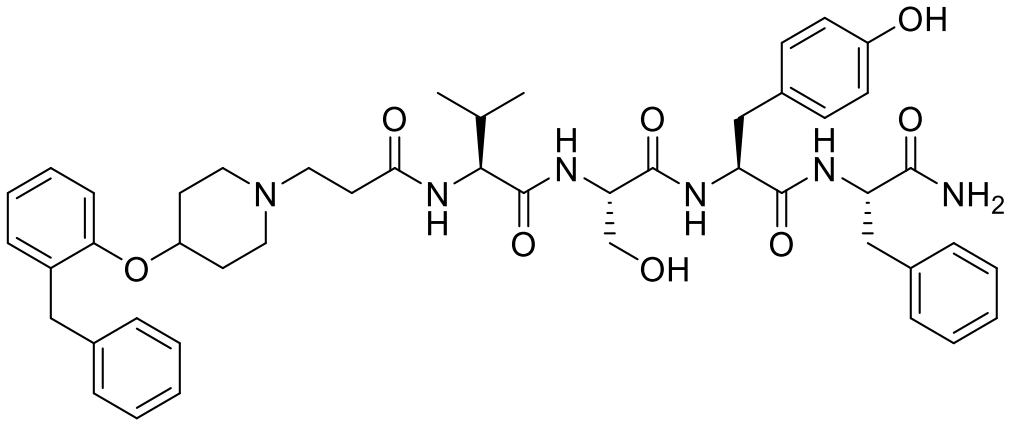

Compound synthesised using General Procedure 2 and purified using *System 4* to give a white solid (0.81mg, 1µmol, 2%). **HRMS** (Bruker MicroTOF)(*m/z*): Calculated $(M+H)^+$ for $C_{47}H_{58}N_6O_8$ = 835.4389; Measured = 835.4369; Error = 2.4ppm. **Analytical HPLC** (System 2): 93% purity; t_R = 15.15 min.

***tert*-Butyl 2-(dimethoxymethyl)-1*H*-pyrrole-1-carboxylate 78**

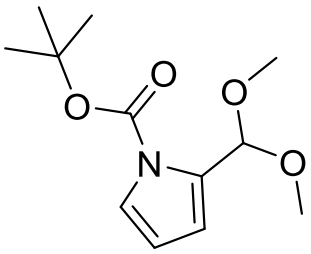

1g (10.52mmol) of 2-formylpyrrole and 2.525g (11.57mmol) of di-*tert*-butyl dicarbonate were dissolved in 20mL of DCM, treated with 1.7mL (11.57mmol) of triethylamine and 64mg (0.526mmol) of 4-dimethylaminopyridine and stirred for 30 min at RT. The reaction mixture was then filtered through a silica plug washing with DCM and monitored using TLC. The filtrate was concentrated and dried over rotary evaporator and vacuum oven to afford a pale brown oil (2.044g, 10.4mmol, 99%). 1g (5.122mmol) of the oil was dissolved in 5mL of MeOH, subsequently treated with 1.1mL (10.245mmol) of trimethyl orthoformate and 19.5mg (0.1024mmol) of p-toluenesulfonic acid and left to stir for 3 hr at RT. The resulting reaction mixture was diluted with 10mL of sat. aq. $NaHCO_3$ and 10mL of water, extracted with EtOAc and the resulting organic layer washed with sat. brine, dried over $MgSO_4$, filtered and concentrated over rotary evaporator to afford a dark brown gum (1.07g, 4.46mmol, 87%)

^{1}H NMR (400 MHz, $CDCl_3$) δ 7.20 (dd, *J* = 3.3, 1.9 Hz, 1H, Pyrrole C5**H**), 6.45 – 6.39 (m, 1H, Pyrrole C3**H**), 6.12 – 6.08 (m, 1H, Pyrrole C4**H**), 5.88 (s, 1H, -C**H**$(OMe)_2$), 3.32 (s, 6H, 2 x -OC**H$_3$**), 1.58 (s, 9H, -OC(C**H$_3$**)$_3$).)

^{13}C NMR (101 MHz, $CDCl_3$) δ 148.85, 131.42, 122.50, 113.40, 109.78, 98.43, 83.85, 53.35, 27.96.

(5-Formyl-1*H*-pyrrol-2-yl)boronic acid 79

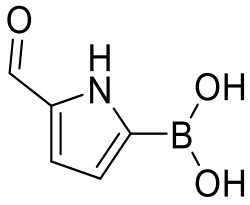

1.2g (5mmol) of **78** and 1.8mL (7.5mmol) of triisopropylborate were dissolved in 6mL of dry THF and cooled to 0°C under N_2. The mixture was treated with dropwise with 6.5mL (13mmol) of lithium diisopropylamide (2.0 M in THF/heptane/ethylbenzene) over a 15 min period and left to stir for 30 min. The reaction mixture was then quenched with sat. NH_4Cl and poured into a stirred 25mL aq. solution of 10% $NaHSO_4$ and heated to 70°C for 2 hr. The pH of the mixture was adjusted to approximately 2 by adding more $NaHSO_4$. The organics were then extracted with EtOAc, the organic layer washed with sat. brine, dried over $MgSO_4$, filtered and concentrated under rotary evaporator to afford a black gum. This was subsequently triturated with 10mL of diisopropyl ether/hexane (1:1) to afford a black solid (235mg, 1.69mmol, 34%).

^{1}H NMR (400 MHz, DMSO-d_6) δ 11.67 (s, 1H, Pyrrole-N1**H**), 9.56 (s, 1H, -C**H**O), 8.18 (s, 2H, -B(O**H**)$_2$), 6.96 (dd, *J* = 3.7, 2.2 Hz, 1H, Pyrrole-C4**H**), 6.75 (dd, *J* = 3.7, 2.2 Hz, 1H, Pyrrole-C3**H**).

^{13}C NMR (101 MHz, DMSO-d_6) δ 180.06, 135.53, 120.02, 119.28 (N.B. C2 carbon not observed due to the quadrupolar boron)

LCMS: *m/z* of $(M+H)^+$ too small to be observable (<150 Mw); t_R = 2.43 min.

5-(Thiophen-2-yl)-1*H*-pyrrole-2-carbaldehyde 71

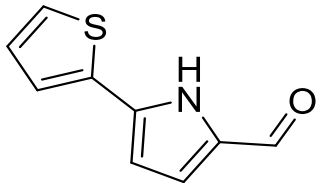

235mg (1.69mmol) of **79** and 140uL (1.44mmol) of 2-bromothiophene were dissolved in 15mL of 10% water/dioxane and degassed by bubbling N_2 for 15 mins. 178mg (1.69mmol) of Na_2CO_3 and 50mg (0.071mmol) of $Pd(PPh_3)_2Cl_2$ were added and heated to 100°C under N_2 for 3 hr. The resulting reaction mixture was cooled to RT over time, diluted with 15mL of water, extracted with diethyl ether and the resulting organic layer was washed with sat. brine, dried over $MgSO_4$, filtered, concentrated over rotary evaporator and purified by column chromatography (EtOAc:hexane = 15:85) to afford a yellowish orange solid (82mg, 0.46mmol, 32%).

^{1}H NMR (400 MHz, $CDCl_3$) δ 9.96 (s, 1H, Pyrrole N1**H**), 9.49 (s, 1H, -C**H**O), 7.38 (d, *J* = 3.6 Hz, 1H, Thiophene-C3**H**), 7.32 (d, *J* = 5.1 Hz, 1H, Thiophene-C5**H**), 7.11 – 7.06 (m, 1H, Thiophene-C4**H**), 7.01 – 6.97 (m, 1H, Pyrrole-C4**H**), 6.55 – 6.50 (m, 1H, Pyrrole-C3**H**).

^{13}C NMR (101 MHz, $CDCl_3$) δ 178.76, 134.87, 133.85, 132.95, 128.33, 125.94, 124.54, 123.12, 109.54.

LCMS: *m/z* of $(M+H)^+$ = 178.1; t_R = 2.61 min.

Tributyl(4-methoxybenzyl)phosphonium chloride 80

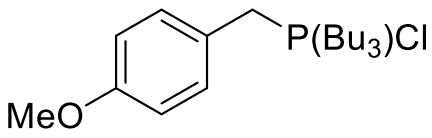

2mL (15mmol) of 4-methoxybenzyl chloride and 6mL (22.5mmol) of tributylphosphine were dissolved in 15mL of dry toluene and heated under reflux for 18 hrs under N_2. The reaction mixture was left to cool and concentrated by blowing N_2, which was subsequently triturated with diethyl ether, filtered and dried in a vacuum oven to afford the product, a white, hygroscopic solid (4.618g, 12.9mmol, 86%).

^{1}H NMR (400 MHz, DMSO-d_6) δ 7.28 (dd, *J* = 8.8, 2.4 Hz, 2H, Ph-C2**H**), 6.98 (d, *J* = 8.5 Hz, 2H, Ph-C3**H**), 3.79 (d, *J* = 14.9 Hz, 2H, -C**H$_2$**P-), 3.75 (s, 3H, -OC**H$_3$**), 2.26 – 2.03 (m, 6H, 3 x -PC**H$_2$**$CH_2CH_2CH_3$), 1.44 – 1.33 (m, 12H, 3 x -PCH_2C**H$_2$**C**H$_2$**CH_3), 0.91 – 0.86 (m, 9H, 3 x -$PCH_2CH_2CH_2$C**H$_3$**).

^{13}C NMR (101 MHz, DMSO-d_6) δ 158.94 (d, *J* = 3.4 Hz), 131.09 (d, *J* = 4.8 Hz), 120.61 (d, *J* = 8.5 Hz), 114.57 (d, *J* = 2.7 Hz), 55.17, 24.53 (d, *J* = 44.6 Hz), 23.35 (d, *J* = 15.6 Hz), 22.52 (d, *J* = 4.6 Hz), 17.27 (d, *J* = 47.0 Hz), 13.22.

LCMS: *m/z* of $(M\text{-}Cl)^+$ = 324.4; t_R = 2.39 min.

(*E*)-2-(4-Methoxystyryl)-1*H*-pyrrole 81

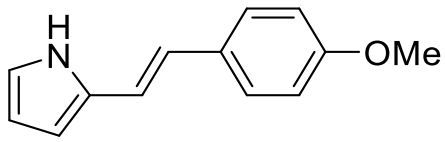

1g (2.79mmol) of **80** was transferred to a microwave vial, treated with a solution of 2.8M NaOH (112mg in 1mL water, 2.79mmol), vortexed for 1 min and sonicated for 3 min resulting in a white suspension. 239mg (2.51mmol) of 2-formylpyrrole was added into the vial and heated in the MW to 100°C for 25 min. The reaction mixture was diluted with water, extracted with DCM and the resulting organic layer was washed with brine, dried over $MgSO_4$ and filtered. The filtrate was washed through a silica plug with DCM monitored by TLC and the filtrate dried under rotary evaporator to afford a bluish green solid (380mg, 1.91mmol, 76%).

^{1}H NMR (400 MHz, $CDCl_3$) δ 8.30 (s, 1H), 7.41 – 7.34 (m, 2H, 2 x Ph-C2**H**), 6.90 – 6.87 (m, 2H, 2 x Ph-C3**H**), 6.84 (d, *J* = 16.6 Hz, 1H, -CHC**H**Ph), 6.82 – 6.76 (m, 1H, Pyrrole-C5**H**), 6.63 (d, *J* = 16.5 Hz, 1H, -C**H**CHPh), 6.33 – 6.30 (m, 1H, Pyrrole-C3**H**), 6.28 – 6.21 (m, 1H, Pyrrole-C4**H**), 3.82 (s, 3H, -OC**H$_3$**).

^{13}C NMR (101 MHz, $CDCl_3$) δ 158.96, 131.20, 130.45, 127.13, 123.26, 118.83, 117.26, 114.29, 110.04, 108.53, 55.47.

LCMS: *m/z* of $(M+H)^+$ = 200.0; t_R = 2.93 min.

(*E*)-2-(4-(Prop-2-yn-1-yloxy)styryl)-1*H*-pyrrole 72

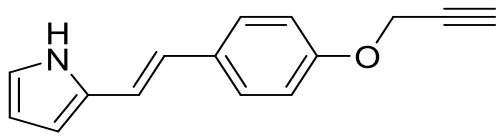

200mg (1mmol) of **81** was dissolved in degassed, anhydrous DMF (6mL) under N_2 was treated with 168mg of sodium ethanethiolate (2mmol) and heated to 145°C for 18 hrs. The reaction mixture was then diluted with ethyl acetate (30mL) and washed with 0.5M NH_4Cl (5 x 30mL), sat. brine, dried over $MgSO_4$, filtered and concentrated in vacuo to afford a black solid. This was dissolved in acetonitrile (5mL) and treated with 208mg of K_2CO_3 (1.5mmol) and heated to reflux under N_2 for 30 min. This was left to cool at rt, treated with 100µL (1.1mmol) of propargyl bromide and heated to reflux for 18 hr. This was left to cool, the solids were filtered off, washed with acetonitrile (3 x 10 mL), filtrate evaporated under vacuum and placed in a vacuum oven to dry which gave a grey solid (197mg, 0.88mmol, 88%).

^{1}H NMR (400 MHz, $CDCl_3$) δ 8.32 (s, 1H, Pyrrole **H**), 7.40 – 7.33 (m, 2H, 2 x Ph-C2**H**), 6.99 – 6.91 (m, 2H, 2 x Ph-C3**H**), 6.85 (d, *J* = 16.5 Hz, 1H, -CHC**H**Ph), 6.81 – 6.77 (m, 1H, Pyrrole-C5**H**), 6.62 (d, *J* = 16.5 Hz, 1H, -C**H**CHPh), 6.36 – 6.30 (m, 1H, Pyrrole-C3**H**), 6.28 – 6.21 (m, 1H, Pyrrole-C4**H**), 4.70 (d, *J* = 2.4 Hz, 2H, OC**H$_2$**C≡CH), 2.53 (t, *J* = 2.4 Hz, 1H, -$OCH_2C{\equiv}C$**H**).

^{13}C NMR (101 MHz, $CDCl_3$) δ 156.77, 131.34, 131.04, 127.06, 122.97, 118.98, 117.68, 115.26, 109.98, 108.63, 78.66, 75.74, 55.98.

LCMS: *m/z* of $(M+H)^+$ = 223.8; t_R = 2.94 min.

(*E*)-5,5-Difluoro-7-(4-(prop-2-yn-1-yloxy)styryl)-3-(thiophen-2-yl)-5*H*-5λ^4-dipyrrolo[1,2-*c*:2',1'-*f*][1,3,2]diazaborinin-4-ium 70

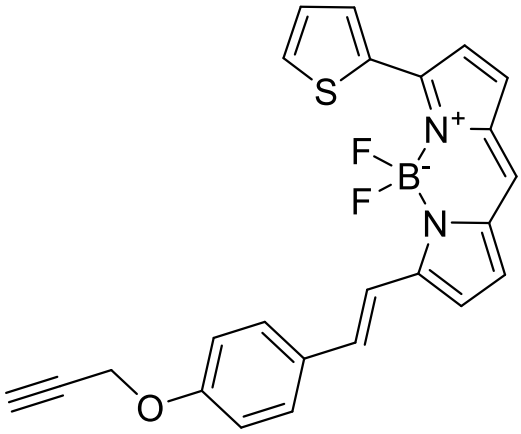

151mg (0.85mmol) of **71** and 190mg (0.85mmol) of **72** were dissolved in a mixture of dry DCM/MeOH (10:1, 33mL) and degassed for 15 mins. The reaction flask was placed under N_2, treated dropwise with 80µL (0.85mmol) of $POCl_3$ and stirred at RT for 15 hr in the dark. The mixture was concentrated by blowing N_2, diluted in 150mL of DCM, treated with 1.4mL (10.22mmol) of DIPEA and 1.25mL (10.22mmol) of boron trifluoride diethyl etherate and allowed to stir in the dark under N_2 for 2 hr at RT. The reaction mixture was then washed with brine, dried over $MgSO_4$, filtered and concentrated under rotary evaporator. The resulting mixture was purified by column chromatography (20% EtOAc/hexane) to afford 251mg of red, iridescent solid (251mg, 0.58mmol, 69%).

^{1}H NMR (400 MHz, DMSO-d_6) δ 8.05 (dd, *J* = 3.8, 1.1 Hz, 1H, Thiophene-C**H**), 7.84 (dd, *J* = 5.0, 1.0 Hz, 1H, Thiophene-C**H**), 7.75 (d, *J* = 16.3 Hz, 1H, -CHC**H**Ph), 7.65 – 7.59 (m, 3H, 3 x Ar-C**H**), 7.41 (d, *J* = 16.2 Hz, 1H, -C**H**CHPh), 7.38 (d, *J* = 4.7 Hz, 1H, Ar-C**H**), 7.33 – 7.26 (m, 3H, 3 x Ar-C**H**), 7.12 (d, *J* = 8.8 Hz, 2H, Ar-C**H**), 6.96 (d, *J* = 4.3 Hz, 1H, Ar-C**H**), 4.88 (d, *J* = 2.4 Hz, 2H, -OC**H$_2$**C≡CH), 3.63 (t, *J* = 2.4 Hz, 1H, -OCH$_2$C≡C**H**)

^{13}C NMR (101 MHz, DMSO) δ 158.63, 156.36, 147.69, 138.74, 136.46, 136.37, 133.68, 131.29, 130.25, 129.68, 129.22, 129.03, 128.94, 125.17, 119.41, 118.23, 116.08, 116.06, 115.65, 78.91, 78.58, 55.63.

HRMS (Bruker MicroTOF)(*m/z*): Calculated $(M+H)^+$ for $C_{24}H_{17}B_1F_2N_2O_1S_1$ = 431.1195; Measured = 431.1206; Error = 1.4ppm.

LCMS: *m/z* of $(M+H)^+$ = 430.8; t_R = 3.23 min.

(*S*)-*N*1-((*S*)-1-Amino-3-azido-1-oxopropan-2-yl)-2-((S)-2-((S)-2-(3-(4-(2-benzylphenoxy)piperidin-1-yl)propanamido)-3-methylbutanamido)-3-hydroxypropanamido) succinamide 82

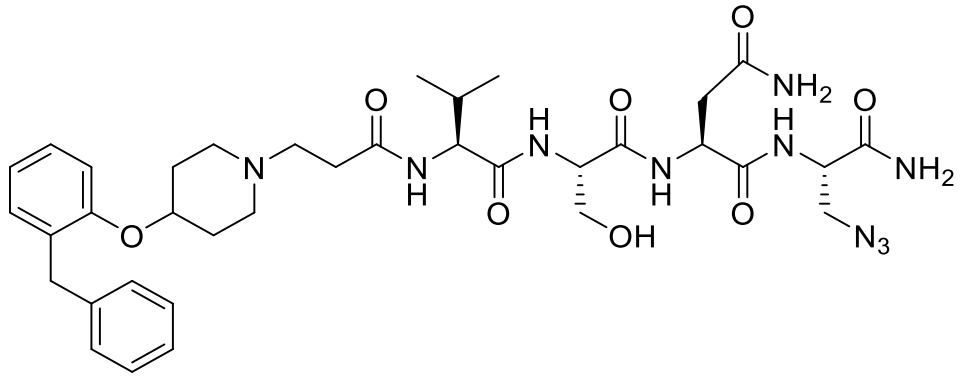

Compound synthesised using General Procedure 2 and purified using *System 7* to give a white solid (0.5mg, 0.7µmol, 2%). **HRMS** (Bruker MicroTOF)(*m/z*): Calculated $(M+H)^+$ for $C_{36}H_{50}N_{10}O_8$ = 751.3886; Measured = 751.3859; Error = 3.6ppm.

(*S*)-5-(((*S*)-4-Amino-1-(((*S*)-1-amino-3-azido-1-oxopropan-2-yl)amino)-1,4-dioxobutan-2-yl)amino)-4-((*S*)-2-(3-(4-(2-benzylphenoxy)piperidin-1-yl)propanamido)-3-methylbutanamido)-5-oxopentanoic acid 83

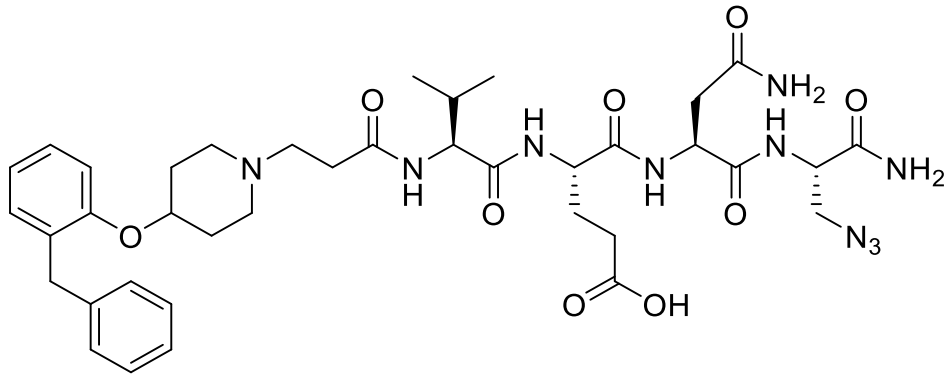

Compound synthesised using General Procedure 2 and purified using *System 7* to give a white solid (0.5mg, 0.6µmol, 2%). **HRMS** (Bruker MicroTOF)(*m/z*): Calculated $(M+H)^+$ for $C_{38}H_{52}N_{10}O_9$ = 815.3811; Measured = 815.3770; Error = 5.0ppm.

(*S*)-*N*-((*S*)-1-Amino-3-azido-1-oxopropan-2-yl)-2-((S)-2-((S)-2-(3-(4-(2-benzylphen-oxy)piperidin-1-yl)propanamido)propanamido)propanamido)propanamide 84

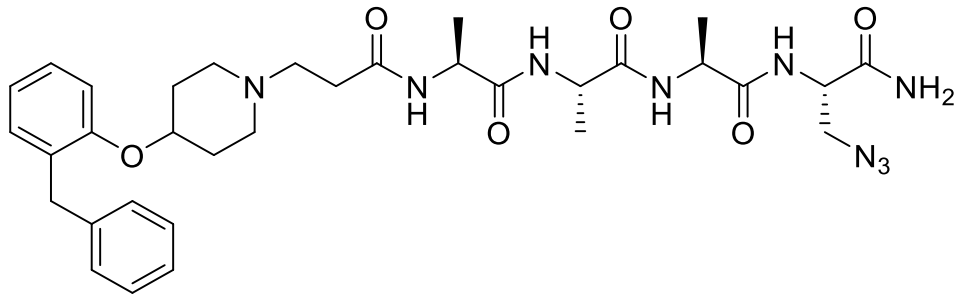

Compound synthesised using General Procedure 2 and purified using *System 7* to give a white solid (0.6mg, 0.9µmol, 2%). **HRMS** (Bruker MicroTOF)(*m/z*): Calculated $(M+H)^+$ for $C_{33}H_{45}N_9O_6$ = 664.3566; Measured = 664.3578; Error = 1.9ppm.

(*S*)-*N*1-((*S*)-1-Amino-3-(4-((4-((*E*)-2-(5,5-difluoro-7-(thiophen-2-yl)-5*H*-5λ^4,6λ^4-dipyrrolo[1,2-*c*:2',1'-*f*][1,3,2]diazaborinin-3-yl)vinyl)phenoxy)methyl)-1*H*-1,2,3-triazol-1-yl)-1-oxopropan-2-yl)-2-((*S*)-2-((*S*)-2-(3-(4-(2-benzylphenoxy)piperidin-1-yl)propanamido)-3-methylbutanamido)-3-hydroxypro-panamido)succinimide 75

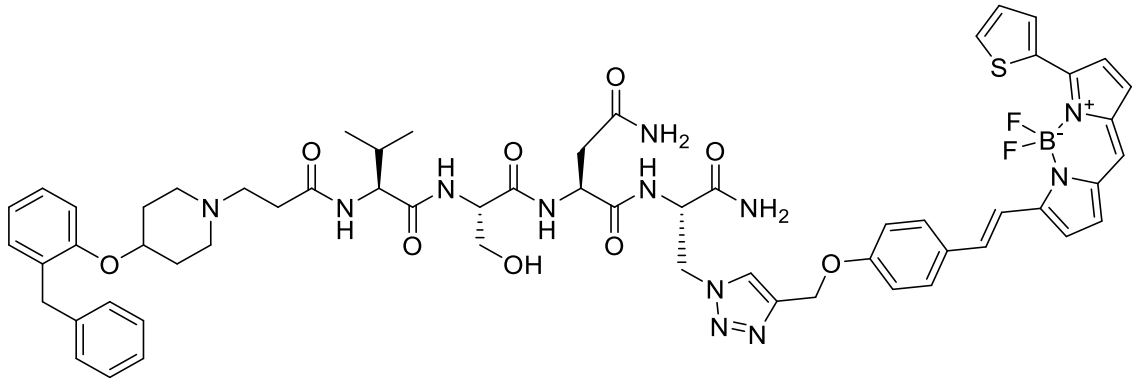

Compound synthesised using General Procedure 3 with 0.5mg (0.7µmol) of **79** and purified using *System 8* to give a blue solid (0.33mg, 0.4µmol, 67%). **HRMS** (Bruker MicroTOF)(*m/z*): Calculated $(M+H)^+$ for $C_{60}H_{67}B_1F_2N_{12}O_9S_1$ = 1181.5009; Measured = 1181.4954; Error = 5.5ppm. **Analytical HPLC** (System 2): 96% purity; t_R = 15.90 min.

(*S*)-5-(((*S*)-4-Amino-1-(((*S*)-1-amino-3-(4-((4-((*E*)-2-(5,5-difluoro-7-(thiophen-2-yl)-5*H*-5λ^4,6λ^4-dipyrrolo[1,2-*c*:2',1'-*f*][1,3,2]diazaborinin-3-yl)vinyl)phenoxy) methyl)-1*H*-1,2,3-triazol-1-yl)-1-oxopropan-2-yl)amino)-1,4-dioxobutan-2-yl)amino)-4-((*S*)-2-(3-(4-(2-benzylphenoxy)piperidin-1-yl)propanamido)-3-methylbutanamido)-5-oxopentanoic acid 76

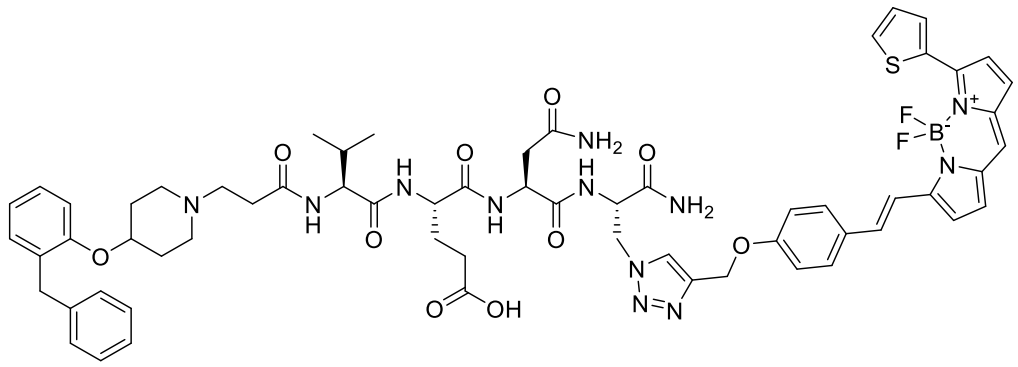

Compound synthesised using General Procedure 3 with 0.5mg (0.6µmol) of **80** and purified using *System 8* to give a blue solid (0.45mg, 0.4µmol, 60%). **HRMS** (Bruker MicroTOF)(*m/z*): Calculated $(M+H)^+$ for $C_{62}H_{69}B_1F_2N_{12}O_{10}S_1$ = 1223.5114; Measured = 1223.5051; Error = 0.3ppm. **Analytical HPLC** (System 2): 95% purity; t_R = 16.21 min.

(*S*)-*N*-((*S*)-1-Amino-3-(4-((4-((*E*)-2-(5,5-difluoro-7-(thiophen-2-yl)-5*H*-5λ^4,6λ^4-dipyrrolo[1,2-*c*:2',1'-*f*][1,3,2]diazaborinin-3-yl)vinyl)phenoxy)methyl)-1*H*-1,2,3-triazol-1-yl)-1-oxopropan-2-yl)-2-((*S*)-2-((*S*)-2-(3-(4-(2-benzylphenoxy)piperidin-1-yl)propanamido)propanamido)propanamido)-propanamide 77

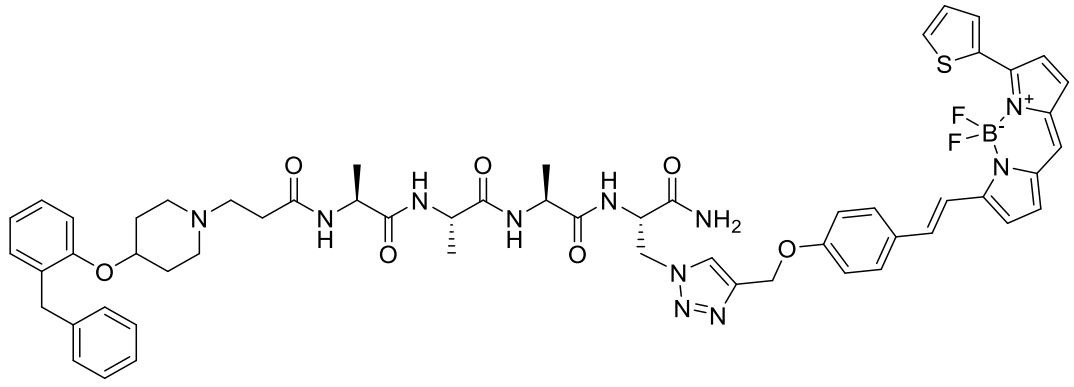

Compound synthesised using General Procedure 3 with 0.6mg (0.9µmol) of **81** and purified using *System 8* to give a blue solid (0.77mg, 0.7µmol, 79%). **HRMS** (Bruker MicroTOF)(*m/z*): Calculated $(M+H)^+$ for $C_{57}H_{62}B_1F_2N_{11}O_7S_1$ = 1094.4688; Measured = 1094.4711; Error = 0.3ppm. **Analytical HPLC** (System 2): 99% purity; t_R = 15.85 min.

(*E*)-3-(Dibenzo[*b*,*e*]oxepin-11(6*H*)-ylidene)-*N*-methylpropan-1-amine 85

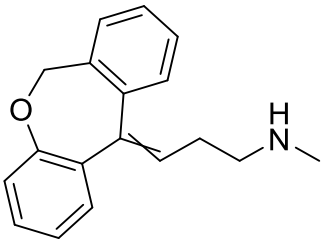

500mg (1.6mmol) of doxepin hydrochloride with a reported *E:Z* isomeric ratio of 85:15 was dissolved in 25mL of dichloromethane and washed with 25mL of saturated sodium bicarbonate solution to liberate the free base. The resulting organic layer was dried with brine wash and $MgSO_4$, filtered and concentrated using rotary evaporation. Doxepin was then dissolved in 5mL of chloroform, subsequently treated with 240µL (1.74mmol) of trichloroethyl-chloroformate and 243µL (1.74mmol) of triethylamine and left to stir at room temperature for 6 hrs. The resulting mixture was dried using rotary evaporator and purified using column chromatography (hexane:EtOAc = 80:20). The eluents with the product were combined, dried under rotary evaporation to give 536mg of product appearing as a yellow oil.

491mg (1.114mmol) of the oil was dissolved in 4mL of THF, transferred to a 2-necked RBF placed under N_2 environment and subsequently treated with 1mL of 1M NaH_2PO_4 (1mmol) and 1g (16.7mmol) of zinc powder and left to stir overnight. The resulting mixture was acidified with 2M HCl and washed three times with dichloromethane. The pH of the aqueous layer was then adjusted to 14 and extracted three times with dichloromethane. The resulting organic layer was dried by brine wash and $MgSO_4$, concentrated and dried under rotary evaporation to give a pale-yellow oil (170mg, 0.64mmol, 45% over 2 steps). *E*:*Z* ratio of 79:21 determined by 1H NMR.

^{1}H NMR (*E*-isomer) (400 MHz, $CDCl_3$) δ 7.40 – 7.21 (m, 5H, Ar-C**H**), 7.16 – 7.09 (m, 1H, Ar-C**H**), 6.92 – 6.82 (m, 1H, Ar-C**H**), 6.76 (dd, *J* = 8.2, 1.3 Hz, 1H, Ar-C**H**), 6.02 (t, *J* = 7.4 Hz, 1H, -CC**H**CH_2-), 5.54 (br s, 1H, PhOC**H_2**Ph), 4.83 (br s, 1H, PhOC**H_2**Ph), 2.71 (t, *J* = 7.1 Hz, 2H, -C**H_2**CH_2N-), 2.44 – 2.36 (m, 5H, -CH_2C**H_2**N- and -NC**H_3**).

^{13}C NMR (*E*-isomer) (101 MHz, $CDCl_3$) δ 155.19, 141.22, 140.91, 134.34, 130.21, 129.63, 129.19, 128.71, 128.30, 128.07, 127.93, 127.36, 121.10, 119.31, 70.23, 51.68, 36.20, 29.65.

LCMS: *m/z* of $(M+H)^+$ = 265.7; t_R = 2.16 min.

Methyl (*E*)-3-((3-(dibenzo[*b,e*]oxepin-11(6*H*)-ylidene)propyl)(methyl)amino)-propanoate 86

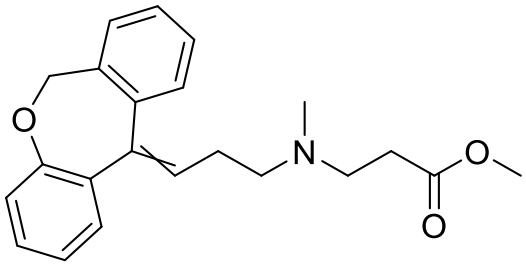

161mg (0.61mmol) of **85** was dissolved in 5mL of 1,2-dichloroethane (DCE) in a 50mL RBF and heated to 75°C under reflux. 660µL (7.32mmol) of methyl acrylate and approximately 1mL (5.75mmol, 9eq) of DIPEA was added into the RBF and left to react for overnight. DCE and excess methyl acrylate were removed using rotary evaporator and the crude was purified using column chromatography (hexane:EtOAc:Et_3N = 80:20:1) to give pale yellow oil as the product (148mg, 0.42mmol, 69%). *E*:*Z* ratio of 79:21 determined by 1H NMR.

^{1}H NMR (*E*-isomer) (400 MHz, $CDCl_3$) δ 7.40 – 7.19 (m, 5H, Ar-C**H**), 7.15 – 7.06 (m, 1H, Ar-C**H**), 6.91 – 6.82 (m, 1H, Ar-C**H**), 6.75 (dd, *J* = 8.1, 1.3 Hz, 1H, Ar-C**H**), 6.01 (t, *J* = 7.4 Hz, 1H, -CC**H**CH_2-), 5.54 (v br s, 1H, PhOC**H_2**Ph), 4.84 (v br s, 1H, PhOC**H_2**Ph), 3.62 (s, 3H, COOC**H_3**), 2.66 (t, *J* = 7.2 Hz, 2H, -NC**H_2**CH_2CO-), 2.48 (t, *J* = 7.3 Hz, 2H, -CH_2C**H_2**N-), 2.43 (t, *J* = 7.2 Hz, 2H, -NCH_2C**H_2**CO-), 2.37 – 2.27 (m, 2H, -C**H_2**CH_2N-), 2.14 (s, 3H, -NC**H_3**).

^{13}C NMR (*E*-isomer) (101 MHz, $CDCl_3$) δ 173.13, 155.19, 141.40, 140.06, 134.43, 130.25, 130.20, 129.05, 128.64, 128.24, 127.98, 127.84, 127.52, 121.05, 119.23, 70.21, 57.14, 52.82, 51.72, 41.83, 32.54, 27.34.

LCMS: *m/z* of $(M+H)^+$ = 351.6; t_R = 2.21 min.

HRMS (Bruker MicroTOF)(*m/z*): Calculated $(M+Na)^+$ for $C_{22}H_{25}N_1O_3$ = 374.1727; Measured $(M+Na)^+$ = 374.1740; Error = 3.5ppm.

(*E*)-3-((3-(Dibenzo[*b,e*]oxepin-11(6*H*)-ylidene)propyl)(methyl)amino)propanoic acid 87

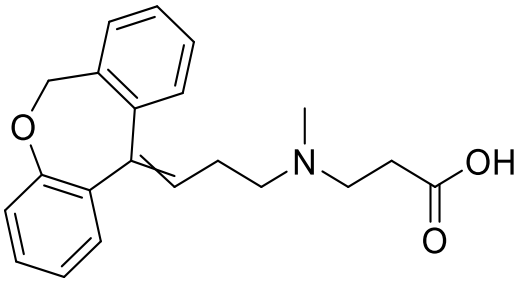

140mg (0.4mmol) of **86** was dissolved in 2.5mL of THF in a 50mL RBF. 112mg of NaOH was dissolved in 5mL of deionised water and 2.5mL (56mg, 1.4mmol) of the resulting solution was added dropwise into the reaction mixture and left to stir at room temperature for 1 hr. THF was removed from the reaction mixture via rotary evaporator and the pH was adjusted to 6. The reaction mixture was then diluted with 20mL of deionised water and extracted for four times with chloroform (50mL x 4). The resulting organic layer was washed with brine, dried with $MgSO_4$, filtered and dried using rotary evaporator to give the product as a pale-yellow gum (130mg, 0.39mmol, 96%). *E*:*Z* ratio of 79:21 determined by 1H NMR.

^{1}H NMR (*E*-isomer) (400 MHz, CD_3OD) δ 7.46 – 7.36 (m, 3H, Ar-C**H**), 7.33 – 7.28 (m, 2H, Ar-C**H**), 7.15 – 7.09 (m, 1H, Ar-C**H**), 6.90 – 6.85 (m, 1H, Ar-C**H**), 6.71 (dd, *J* = 8.3, 1.3 Hz, 1H, Ar-C**H**), 6.01 (t, *J* = 7.4 Hz, 1H, -CC**H**CH_2-), 5.55 (v br s, 1H, PhOC**H_2**Ph), 5.21 (v br s, 1H, PhOC**H_2**Ph), 3.20 (t, *J* = 7.4 Hz, 2H, -CH_2C**H_2**N-), 3.16 (t, *J* = 6.4 Hz, 2H, -NCH_2C**H_2**CO-), 2.67 – 2.60 (m, 2H, -C**H_2**CH_2N-), 2.65 (s, 3H, -NC**H_3**), 2.48 (t, *J* = 6.4 Hz, 2H, -NC**H_2**CH_2CO-).

^{13}C NMR (*E*-isomer) (101 MHz, CD_3OD) δ 177.70, 156.68, 144.55, 141.63, 136.00, 131.09, 130.48, 129.92, 129.53, 129.48, 128.59, 127.86, 126.07, 122.10, 120.22, 70.91, 56.24, 54.79, 39.65, 31.05, 25.75.

LCMS: *m/z* of $(M+H)^+$ = 337.6; t_R = 0.32 min (protonated), 2.23 min.

HRMS (Bruker MicroTOF)(*m/z*): Calculated $(M+H)^+$ for $C_{21}H_{23}N_1O_3$ = 338.1751; Measured = 338.1758; Error = 2.1ppm.

(*S*)-*N*1-(3-(((S)-1-Amino-5-azido-1-oxopentan-2-yl)amino)-3-oxopropyl)-2-((*S*)-2-((*S*)-2-(3-(4-(2-benzylphenoxy)piperidin-1-yl)propanamido)-3-methylbutanamido)-3-hydroxypropanamido)succinamide 88

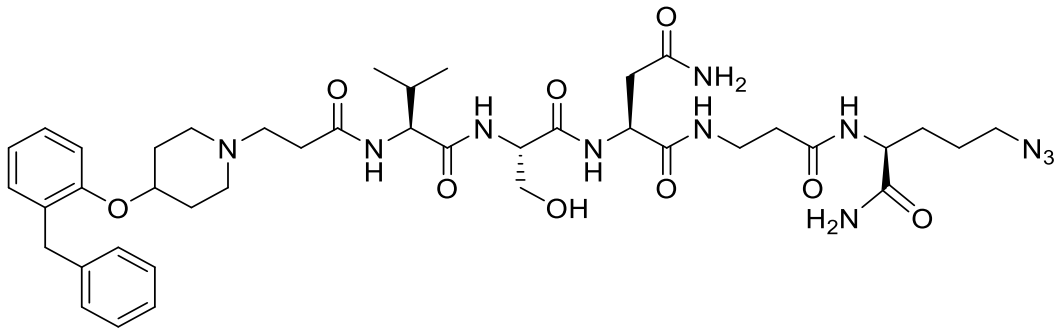

Compound synthesised using General Procedure 1 and purified using *System 7* to give a white solid (1.8mg, 2.1µmol, 5%). **HRMS** (Bruker MicroTOF)(*m/z*): Calculated $(M+H)^+$ for $C_{41}H_{59}N_{11}O_9$ = 850.4570; Measured = 850.4596; Error = 3.1ppm. **Analytical HPLC** (System 2): 91% purity; t_R = 12.50 min.

(S)-5-Azido-2-((6S,9S,12S)-16-(4-(2-benzylphenoxy)piperidin-1-yl)-6,9,12-trimethyl-5,8,11,14-tetraoxo-4,7,10,13-tetraazahexadecanamido)pentanamide 89

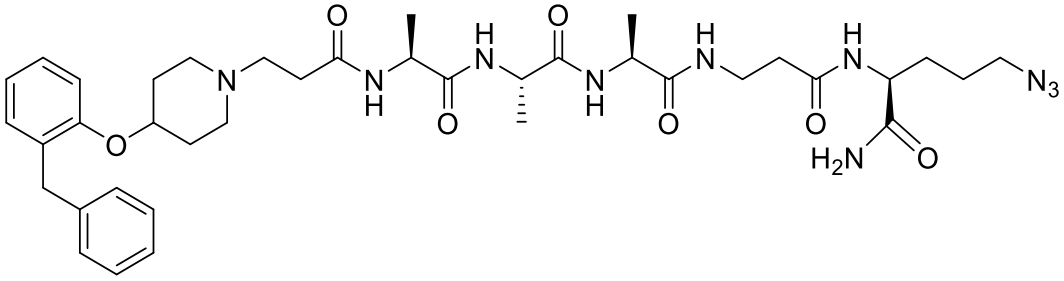

Compound synthesised using General Procedure 1 and purified using *System 7* to give a white solid (2.2mg, 2.9µmol, 7%). **HRMS** (Bruker MicroTOF)(*m/z*): Calculated $(M+H)^+$ for $C_{38}H_{54}N_{10}O_7$ = 763.4250; Measured = 763.4274; Error = 3.1ppm. **Analytical HPLC** (System 2): 92% purity; t_R = 12.39 min.

(*S*)-*N*1-(3-(((S)-1-Amino-5-azido-1-oxopentan-2-yl)amino)-3-oxopropyl)-2-((*S*)-2-((*S*)-2-(3-(((*E*)-3-(dibenzo[*b,e*]oxepin-11(6*H*)-ylidene)propyl)amino)propanamido)-3-methylbutanamido)-3-hydroxypropanamido)succinimide 90

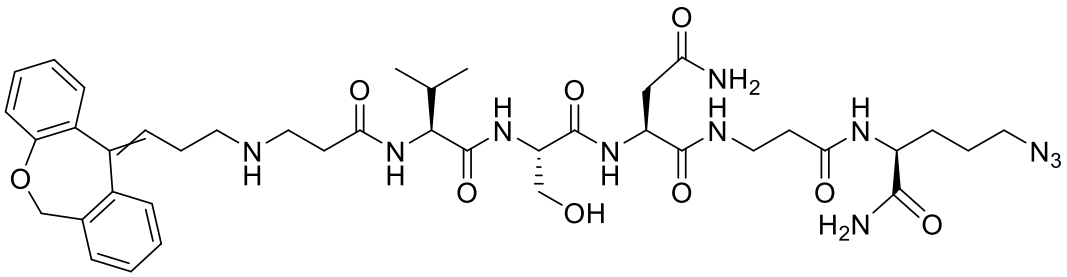

Compound synthesised using General Procedure 1 and purified using *System 7* to give a white solid (3.3mg, 3.9µmol, 10%). **HRMS** (Bruker MicroTOF)(*m/z*): Calculated $(M+H)^+$ for $C_{41}H_{57}N_{11}O_9$ = 848.4413; Measured = 848.4459; Error = 5.3ppm. **Analytical HPLC** (System 2): 92% purity; t_R = 12.43 min.

(*S*)-5-Azido-2-((6*S*,9*S*,12*S*,*E*)-20-(dibenzo[*b,e*]oxepin-11(6*H*)-ylidene)-6,9,12-trimethyl-5,8,11,14-tetraoxo-4,7,10,13,17-pentaazaicosanamido)pentanamide 91

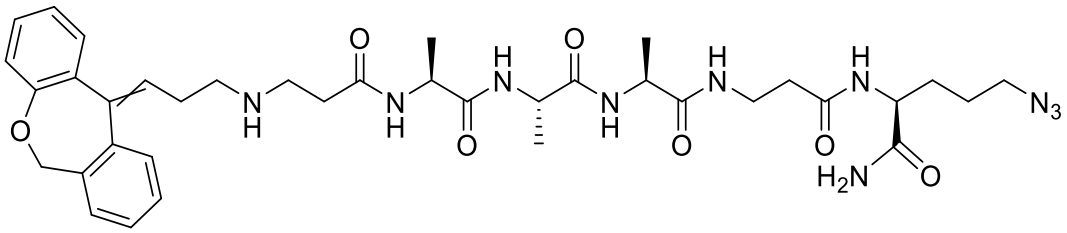

Compound synthesised using General Procedure 1 and purified using *System 7* to give a white solid (3.4mg, 4.5µmol, 11%). **HRMS** (Bruker MicroTOF)(*m/z*): Calculated $(M+H)^+$ for $C_{38}H_{52}N_{10}O_7$ = 761.4093; Measured = 761.4097; Error = 0.5ppm. **Analytical HPLC** (System 2): 94% purity; t_R = 12.38 min.

(*S*)-*N*1-(3-(((*S*)-1-Amino-5-(4-((4-((*E*)-2-(5,5-difluoro-7-(thiophen-2-yl)-5*H*-5λ^4,6λ^4-dipyrrolo[1,2-*c*:2',1'-*f*][1,3,2]diazaborinin-3-yl)vinyl)phenoxy)methyl)-1*H*-1,2,3-triazol-1-yl)-1-oxopentan-2-yl)amino)-3-oxopropyl)-2-((S)-2-((S)-2-(3-(4-(2-benzylphenoxy)piperidin-1-yl)propanamido)-3-methylbutanamido)-3-hydroxypropanamido)succinamide 92

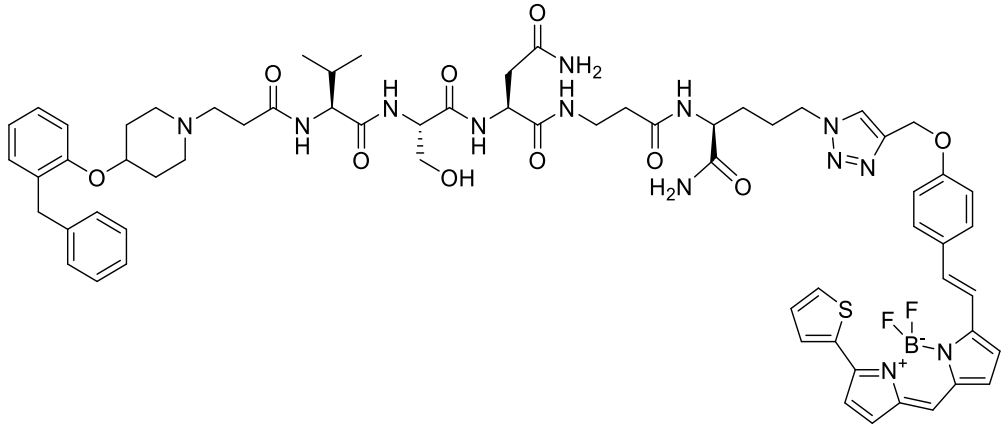

Compound synthesised using General Procedure 3 with 0.9mg (1.1µmol) of **88** and purified using *System 8* to give a blue solid (0.73mg, 0.6µmol, 54%). **HRMS** (Bruker MicroTOF)(*m/z*): Calculated $(M+H)^+$ for $C_{65}H_{76}B_1F_2N_{13}O_{10}S_1$ = 1280.5693; Measured = 1280.5718; Error = 1.1ppm. **Analytical HPLC** (System 2): 99% purity; t_R = 15.92 min**.**

(*S*)-2-((6*S*,9*S*,12*S*)-16-(4-(2-Benzylphenoxy)piperidin-1-yl)-6,9,12-trimethyl-5,8,11,14-tetraoxo-4,7,10,13-tetraazahexadecanamido)-5-(4-((4-((*E*)-2-(5,5-difluoro-7-(thiophen-2-yl)-5*H*-5λ^4,6λ^4-dipyrrolo[1,2-*c*:2',1'-*f*][1,3,2]diazaborinin-3-yl)vinyl)phenoxy)methyl)-1*H*-1,2,3-triazol-1-yl)pentanamide 93

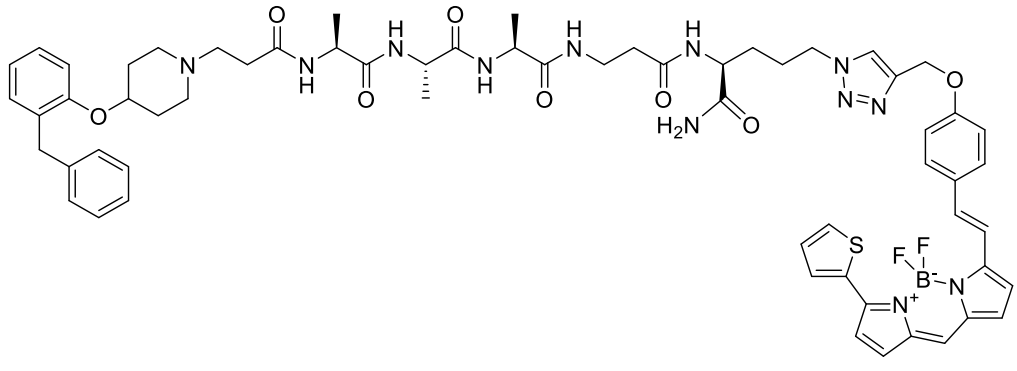

Compound synthesised using General Procedure 3 with 1.1mg (1.4µmol) of **89** and purified using *System 8* to give a blue solid (0.78mg, 0.7µmol, 45%). **HRMS** (Bruker MicroTOF)(*m/z*): Calculated $(M+H)^+$ for $C_{62}H_{71}B_1F_2N_{12}O_8S_1$ = 1193.5372; Measured = 1193.5443; Error = 5.1ppm. **Analytical HPLC** (System 2): 99% purity; t_R = 15.95 min**.**

(*S*)-*N*1-(3-(((*S*)-1-amino-5-(4-((4-((*E*)-2-(5,5-difluoro-7-(thiophen-2-yl)-5*H*-5λ^4,6λ^4-dipyrrolo[1,2-*c*:2',1'-*f*][1,3,2]diazaborinin-3-yl)vinyl)phenoxy)methyl)-1*H*-1,2,3-triazol-1-yl)-1-oxopentan-2-yl)amino)-3-oxopropyl)-2-((*S*)-2-((*S*)-2-(3-(((*E*)-3-(dibenzo[*b,e*]oxepin-11(6*H*)-ylidene)propyl)amino)propanamido)-3-methylbutamido)-3-hydroxypropanamido)succinimide 94

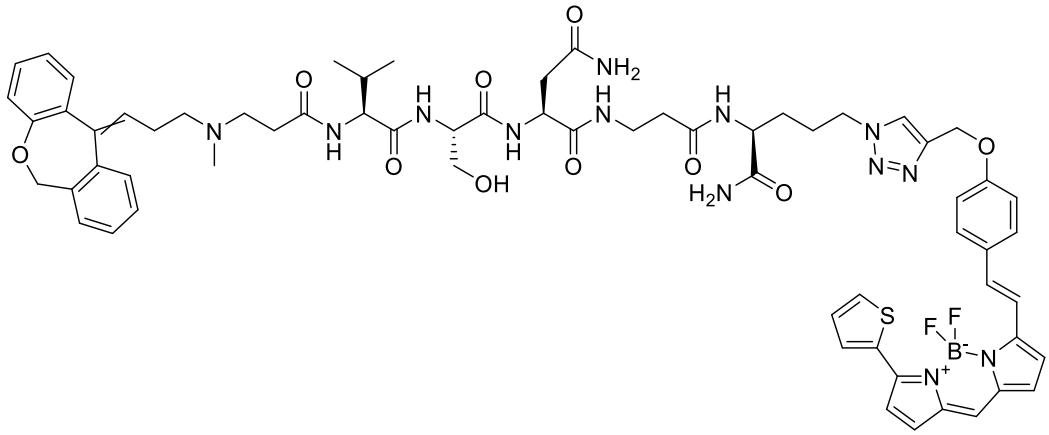

Compound synthesised using General Procedure 3 with 1.6mg (1.9µmol) of **90** and purified using *System 8* to give a blue solid (0.79mg, 0.6µmol, 33%). **HRMS** (Bruker MicroTOF)(*m/z*): Calculated $(M+H)^+$ for $C_{65}H_{74}B_1F_2N_{13}O_{10}S_1$ = 1278.5536; Measured = 1278.5584; Error = 2.9ppm. **Analytical HPLC** (System 2): 99% purity; t_R = 16.35 min**.**

(*S*)-2-((6*S*,9*S*,12*S*,*E*)-20-(Dibenzo[*b,e*]oxepin-11(6*H*)-ylidene)-6,9,12-trimethyl-5,8,11,14-tetraoxo-4,7,10,13,17-pentaazaicosanamido)-5-(4-((4-((E)-2-(5,5-difluoro-7-(thiophen-2-yl)-5*H*-5λ^4,6λ^4-dipyrrolo[1,2-*c*:2',1'-*f*][1,3,2]diazaborinin-3-yl)vinyl)phenoxy)methyl)-1*H*-1,2,3-triazol-1-yl)pentanamide 95

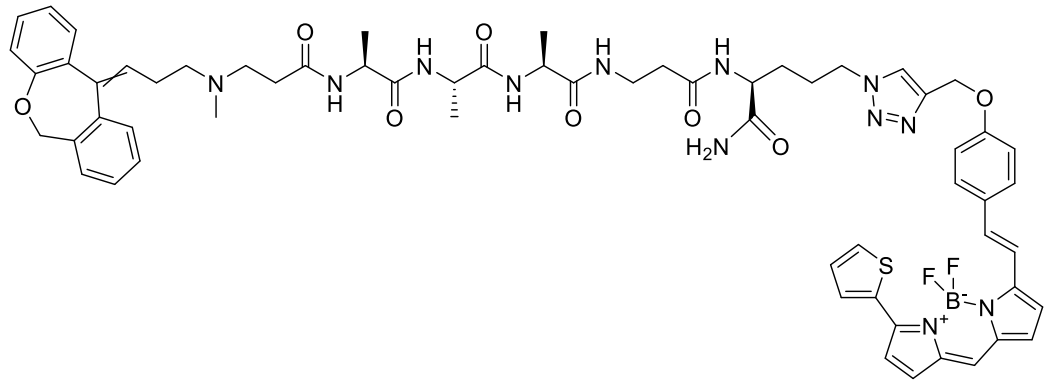

Compound synthesised using General Procedure 3 with 1.7mg (2.2µmol) of **91** and purified using *System 8* to give a blue solid (0.88mg, 0.7µmol, 33%). **HRMS** (Bruker MicroTOF)(*m/z*): Calculated $(M+H)^+$ for $C_{62}H_{69}B_1F_2N_{12}O_8S_1$ = 1191.5216; Measured = 1191.5283; Error = 3.1ppm. **Analytical HPLC** (System 2): 99% purity; t_R = 16.23 min

(*S*)-2-((*S*)-2-((*S*)-2-(3-(4-(2-Benzylphenoxy)piperidin-1-yl)propanamido)-3-methyl butanamido)-3-hydroxypropanamido)-*N*1-(3-(((*S*)-1,6-diamino-1-oxohexan-2-yl) amino)-3-oxopropyl)succinamide 96.

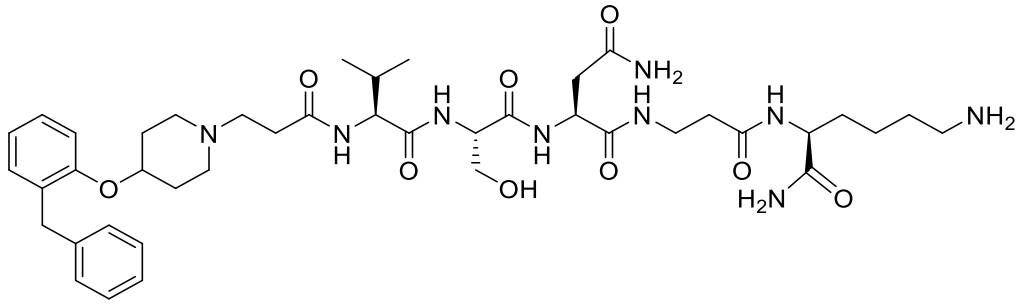

Compound synthesised using General Procedure 2 and purified using *System 5* to give a white solid (1.4mg, 1.7µmol, 4%). **HRMS** (Bruker MicroTOF)(*m/z*): Calculated $(M+H)^+$ for $C_{42}H_{63}N_9O_9$ = 838.4822; Measured = 838.4829; Error = 0.9ppm. **Analytical HPLC** (System 2): 99% purity; t_R = 11.77 min.

(*S*)-2-((*S*)-2-((*S*)-2-(3-(4-(2-Benzylphenoxy)piperidin-1-yl)propanamido)-3-methyl butanamido)-propanamido)-*N*1-(3-(((*S*)-1,6-diamino-1-oxohexan-2-yl)amino)-3-oxo-propyl)succinamide 97.

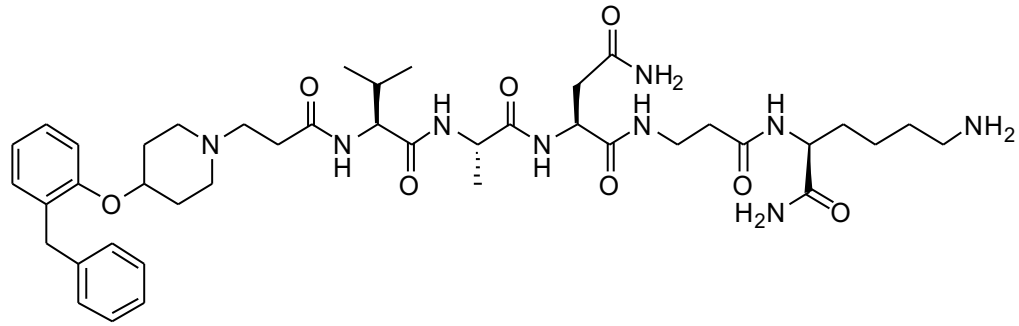

Compound synthesised using General Procedure 2 and purified using *System 5* to give a white solid (2.4mg, 2.9µmol, 7%). **HRMS** (Bruker MicroTOF)(*m/z*): Calculated $(M+H)^+$ for $C_{42}H_{63}N_9O_8$ = 822.4872; Measured = 822.4879; Error = 0.8ppm. **Analytical HPLC** (System 2): 99% purity; t_R = 11.82 min.

(*S*)-2-((*S*)-2-((*2S,3R*)-2-(3-(4-(2-Benzylphenoxy)piperidin-1-yl)propanamido)-3-hydroxybutanamido)-3-hydroxy-propanamido)-*N*1-(3-(((S)-1,6-diamino-1-oxohexan-2-yl)amino)-3-oxopropyl)succinamide 98.

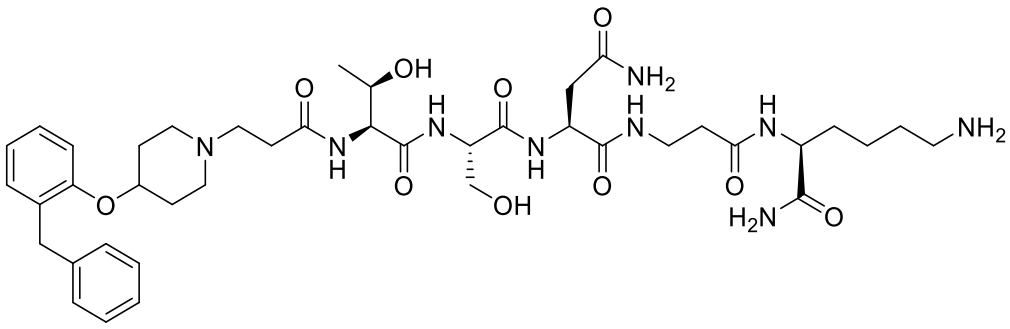

Compound synthesised using General Procedure 2 and purified using *System 5* to give a white solid (1.4mg, 1.7µmol, 4%). **HRMS** (Bruker MicroTOF)(*m/z*): Calculated $(M+H)^+$ for $C_{41}H_{64}N_9O_{10}$ = 840.4614; Measured = 840.4581; Error = 3.9ppm. **Analytical HPLC** (System 2): 99% purity; t_R = 11.45 min.

(*S*)-2-((*S*)-2-((*2S,3R*)-2-(3-(4-(2-Benzylphenoxy)piperidin-1-yl)propanamido)-3-hydroxybutanamido)-propanamido)-*N*1-(3-(((*S*)-1,6-diamino-1-oxohexan-2-yl)amino)-3-oxopropyl)succinamide 99.

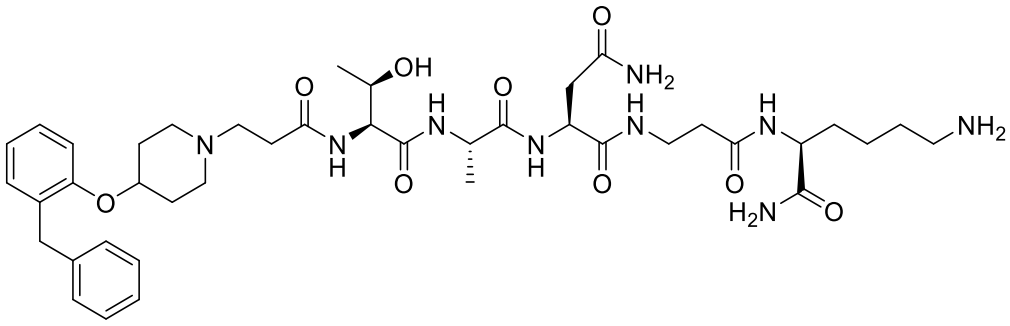

Compound synthesised using General Procedure 2 and purified using *System 5* to give a white solid (1.9mg, 2.3µmol, 6%). **HRMS** (Bruker MicroTOF)(*m/z*): Calculated $(M+H)^+$ for $C_{41}H_{61}N_9O_9$ = 824.4665; Measured = 824.4663; Error = 0.2ppm. **Analytical HPLC** (System 2): 99% purity; t_R = 11.52 min.

(*S*)-6-Amino-2-((*6S,9S,12S*)-16-(4-(2-benzylphenoxy)piperidin-1-yl)-6-(4-hydroxybenzyl)-9-(hydroxymethyl)-12-isopropyl-5,8,11,14-tetraoxo-4,7,10,13-tetraazahexadecanamido)hexanamide 100.

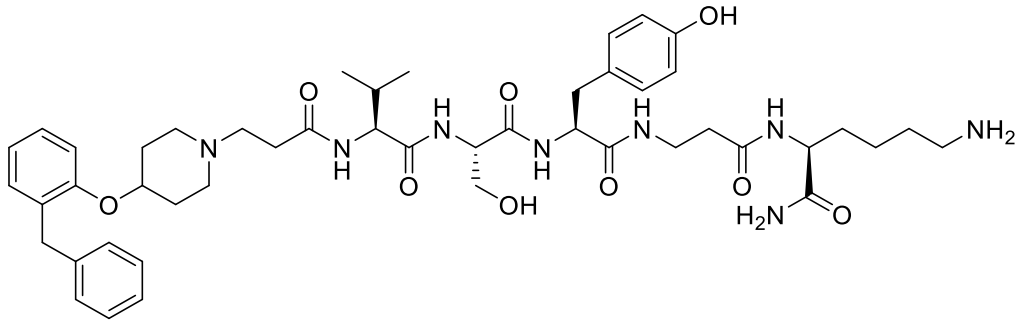

Compound synthesised using General Procedure 2 and purified using *System 5* to give a white solid (1.9mg, 2.1µmol, 5%). **HRMS** (Bruker MicroTOF)(*m/z*): Calculated $(M+H)^+$ for $C_{47}H_{66}N_8O_9$ = 887.5026; Measured = 887.5032; Error = 0.8ppm. **Analytical HPLC** (System 2): 99% purity; t_R = 12.23 min.

(*S*)-6-Amino-2-((6*S*,9*S*,12*S*)-16-(4-(2-benzylphenoxy)piperidin-1-yl)-6-(4-hydroxybenzyl)-12-isopropyl-9-methyl-5,8,11,14-tetraoxo-4,7,10,13-tetraazahexadecanamido)hexanamide 101.

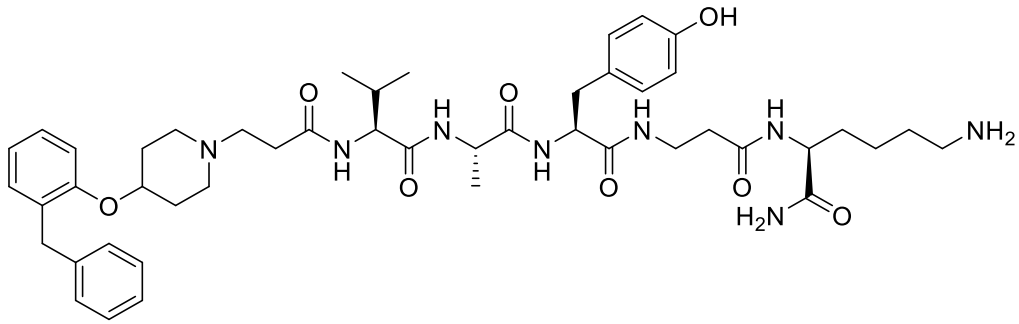

Compound synthesised using General Procedure 2 and purified using *System 5* to give a white solid (2.4mg, 2.8µmol, 7%). **HRMS** (Bruker MicroTOF)(*m/z*): Calculated $(M+H)^+$ for $C_{47}H_{66}N_8O_8$ = 871.5076; Measured = 871.5036; Error = 4.7ppm. **Analytical HPLC** (System 2): 99% purity; t_R = 12.34 min.

(*S*)-6-Amino-2-((*6S,9S,12S*)-16-(4-(2-benzylphenoxy)piperidin-1-yl)-6-(4-hydroxybenzyl)-12-((*R*)-1-hydroxyethyl)-9-(hydroxymethyl)-5,8,11,14-tetraoxo-4,7,10,13-tetraazahexadecanamido)hexanamide 102.

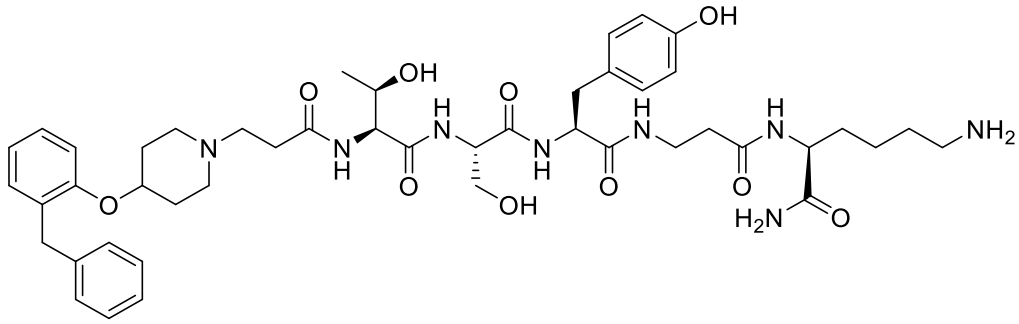

Compound synthesised using General Procedure 2 and purified using *System 5* to give a white solid (1.9mg, 2.1µmol, 5%). **HRMS** (Bruker MicroTOF)(*m/z*): Calculated $(M+H)^+$ for $C_{46}H_{64}N_8O_{10}$ = 889.4818; Measured = 889.4811; Error = 0.9ppm. **Analytical HPLC** (System 2): 98% purity; t_R = 11.85 min.

(*S*)-6-Amino-2-((*6S,9S,12S*)-16-(4-(2-benzylphenoxy)piperidin-1-yl)-6-(4-hydroxy benzyl)-12-((*R*)-1-hydroxyethyl)-9-methyl-5,8,11,14-tetraoxo-4,7,10,13-tetraaza hexadecanamido)hexanamide 103.

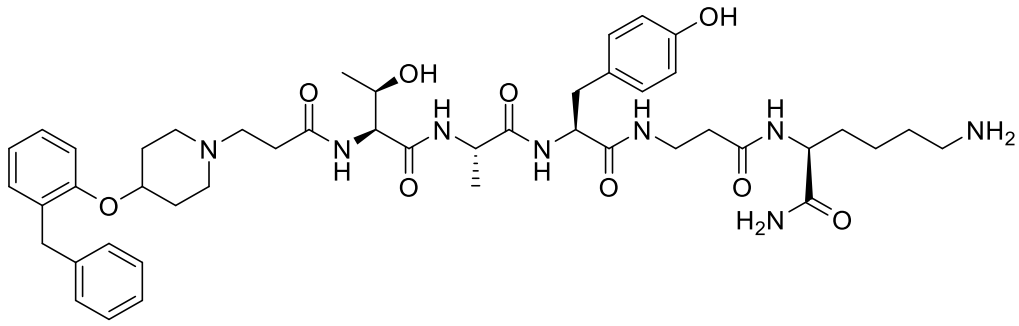

Compound synthesised using General Procedure 2 and purified using *System 5* to give a white solid (2.3mg, 2.6µmol, 7%). **HRMS** (Bruker MicroTOF)(*m/z*): Calculated $(M+H)^+$ for $C_{46}H_{64}N_8O_9$ = 873.4869; Measured = 873.4842; Error = 3.10ppm. **Analytical HPLC** (System 2): 99% purity; t_R = 12.00 min.

(*S*)-2-((*S*)-2-((2*S*,3*S*)-2-(3-(4-(2-Benzylphenoxy)piperidin-1-yl)propanamido)-3-methylpentanamido)-3-hydroxypropanamido)-*N*1-(3-(((*S*)-1,6-diamino-1-oxohexan-2-yl)amino)-3-oxopropyl)succinamide 104

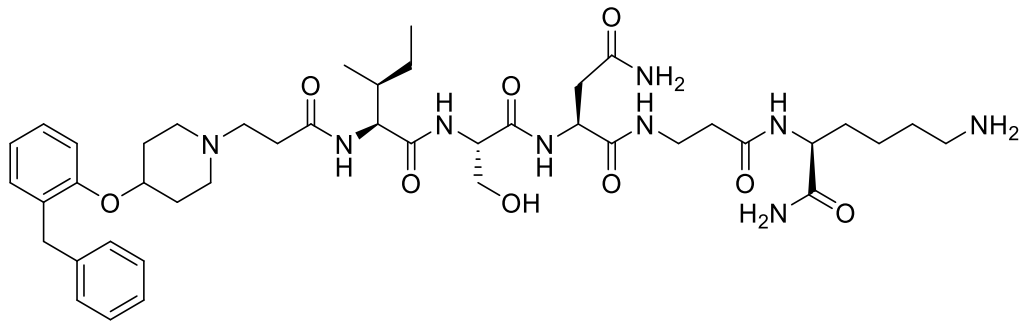

Compound synthesised using General Procedure 2 and purified using *System 5* to give a white solid (2.3mg, 2.6µmol, 7%). **HRMS** (Bruker MicroTOF)(*m/z*): Calculated $(M+H)^+$ for $C_{43}H_{65}N_9O_9$ = 852.4978; Measured = 852.4969; Error = 1ppm. **Analytical HPLC** (System 2): 99% purity; t_R = 12.30 min.

(*S*)-2-((*S*)-2-((*S*)-2-(3-(4-(2-Benzylphenoxy)piperidin-1-yl)propanamido)-4-methylpentanamido)-3-hydroxypropanamido)-*N*1-(3-(((*S*)-1,6-diamino-1-oxohexan-2-yl)amino)-3-oxopropyl)succinamide 105

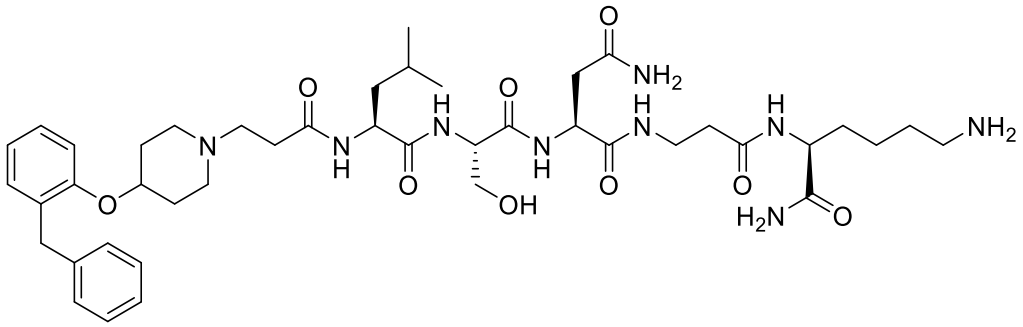

Compound synthesised using General Procedure 2 and purified using *System 5* to give a white solid (1.3mg, 1.5µmol, 4%). **HRMS** (Bruker MicroTOF)(*m/z*): Calculated $(M+H)^+$ for $C_{43}H_{65}N_9O_9$ = 852.4978; Measured = 852.4964; Error = 1.7ppm. **Analytical HPLC** (System 2): 94% purity; tR = 12.62 min.

(*S*)-6-Amino-2-((*6S,9S,12S*)-12-benzyl-16-(4-(2-benzylphenoxy)piperidin-1-yl)-6,9-dimethyl-5,8,11,14-tetraoxo-4,7,10,13-tetraazahexadecanamido)hexanamide 106

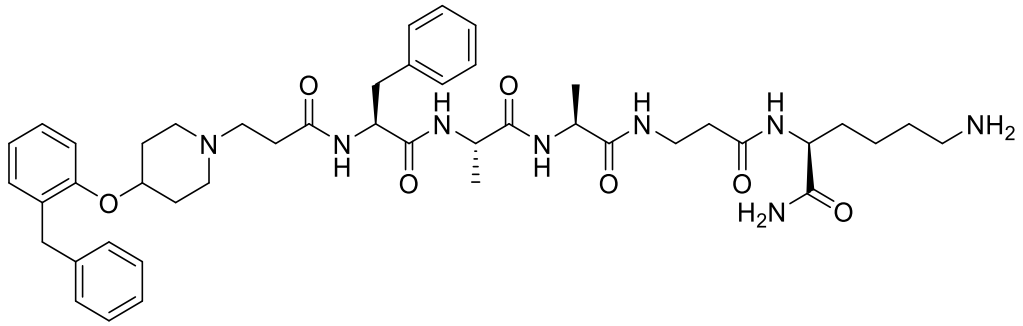

Compound synthesised using General Procedure 2 and purified using *System 5* to give a white solid (2.5mg, 3µmol, 8%). **HRMS** (Bruker MicroTOF)(*m/z*): Calculated $(M+H)^+$ for $C_{45}H_{62}N_8O_7$ = 827.4814; Measured = 827.4807; Error = 0.9ppm. **Analytical HPLC** (System 2): 99% purity; t_R = 13.02 min.

(*S*)-*N*1-(3-(((*S*)-1-Amino-6-(2-(4-((*E*)-2-(5,5-difluoro-7-(thiophen-2-yl)-5*H*-5λ^4,6λ^4-dipyrrolo[1,2-*c*:2',1'-*f*][1,3,2]diazaborinin-3-yl)vinyl)phenoxy)acetamido)-1-oxohexan-2-yl)amino)-3-oxopropyl)-2-((*S*)-2-((*S*)-2-(3-(4-(2-benzylphenoxy)piperidin-1-yl)propanamido)-3-methylbutanamido)-3-hydroxypropanamido) succinamide 107.

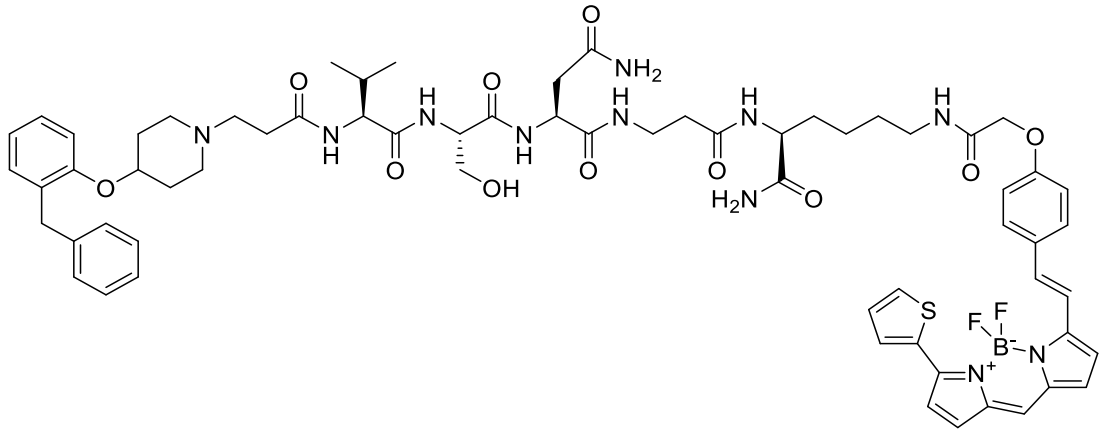

Compound synthesised using General Procedure 4 with 1.4mg (1.7µmol) of **96** and purified using *System 6* to give a blue solid (0.73mg, 0.6µmol, 34%). **HRMS** (Bruker MicroTOF)(*m/z*): Calculated $(M+H)^+$ for $C_{65}H_{78}B_1F_2N_{11}O_{11}S_1$ = 1270.5737; Measured = 1270.5687; Error = 4.7ppm. **Analytical HPLC** (System 2): 99% purity; t_R = 17.97 min.

(*S*)-*N*1-(3-(((*S*)-1-Amino-6-(2-(4-((*E*)-2-(5,5-difluoro-7-(thiophen-2-yl)-5*H*-5λ^4,6λ^4-dipyrrolo[1,2-*c*:2',1'-*f*][1,3,2] diazaborinin-3-yl)vinyl)phenoxy)acetamido)-1-oxohexan-2-yl)amino)-3-oxopropyl)-2-((*S*)-2-((*S*)-2-(3-(4-(2-benzylphenoxy) piperidin-1-yl)propanamido)-3-methylbutanamido)propanamido)succinamide 108

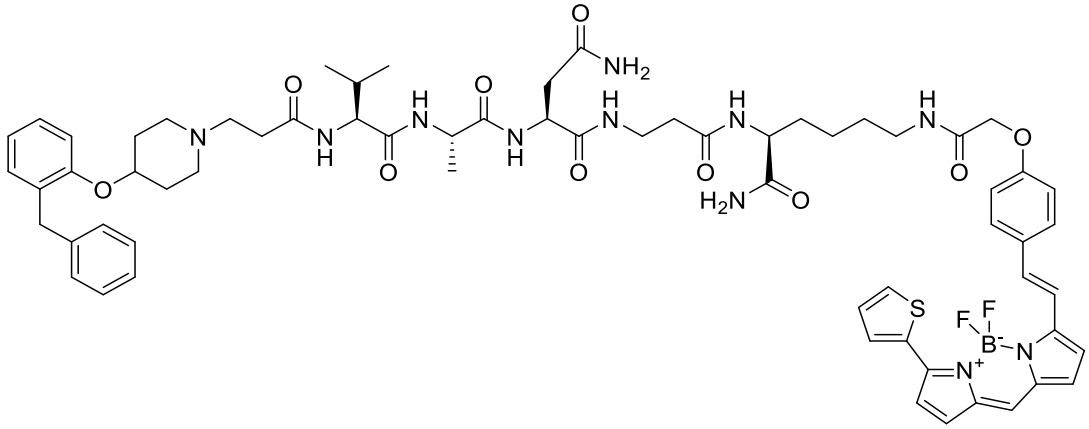

Compound synthesised using General Procedure 4 with 2.4mg (2.9µmol) of **97** and purified using *System 6* to give a blue solid (1.65mg, 1.3µmol, 45%). **HRMS** (Bruker MicroTOF)(*m/z*): Calculated $(M+H)^+$ for $C_{65}H_{78}B_1F_2N_{11}O_{10}S_1$ = 1254.5788; Measured = 1254.5761; Error = 3.0ppm. **Analytical HPLC** (System 2): 99% purity; t_R = 18.15 min.

(*S*)-*N*1-(3-(((*S*)-1-Amino-6-(2-(4-((*E*)-2-(5,5-difluoro-7-(thiophen-2-yl)-5*H*-5λ^4,6λ^4-dipyrrolo[1,2-*c*:2',1'-*f*][1,3,2]diazaborinin-3-yl)vinyl)phenoxy)acetamido)-1-oxohexan-2-yl)amino)-3-oxopropyl)-2-((*S*)-2-((*2S,3R*)-2-(3-(4-(2-benzylphenoxy)piperidin-1-yl)propanamido)3-hydroxybutanamido)-3-hydroxypropanamido)succinamide 109

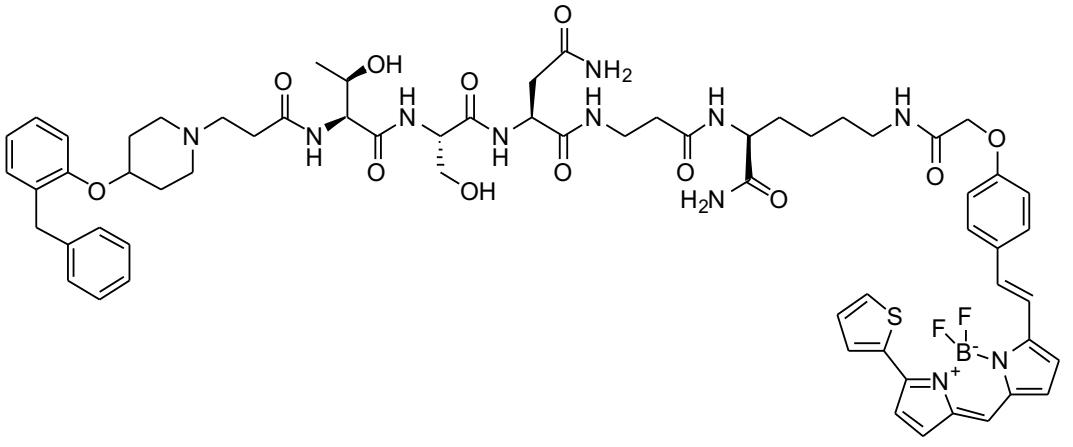

Compound synthesised using General Procedure 4 with 1.4mg (1.7µmol) of **98** and purified using *System 6* to give a blue solid (0.83mg, 0.7µmol, 39%). **HRMS** (Bruker MicroTOF)(*m/z*): Calculated $(M+H)^+$ for $C_{64}H_{76}B_1F_2N_{11}O_{12}S_1$ = 1272.5530; Measured = 1272.5508; Error = 2.5ppm. **Analytical HPLC** (System 2): 99% purity; t_R = 17.50 min.

(*S*)-*N*1-(3-(((*S*)-1-Amino-6-(2-(4-((*E*)-2-(5,5-difluoro-7-(thiophen-2-yl)-5*H*-5λ^4,6λ^4-dipyrrolo[1,2-*c*:2',1'-*f*][1,3,2]diazaborinin-3-yl)vinyl)phenoxy)acetamido)-1-oxohexan-2-yl)amino)-3-oxopropyl)-2-((*S*)-2-((*2S,3R*)-2-(3-(4-(2-benzylphenoxy)piperidin-1-yl)propanamido)-3-hydroxybutanamido)-propanamido)succinamide 110.

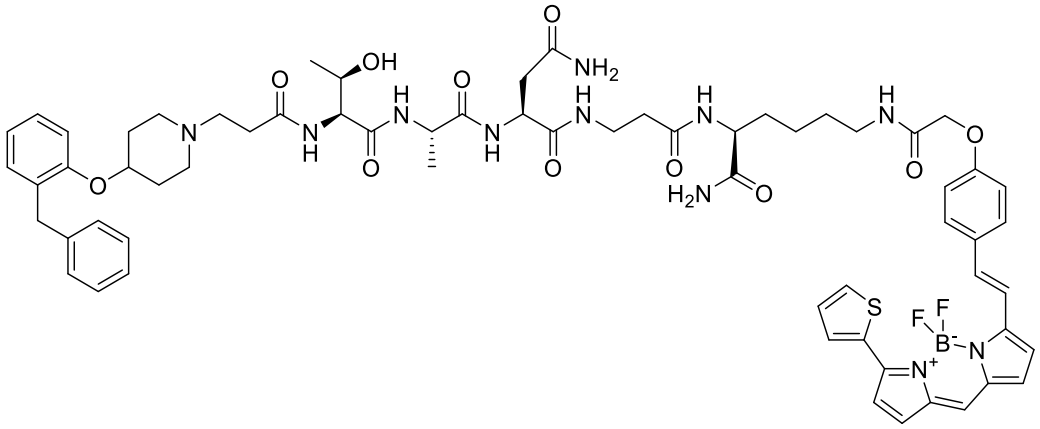

Compound synthesised using General Procedure 4 with 1.9mg (2.3µmol) of **99** and purified using *System 6* to give a blue solid (0.95mg, 0.8µmol, 33%). **HRMS** (Bruker MicroTOF)(*m/z*): Calculated (M+H)$^+$ for $C_{64}H_{76}B_1F_2N_{11}O_{11}S_1$ = 1256.5580; Measured = 1256.5538; Error = 4.2ppm. **Analytical HPLC** (System 2): 99% purity; t_R = 17.68 min.

(*S*)-2-((*6S,9S,12S*)-16-(4-(2-Benzylphenoxy)piperidin-1-yl)-6-(4-hydroxybenzyl)-9-(hydroxymethyl)-12-isopro-pyl-5,8,11,14-tetraoxo-4,7,10,13-tetraazahexadecan amido)-6-(2-(4-((*E*)-2-(5,5-difluoro-7-(thiophen-2-yl)-5*H*-5λ^4,6λ^4-dipyrrolo[1,2-*c*:2',1'-*f*][1,3,2]diazaborinin-3-yl)-vinyl)phenoxy)acetam-ido)-hexanamide 111.

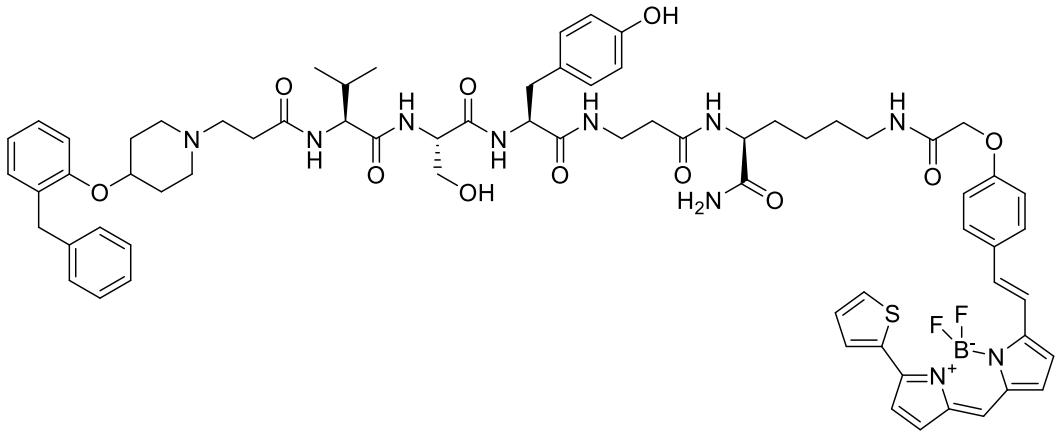

Compound synthesised using General Procedure 4 with 1.9mg (2.1µmol) of **100** and purified using *System 6* to give a blue solid (1.11mg, 0.8µmol, 39%). **HRMS** (Bruker MicroTOF)(*m/z*): Calculated (M+H)$^+$ for $C_{70}H_{81}B_1F_2N_{10}O_{11}S_1$ = 1319.5941; Measured = 1319.5883; Error = 5.2ppm. **Analytical HPLC** (System 2): 97% purity; t_R = 18.52 min.

(*S*)-2-((*6S,9S,12S*)-16-(4-(2-Benzylphenoxy)piperidin-1-yl)-6-(4-hydroxybenzyl)-12-isopropyl-9-methyl-5,8,11,14-tetraoxo-4,7,10,13-tetraazahexadecanamido)-6-(2-(4-((*E*)-2-(5,5-difluoro-7-(thiophen-2-yl)-5*H*-5λ^4,6λ^4-di-pyrrolo[1,2-*c*:2',1'-*f*][1,3,2] diazaborinin-3-yl)vinyl)phen-oxy)acetamido)-hexanamide 112.

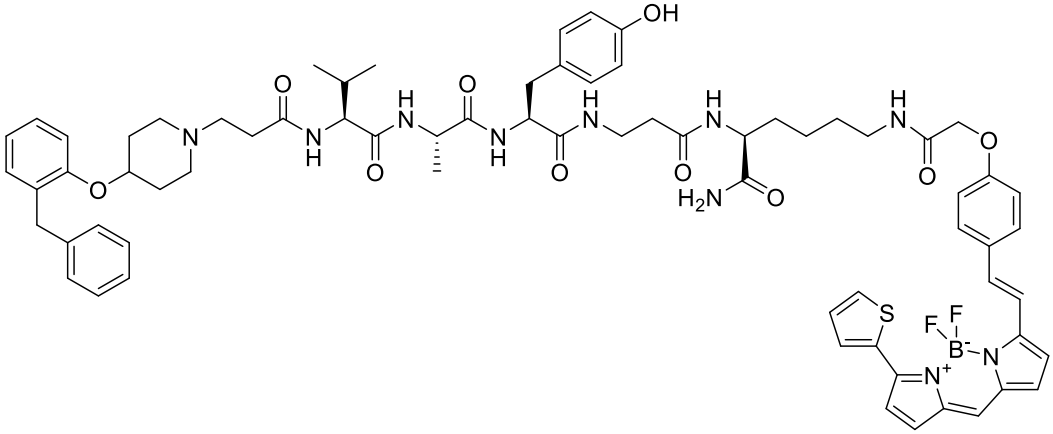

Compound synthesised using General Procedure 4 with 2.4mg (2.8µmol) of **101** and purified using *System 6* to give a blue solid (0.96mg, 0.7µmol, 27%). **HRMS** (Bruker MicroTOF)(*m/z*): Calculated $(M+H)^+$ for $C_{70}H_{81}B_1F_2N_{10}O_{10}S_1$ = 1303.5992; Measured = 1303.5943; Error = 4.6ppm. **Analytical HPLC** (System 2): 99% purity; t_R = 18.75 min.

(*S*)-2-((*6S,9S,12S*)-16-(4-(2-Benzylphenoxy)piperidin-1-yl)-6-(4-hydroxybenzyl)-12-((*R*)-1-hydroxy-ethyl)-9-(hy-droxymethyl)-5,8,11,14-tetraoxo-4,7,10,13-tetraazahexadecanamido)-6-(2-(4-((*E*)-2-(5,5-difluoro-7-(thiophen-2-yl)-5*H*-5λ^4,6λ^4-dipyrrolo[1,2-*c*:2',1'-*f*][1,3,2]diazaborinin-3-yl)vinyl) phenoxy)acetamido)hexanamide 113.

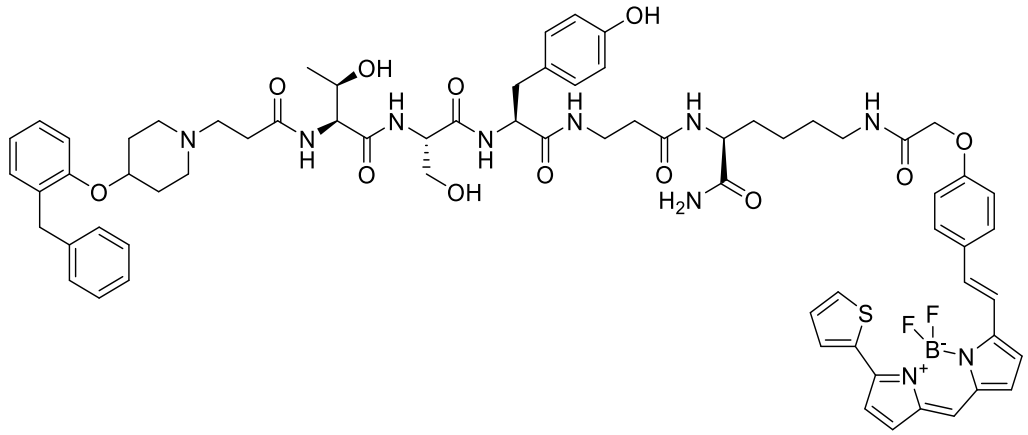

Compound synthesised using General Procedure 4 with 1.9mg (2.1µmol) of **102** and purified using *System 6* to give a blue solid (0.77mg, 0.6µmol, 27%). **HRMS** (Bruker MicroTOF)(*m/z*): Calculated $(M+H)^+$ for $C_{69}H_{79}B_1F_2N_{10}O_{12}S_1$ = 1321.5734; Measured = 1321.5741; Error = 0.3ppm. **Analytical HPLC** (System 2): 99% purity; t_R = 18.02 min.

(*S*)-2-((*6S,9S,12S*)-16-(4-(2-Benzylphenoxy)piperidin-1-yl)-6-(4-hydroxybenzyl)-12-((*R*)-1-hydroxyethyl)-9-me-thyl-5,8,11,14-tetraoxo-4,7,10,13-tetraazahexadecanamido)-6-(2-(4-((*E*)-2-(5,5-difluoro-7-(thiophen-2-yl)-5*H*-5λ^4,6λ^4-dipyrrolo[1,2-*c*:2',1'-*f*][1,3,2]diazaborinin-3-yl)vinyl)phenoxy)acetamido)hexanamide 114

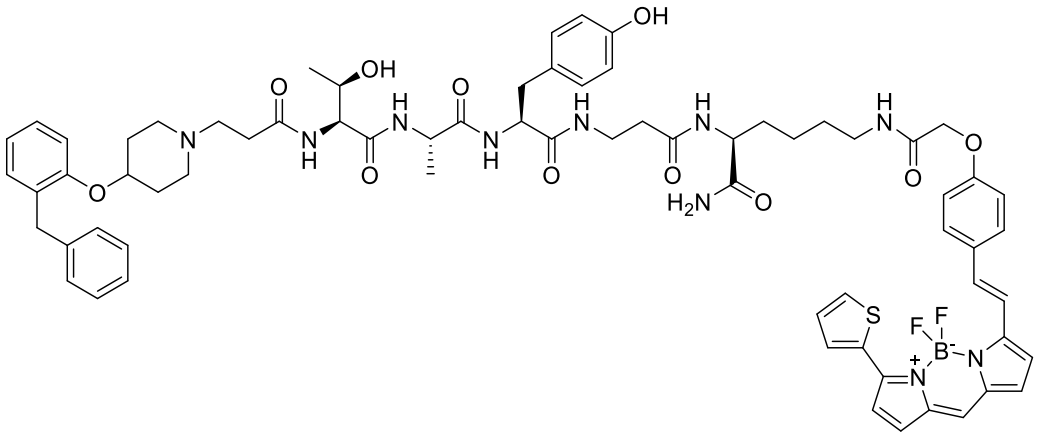

Compound synthesised using General Procedure 4 with 2.3mg (2.6µmol) of **103** and purified using *System 6* to give a blue solid (1.04mg, 0.8µmol, 30%). **HRMS** (Bruker MicroTOF)(*m/z*): Calculated $(M+H)^+$ for $C_{69}H_{79}B_1F_2N_{10}O_{11}S_1$ = 1305.5784; Measured = 1305.5757; Error = 3.0ppm. **Analytical HPLC** (System 2): 99% purity; t_R = 18.28 min.

(*S*)-*N*1-(3-(((S)-1-Amino-6-(2-(4-((*E*)-2-(5,5-difluoro-7-(thiophen-2-yl)-5*H*-5λ^4,6λ^4-dipyrrolo[1,2-*c*:2',1'-*f*][1,3,2]diazaborinin-3-yl)vinyl)phenoxy)acetamido)-1-oxohexan-2-yl)amino)-3-oxopropyl)-2-((*S*)-2-((2*S*,3*S*)-2-(3-(4-(2-benzylphenoxy)piperidin-1-yl)propanamido)-3-methylpentanamido)-3-hydroxypropanamido)succinamide115

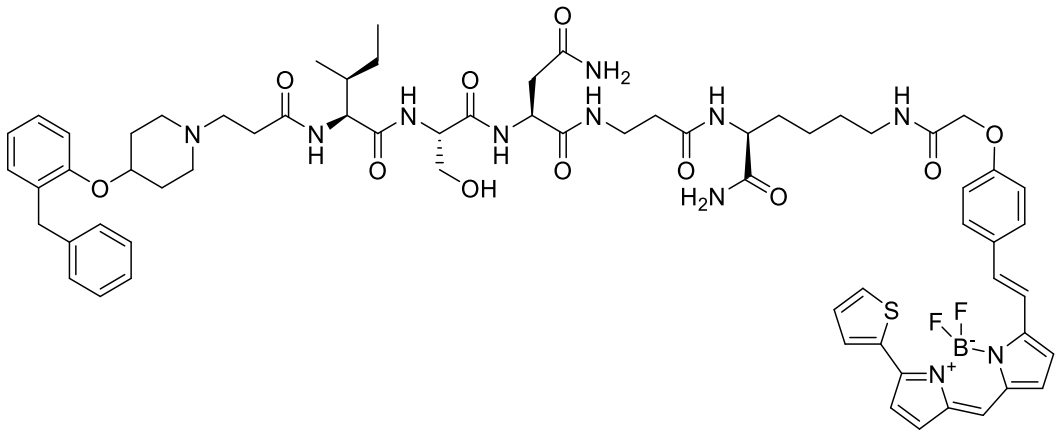

Compound synthesised using General Procedure 4 with 2.3mg (2.7µmol) of **104** and purified using *System 6* to give a blue solid (1.02mg, 0.8µmol, 29%). **HRMS** (Bruker MicroTOF)(*m/z*): Calculated $(M+H)^+$ for $C_{66}H_{80}B_1F_2N_{11}O_{11}S_1$ = 1284.5893; Measured = 1284.5828; Error = 5.9ppm. **Analytical HPLC** (System 2): 95% purity; t_R = 17.92 min.

(*S*)-*N*1-(3-(((S)-1-Amino-6-(2-(4-((*E*)-2-(5,5-difluoro-7-(thiophen-2-yl)-5*H*-5λ^4,6λ^4-dipyrrolo[1,2-*c*:2',1'-*f*][1,3,2]diazaborinin-3-yl)vinyl)phenoxy)acetamido)-1-oxohexan-2-yl)amino)-3-oxopropyl)-2-((*S*)-2-((*S*)-2-(3-(4-(2-benzylphenoxy)piperidin-1-yl)propanamido)-4-methylpentanamido)-3-hydroxypropanamido)succinimide 116

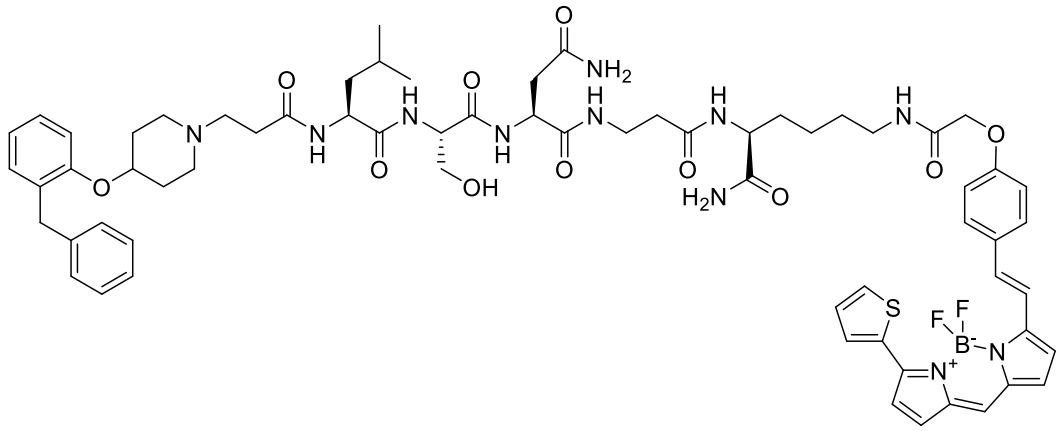

Compound synthesised using General Procedure 4 with 1.3mg (1.5µmol) of **105** and purified using *System 6* to give a blue solid (0.59mg, 0.4µmol, 29%). **HRMS** (Bruker MicroTOF)(*m/z*): Calculated $(M+H)^+$ for $C_{66}H_{80}B_1F_2N_{11}O_{11}S_1$ = 1284.5893; Measured = 1284.5844; Error = 4.6ppm. **Analytical HPLC** (System 2): 95% purity; t_R = 18.03 min.

(*S*)-2-((6*S*,9*S*,12*S*)-12-Benzyl-16-(4-(2-benzylphenoxy)piperidin-1-yl)-6,9-dimethyl-5,8,11,14-tetraoxo-4,7,10,13-tetraazahexadecanamido)-6-(2-(4-((*E*)-2-(5,5-difluoro-7-(thiophen-2-yl)-5*H*-5λ^4,6λ^4-dipyrr-olo[1,2-*c*:2',1'-*f*][1,3,2]diazaborinin-3-yl)vinyl)phenoxy)acetamido)hexanamide 117

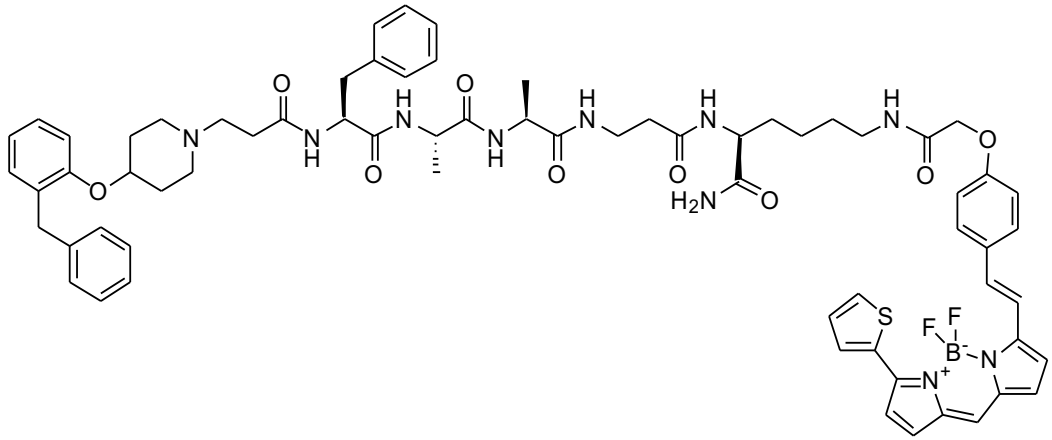

Compound synthesised using General Procedure 4 with 2.5mg (3µmol) of **106** and purified using *System 6* to give a blue solid (1.18mg, 0.9µmol, 30%). **HRMS** (Bruker MicroTOF)(*m/z*): Calculated $(M+H)^+$ for $C_{68}H_{77}B_1F_2N_{10}O_9S_1$ = 1259.5730; Measured = 1259.5783; Error = 3.4ppm. **Analytical HPLC** (System 2): 99% purity; t_R = 18.67 min.

Methyl (*E*)-2-(4-(2-(1*H*-pyrrol-2-yl)vinyl)phenoxy)acetate 118

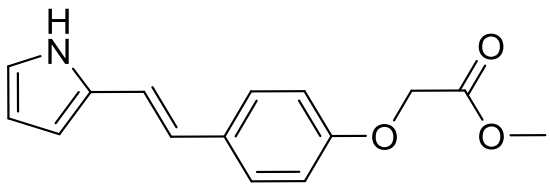

50mg (0.25mmol) of **76** dissolved in degassed, anhydrous DMF (3mL) under N_2 was treated with 63mg of sodium ethanethiolate (0.75mmol) and heated to 145°C for 18 hrs. The reaction mixture was then diluted with ethyl acetate (30mL) and washed with 0.5M NH_4Cl (5 x 20mL), followed by brine, dried over $MgSO_4$, filtered and concentrated in vacuo to afford a black solid. This was dissolved in acetonitrile (5mL), treated with K_2CO_3 (52mg, 0.375 mmol) and heated to reflux under N_2 for 30 min. This was cooled to RT, treated with methyl bromoacetate (26µL, 0.275mmol) and heated to reflux for 18 hr. This was then left to cool, acetonitrile was removed by rotary evaporator and the reaction mixture was dissolved in 50mL of ethyl acetate, followed by washings with water (3 x 50 mL) and brine, dried over $MgSO_4$, filtered, the resulting filtrate evaporated under rotary evaporator and placed in a vacuum oven to dry which gave a greenish black solid (44mg, 0.17mmol, 69%).

^{1}H NMR (400 MHz, $CDCl_3$) δ 8.35 (s, 1H, Pyrrole **H**), 7.35 (d, *J* = 8.8 Hz, 2H, 2 x Ph-C2**H**), 6.87 (d, *J* = 8.8 Hz, 2H, 2 x Ph-C3**H**), 6.85 (d, *J* = 16.7 Hz, 1H, -CHC**H**Ph), 6.81 – 6.77 (m, 1H, Pyrrole-C5**H**), 6.61 (d, *J* = 16.5 Hz, 1H, -C**H**CHPh), 6.34 – 6.29 (m, 1H, Pyrrole-C3**H**), 6.27 – 6.20 (m, 1H, Pyrrole-C3**H**), 4.64 (s, 2H, -OC**H$_2$**-), 3.81 (s, 3H, -OC**H$_3$**).
^{13}C NMR (101 MHz, $CDCl_3$) δ 169.52, 157.04, 131.62, 131.05, 127.19, 122.88, 118.99, 117.86, 115.03, 114.28, 110.07, 108.77, 65.55, 52.44.

LCMS: *m/z* of $(M+H)^+$ = 257.8; t_R = 2.81 min.

Methyl (*E*)-2-(4-(2-(5,5-difluoro-7,9-dimethyl-5*H*-5λ^4,6λ^4-dipyrrolo[1,2-*c*:2',1'-*f*][1,3, 2]diaza-borinin-3-yl)vinyl)phenoxy)acetate 119

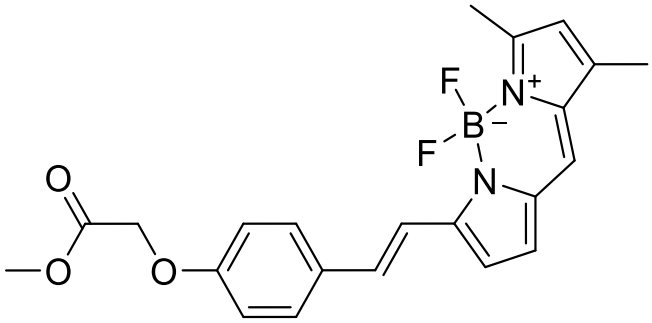

44mg (0.171mmol) of **118** and 21mg (0.171mmol) of 3,5-dimethyl-1*H*-pyrrole-2-carboxaldehyde were dissolved in 10mL of dry DCM and degassed for 15 mins. The reaction flask was placed under N_2, treated dropwise with 16µL (0.171mmol) of $POCl_3$ and stirred at RT for 2 hrs in the dark. The mixture was subsequently diluted with 40mL of DCM, treated with 0.3mL (2.05mmol) of DIPEA and 0.25mL (2.05mmol) of boron trifluoride diethyl etherate and stirred in the dark under N_2 for 18 hr at RT. The reaction mixture was then washed with brine, dried over $MgSO_4$, filtered and concentrated under rotary evaporator. The resulting gum was purified by column chromatography (EtOAc:hexane = 5:95 to 50:50) to afford a dark purple solid (13mg, 0.032mmol, 19%).

^{1}H NMR (400 MHz, DMSO-d_6) δ 7.62 (s, 1H, Ar-C**H**), 7.60 – 7.45 (m, 3H, Ar-C**H**), 7.30 (d, *J* = 16.4 Hz, 1H, -C**H**CHPh), 7.18 (d, *J* = 4.3 Hz, 1H, Ar-C**H**), 7.09 (d, *J* = 4.3 Hz, 1H, Ar-C**H**), 7.00 (d, *J* = 8.8 Hz, 2H, 2 x Ph-C3**H**), 6.28 (s, 1H, Ar-C**H**), 4.84 (s, 2H, -OC**H$_2$**-), 3.70 (s, 3H, -OC**H$_3$**), 2.48 (s, 3H, Pyrrole C3-C**H$_3$**), 2.25 (s, 3H, Pyrrole C5-C**H$_3$**).

^{13}C NMR (101 MHz, DMSO) δ 169.02, 158.50, 157.77, 153.17, 142.85, 135.79, 134.67, 134.49, 129.52, 129.43, 128.56, 123.36, 119.94, 116.45, 115.75, 115.24, 64.63, 51.89, 14.56, 11.04.

LCMS: *m/z* of $(M+H)^+$ = 410.9; t_R = 3.10 min.

(*E*)-2-(4-(2-(5,5-Difluoro-7,9-dimethyl-5*H*-5λ^4,6λ^4-dipyrrolo[1,2-*c*:2',1'-*f*][1,3,2]di-aza-borinin-3-yl)vinyl)phenoxy)acetic acid 120

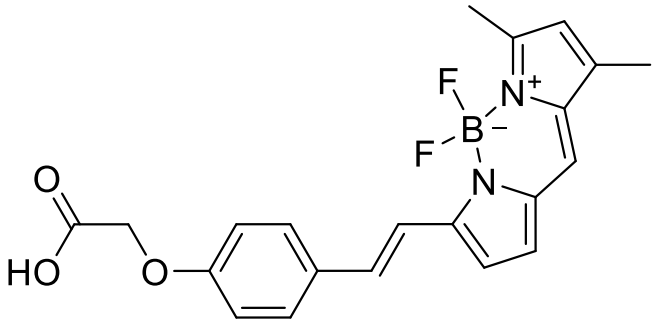

13mg (0.032mmol) of **119** dissolved in THF:H_2O (1.5mL:0.75mL) was treated with 50µL of 85% H_3PO_4 and heated under reflux at 65°C for 90 hr under N_2. The reaction mixture was concentrated under rotary evaporator, diluted in 25mL of DCM, washed with brine, dried over $MgSO_4$, filtered and concentrated under rotary evaporator. The concentrate was purified by column chromatography (MeOH:DCM = 10:90 to 25:75) to afford a dark purple solid (12mg, 0.030mmol, 92%).

^{1}H NMR (400 MHz, DMSO-d_6) δ 13.11 (s, 1H, COO**H**), 7.64 (s, 1H, Ar-C**H**), 7.61 – 7.47 (m, 3H, Ar-C**H**), 7.31 (d, *J* = 16.4 Hz, 1H, -C**H**CHPh), 7.19 (d, *J* = 4.4 Hz, 1H, Ar-C**H**), 7.12 (d, *J* = 4.3 Hz, 1H, Ar-C**H**), 7.00 (d, *J* = 8.8 Hz, 2H, 2 x Ph-C3**H**), 6.29 (s, 1H, Ar-C**H**), 4.73 (s, 2H, -OC**H$_2$**-), 2.50 (s, 3H, Pyrrole C3-C**H$_3$**), 2.26 (s, 3H, Pyrrole C5-C**H$_3$**).

^{13}C NMR (101 MHz, DMSO) δ 169.85, 158.70, 157.60, 153.27, 142.72, 135.95, 134.68, 134.42, 129.47, 129.27, 128.53, 123.34, 119.84, 116.26, 115.81, 115.17, 64.56, 14.55, 11.04.

LCMS: *m/z* of $(M+H)^+$ = 395.7; t_R = 2.96 min.

3-(5,5-Difluoro-7-(thiophen-2-yl)-5*H*-5λ^4,6λ^4-dipyrrolo[1,2-*c*:2',1'-*f*][1,3,2]diaza-borini-n-3-yl)propanoic acid 121

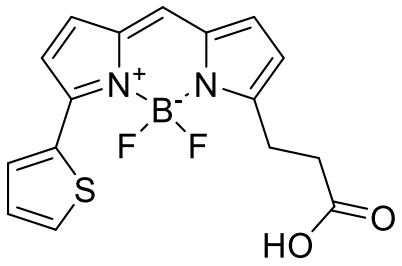

50mg (0.282mmol) of **71** and 44mg (0.282mmol) of methyl 3-(1H-pyrrol-2-yl)propanoate were dissolved in 10mL of dry DCM and degassed for 15 mins. The reaction flask was placed under N_2, treated dropwise with 29µL (0.311mmol) of $POCl_3$ and stirred at RT for 2 hrs in the dark. The mixture was subsequently diluted with 40mL of DCM, treated with 0.85mL (3.39mmol) of DIPEA and 1.25mL (3.39mmol) of boron trifluoride diethyl etherate and stirred in the dark under N_2 for 18 hr at RT. The reaction mixture was then washed with brine, dried over $MgSO_4$, filtered and concentrated under rotary evaporator. The resulting gum was purified by column chromatography (EtOAc:hexane = 5:95 to 30:70), dried under rotary evaporator, re-dissolved in THF:H_2O (1.8mL:0.9mL), treated with 0.1mL of 85% H_3PO_4 and heated under reflux at 65°C for 90 hr under N_2. The reaction mixture was concentrated under rotary evaporator, diluted in 30mL of DCM, washed with brine, dried over $MgSO_4$, filtered and concentrated under rotary evaporator. The concentrate was purified by column chromatography (MeOH:DCM = 5:95 to 7.5:92.5) to afford a dark purple solid (15mg, 0.043mmol, 15%).

^{1}H NMR (400 MHz, DMSO-d_6) δ 12.36 (s, 1H, COO**H**), 8.03 (dd, *J* = 3.8, 1.1 Hz, 1H, Thiophene-C**H**), 7.85 (dd, *J* = 5.1, 1.0 Hz, 1H, Thiophene-C**H**), 7.70 (s, 1H, Ar-C**H**), 7.35 (d, *J* = 4.3 Hz, 1H, Ar-C**H**), 7.29 (d, *J* = 4.2 Hz, 1H, Ar-C**H**), 7.26 (dd, *J* = 5.0, 3.8 Hz, 1H, Thiophene-C**H**), 6.98 (d, *J* = 4.3 Hz, 1H, Ar-C**H**), 6.55 (d, *J* = 4.2 Hz, 1H, Ar-C**H**), 3.17 (t, *J* = 7.7 Hz, 2H, -C**H$_2$**CH$_2$COOH), 2.69 (t, *J* = 7.7 Hz, 2H, -CH$_2$C**H$_2$**COOH).

^{13}C NMR (101 MHz, DMSO) δ 173.32, 160.95, 149.42, 136.29, 134.58, 133.23, 131.40, 131.04, 130.99, 128.91, 128.03, 119.95, 119.01, 32.08, 23.85. (1 Carbon missing)

LCMS: *m/z* of $(M+H)^+$ not observable; t_R = 2.80 min.

HRMS (Bruker MicroTOF)(*m/z*): Calculated $(M-H)^-$ for $C_{16}H_{13}B_1F_2N_2O_2S_1$ = 345.0686; Measured = 345.0680; Error = 2.7ppm..

(*S*)-*N*1-(3-(((*S*)-1-Amino-6-(6-(2-(4-((*E*)-2-(5,5-difluoro-7-(thiophen-2-yl)-5*H*-4λ^4,5λ^4-dipyrrolo[1,2-*c*:2',1'-*f*][1,3,2]diazaborinin-3-yl)vinyl)phenoxy)acetamido)hexanamido)-1-oxohexan-2-yl)amino)-3-oxopropyl)-2-((*S*)-2-((*S*)-2-(3-(4-(2-benzylphenoxy)piperidin-1-yl)propanamido)-3-methylbutanamido)-3-hydroxypropanamido) succinamide 122

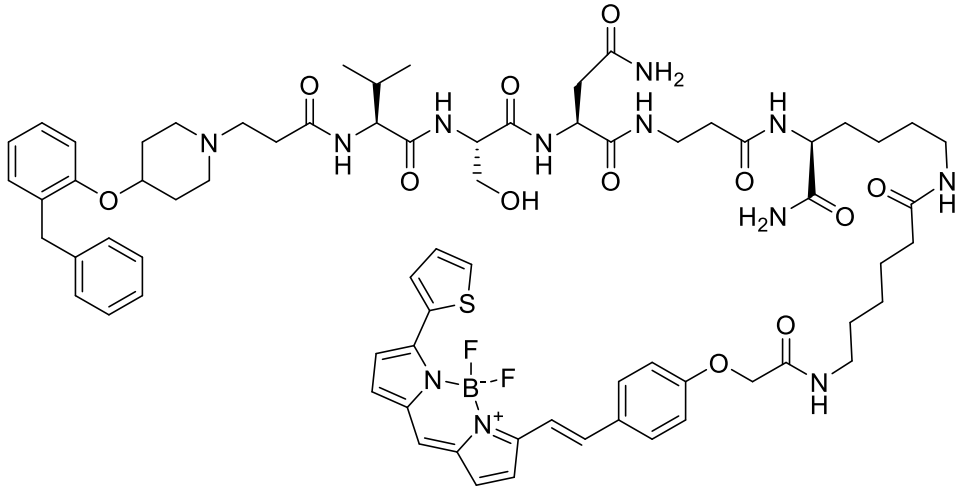

Compound synthesised using General Procedure 5 with 1.3mg (1.6µmol) of **96** and purified using *System 9* to give a blue solid (1.28mg, 0.9µmol, 58%). **HRMS** (Bruker MicroTOF)(*m/z*): Calculated $(M+H)^+$ for $C_{71}H_{89}B_1F_2N_{12}O_{12}S_1$ = 1383.6578; Measured = 1383.6513; Error = 5.5ppm. **Analytical HPLC** (System 2): 99% purity; t_R = 16.31min.

(*S*)-*N*^{1}-(3-(((*S*)-1-Amino-6-(2-(4-((*E*)-2-(5,5-difluoro-7,9-dimethyl-5*H*-5λ^4,6λ^4-dipyrrolo[1,2-*c*:2',1'-*f*][1,3,2]diazaborinin-3-yl)vinyl)phenoxy)acetamido)-1-oxohexan-2-yl)amino)-3-oxopropyl)-2-((*S*)-2-((*S*)-2-(3-(4-(2-benzylphenoxy)piperidin-1-yl) propanamido)-3-methylbutanamido)-3-hydroxypropanamido)succinimide 123

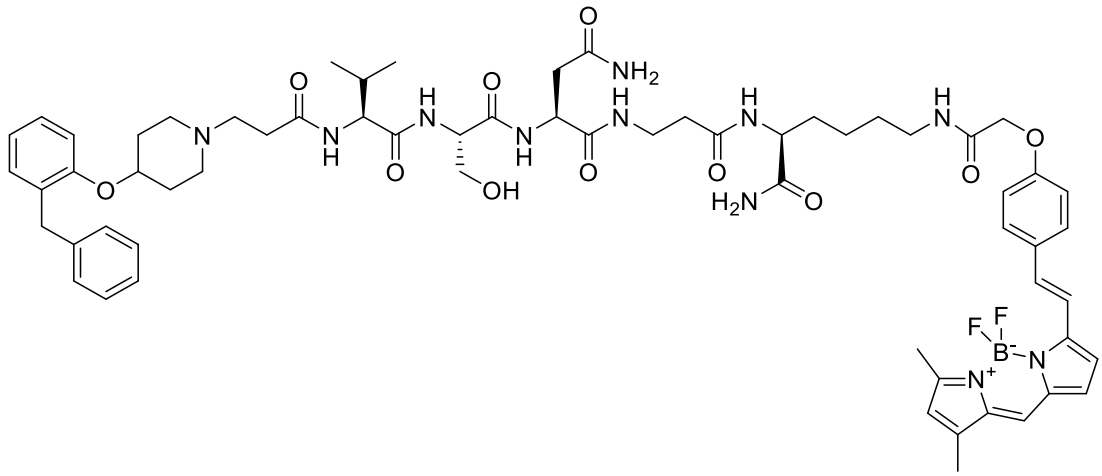

Compound synthesised using General Procedure 4 with 0.6mg (0.7µmol) of **96** and purified using *System 8* to give a purple solid (0.61mg, 0.5µmol, 69%). **HRMS** (Bruker MicroTOF)(*m/z*): Calculated $(M+H)^+$ for $C_{63}H_{80}B_1F_2N_{11}O_{11}$ = 1216.6173; Measured = 1216.6214; Error = 2.5ppm. **Analytical HPLC** (System 2): 95% purity; tR = 15.65min.

(*S*)-*N*^{1}-(3-(((*S*)-1-Amino-6-(3-(5,5-difluoro-7-(thiophen-2-yl)-5*H*-5λ^4,6λ^4-dipyrrolo [1,2-*c*:2',1'-*f*][1,3,2]diazaborinin-3-yl)propanamido)-1-oxohexan-2-yl)amino)-3-oxopropyl)-2-((*S*)-2-((*S*)-2-(3-(4-(2-benzylphenoxy)piperidin-1-yl)propanamido)-3-methylbutanamido)-3-hydroxypropanamido)succinamide 124

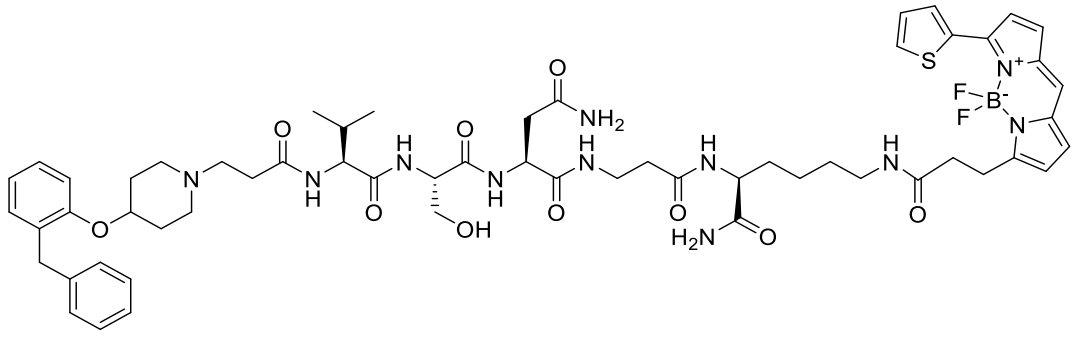

Compound synthesised using General Procedure 4 with 0.4mg (0.5µmol) of **96** and purified using *System 9* to give a purple solid (0.37mg, 0.3µmol, 66%). **HRMS** (Bruker MicroTOF)(*m/z*): Calculated $(M+H)^+$ for $C_{58}H_{74}B_1F_2N_{11}O_{10}S_1$ = 1166.5475; Measured = 1166.5450; Error = 2.9ppm. **Analytical HPLC** (System 2): 96% purity; t_R = 14.80min.

(*S*)-*N*1-(3-(((*S*)-1-Amino-6-(3-(5,5-difluoro-7,9-dimethyl-5*H*-4λ^4,5λ^4-dipyrrolo[1,2-*c*:2',1'-*f*][1,3,2]diazaborinin-3-yl)propanamido)-1-oxohexan-2-yl)amino)-3-oxopropyl)-2-((*S*)-2-((*S*)-2-(3-(4-(2-benzylphenoxy)piperidin-1-yl)propanamido)-3-methylbutanamido)-3-hydroxypropanamido)succinamide 125

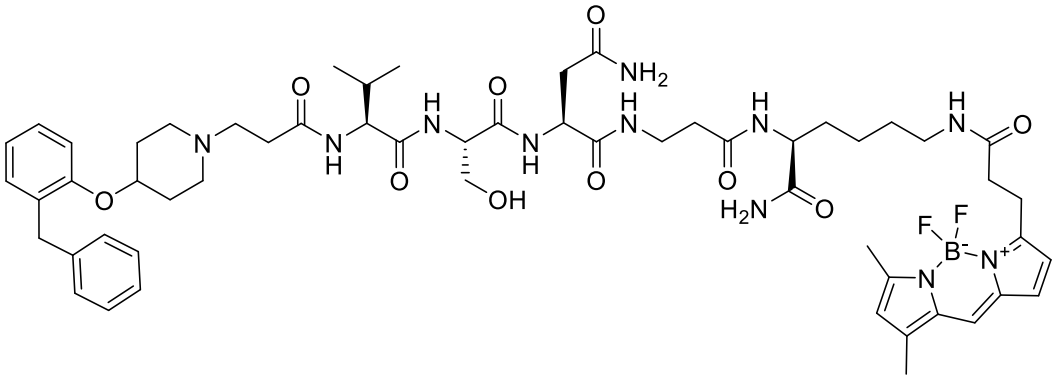

Compound synthesised using General Procedure 5 with 0.6mg (0.7µmol) of **96** and purified using *System 9* to give a green solid (0.65mg, 0.6µmol, 80%). **HRMS** (Bruker MicroTOF)(*m/z*): Calculated $(M+H)^+$ for $C_{56}H_{76}B_1F_2N_{11}O_{10}$ = 1112.5911; Measured = 1112.5966; Error = 4.1ppm. **Analytical HPLC** (System 2): 99% purity; t_R = 14.36min.

(*S*)-*N*1-(3-(((*S*)-1-Amino-6-(6-(3-(5,5-difluoro-7,9-dimethyl-5*H*-4λ^4,5λ^4-dipyrrolo [1,2-*c*:2',1'-*f*][1,3,2]diazaborinin-3-yl)propanamido)hexanamido)-1-oxohexan-2-yl)amino)-3-oxopropyl)-2-((*S*)-2-((*S*)-2-(3-(4-(2-benzylphenoxy)piperidin-1-yl)propanamido)-3-methylbutanamido)-3-hydroxypropanamido)succinamide 126

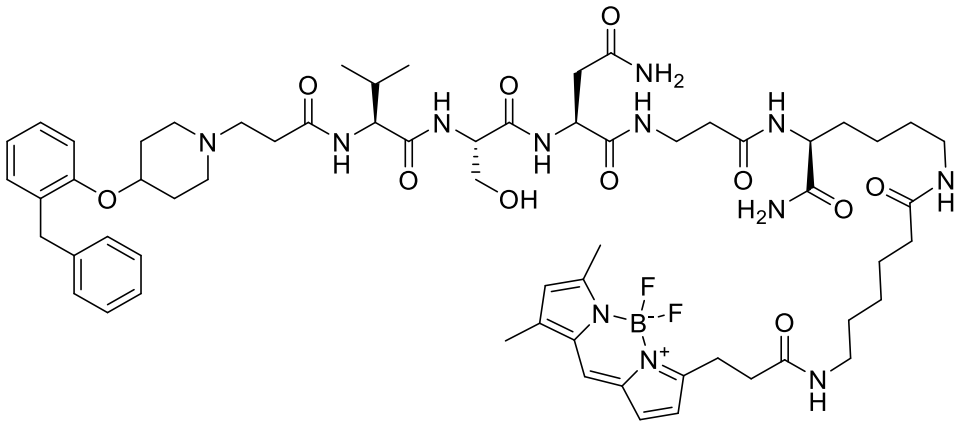

Compound synthesised using General Procedure 5 with 1.3mg (1.6µmol) of **96** and purified using *System 9* to give a green solid (0.81mg, 0.7µmol, 41%). **HRMS** (Bruker MicroTOF)(*m/z*): Calculated $(M+H)^+$ for $C_{62}H_{87}B_1F_2N_{12}O_{11}$ = 1225.6751; Measured = 1225.6712; Error = 4.0ppm. **Analytical HPLC** (System 2): 99% purity; t_R = 14.62min.

1-((5*S*,8*S*,11*S*,18*S*)-11-(2-Amino-2-oxoethyl)-1-(4-(2-benzylphenoxy)piperidin-1-yl)-18-carbamoyl-8-(hydroxymethyl)-5-isopropyl-3,6,9,12,16,24-hexaoxo-4,7,10,13,17,23-hexaazanonacosan-29-yl)-3,3-dimethyl-2-((1*E*,3*E*)-5-((*E*)-1,3,3-trimethyl-5-sulfonatoindolin-2-ylidene)penta-1,3-dien-1-yl)-3*H*-indol-1-ium-5-sulfonate 127

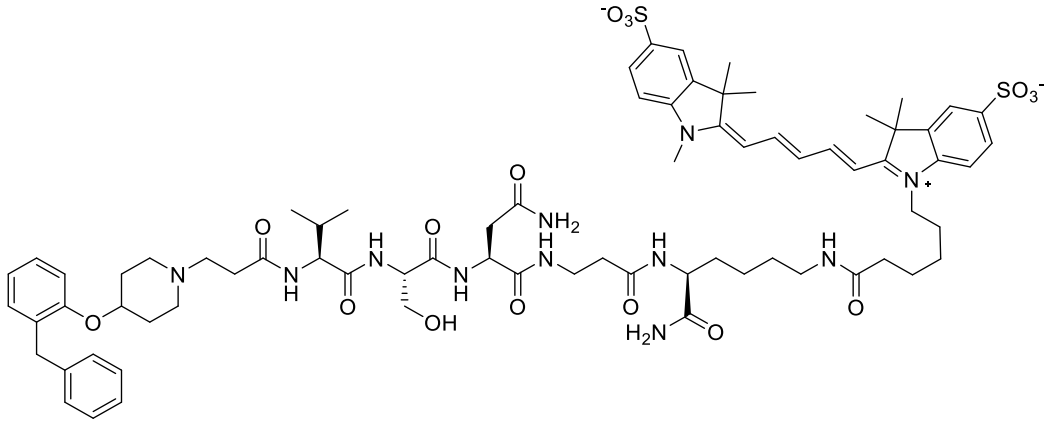

Compound synthesised using General Procedure 5 with 1.3mg (1.6µmol) of **96** and purified using *System 9* to give a. blue solid (1.12mg, 0.8µmol, 48%). **HRMS** (Bruker MicroTOF)(*m/z*): Calculated M^- for $C_{74}H_{98}N_{11}O_{16}S_2$ = 1460.6640; Measured = 1460.6607; Error = 2.2ppm. **Analytical HPLC** (System 2): 95% purity; t_R = 14.36min.

***N*-((5*S*,8*S*,11*S*,18*S*)-5-Benzyl-1-(4-(2-benzylphenoxy)piperidin-1-yl)-18-carbamoyl-8,11-dimethyl-3,6,9,12,16-pentaoxo-4,7,10,13,17-pentaazadocosan-22-yl)-6-(2-(4-((*E*)-2-(5,5-difluoro-7-(thiophen-2-yl)-5*H*-4λ^4,5λ^4-dipyrrolo[1,2-*c*:2',1'-*f*][1,3,2]diazaborinin-3-yl)vinyl)phenoxy)acetamido)hexanamide 128**

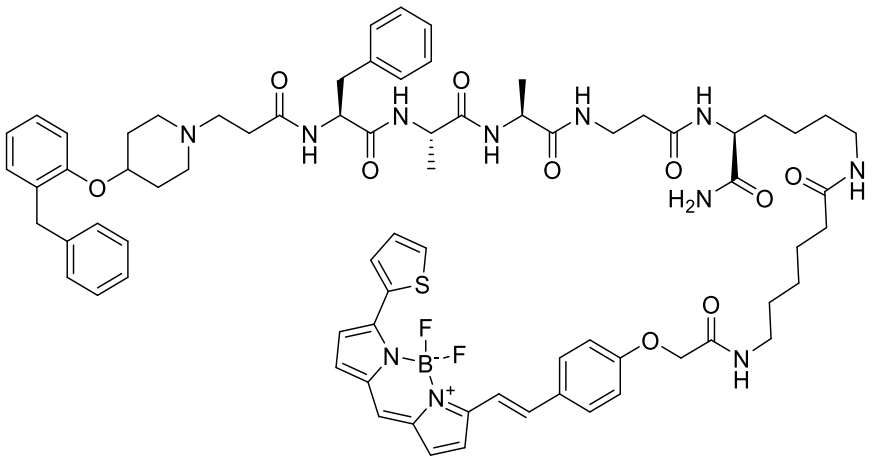

Compound synthesised using General Procedure 5 with 1.3mg (1.6µmol) of **106** and purified using *System 9* to give a blue solid (1.81mg, 1.3µmol, 82%). **HRMS** (Bruker MicroTOF)(*m/z*): Calculated $(M+H)^+$ for $C_{74}H_{88}B_1F_2N_{11}O_{10}S_1$ = 1372.7570; Measured = 1372.6578; Error = 0.3ppm. **Analytical HPLC** (System 2): 99% purity; t_R = 16.89min.

(*S*)-2-((6*S*,9*S*,12*S*)-12-Benzyl-16-(4-(2-benzylphenoxy)piperidin-1-yl)-6,9-dimethyl-5,8,11,14-tetraoxo-4,7,10,13-tetraazahexadecanamido)-6-(2-(4-((*E*)-2-(5,5-difluoro-7,9-dimethyl-5*H*-5λ^4,6λ^4-dipyrrolo[1,2-*c*:2',1'-*f*][1,3,2]diazaborinin-3-yl)vinyl)phenoxy)acetamido)hexanamide 129

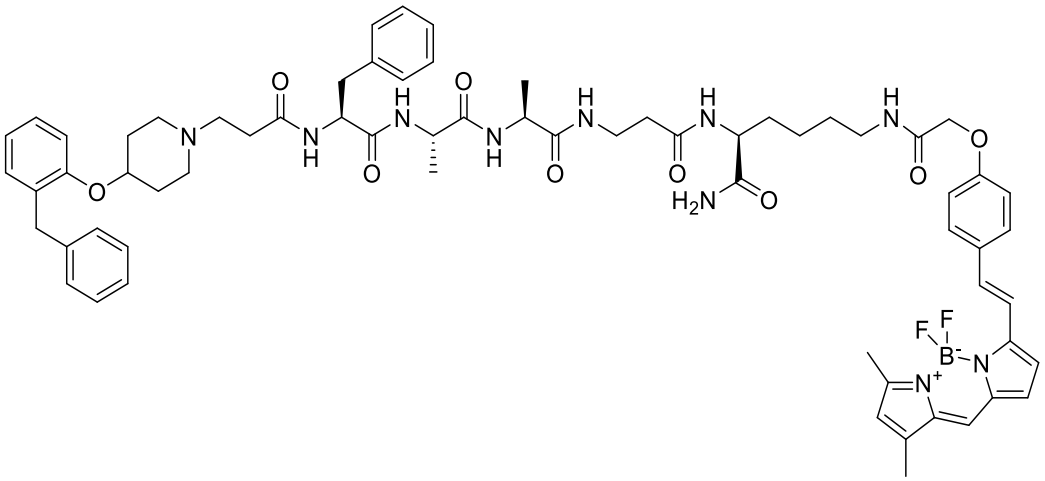

Compound synthesised using General Procedure 4 with 0.5mg (0.6µmol) of **106** and purified using *System 8* to give a purple solid (0.61mg, 0.5µmol, 79%). **HRMS** (Bruker MicroTOF)(*m/z*): Calculated $(M+H)^+$ for $C_{66}H_{79}B_1F_2N_{10}O_9$ = 1205.6165; Measured = 1205.6199; Error = 1.9ppm. **Analytical HPLC** (System 2): 96% purity; t_R = 15.47min.

(*S*)-2-((6*S*,9*S*,12*S*)-12-Benzyl-16-(4-(2-benzylphenoxy)piperidin-1-yl)-6,9-dimethyl-5,8,11,14-tetraoxo-4,7,10,13-tetraazahexadecanamido)-6-(3-(5,5-difluoro-7-(thiophen-2-yl)-5*H*-5λ^4,6λ^4-dipyrrolo[1,2-*c*:2',1'-*f*][1,3,2]diazaborinin-3-yl)propanamido) hexanamide 130

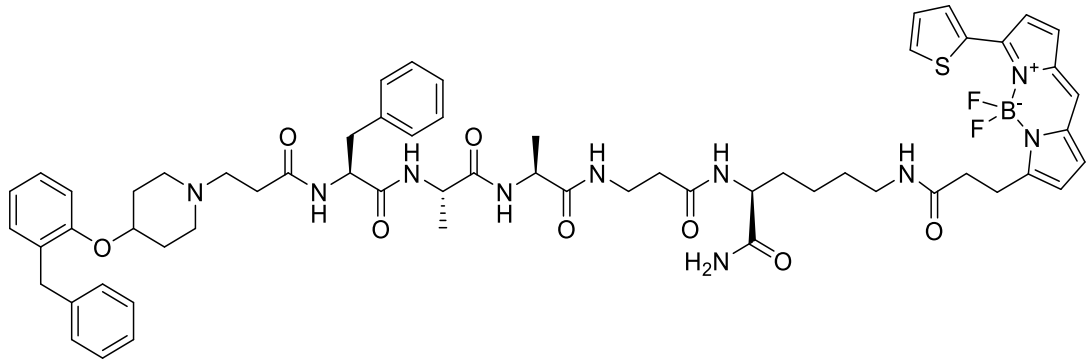

Compound synthesised using General Procedure 4 with 0.4mg (0.5µmol) of **106** and purified using *System 9* to give a purple solid (0.32mg, 0.3µmol, 58%). **HRMS** (Bruker MicroTOF)(*m/z*): Calculated $(M+H)^+$ for $C_{61}H_{73}B_1F_2N_{10}O_8S_1$ = 1155.5467; Measured = 1155.5496; Error = 1.6ppm. **Analytical HPLC** (System 2): 96% purity; tR = 15.48min.

(*S*)-2-((6*S*,9*S*,12*S*)-12-Benzyl-16-(4-(2-benzylphenoxy)piperidin-1-yl)-6,9-dimethyl-5,8,11,14-tetraoxo-4,7,10,13-tetraazahexadecanamido)-6-(3-(5,5-difluoro-7,9-dimethyl-5*H*-4λ^4,5λ^4-dipyrrolo[1,2-*c*:2',1'-*f*][1,3,2]diazaborinin-3-yl)propanamido)hexanamide 131

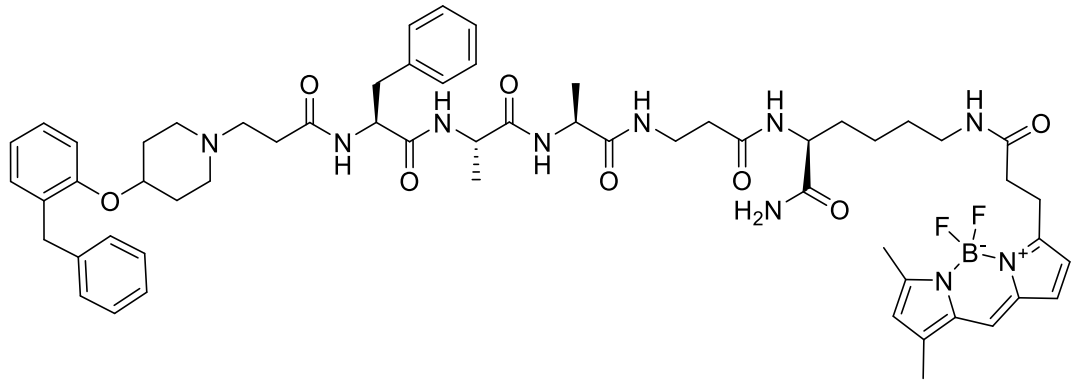

Compound synthesised using General Procedure 5 with 0.6mg (0.7µmol) of **106** and purified using *System 9* to give a green solid (0.66mg, 0.6µmol, 79%). **HRMS** (Bruker MicroTOF)(*m/z*): Calculated $(M+H)^+$ for $C_{59}H_{75}B_1F_2N_{10}O_8$ = 1101.5903; Measured = 1101.5961; Error = 4.4ppm. **Analytical HPLC** (System 2): 99% purity; t_R = 15.12min.

***N*-((5*S*,8*S*,11*S*,18*S*)-5-Benzyl-1-(4-(2-benzylphenoxy)piperidin-1-yl)-18-carbamoyl-8,11-dimethyl-3,6,9,12,16-pentaoxo-4,7,10,13,17-pentaazadocosan-22-yl)-6-(3-(5,5-difluoro-7,9-dimethyl-5*H*-4λ^4,5λ^4-dipyrrolo[1,2-*c*:2',1'-*f*][1,3,2]diazaborinin-3-yl)propanamido)hexanamide 132**

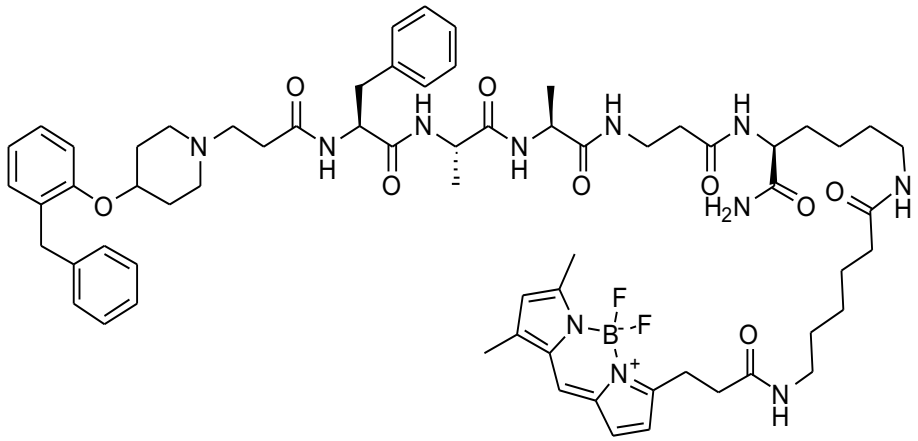

Compound synthesised using General Procedure 5 with 1.3mg (1.6µmol) of **106** and purified using *System 9* to give a green solid (1.16mg, 1µmol, 60%). **HRMS** (Bruker MicroTOF)(*m/z*): Calculated $(M+H)^+$ for $C_{65}H_{86}B_1F_2N_{11}O_9$ = 1214.6744; Measured = 1214.6816; Error = 5.1ppm. **Analytical HPLC** (System 2): 99% purity; t_R = 15.23min.

1-((5*S*,8*S*,11*S*,18*S*)-5-Benzyl-1-(4-(2-benzylphenoxy)piperidin-1-yl)-18-carbamoyl-8,11-dimethyl-3,6,9,12,16,24-hexaoxo-4,7,10,17,23-pentaazaoctacosan-28-yl)-3,3-dimethyl-2-((1*E*,3*E*)-5-((*E*)-1,3,3-trimethyl-5-sulfonatoindolin-2-ylidene)penta-1,3-dien-1-yl)-3*H*-indol-1-ium-5-sulfonate 133

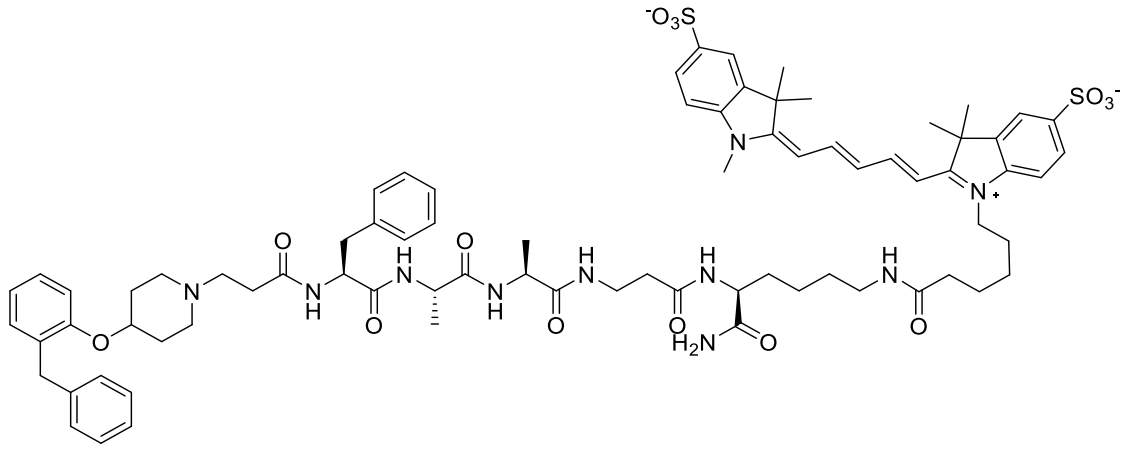

Compound synthesised using General Procedure 5 with 1.3mg (1.6µmol) of **106** and purified using *System 9* to give a blue solid (1.29mg, 0.9µmol, 56%). **HRMS** (Bruker MicroTOF)(*m/z*): Calculated M^- for $C_{77}H_{87}N_{10}O_{14}S_2$ = 1449.6633; Measured = 1449.6576; Error = 3.9ppm. **Analytical HPLC** (System 2): 98% purity; t_R = 15.23min.

6.2 Pharmacology

Materials

Fetal calf serum was obtained from PAA Laboratories (Wokingham, UK), furimazine from Promega (Southampton, UK) and all other chemicals and reagents were obtained from Sigma-Aldrich (Gillingham, UK) and Tocris Bioscience (Bristol, UK).

Cell Culture

Nluc-tagged H_1R expressing HEK293T cells, H_1R-YFP expressing CHO cells and wildtype H_1R expressing CHO cells were prepared as detailed in Stoddart et al[3]. HEK293T cells were maintained in Dulbecco's modified Eagles medium (DMEM) supplemented with 10% fetal calf serum whereas CHO cells were maintained in Dulbecco's modified Eagles medium nutrient mix F12 (DMEM/F12) supplemented with 10% fetal calf serum and 2mM of L-glutamine. All cell lines were maintained in T-75 flasks at 37°C in a humidified atmosphere of air with 5% CO_2. All cell culture

procedures including cell plating for assays were performed in a class II laminar flow hood using sterile techniques.

Spectral Characterisation of Fluorescent Ligands

Fluorescent ligands were diluted to 0.1mM with either Hank's Balanced Salt Solution (HBSS; 145 mmol/L NaCl, 5 mmol/L KCl, 1.7 mmol/ $CaCl_2$, 1mmol/L $MgSO_4$, 10 mmol/L HEPES, 2mmol/L sodium pyruvate, 1.5 mmol/L $NaHCO_3$, 10 mmol/L D-glucose, pH7.4) or DMSO and 100µL of the dilution were transferred to black-walled, clear-bottom 96-well plates. Plates were then placed in multi-well fluorometric imaging plate reader FlexStation3 (Molecular Devices, Sunnyvale, CA). The excitation spectrum was determined by measuring the intensity of emission at a fixed wavelength (580nm for **32**, 620nm for **123-124**, **129-130**) after excitation with light of wavelengths ranging from 300-540nm for **32** and 450-580nm for **123-124**, **129-130**). The emission spectrum was determined by measuring the intensity of light emitted across a range of wavelengths (510-700nm for **32** and 550-700nm for **123-124**, **129-130**) when excited with light at 460nm for **32** and 500nm for **123-124**, **129-130**).

Transfection and Preparation of Cell Homogenates

HEK293T cells were transiently transfected with 2.5 µg cDNA encoding Nluc-H_3R or Nluc-H_4R and 2.5 µg empty pcDEF3 vector using the polyethylenimine method as described previously in Mocking et al[72]. Two days after transfection, cells were collected in phosphate-buffered saline (PBS), centrifuged at 1900 g for 10 minutes and cell pellet was stored at -20°C until day of experiment. Pellet was resuspended in HBSS buffer and cells were disrupted using a Branson sonifier 250 (Boom bv., Meppel, the Netherlands) prior to use in NanoBRET binding assay.

NanoBRET Binding Assays

For whole cell NanoBRET assays, HEK293T cells stably expressing Nluc-tagged H_1R were seeded in white 96-well microplates and grown for 24 hr prior to experimentation in normal growth medium. The media was replaced with HBSS right before experimentation. For saturation binding experiments, the required concentrations of fluorescent ligand and the competing unlabelled ligand mepyramine (final concentration of 10µM) were added simultaneously to the plate

and incubated for 2 h at 37°C in the absence of CO_2. For competition binding experiments, the required concentrations of unlabelled ligand and the competing fluorescent ligand **11** (final concentration of 25nM) were added simultaneously and incubated for 2 h at 37°C in the absence of CO_2. For membrane NanoBRET saturation binding experiments, cell homogenates expressing the Nluc-H_3R or Nluc-H_4R were incubated with the required concentrations of fluorescent ligand in the absence and presence of 10μM clobenpropit in HBSS for 2 hours at 25°C. For all NanoBRET binding experiments, 10μM of the NanoGlo substrate (Promega) was added to each well after the incubation period and fluorescence and luminescence emissions measured after 5 min. For association kinetic experiments, 10μM furimazine was added to each well and incubated at room temperature in the dark for 15 min to allow for stabilisation of luminescence signal. The required concentration of fluorescent ligand in the presence or absence of 10μM of doxepin was added simultaneously and the plates were read immediately with each well being read once per min for 90 min. Fluorescence and luminescence were read simultaneously using a PHERAstar FS plate reader (BMG Labtech, Aylesbury, UK) at 37°C. Luminescence was measured at 392.5-467.5nm for green-shifted fluorescent ligands and 420-500nm for orange and red-shifted fluorescent ligands. Fluorescence was measured at 512.5-547.5nm for green-shifted fluorescent ligands, >550nm (longpass) for orange-shifted fluorescent ligands and >610nm (longpass) for red-shifted fluorescent ligands. The raw BRET ratio was calculated by dividing the fluorescence value by the luminescence value.

Intracellular Calcium Mobilisation Assay

CHO H_1R cells were grown to confluence in black-walled, clear-bottom 96-well plates. On the day of the experiment, the media was replaced with 100μL of HBSS containing 2.5nM probenecid, 2.3μM Fluo-4AM (Invitrogen, Carlsbad, CA), 0.023% Pluronic F-127, 0.5nM Brilliant Black BN and the plate incubated for 1 hr at 37°C in the dark. Plates were then placed in multi-well fluorometric imaging plate reader FlexStation3 (Molecular Devices, Sunnyvale, CA) and Fluo-4 fluorescence was measured at 520nm (excitation at 485nm) every 1.52s for 200s. HBSS only or HBSS containing the required concentration of histamine was added after 15s. For each well the peak maximum-minimum maximum change in fluorescence value was taken and plotted against concentration of histamine to give a dose-response curve.

Confocal Imaging

H_1R-YFP expressing CHO cells were grown to approximately 80% confluency on an 8-well Labtek chambered coverglass (Nunc Nalgene). On the day of experiment, the cells were washed twice with 200µL of HBSS and subsequently incubated in the presence or absence of 10µM mepyramine for 30 min at 37°C in humidified air with 0% CO_2. The required concentration of fluorescent ligand was added to the wells and incubated for another 30 min at 37°C. Images were acquired using a Zeiss LSM710 confocal microscope (Carl Zeiss GmbH, Hena, Germany) fitted with a 63x plan-Apochromat NA1.3 Ph3 oil-immersion lens. For YFP, a 488nm argon laser was used for excitation and emission was detected using a BP505-30 filter. For BODIPY630/650 fluorophore, a 633nm helium-neon laser was used for excitation and emission was detected using a 650nm long pass filter. A pinhole of 1 Airy Unit was used and fixed laser power, gain and offset for the BODIPY630/650 containing compounds were kept constant across all experiments.

Data Analysis

All data were analysed and presented using Prism 7 (GraphPad Software, San Diego, CA). Total and non-specific saturation binding curves from NanoBRET saturation binding assay were fitted simultaneously using equation (1):

$$\text{BRET Ratio} = \frac{B_{max} \times [B]}{[B] + K_D} + \big((M \times [B]) + C\big) \quad (1)$$

where B_{max} is the maximal response, [B] is the concentration of fluorescent ligand in nM, K_D is the equilibrium dissociation constant in nM, M is the slope of the non-specific component and C is the intercept with the Y-axis.

NanoBRET competition binding curves were fitted using the Cheng-Prusoff equation (2):

$$K_i = \frac{IC_{50}}{1 + \frac{[L]}{K_D}} \quad (2)$$

where [L] is the concentration of the fluorescent ligand **11** in nM and K_D is the equilibrium dissociation constant of **11** in nM (K_D = 8nM). The IC_{50} is calculated as in equation (3):

$$\% \text{ inhibition of specific binding} = \frac{100 \times [A]}{[A] + IC_{50}} \quad (3)$$

where [A] is the concentration of the unlabelled competing drug and IC50 is the molar concentration of this competing ligand required to inhibit 50% of the specific binding of the concentration [L] of the fluorescent ligand.

For the NanoBRET association kinetic experiments, BRET ratio was determined for each concentration of fluorescent ligand at each time point in the presence or absence of 10µM of doxepin. Specific binding was calculated from the subtraction of non-specific binding from total binding. The k_{on}, k_{off} and K_D values were obtained from the data using equation (4):

$$K_D = \frac{k_{off}}{k_{on}} \quad (4)$$

where K_D is the equilibrium dissociation constant and k_{off} is the dissociation rate constant of the ligand in min^{-1}. k_{on} is the association rate constant in $M^{-1}\,min^{-1}$ and is calculated as follows in the equation (5):

$$k_{on} = \frac{k_{obs} - k_{off}}{[L]} \quad (5)$$

where [L] is the ligand concentration in M and k_{obs} is calculated from global fitting of the data to the following equation which expresses monoexponential association function (6):

$$Y = Y_{max}(1 - e^{-k_{obs}t}) \quad (6)$$

where Y_{max} equals levels of binding at infinite time (t) and k_{obs} is the rate constant for the observed rate of association.

For the calcium mobilisation experiments, estimated affinity values (pK_B) were calculated from the shift in agonist concentration response curves in the presence of the fluorescent antagonists using equation (7):

$$\mathrm{DR} = 1 + \frac{[B]}{K_B} \tag{7}$$

where DR (dose ratio) is the ratio of the agonist concentration required to stimulate an identical response in the presence and absence of antagonist, [B]. DR was determined from the EC_{25} value as there was a decrease in observed maximal efficacy of histamine in the presence of all ten fluorescent antagonists. The EC_{25} value was determined from the non-linear regression fit of the normalised maximum-minimum fluorescence values using the equation (8):

$$\mathrm{Y} = Y_{min} + \frac{Y_{max} - Y_{min}}{1 + 10^{logEC_{50} - x}} \tag{8}$$

where Y_{min} and Y_{max} are the lowest and highest normalised maximum-minimum fluorescence value and EC_{50} is the concentration of the histamine at 50% response.

6.3 Computational Modelling

Molecular Docking

The H_1R crystal structure (PDB code: 3RZE) was obtained from the protein data bank and prepared by using Protein Preparation Wizard within Maestro of the Schrodinger modelling suite. Missing atoms (in K442, R481) and missing residues (F168-V174 in extracellular loop 2) were modelled, phosphate ion, water molecule and *Z*-isomer of Doxepin (D7V) were removed retaining only the *E*-isomer (5EH), hydrogen bonding were optimised using PROPKA at pH 7 and the protein structure was minimised using OPLS3 force field. Ligands for docking were prepared and minimised using LigPrep within the modelling suite and docked into the receptor using Glide under XP (extra precision) mode without imposing any restraints using OPLS3 force field and flexible ligand sampling. The binding poses that formed the crucial salt bridge interaction

with Asp107 were selected and their poses and glide scores examined using Maestro within the Schrodinger modelling suite. Only one binding pose was obtained for the docking of **107**. This was modelled using PyMOL 2.1.1 to include amino acid labels and distance measurements between the fluorescent ligand and nearby receptor residues.

Membrane Bilayer Modelling

The T4-lysozyme of the H_1R crystal structure (PDB: 3RZE) was truncated and the membrane bilayer modelled using ProBLM web server[156] by uploading the receptor PDB file as input and selecting POPC-75x75 (phospholiphase C) as the membrane file on the server. The membrane bilayer model was subsequently aligned with the docking pose of compound 107 using PyMOL 2.1.1.

Chapter 7: References

1. Massari, N. A., Nicoud, M. B., and Medina, V. A. (2020) Histamine receptors and cancer pharmacology: an update, *Br. J. Pharmacol.* **2020**; 177(3), 516–538.

2. Medina, V. A.; Rivera, E. S., Histamine receptors and cancer pharmacology. *Br. J. Pharmacol.* **2010,** *161* (4), 755-767.

3. Stoddart, L. A.; Vernall, A. J.; Bouzo-Lorenzo, M.; Bosma, R.; Kooistra, A. J.; de Graaf, C.; Vischer, H. F.; Leurs, R.; Briddon, S. J.; Kellam, B.; Hill, S. J., Development of novel fluorescent histamine H1-receptor antagonists to study ligand-binding kinetics in living cells. *Sci. Rep.* **2018,** *8* (1), 1572.

4. Shimamura, T.; Shiroishi, M.; Weyand, S.; Tsujimoto, H.; Winter, G.; Katritch, V.; Abagyan, R.; Cherezov, V.; Liu, W.; Han, G. W., Structure of the human histamine H_1 receptor complex with doxepin. *Nature* **2011,** *475* (7354), 65-70.

5. Overington, J. P.; Al-Lazikani, B.; Hopkins, A. L., How many drug targets are there? *Nat. Rev. Drug Discov.* **2006,** *5* (12), 993-996.

6. Bjarnadóttir, T. K.; Gloriam, D. E.; Hellstrand, S. H.; Kristiansson, H.; Fredriksson, R.; Schiöth, H. B., Comprehensive repertoire and phylogenetic analysis of the G protein-coupled receptors in human and mouse. *Genomics* **2006,** *88* (3), 263-273.

7. Santos, R.; Ursu, O.; Gaulton, A.; Bento, A. P.; Donadi, R. S.; Bologa, C. G.; Karlsson, A.; Al-Lazikani, B.; Hersey, A.; Oprea, T. I.; Overington, J. P., A comprehensive map of molecular drug targets. *Nat. Rev. Drug Discov.* **2016,** *16*, 19.

8. Foord, S. M.; Bonner, T. I.; Neubig, R. R.; Rosser, E. M.; Pin, J. P.; Davenport, A. P.; Spedding, M.; Harmar, A. J., International Union of Pharmacology. XLVI. G Protein-Coupled Receptor List. *Pharmacol. Rev.* **2005,** *57* (2), 279-288.

9. Rasmussen, S. G. F.; Choi, H. J.; Rosenbaum, D. M.; Kobilka, T. S.; Thian, F. S.; Edwards, P. C.; Burghammer, M.; Ratnala, V. R. P.; Sanishvili, R.; Fischetti, R. F.; Schertler, G. F. X.; Weis, W. I.; Kobilka, B. K., Crystal structure of the human β2 adrenergic G-protein-coupled receptor. *Nature* **2007,** *450*, 383.

10. Lee, Y.; Basith, S.; Choi, S., Recent Advances in Structure-Based Drug Design Targeting Simulations. *J. Med. Chem.* **2018,** *61* (1), 1-46.

over two steps 0in cancer. *Nat. Rev. Drug Discov.* **2011,** *10* (1), 47-60.

12. Pfleger, J.; Gresham, K.; Koch, W. J., G protein-coupled receptor kinases as therapeutic targets in the heart. *Nat. Rev. Cardiol.* **2019**.

13. Thomsen, W.; Frazer, J.; Unett, D., Functional assays for screening GPCR targets. *Curr Opin Biotechnol* **2005,** *16* (6), 655-665.

14. Shenoy, S. K.; Lefkowitz, R. J., Seven-Transmembrane Receptor Signaling Through beta-Arrestin. *Science's STKE* **2005,** *2005* (308), cm10.

15. Ma, L.; Pei, G., β-arrestin signaling and regulation of transcription. *J. Cell Sci* **2007,** *120* (2), 213-218.

16. Kang, J.; Shi, Y.; Xiang, B.; Qu, B.; Su, W.; Zhu, M.; Zhang, M.; Bao, G.; Wang, F.; Zhang, X.; Yang, R.; Fan, F.; Chen, X.; Pei, G.; Ma, L., A Nuclear Function of beta-Arrestin1 in GPCR Signaling: Regulation of Histone Acetylation and Gene Transcription. *Cell* **2005,** *123* (5), 833-847.

17. Pierce, K. L.; Lefkowitz, R. J., Classical and new roles of beta-arrestins in the regulation of G-protein-coupled receptors. *Nat. Rev. Neurosci* **2001,** *2* (10), 727-733.

18. Lefkowitz, R. J.; Shenoy, S. K., Transduction of Receptor Signals by beta-Arrestins. *Science* **2005,** *308* (5721), 512-517.

19. Wang, P.; Gao, H.; Ni, Y.; Wang, B.; Wu, Y.; Ji, L.; Qin, L.; Ma, L.; Pei, G., beta-Arrestin 2 Functions as a G-Protein-coupled Receptor-activated Regulator of Oncoprotein Mdm2. *J. Biol. Chem* **2003,** *278* (8), 6363-6370.

20. Witherow, D. S.; Garrison, T. R.; Miller, W. E.; Lefkowitz, R. J., β-Arrestin inhibits NF-κB activity by means of its interaction with the NF-κB inhibitor IκBα. *Proc. Natl. Acad. Sci. U.S.A* **2004,** *101* (23), 8603-8607.

21. Gao, H.; Sun, Y.; Wu, Y.; Luan, B.; Wang, Y.; Qu, B.; Pei, G., Identification of beta-Arrestin2 as a G Protein-Coupled Receptor-Stimulated Regulator of NF-kappaB Pathways. *Mol. Cell* **2004,** *14* (3), 303-317.

22. Claing, A.; Laporte, S. A.; Caron, M. G.; Lefkowitz, R. J., Endocytosis of G protein-coupled receptors: roles of G protein-coupled receptor kinases and beta-arrestin proteins. *Prog. Neurobiol* **2002,** *66* (2), 61-79.

23. Shenoy, S. K.; McDonald, P. H.; Kohout, T. A.; Lefkowitz, R. J., Regulation of Receptor Fate by Ubiquitination of Activated β_2-Adrenergic Receptor and β-Arrestin. *Science* **2001,** *294* (5545), 1307-1313.

24. Congreve, M.; Oswald, C.; Marshall, F. H., Applying Structure-Based Drug Design Approaches to Allosteric Modulators of GPCRs. *Trends Pharmacol. Sci.* **2017,** *38* (9), 837-847.

25. Christopoulos, A., Allosteric binding sites on cell-surface receptors: novel targets for drug discovery. *Nat. Rev. Drug Discov.* **2002,** *1* (3), 198-210.

26. Gentry, P. R.; Sexton, P. M.; Christopoulos, A., Novel Allosteric Modulators of G Protein-coupled Receptors. *J. Biol. Chem* **2015,** *290* (32), 19478-19488.

27. Christopoulos, A., Advances in G Protein-Coupled Receptor Allostery: From Function to Structure. *Mol. Pharmacol* **2014,** *86* (5), 463-478.

28. May, L. T.; Leach, K.; Sexton, P. M.; Christopoulos, A., Allosteric Modulation of G Protein–Coupled Receptors. *Annu. Rev. Pharmacol. Toxicol.* **2007,** *47* (1), 1-51.

29. Christopoulos, A.; Changeux, J.-P.; Catterall, W. A.; Fabbro, D.; Burris, T. P.; Cidlowski, J. A.; Olsen, R. W.; Peters, J. A.; Neubig, R. R.; Pin, J.-P.; Sexton, P. M.; Kenakin, T. P.; Ehlert, F. J.; Spedding, M.; Langmead, C. J., International Union of Basic and Clinical Pharmacology. XC. Multisite Pharmacology: Recommendations for the Nomenclature of Receptor Allosterism and Allosteric Ligands. *Pharmacol. Rev.* **2014,** *66* (4), 918-947.

30. Valant, C.; Lane, J. R.; Sexton, P. M.; Christopoulos, A., The Best of Both Worlds? Bitopic Orthosteric/Allosteric Ligands of G Protein–Coupled Receptors. *Annu. Rev. Pharmacol. Toxicol.* **2012,** *52* (1), 153-178.

31. Christopher, J. A.; Orgován, Z.; Congreve, M.; Doré, A. S.; Errey, J. C.; Marshall, F. H.; Mason, J. S.; Okrasa, K.; Rucktooa, P.; Serrano-Vega, M. J.; Ferenczy, G. G.; Keserű, G. M., Structure-Based Optimization Strategies for G Protein-Coupled Receptor (GPCR) Allosteric Modulators: A Case Study from Analyses of New Metabotropic Glutamate Receptor 5 (mGlu5) X-ray Structures. *J. Med. Chem.* **2019,** *62* (1), 207-222.

32. Thal, D. M.; Glukhova, A.; Sexton, P. M.; Christopoulos, A., Structural insights into G-protein-coupled receptor allostery. *Nature* **2018,** *559* (7712), 45-53.

33. Wold, E. A.; Chen, J.; Cunningham, K. A.; Zhou, J., Allosteric Modulation of Class A GPCRs: Targets, Agents, and Emerging Concepts. *J. Med. Chem.* **2019,** *62* (1), 88-127.

34. Neubig, R. R.; Spedding, M.; Kenakin, T.; Christopoulos, A., International Union of Pharmacology Committee on Receptor Nomenclature and Drug Classification. XXXVIII. Update on Terms and Symbols in Quantitative Pharmacology. *Pharmacol. Rev.* **2003,** *55* (4), 597-606.

35. Yung-Chi, C.; Prusoff, W. H., Relationship between the inhibition constant (KI) and the concentration of inhibitor which causes 50 per cent inhibition (I50) of an enzymatic reaction. *Biochem. Pharmacol* **1973,** *22* (23), 3099-3108.

36. Motulsky, H. J.; Mahan, L. C., The kinetics of competitive radioligand binding predicted by the law of mass action. *Mol. Pharmacol* **1984,** *25* (1), 1-9.

37. Rang, H. P.; Ritter, J. M.; Flower, R. J.; Henderson, G., *Rang & Dale's Pharmacology*. 8 ed.; Churchill Livingstone: Edinburgh, 2015.

38. Milligan, G., Principles: Extending the utility of [35S]GTPgammaS binding assays. *Trends Pharmacol. Sci.* **2003,** *24* (2), 87-90.

39. Wise, A.; Jupe, S. C.; Rees, S., The Identification of Ligands at Orphan G-Protein Coupled Receptors. *Annu. Rev. Pharmacol. Toxicol.* **2004,** *44* (1), 43-66.

40. Robas, N. M.; Fidock, M. D., Identification of Orphan G Protein-Coupled Receptor Ligands Using FLIPR® Assays. In *Receptor Binding Techniques*, Davenport, A. P., Ed. Humana Press: Totowa, NJ, 2005; pp 17-26.

41. Williams, C., cAMP detection methods in HTS: selecting the best from the rest. *Nat. Rev. Drug Discov.* **2004,** *3* (2), 125-135.

42. McGrath, J. C.; Daly, C. J., Use of fluorescent ligands and receptors to visualize adrenergic receptors. In *The Adrenergic Receptors*, Springer: 2006; pp 151-172.

43. Kuder, K.; Kiec-Kononowicz, K., Fluorescent GPCR ligands as new tools in pharmacology. *Curr. Med. Chem* **2008,** *15* (21), 2132-2143.

44. Tomasch, M.; Schwed, J. S.; Weizel, L.; Stark, H., Novel chalcone-based fluorescent human histamine h(3) receptor ligands as pharmacological tools. *Front Syst Neurosci* **2012,** *6*, 14.

45. Tomasch, M.; Schwed, J. S.; Paulke, A.; Stark, H., Bodilisant-a novel fluorescent, highly affine histamine h3 receptor ligand. *ACS Med Chem Lett* **2013,** *4* (2), 269-73.

46. Leopoldo, M.; Lacivita, E.; Berardi, F.; Perrone, R., Developments in fluorescent probes for receptor research. *Drug Discov Today* **2009,** *14* (13-14), 706-12.

47. Vernall, A. J.; Stoddart, L. A.; Briddon, S. J.; Ng, H. W.; Laughton, C. A.; Doughty, S. W.; Hill, S. J.; Kellam, B., Conversion of a non-selective adenosine receptor antagonist into A3-selective high affinity fluorescent probes using peptide-based linkers. *Org Biomol Chem* **2013,** *11* (34), 5673-82.

48. Rose, R. H.; Briddon, S. J.; Hill, S. J., A novel fluorescent histamine H1 receptor antagonist demonstrates the advantage of using fluorescence correlation spectroscopy to study the binding of lipophilic ligands. *Br. J. Pharmacol.* **2012,** *165* (6), 1789-800.

49. Iliopoulos-Tsoutsouvas, C.; Kulkarni, R. N.; Makriyannis, A.; Nikas, S. P., Fluorescent probes for G-protein-coupled receptor drug discovery. *Expert Opin. Drug Discov* **2018,** *13* (10), 933-947.

50. Monici, M., Cell and tissue autofluorescence research and diagnostic applications. In *Biotechnology Annual Review*, Elsevier: 2005; Vol. 11, pp 227-256.

51. Soave, M.; Briddon, S. J.; Hill, S. J.; Stoddart, L. A., Fluorescent ligands: Bringing light to emerging GPCR paradigms. *Br. J. Pharmacol.* **2020,** *177* (5), 978-991.

52. Stoddart, L. A.; Kilpatrick, L. E.; Briddon, S. J.; Hill, S. J., Probing the pharmacology of G protein-coupled receptors with fluorescent ligands. *Neuropharmacology* **2015,** *98*, 48-57.

53. Machleidt, T.; Woodroofe, C. C.; Schwinn, M. K.; Méndez, J.; Robers, M. B.; Zimmerman, K.; Otto, P.; Daniels, D. L.; Kirkland, T. A.; Wood, K. V., NanoBRET—A Novel BRET Platform for the Analysis of Protein–Protein Interactions. *ACS Chem. Biol* **2015,** *10* (8), 1797-1804.

54. Los, G. V.; Encell, L. P.; McDougall, M. G.; Hartzell, D. D.; Karassina, N.; Zimprich, C.; Wood, M. G.; Learish, R.; Ohana, R. F.; Urh, M.; Simpson, D.; Mendez, J.; Zimmerman, K.; Otto, P.; Vidugiris, G.; Zhu, J.; Darzins, A.; Klaubert, D. H.; Bulleit, R. F.; Wood, K. V., HaloTag: A Novel Protein Labeling Technology for Cell Imaging and Protein Analysis. *ACS Chem. Biol* **2008,** *3* (6), 373-382.

55. Keppler, A.; Gendreizig, S.; Gronemeyer, T.; Pick, H.; Vogel, H.; Johnsson, K., A general method for the covalent labeling of fusion proteins with small molecules in vivo. *Nature Biotechnol.* **2003,** *21* (1), 86-89.

56. Gautier, A.; Juillerat, A.; Heinis, C.; Corrêa, I. R.; Kindermann, M.; Beaufils, F.; Johnsson, K., An Engineered Protein Tag for Multiprotein Labeling in Living Cells. *Chem. Biol.* **2008,** *15* (2), 128-136.

57. Pfleger, K. D. G.; Eidne, K. A., Illuminating insights into protein-protein interactions using bioluminescence resonance energy transfer (BRET). *Nat. Methods* **2006,** *3* (3), 165-174.

58. Hall, M. P.; Unch, J.; Binkowski, B. F.; Valley, M. P.; Butler, B. L.; Wood, M. G.; Otto, P.; Zimmerman, K.; Vidugiris, G.; Machleidt, T.; Robers, M. B.; Benink, H. A.; Eggers, C. T.; Slater, M. R.; Meisenheimer, P. L.; Klaubert, D. H.; Fan, F.; Encell, L. P.; Wood, K. V., Engineered Luciferase Reporter from a Deep Sea Shrimp Utilizing a Novel Imidazopyrazinone Substrate. *ACS Chem. Biol* **2012,** *7* (11), 1848-1857.

59. Hiblot, J.; Yu, Q.; Sabbadini, M. D. B.; Reymond, L.; Xue, L.; Schena, A.; Sallin, O.; Hill, N.; Griss, R.; Johnsson, K., Luciferases with Tunable Emission Wavelengths. *Angew. Chem* **2017,** *129* (46), 14748-14752.

60. Wu, P. G.; Brand, L., Resonance Energy Transfer: Methods and Applications. *Anal. Biochem* **1994,** *218* (1), 1-13.

61. Dacres, H.; Michie, M.; Wang, J.; Pfleger, K. D. G.; Trowell, S. C., Effect of enhanced Renilla luciferase and fluorescent protein variants on the Förster distance of Bioluminescence resonance energy transfer (BRET). *Biochem. Biophys. Res. Commun* **2012,** *425* (3), 625-629.

62. Stoddart, L. A.; Kilpatrick, L. E.; Hill, S. J., NanoBRET Approaches to Study Ligand Binding to GPCRs and RTKs. *Trends Pharmacol. Sci.* **2018,** *39* (2), 136-147.

63. Zwier, J. M.; Roux, T.; Cottet, M.; Durroux, T.; Douzon, S.; Bdioui, S.; Gregor, N.; Bourrier, E.; Oueslati, N.; Nicolas, L.; Tinel, N.; Boisseau, C.; Yverneau, P.; Charrier-Savournin, F.; Fink, M.; Trinquet, E., A Fluorescent Ligand-Binding Alternative Using Tag-lite® Technology. *J. Biomol. Screen.* **2010,** *15* (10), 1248-1259.

64. Young, S. M.; Bologa, C.; Prossnitz, E. R.; Oprea, T. I.; Sklar, L. A.; Edwards, B. S., High-Throughput Screening with HyperCyt® Flow Cytometry to Detect Small Molecule Formylpeptide Receptor Ligands. *J. Biomol. Screen.* **2005,** *10* (4), 374-382.

65. Allen, M.; Reeves, J.; Mellor, G., High Throughput Fluorescence Polarization: A Homogeneous Alternative to Radioligand Binding for Cell Surface Receptors. *J. Biomol. Screen.* **2000,** *5* (2), 63-69.

66. Stoddart, L. A.; Johnstone, E. K. M.; Wheal, A. J.; Goulding, J.; Robers, M. B.; Machleidt, T.; Wood, K. V.; Hill, S. J.; Pfleger, K. D. G., Application of BRET to monitor ligand binding to GPCRs. *Nat. Methods* **2015,** *12*, 661.

67. Soave, M.; Stoddart, L. A.; Brown, A.; Woolard, J.; Hill, S. J., Use of a new proximity assay (NanoBRET) to investigate the ligand-binding characteristics of three fluorescent ligands to the human β1-adrenoceptor expressed in HEK-293 cells. *Pharmacol. res. perspect.* **2016,** *4* (5), e00250.

68. Hansen, A. H.; Sergeev, E.; Pandey, S. K.; Hudson, B. D.; Christiansen, E.; Milligan, G.; Ulven, T., Development and Characterization of a Fluorescent Tracer for the Free Fatty Acid Receptor 2 (FFA2/GPR43). *J. Med. Chem.* **2017,** *60* (13), 5638-5645.

69. Kilpatrick, L. E.; Friedman-Ohana, R.; Alcobia, D. C.; Riching, K.; Peach, C. J.; Wheal, A. J.; Briddon, S. J.; Robers, M. B.; Zimmerman, K.; Machleidt, T.; Wood, K. V.; Woolard, J.; Hill, S. J., Real-time analysis of the binding of fluorescent VEGF165a to VEGFR2 in living cells: Effect of receptor tyrosine kinase inhibitors and fate of internalized agonist-receptor complexes. *Biochem. Pharmacol* **2017,** *136*, 62-75.

70. Conroy, S.; Kindon, N. D.; Glenn, J.; Stoddart, L. A.; Lewis, R. J.; Hill, S. J.; Kellam, B.; Stocks, M. J., Synthesis and Evaluation of the First Fluorescent Antagonists of the Human P2Y2 Receptor Based on AR-C118925. *J. Med. Chem.* **2018,** *61* (7), 3089-3113.

71. Wang, J.-H.; Shao, X.-X.; Hu, M.-J.; Wei, D.; Liu, Y.-L.; Xu, Z.-G.; Guo, Z.-Y., A novel BRET-based binding assay for interaction studies of relaxin family peptide receptor 3 with its ligands. *Amino Acids* **2017,** *49* (5), 895-903.

72. Mocking, T. A. M.; Verweij, E. W. E.; Vischer, H. F.; Leurs, R., Homogeneous, Real-Time NanoBRET Binding Assays for the Histamine H_3 and H_4 Receptors on Living Cells. *Mol. Pharmacol* **2018,** *94* (6), 1371-1381.

73. Bouzo-Lorenzo, M.; Stoddart, L. A.; Xia, L.; IJzerman, A. P.; Heitman, L. H.; Briddon, S. J.; Hill, S. J., A live cell NanoBRET binding assay allows the study of ligand-binding kinetics to the adenosine A3 receptor. *Purinergic Signal.* **2019**.

74. Robers, M. B.; Dart, M. L.; Woodroofe, C. C.; Zimprich, C. A.; Kirkland, T. A.; Machleidt, T.; Kupcho, K. R.; Levin, S.; Hartnett, J. R.; Zimmerman, K.; Niles, A. L.; Ohana, R. F.; Daniels, D. L.; Slater, M.; Wood, M. G.; Cong, M.; Cheng, Y.-Q.; Wood, K. V., Target engagement and drug residence time can be observed in living cells with BRET. *Nat. Commun.* **2015,** *6*, 10091.

75. Stoddart, L. A.; White, C. W.; Nguyen, K.; Hill, S. J.; Pfleger, K. D. G., Fluorescence- and bioluminescence-based approaches to study GPCR ligand binding. *Br. J. Pharmacol.* **2016,** *173* (20), 3028-3037.

76. Alcobia, D. C.; Ziegler, A. I.; Kondrashov, A.; Comeo, E.; Mistry, S.; Kellam, B.; Chang, A.; Woolard, J.; Hill, S. J.; Sloan, E. K., Visualizing Ligand Binding to a GPCR In Vivo Using NanoBRET. *iScience* **2018,** *6*, 280-288.

77. Dale, N. C.; Johnstone, E. K. M.; White, C. W.; Pfleger, K. D. G., NanoBRET: The Bright Future of Proximity-Based Assays. *Front. Bioeng. Biotechnol.* **2019,** *7* (56).

78. Stoddart, Leigh A.; Vernall, Andrea J.; Denman, Jessica L.; Briddon, Stephen J.; Kellam, B.; Hill, Stephen J., Fragment Screening at Adenosine-A3 Receptors in Living Cells Using a Fluorescence-Based Binding Assay. *Chem. Biol.* **2012,** *19* (9), 1105-1115.

79. Gherbi, K.; Briddon, S. J.; Hill, S. J., Detection of the secondary, low-affinity β1-adrenoceptor site in living cells using the fluorescent CGP 12177 derivative BODIPY-TMR-CGP. *Br. J. Pharmacol.* **2014,** *171* (23), 5431-5445.

80. May, L. T.; Self, T. J.; Briddon, S. J.; Hill, S. J., The Effect of Allosteric Modulators on the Kinetics of Agonist-G Protein-Coupled Receptor Interactions in Single Living Cells. *Mol. Pharmacol* **2010,** *78* (3), 511-523.

81. Gherbi, K.; May, L. T.; Baker, J. G.; Briddon, S. J.; Hill, S. J., Negative cooperativity across β1-adrenoceptor homodimers provides insights into the nature of the secondary low-affinity CGP 12177 β1-adrenoceptor binding conformation. *The FASEB Journal* **2015,** *29* (7), 2859-2871.

82. May, L. T.; Bridge, L. J.; Stoddart, L. A.; Briddon, S. J.; Hill, S. J., Allosteric interactions across native adenosine-A3 receptor homodimers: quantification using single-cell ligand-binding kinetics. *The FASEB Journal* **2011,** *25* (10), 3465-3476.

83. Vernall, A. J.; Hill, S. J.; Kellam, B., The evolving small‐molecule fluorescent‐conjugate toolbox for Class A GPCRs. *Br. J. Pharmacol.* **2014,** *171* (5), 1073-1084.

84. Bohme, I.; Beck-Sickinger, A. G., Illuminating the life of GPCRs. *Cell Commun Signal* **2009,** *7*, 16.

85. Briddon, S. J.; Hill, S. J., Pharmacology under the microscope: the use of fluorescence correlation spectroscopy to determine the properties of ligand-receptor complexes. *Trends Pharmacol. Sci.* **2007,** *28* (12), 637-645.

86. Briddon, S. J.; Kilpatrick, L. E.; Hill, S. J., Studying GPCR Pharmacology in Membrane Microdomains: Fluorescence Correlation Spectroscopy Comes of Age. *Trends Pharmacol. Sci.* **2018,** *39* (2), 158-174.

87. Pramanik, A.; Rigler, R., Ligand-Receptor Interactions in the Membrane of Cultured Cells Monitored by Fluorescence Correlation Spectroscopy. In *Biological Chemistry*, 2001; Vol. 382, p 371.

88. Zhong, Z.-H.; Pramanik, A.; Ekberg, K.; Jansson, O. T.; Jörnvall, H.; Wahren, J.; Rigler, R., Insulin binding monitored by fluorescence correlation spectroscopy. *Diabetologia* **2001,** *44* (9), 1184-1188.

89. Hegener, O.; Prenner, L.; Runkel, F.; Baader, S. L.; Kappler, J.; Häberlein, H., Dynamics of β2-Adrenergic Receptor−Ligand Complexes on Living Cells. *Biochemistry* **2004,** *43* (20), 6190-6199.

90. Middleton, R. J.; Briddon, S. J.; Cordeaux, Y.; Yates, A. S.; Dale, C. L.; George, M. W.; Baker, J. G.; Hill, S. J.; Kellam, B., New Fluorescent Adenosine A1-Receptor Agonists That Allow Quantification of Ligand−Receptor Interactions in Microdomains of Single Living Cells. *J. Med. Chem.* **2007,** *50* (4), 782-793.

91. Corriden, R.; Kilpatrick, L. E.; Kellam, B.; Briddon, S. J.; Hill, S. J., Kinetic analysis of antagonist-occupied adenosine-A3 receptors within membrane microdomains of individual cells provides evidence of receptor dimerization and allosterism. *The FASEB Journal* **2014,** *28* (10), 4211-4222.

92. Briddon, S. J.; Middleton, R. J.; Cordeaux, Y.; Flavin, F. M.; Weinstein, J. A.; George, M. W.; Kellam, B.; Hill, S. J., Quantitative analysis of the formation and diffusion of A_1-adenosine receptor-antagonist complexes in single living cells. *Proc. Natl. Acad. Sci. U.S.A* **2004,** *101* (13), 4673-4678.

93. Cordeaux, Y.; Briddon, S. J.; Alexander, S. P. H.; Kellam, B.; Hill, S. J., Agonist-occupied A3 adenosine receptors exist within heterogeneous complexes in membrane microdomains of individual living cells. *The FASEB Journal* **2008,** *22* (3), 850-860.

94. Panula, P.; Chazot, P. L.; Cowart, M.; Gutzmer, R.; Leurs, R.; Liu, W. L.; Stark, H.; Thurmond, R. L.; Haas, H. L., International Union of Basic and Clinical Pharmacology. XCVIII. Histamine Receptors. *Pharmacol Rev* **2015,** *67* (3), 601-55.

95. Bruno, B.; Francesca, N.-G.; Shawkat, M. J.; Idoia, O.-M.; Erika, A.-T.; Juan, B.-B.; Gorka, P.-Y.; Aintzane, A.; Maria, D. B., Histamine and Histamine Receptor Antagonists in Cancer Biology. *Inflam. Allergy Drug Targets (Discontinued)* **2010,** *9* (3), 146-157.

96. Falus, A.; Hegyesi, H.; Lázár-Molnár, E.; Pós, Z.; László, V.; Darvas, Z., Paracrine and autocrine interactions in melanoma: histamine is a relevant player in local regulation. *Trends Immunol.* **2001,** *22* (12), 648-652.

97. Rivera, E. S.; Cricco, G. P.; Engel, N. I.; Fitzsimons, C. P.; Martín, G. A.; Bergoc, R. M., Histamine as an autocrine growth factor: an unusual role for a widespread mediator. *Semin. Cancer Biol.* **2000,** *10* (1), 15-23.

98. Fernández-Nogueira, P.; Noguera-Castells, A.; Fuster, G.; Recalde-Percaz, L.; Moragas, N.; López-Plana, A.; Enreig, E.; Jauregui, P.; Carbó, N.; Almendro, V.; Gascón, P.; Bragado, P.; Mancino, M., Histamine receptor 1 inhibition enhances antitumor therapeutic responses through extracellular signal-regulated kinase (ERK) activation in breast cancer. *Cancer Lett.* **2018,** *424*, 70-83.

99. McGrath, J. C.; Arribas, S.; Daly, C. J., Fluorescent ligands for the study of receptors. *Trends Pharmacol. Sci.* **1996,** *17* (11), 393-399.

100. J Kuder, K.; Kiec-Kononowicz, K., Fluorescent GPCR ligands as new tools in pharmacology-update, years 2008-early 2014. *Curr. Med. Chem.* **2014,** *21* (34), 3962-3975.

101. Middleton, R. J.; Kellam, B., Fluorophore-tagged GPCR ligands. *Curr Opin Chem Biol* **2005,** *9* (5), 517-25.

102. Li, L.; Kracht, J.; Peng, S.; Bernhardt, G.; Buschauer, A., Synthesis and pharmacological activity of fluorescent histamine H1 receptor antagonists related to mepyramine. *Bioorg. Med. Chem. Lett.* **2003,** *13* (7), 1245-1248.

103. Kooistra, A. J.; Vischer, H. F.; McNaught-Flores, D.; Leurs, R.; de Esch, I. J. P.; de Graaf, C., Function-specific virtual screening for GPCR ligands using a combined scoring method. *Sci. Rep.* **2016,** *6*, 28288.

104. Church, D. S.; Church, M. K., Pharmacology of Antihistamines. *World Allergy Organ. J.* **2011,** *4* (3), S22-S27.

105. Kuhne, S.; Kooistra, A. J.; Bosma, R.; Bortolato, A.; Wijtmans, M.; Vischer, H. F.; Mason, J. S.; de Graaf, C.; de Esch, I. J.; Leurs, R., Identification of Ligand Binding Hot Spots of the Histamine H1 Receptor following Structure-Based Fragment Optimization. *J. Med. Chem.* **2016,** *59* (19), 9047-9061.

106. Li, L.; Kracht, J.; Peng, S.; Bernhardt, G.; Elz, S.; Buschauer, A., Synthesis and pharmacological activity of fluorescent histamine H2 receptor antagonists related to potentidine. *Bioorg. Med. Chem. Lett.* **2003,** *13* (10), 1717-1720.

107. Malan, S. F.; van Marle, A.; Menge, W. M.; Zuliani, V.; Hoffman, M.; Timmerman, H.; Leurs, R., Fluorescent ligands for the histamine H2 receptor: synthesis and preliminary characterization. *Bioorg Med Chem* **2004,** *12* (24), 6495-503.

108. Xie, S. X.; Petrache, G.; Schneider, E.; Ye, Q. Z.; Bernhardt, G.; Seifert, R.; Buschauer, A., Synthesis and pharmacological characterization of novel fluorescent histamine H2-receptor ligands derived from aminopotentidine. *Bioorg Med Chem Lett* **2006,** *16* (15), 3886-90.

109. Bart, A. E.; Bibinaz, G., Do Histamine receptor 3 antagonists have a place in the therapy for schizophrenia? *Curr. Pharm. Des.* **2015,** *21* (26), 3760-3770.

110. Vohora, D.; Bhowmik, M., Histamine H3 receptor antagonists/inverse agonists on cognitive and motor processes: relevance to Alzheimer's disease, ADHD, schizophrenia, and drug abuse. *Front. Syst. Neurosci.* **2012,** *6*, 72-72.

111. Malek, R.; Arribas, R. L.; Palomino-Antolin, A.; Totoson, P.; Demougeot, C.; Kobrlova, T.; Soukup, O.; Iriepa, I.; Moraleda, I.; Diez-Iriepa, D.; Godyń, J.; Panek, D.; Malawska, B.; Głuch-Lutwin, M.; Mordyl, B.; Siwek, A.; Chabchoub, F.; Marco-Contelles, J.; Kiec-Kononowicz, K.; Egea, J.; de los Ríos, C.; Ismaili, L., New Dual Small Molecules for Alzheimer's Disease Therapy Combining Histamine H3 Receptor (H3R) Antagonism and Calcium Channels Blockade with Additional Cholinesterase Inhibition. *J. Med. Chem.* **2019,** *62* (24), 11416-11422.

112. Amon, M.; Ligneau, X.; Schwartz, J. C.; Stark, H., Fluorescent non-imidazole histamine H3 receptor ligands with nanomolar affinities. *Bioorg Med Chem Lett* **2006,** *16* (7), 1938-40.

113. Cowart, M.; Gfesser, G. A.; Bhatia, K.; Esser, R.; Sun, M.; Miller, T. R.; Krueger, K.; Witte, D.; Esbenshade, T. A.; Hancock, A. A., Fluorescent benzofuran histamine H(3) receptor antagonists with sub-nanomolar potency. *Inflamm Res* **2006,** *55 Suppl 1*, S47-8.

114. Amon, M.; Ligneau, X.; Camelin, J. C.; Berrebi-Bertrand, I.; Schwartz, J. C.; Stark, H., Highly potent fluorescence-tagged nonimidazole histamine H3 receptor ligands. *ChemMedChem* **2007,** *2* (5), 708-16.

115. Kuder, K. J.; Kottke, T.; Stark, H.; Ligneau, X.; Camelin, J. C.; Seifert, R.; Kiec-Kononowicz, K., Search for novel, high affinity histamine H3 receptor ligands with fluorescent properties. *Inflamm Res* **2010,** *59 Suppl 2*, S247-8.

116. Mirzahosseini, A.; Kovács, M.; Kánai, K.; Csutora, P.; Dalmadi, B., BODIPY® FL histamine as a new modality for quantitative detection of histamine receptor upregulation upon IgE sensitization in murine bone marrow-derived mast cells. *Cytometry A* **2015,** *87* (1), 23-31.

117. Korb, O.; Stützle, T.; Exner, T. E., Empirical Scoring Functions for Advanced Protein−Ligand Docking with PLANTS. *J Chem Inf Model* **2009,** *49* (1), 84-96.

118. Yang, L.; Simionescu, R.; Lough, A.; Yan, H., Some observations relating to the stability of the BODIPY fluorophore under acidic and basic conditions. *Dyes Pigm.* **2011,** *91* (2), 264-267.

119. Chauhan, D. P.; Saha, T.; Lahiri, M.; Talukdar, P., BODIPY based 'click on' fluorogenic dyes: application in live cell imaging. *Tetrahedron Lett.* **2014,** *55* (1), 244-247.

120. Kolb, H. C.; Finn, M.; Sharpless, K. B., Click chemistry: diverse chemical function from a few good reactions. *Angew. Chem. Int. Ed.* **2001,** *40* (11), 2004-2021.

121. Tornøe, C. W.; Christensen, C.; Meldal, M., Peptidotriazoles on solid phase:[1, 2, 3]-triazoles by regiospecific copper (I)-catalyzed 1, 3-dipolar cycloadditions of terminal alkynes to azides. *J. Org. Chem.* **2002,** *67* (9), 3057-3064.

122. Huisgen, R., 1,3-Dipolar Cycloadditions. Past and Future. *Angew. Chem. Int. Ed.* **1963,** *2* (10), 565-598.

123. Zhang, L.; Chen, X.; Xue, P.; Sun, H. H.; Williams, I. D.; Sharpless, K. B.; Fokin, V. V.; Jia, G., Ruthenium-catalyzed cycloaddition of alkynes and organic azides. *J. Am. Chem. Soc.* **2005,** *127* (46), 15998-15999.

124. Rostovtsev, V. V.; Green, L. G.; Fokin, V. V.; Sharpless, K. B., A stepwise huisgen cycloaddition process: copper (I) - catalyzed regioselective "ligation" of azides and terminal alkynes. *Angew. Chem* **2002,** *114* (14), 2708-2711.

125. Özçubukçu, S.; Ozkal, E.; Jimeno, C.; Pericàs, M. A., A Highly Active Catalyst for Huisgen 1,3-Dipolar Cycloadditions Based on the Tris(triazolyl)methanol–Cu(I) Structure. *Org. Lett.* **2009,** *11* (20), 4680-4683.

126. Nakamura, T.; Terashima, T.; Ogata, K.; Fukuzawa, S.-i., Copper(I) 1,2,3-Triazol-5-ylidene Complexes as Efficient Catalysts for Click Reactions of Azides with Alkynes. *Org. Lett.* **2011,** *13* (4), 620-623.

127. Yamada, Y. M. A.; Sarkar, S. M.; Uozumi, Y., Amphiphilic Self-Assembled Polymeric Copper Catalyst to Parts per Million Levels: Click Chemistry. *J. Am. Chem. Soc.* **2012,** *134* (22), 9285-9290.

128. Hiroki, H.; Ogata, K.; Fukuzawa, S.-i., 2-Ethynylpyridine-Promoted Rapid Copper (I) Chloride Catalyzed Azide–Alkyne Cycloaddition Reaction in Water. *Synlett* **2013,** *24* (07), 843-846.

129. Worrell, B. T.; Malik, J. A.; Fokin, V. V., Direct evidence of a dinuclear copper intermediate in Cu(I)-catalyzed azide-alkyne cycloadditions. *Science* **2013,** *340* (6131), 457-60.

130. Besanceney-Webler, C.; Jiang, H.; Zheng, T.; Feng, L.; Soriano del Amo, D.; Wang, W.; Klivansky, L. M.; Marlow, F. L.; Liu, Y.; Wu, P., Increasing the Efficacy of Bioorthogonal Click Reactions for Bioconjugation: A Comparative Study. *Angew. Chem. Int. Ed.* **2011,** *50* (35), 8051-8056.

131. Soriano del Amo, D.; Wang, W.; Jiang, H.; Besanceney, C.; Yan, A. C.; Levy, M.; Liu, Y.; Marlow, F. L.; Wu, P., Biocompatible Copper(I) Catalysts for in Vivo Imaging of Glycans. *J. Am. Chem. Soc.* **2010,** *132* (47), 16893-16899.

132. Jiang, H.; Zheng, T.; Lopez-Aguilar, A.; Feng, L.; Kopp, F.; Marlow, F. L.; Wu, P., Monitoring Dynamic Glycosylation in Vivo Using Supersensitive Click Chemistry. *Bioconjug. Chem.* **2014,** *25* (4), 698-706.

133. Agard, N. J.; Baskin, J. M.; Prescher, J. A.; Lo, A.; Bertozzi, C. R., A Comparative Study of Bioorthogonal Reactions with Azides. *ACS Chem. Biol* **2006,** *1* (10), 644-648.

134. MacKenzie, D. A.; Sherratt, A. R.; Chigrinova, M.; Cheung, L. L. W.; Pezacki, J. P., Strain-promoted cycloadditions involving nitrones and alkynes—rapid tunable reactions for bioorthogonal labeling. *Curr Opin Chem Biol* **2014,** *21*, 81-88.

135. Mitsunobu, O.; Yamada, M., Preparation of esters of carboxylic and phosphoric acid via quaternary phosphonium salts. *Bull. Chem. Soc. Jpn.* **1967,** *40* (10), 2380-2382.

136. Fletcher, S., The Mitsunobu reaction in the 21 st century. *Org. Chem. Front.* **2015,** *2* (6), 739-752.

137. Swamy, K. K.; Kumar, N. B.; Balaraman, E.; Kumar, K. P., Mitsunobu and related reactions: advances and applications. *Chem. Rev.* **2009,** *109* (6), 2551-2651.

138. Chan, W. C.; White, P. D., *Fmoc solid phase peptide synthesis : a practical approach / edited by Weng C. Chan and Peter D. White*. Oxford : Oxford University Press: Oxford, 2000.

139. Alnoman, R. B.; Rihn, S.; O'Connor, D. C.; Black, F. A.; Costello, B.; Waddell, P. G.; Clegg, W.; Peacock, R. D.; Herrebout, W.; Knight, J. G., Circularly Polarized Luminescence from Helically Chiral N, N, O, O ‐ Boron ‐ Chelated Dipyrromethenes. *Chem. Eur. J.* **2016,** *22* (1), 93-96.

140. Chan, T. R.; Hilgraf, R.; Sharpless, K. B.; Fokin, V. V., Polytriazoles as Copper(I)-Stabilizing Ligands in Catalysis. *Org. Lett.* **2004,** *6* (17), 2853-2855.

141. Healy, P.; Kildea, J.; Skelton, B.; White, A., Lewis-Base Adducts of Group 11 Metal(I) Compounds. XLIII. Synthesis and Structural Systematics of 1 : 1 Copper(I) Halide/Nitrogen Base Adducts as $[(\text{N-base})_1(\text{CuX})_1]_\infty$ 'Split-Stair' Polymers (X = Cl, Br, I; N-Base = Acridine, Quinaldine and 2,6-Dimethyl- and 2,4,6-Trimethyl-Pyridine). *Aust. J. Chem.* **1989,** *42* (1), 115-136.

142. Baker, J. G.; Middleton, R.; Adams, L.; May, L. T.; Briddon, S. J.; Kellam, B.; Hill, S. J., Influence of fluorophore and linker composition on the pharmacology of fluorescent adenosine A1 receptor ligands. *Br. J. Pharmacol.* **2010,** *159* (4), 772-786.

143. Vernall, A. J.; Stoddart, L. A.; Briddon, S. J.; Hill, S. J.; Kellam, B., Highly Potent and Selective Fluorescent Antagonists of the Human Adenosine A3 Receptor Based on the 1,2,4-Triazolo[4,3-a]quinoxalin-1-one Scaffold. *J. Med. Chem.* **2012,** *55* (4), 1771-1782.

144. Baker, J. G.; Adams, L. A.; Salchow, K.; Mistry, S. N.; Middleton, R. J.; Hill, S. J.; Kellam, B., Synthesis and Characterization of High-Affinity 4,4-Difluoro-4-bora-3a,4a-diaza-s-indacene-

Labeled Fluorescent Ligands for Human β-Adrenoceptors. *J. Med. Chem.* **2011,** *54* (19), 6874-6887.

145. Loudet, A.; Burgess, K., BODIPY Dyes and Their Derivatives: Syntheses and Spectroscopic Properties. *Chem. Rev.* **2007,** *107* (11), 4891-4932.

146. Cusack, K. P.; Wang, Y.; Hoemann, M. Z.; Marjanovic, J.; Heym, R. G.; Vasudevan, A., Design strategies to address kinetics of drug binding and residence time. *Bioorg Med Chem Lett* **2015,** *25* (10), 2019-27.

147. Sykes, D. A.; Stoddart, L. A.; Kilpatrick, L. E.; Hill, S. J., Binding kinetics of ligands acting at GPCRs. *Mol Cell Endocrinol* **2019,** *485*, 9-19.

148. Copeland, R. A.; Pompliano, D. L.; Meek, T. D., Drug-target residence time and its implications for lead optimization. *Nat. Rev. Drug Discov.* **2006,** *5* (9), 730-9.

149. Hoffmann, C.; Castro, M.; Rinken, A.; Leurs, R.; Hill, S. J.; Vischer, H. F., Ligand Residence Time at G-protein-Coupled Receptors-Why We Should Take Our Time To Study It. *Mol Pharmacol* **2015,** *88* (3), 552-60.

150. Gillard, M.; Van Der Perren, C.; Moguilevsky, N.; Massingham, R.; Chatelain, P., Binding characteristics of cetirizine and levocetirizine to human H(1) histamine receptors: contribution of Lys(191) and Thr(194). *Mol Pharmacol* **2002,** *61* (2), 391-9.

151. Schoepke, N.; Church, M. K.; Maurer, M., The inhibition by levocetirizine and fexofenadine of the histamine-induced wheal and flare response in healthy Caucasian and Japanese volunteers. *Acta Derm-Venereol* **2013,** *93* (3), 286-93.

152. Christopoulos, A.; Parsons, A. M.; Lew, M. J.; El-Fakahany, E. E., The assessment of antagonist potency under conditions of transient response kinetics. *Eur. J. Pharmacol.* **1999,** *382* (3), 217-227.

153. Charlton, S. J.; Vauquelin, G., Elusive equilibrium: the challenge of interpreting receptor pharmacology using calcium assays. *Br. J. Pharmacol.* **2010,** *161* (6), 1250-1265.

154. Kenakin, T.; Jenkinson, S.; Watson, C., Determining the Potency and Molecular Mechanism of Action of Insurmountable Antagonists. *J. Pharmacol. Exp. Ther.* **2006,** *319* (2), 710-723.

155. Bosma, R.; Wang, Z.; Kooistra, A. J.; Bushby, N.; Kuhne, S.; van den Bor, J.; Waring, M. J.; de Graaf, C.; de Esch, I. J.; Vischer, H. F.; Sheppard, R. J.; Wijtmans, M.; Leurs, R., Route to Prolonged Residence Time at the Histamine H1 Receptor: Growing from Desloratadine to Rupatadine. *J. Med. Chem.* **2019,** *62* (14), 6630-6644.

156. Kimmett, T.; Smith, N.; Witham, S.; Petukh, M.; Sarkar, S.; Alexov, E., ProBLM web server: protein and membrane placement and orientation package. *Comput Math Methods Med* **2014,** *2014*, 838259.

Appendix

Amino acids, their side groups, 3- and 1-letter code

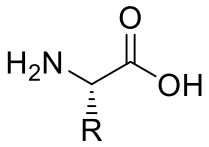

Where R =



Glycine
Gly (G)



Alanine
Ala (A)



Valine
Val (V)

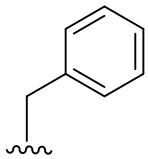

Phenylalanine
Phe (F)

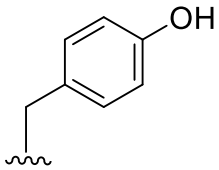

Tyrosine
Tyr (Y)

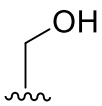

Serine
Ser (S)

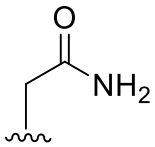

Asparagine
Asn (N)

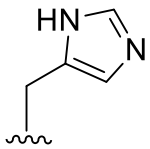

Histidine
His (H)

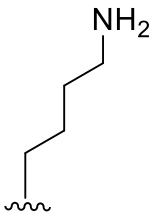

Lysine
Lys (K)

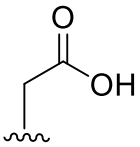

Aspartic acid
Asp (D)

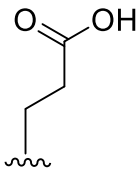

Glutamic acid
Glu (E)

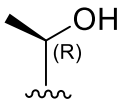

Threonine
Thr (T)

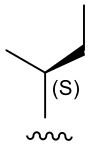

Isoleucine
Iso (I)

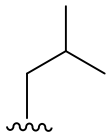

Leucine
Leu (L)

Excitation spectrum for **32** in 10% DMSO/HBSS

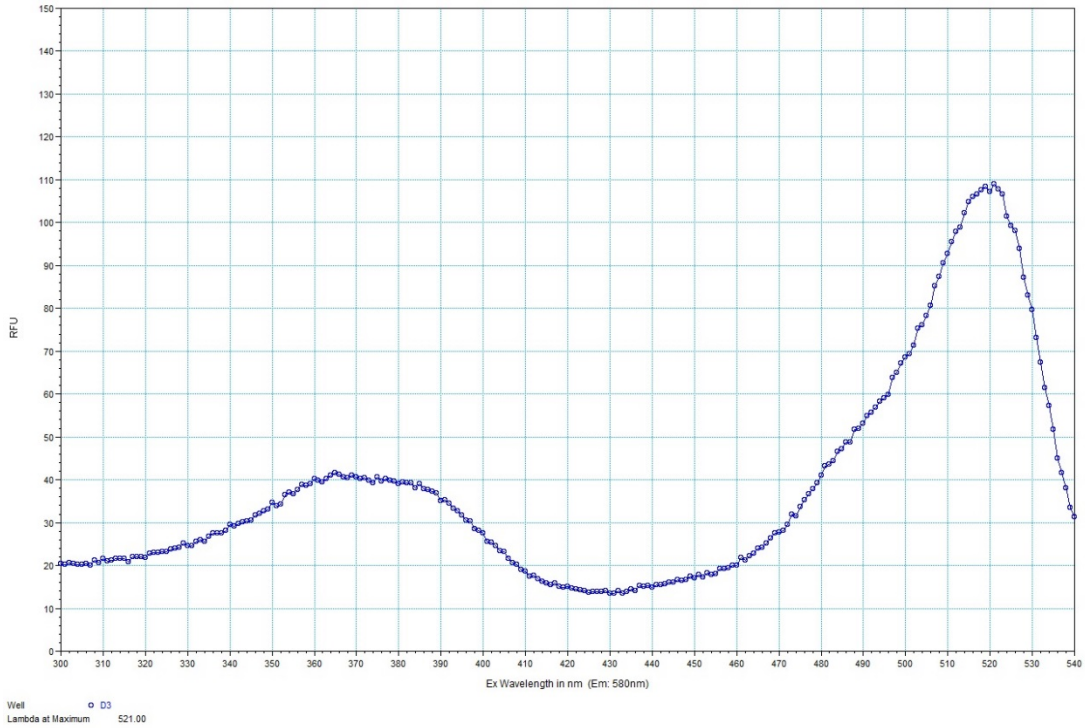

Emission spectrum for **32** in 10% DMSO/HBSS

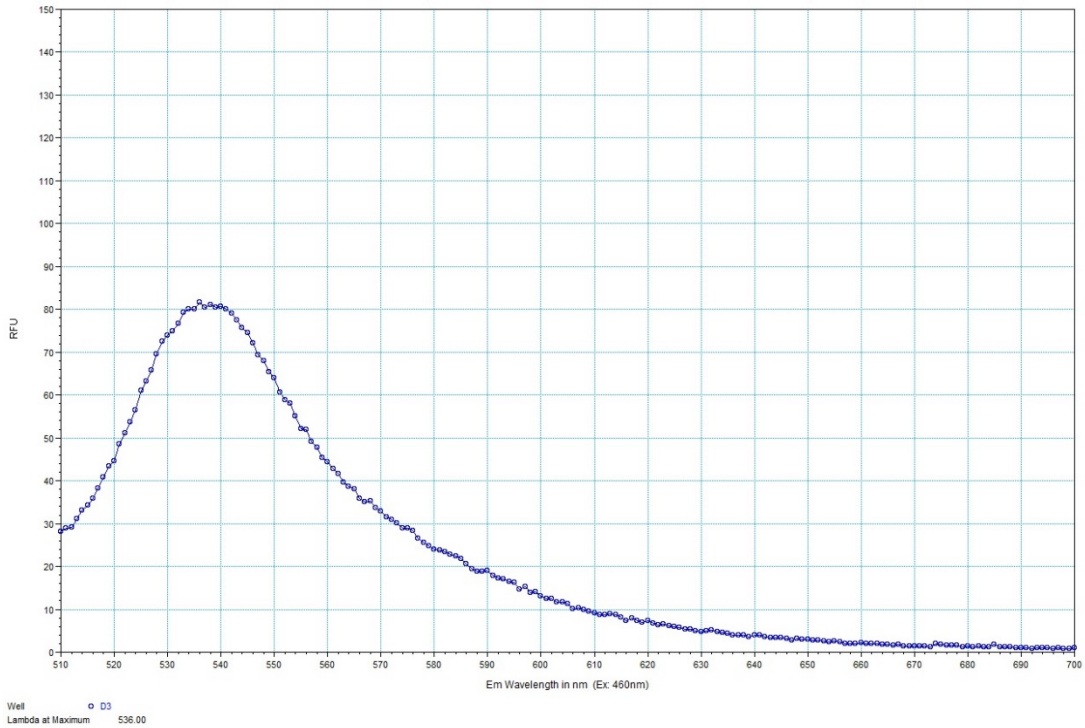

Excitation spectrum for **123** in 10% DMSO/HBSS

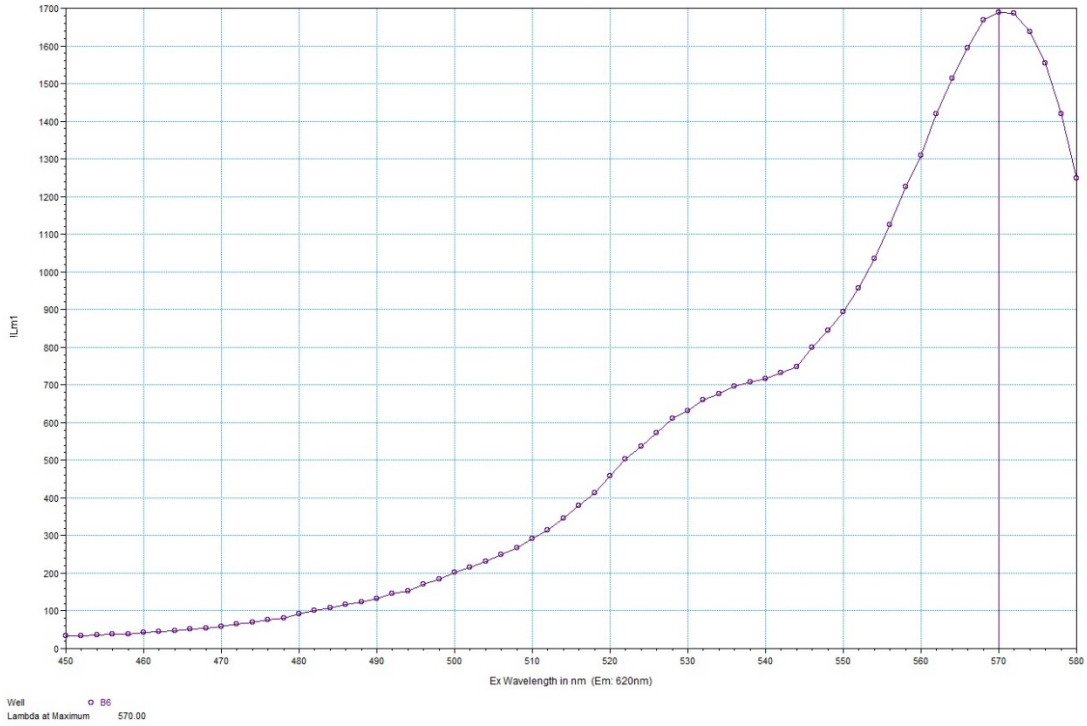

Emission spectrum for **123** in 10% DMSO/HBSS

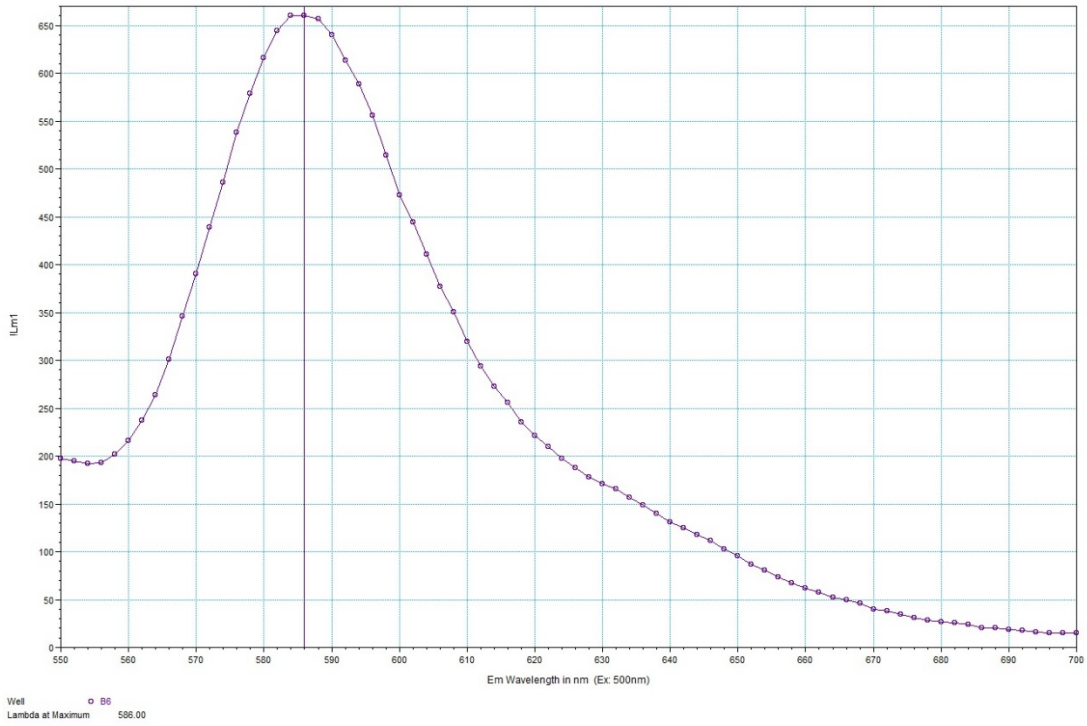

Excitation spectrum for **123** in DMSO

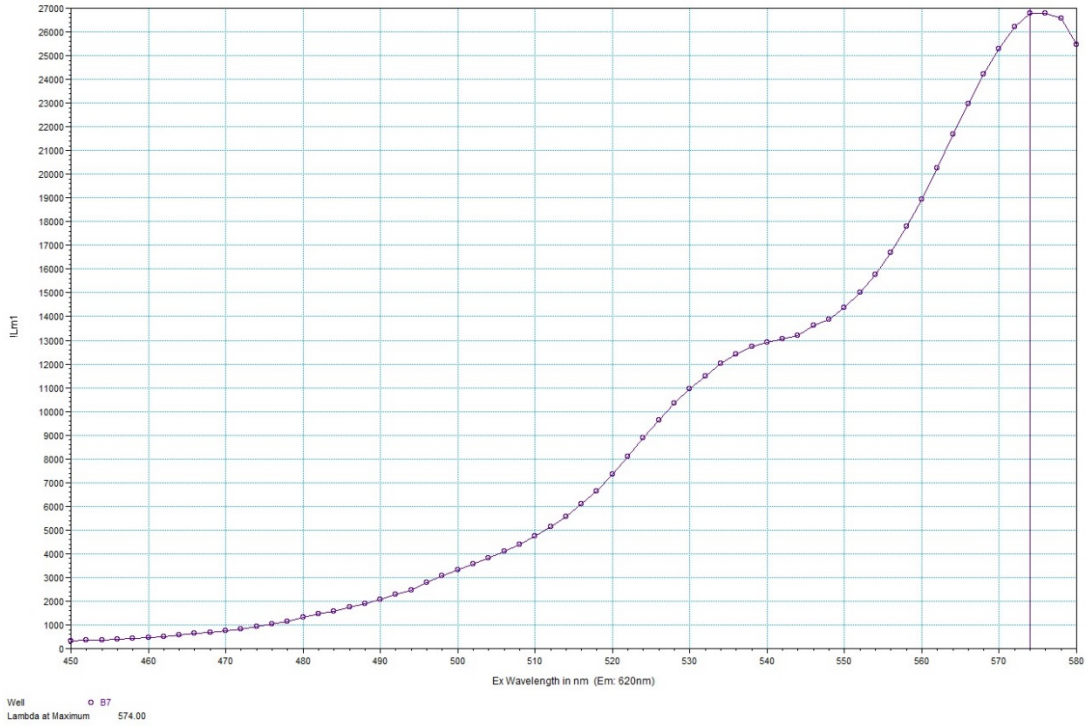

Emission spectrum for **123** in DMSO

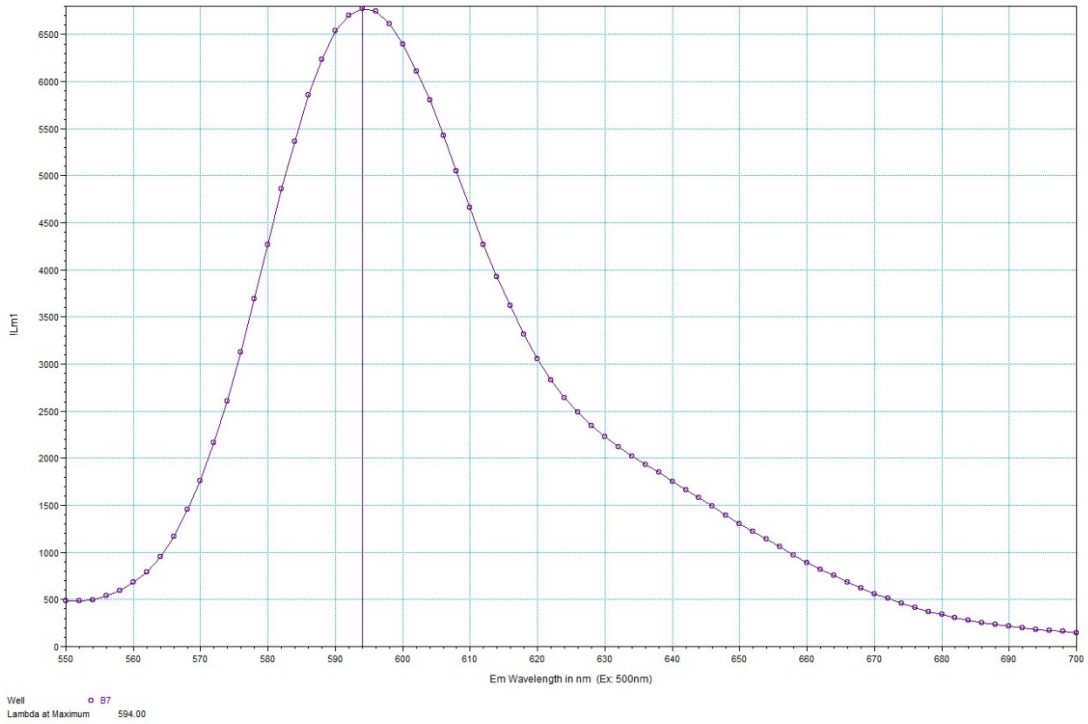

Excitation spectrum for **124** in 10% DMSO/HBSS

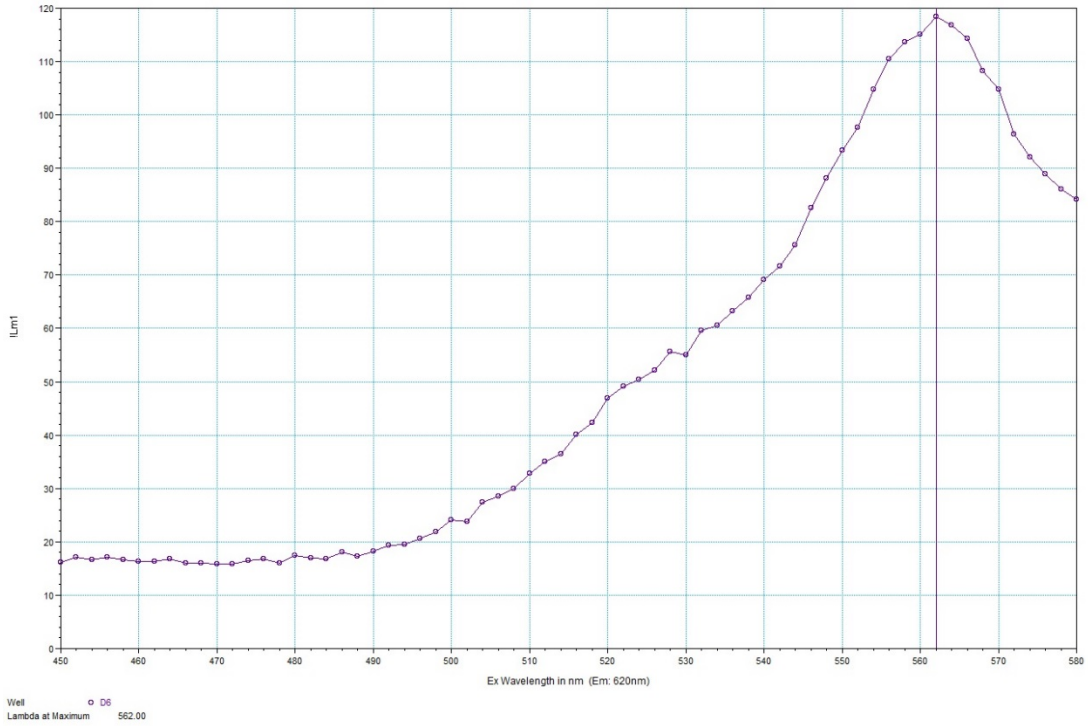

Emission spectrum for **124** in 10% DMSO/HBSS

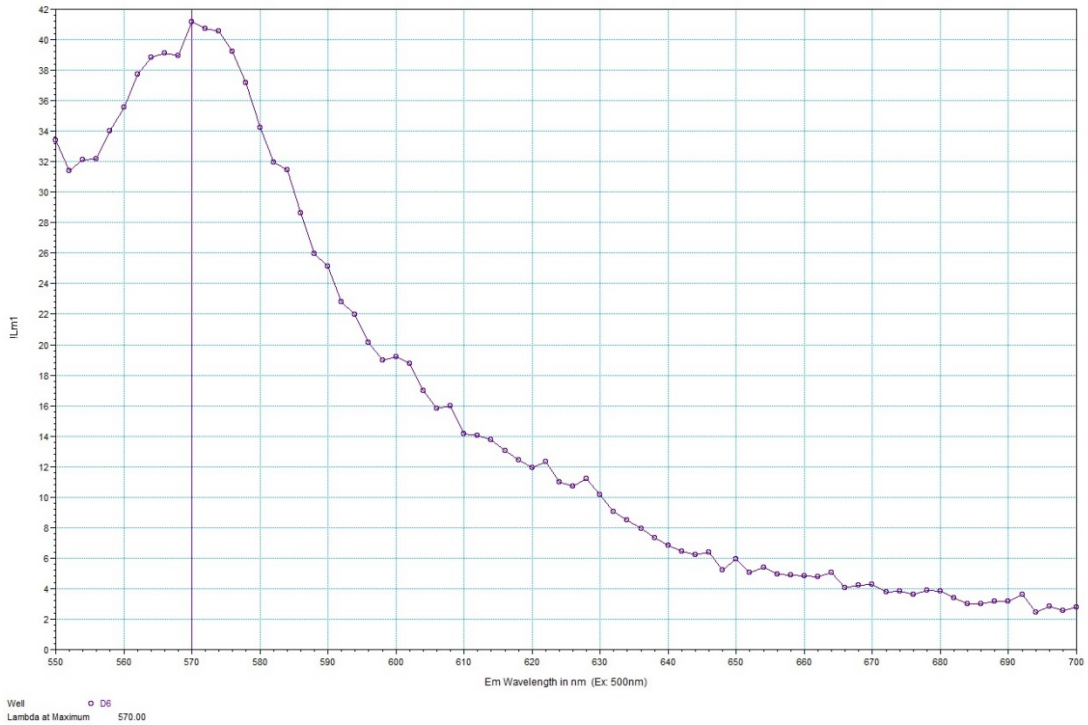

Excitation spectrum for **124** in DMSO

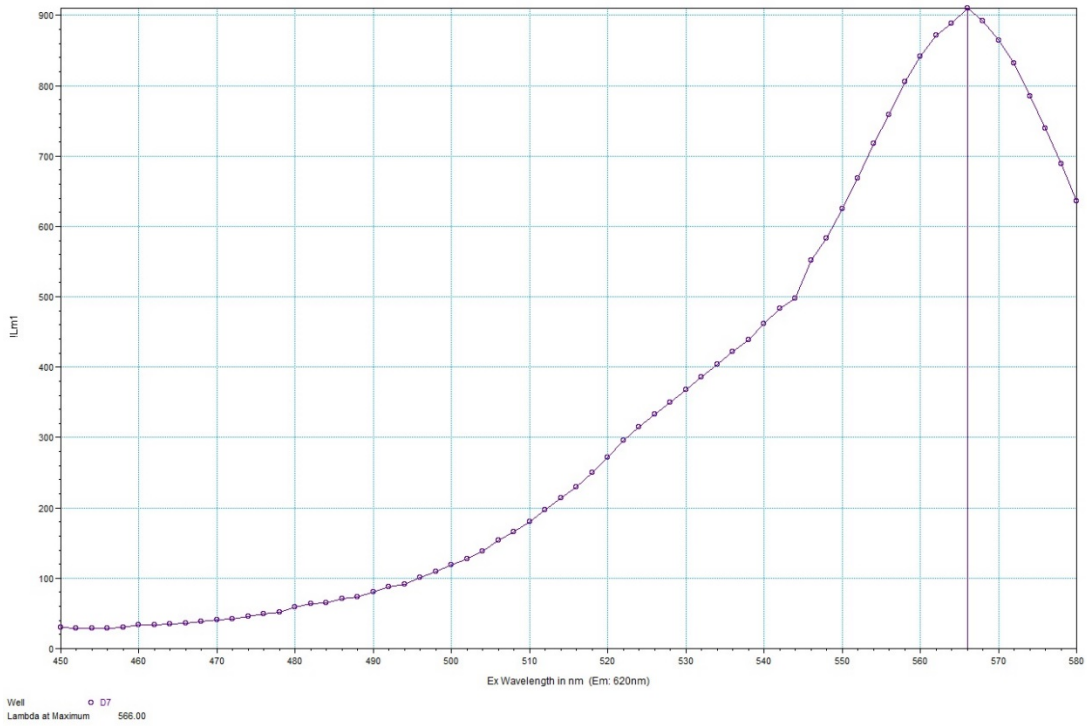

Emission spectrum for **124** in DMSO

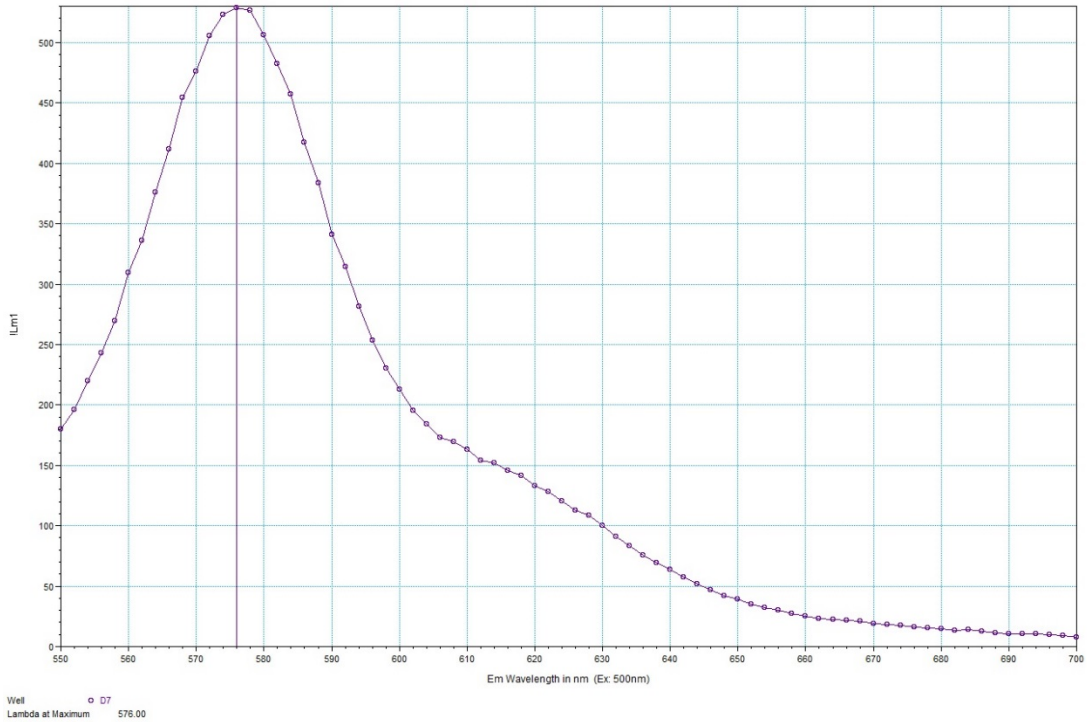

Excitation spectrum for **129** in 10% DMSO/HBSS

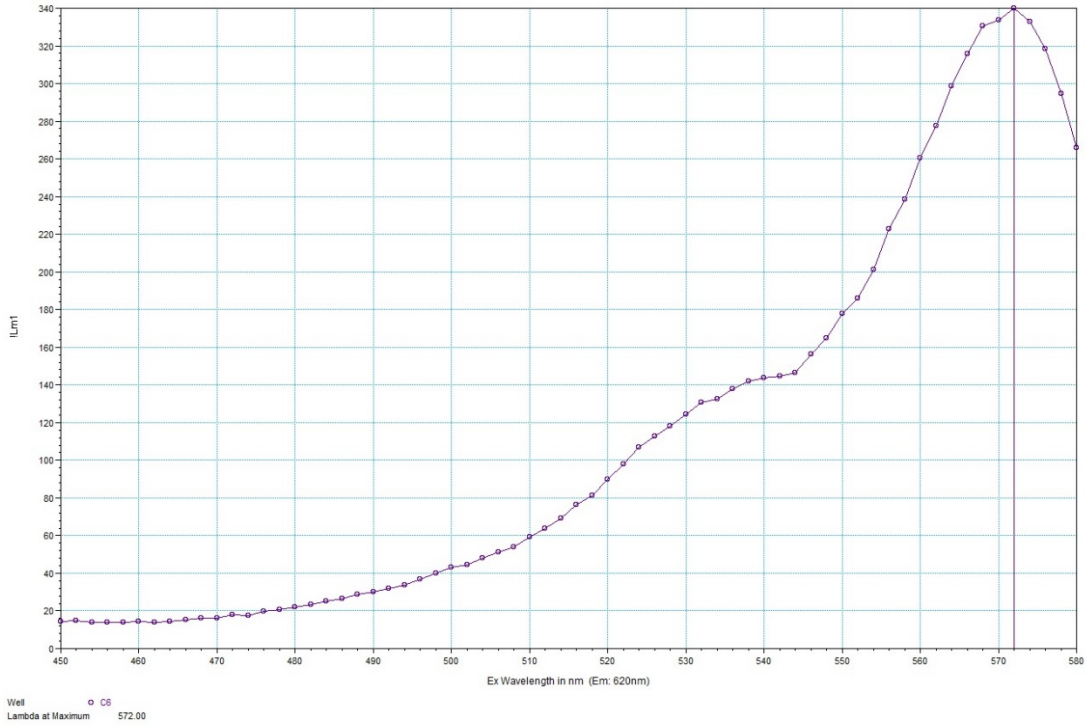

Emission spectrum for **129** in 10% DMSO/HBSS

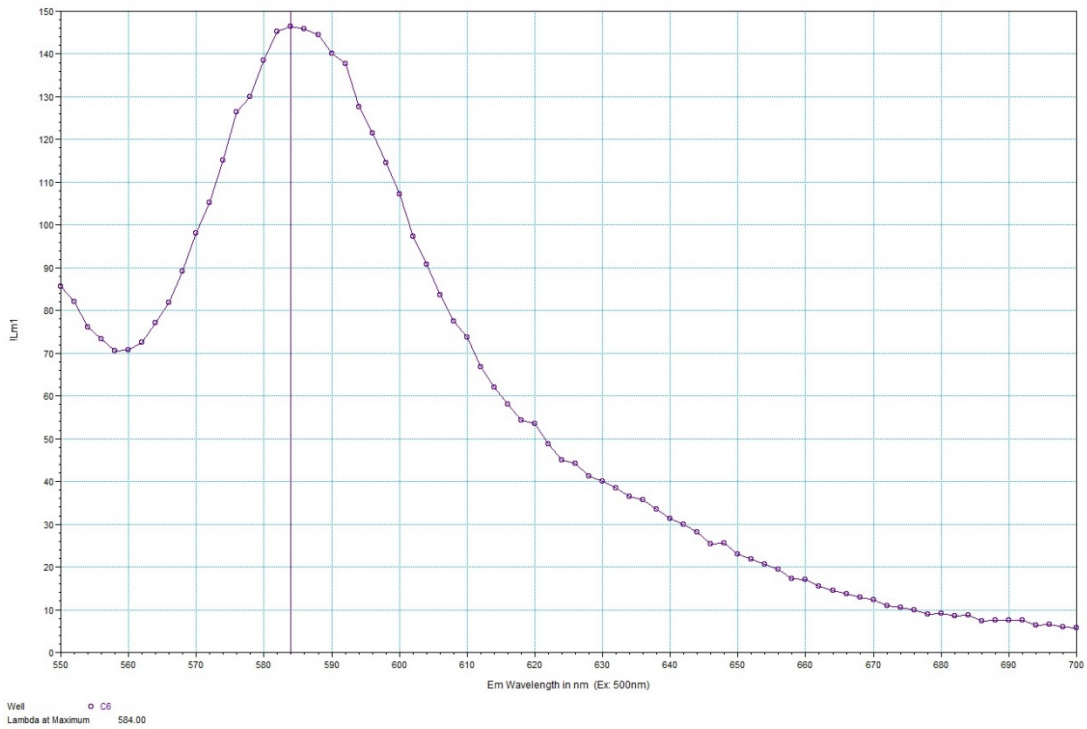

Excitation spectrum for **129** in DMSO

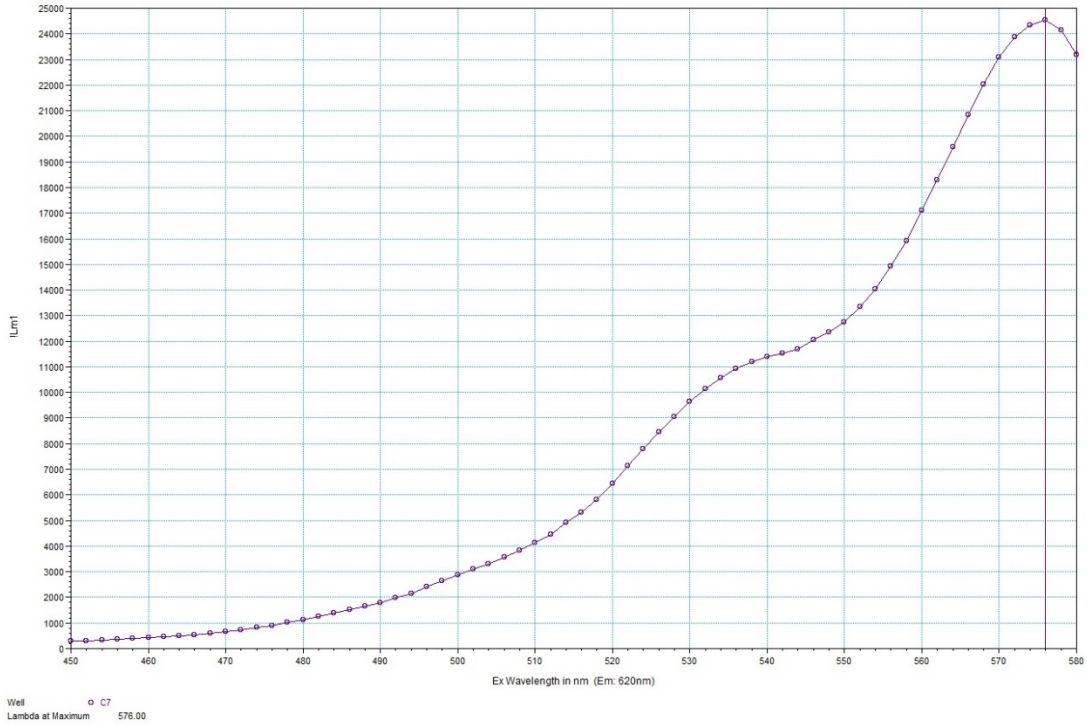

Emission spectrum for **129** in DMSO

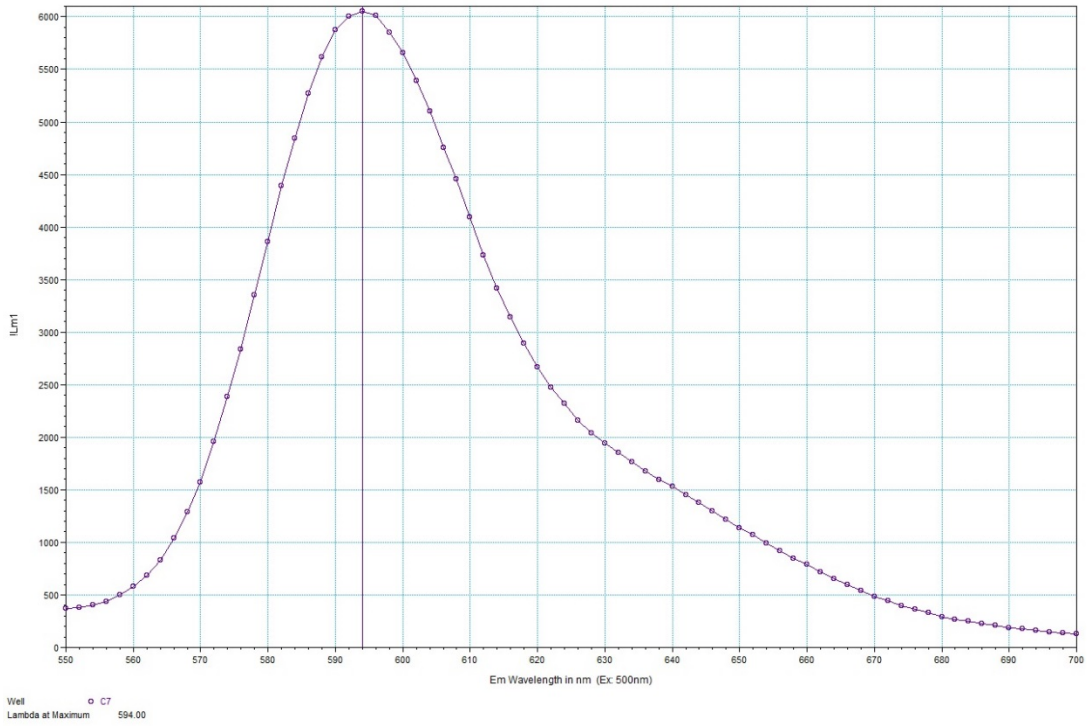

Excitation spectrum for **130** in 10% DMSO/HBSS

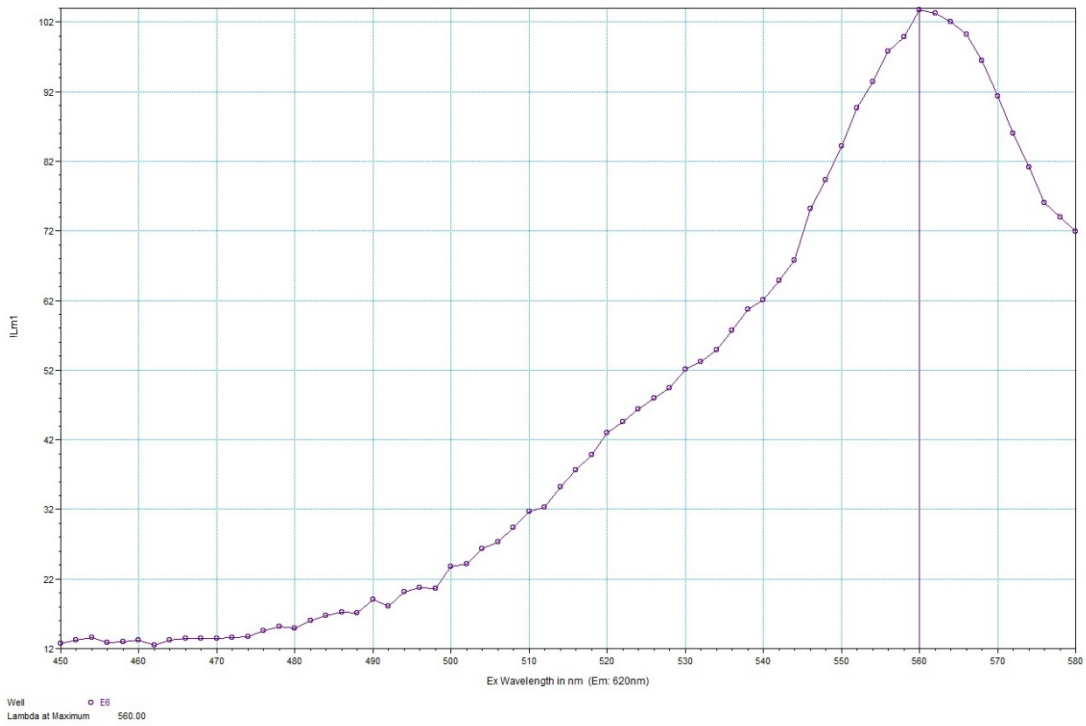

Emission spectrum for **130** in 10% DMSO/HBSS

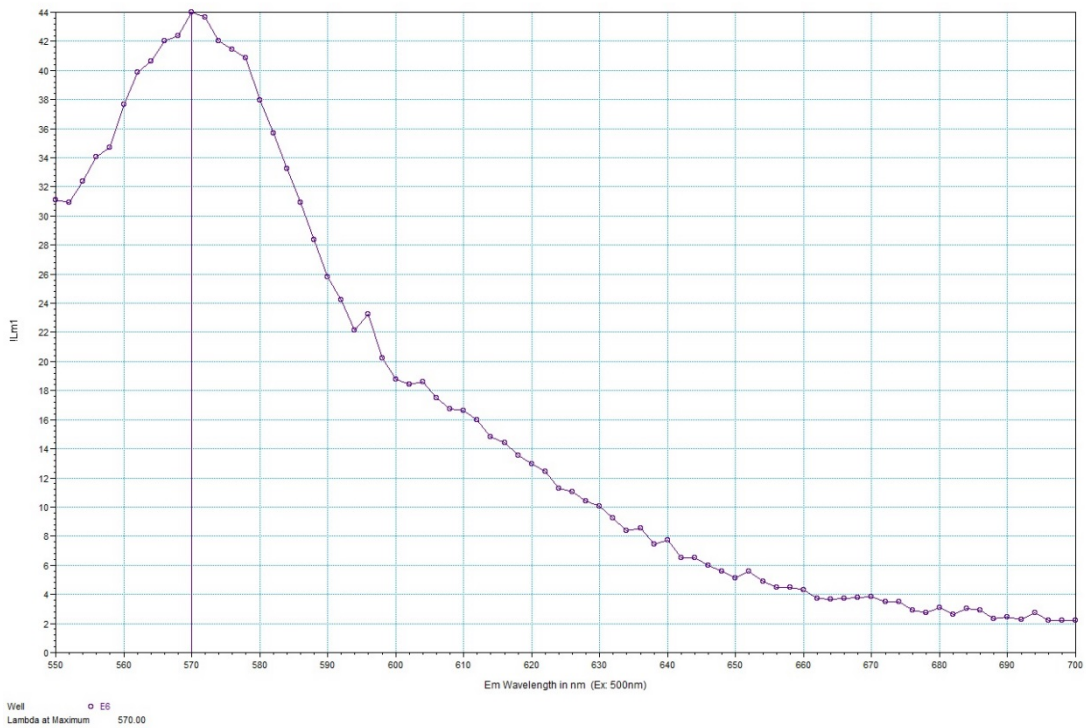

Excitation spectrum for **130** in DMSO

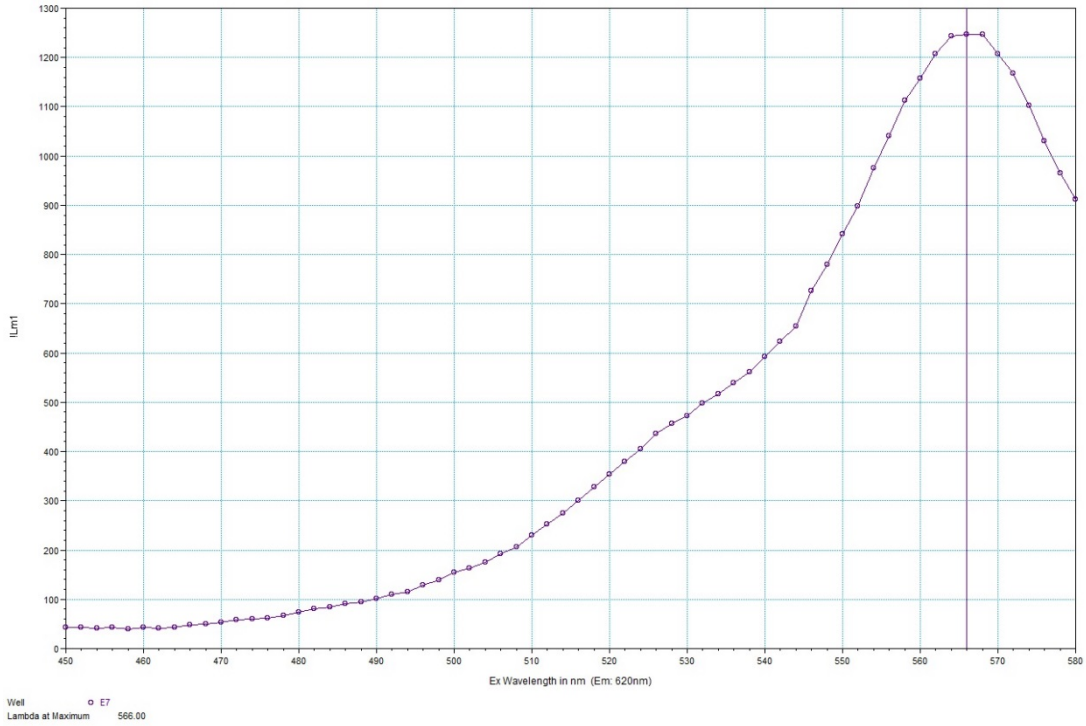

Emission spectrum for **130** in DMSO

